AD-A247 201

ATION PAGE

Form Approved
OMB No. 0704-0188

1. AGENCY USE ONLY (Leave blank)	2. REPORT DATE	3. REPORT TYPE AND DATES COVERED
	23 Dec 1991	Final Technical Report 1 Jul 1986 - 31 Jan 1991

4. TITLE AND SUBTITLE (U)

Diagnostics for Research in Atomization and Turbulent Two-Phase Flows

5. FUNDING NUMBERS

PE - 61102F
PR - 2308
SA - CS
C -

6. AUTHOR(S)

Dr. William D. Bachalo

7. PERFORMING ORGANIZATION NAME(S) AND ADDRESS(ES)

Aerometrics, Inc.
550 Del Rey Avenue, Unit A
Sunnyvale, California 94086

8. PERFORMING ORGANIZATION REPORT NUMBER

AFOSR-TR- 92 0023

9. SPONSORING/MONITORING AGENCY NAME(S) AND ADDRESS(ES)

AFOSR/NA
Building 410
Bolling AFB DC 20332-6448

10. SPONSORING/MONITORING AGENCY REPORT NUMBER

F49620-86-C-0078

11. SUPPLEMENTARY NOTES

12a. DISTRIBUTION/AVAILABILITY STATEMENT

Approved for public release; distribution is unlimited

12b. DISTRIBUTION CODE

13. ABSTRACT (Maximum 200 words)

(See attached sheet.)

14. SUBJECT TERMS	15. NUMBER OF PAGES
CPFF	190
	16. PRICE CODE

17. SECURITY CLASSIFICATION OF REPORT	18. SECURITY CLASSIFICATION OF THIS PAGE	19. SECURITY CLASSIFICATION OF ABSTRACT	20. LIMITATION OF ABSTRACT
Unclassified	Unclassified	Unclassified	UL

Abstract

This investigation focussed on the development of instrumentation for the study of atomization and two-phase turbulent flows including sprays in reacting turbulent flow. Four methods were investigated: the phase Doppler method, ratiometric light scatter detection, Lagrangian frame particle dynamics analyzer, and scattered light heterodyne interferometry. For the phase Doppler technique, the physics of the dual beam light scattering phenomena, the effects of particle morphology on the light scattering, the effects of the nonuniform illumination of the particle, and the consequences of the random particle trajectories were investigated. Sampling statistics were also considered. The ratiometric light scatter detection method was used to size irregular shaped and inhomogeneous particles using the scattered light intensity in the near forward direction. The uncertainty due to the particle trajectory through the beams was removed using an optical deconvolution approach. A Lagrangian method for tracking individual particles was investigated. A rapidly swept light sheet produced a series of images of an individual particle on an array detector, from which the particle's position and velocity were obtained. This method is feasible given sufficient laser power and/or a large enough particle. Scattered light heterodyne interferometry posed significant limitations which indicated that it would not offer significant advantages.

Diagnostics For Research In Atomization and Turbulent Two-Phase Flows

(AFOSR Contract No. F49620-86-0078)
Final Report

b y

Aerometrics, Inc.
550 Del Rey Avenue
Sunnyvale, CA 94086

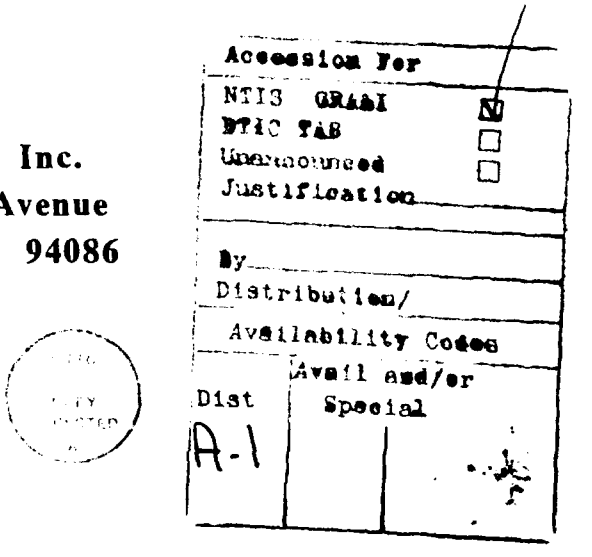

October, 1991

Contents

Diagnostics For Research In Atomization and Turbulent Two-Phase Flows

(AFOSR Contract No. F49620-86-0078)
Final Report

Summary and Overview:

The development of instrumentation for the study of atomization and two-phase turbulent flows including sprays in reacting turbulent flow environments was the primary focus of this research program. Four methods having some unique capabilities were investigated. These methods were the phase Doppler method, ratiometric light scatter detection, Lagrangian frame particle dynamics analyzer, and scattered light heterodyne interferometry. Each of these methods has potential capabilities not available in the others that can add to the experimental information that is needed in the study of these complex flows. Of the methods, the phase Doppler approach is the most advanced and has become a standard instrument for spray and two-phase flow characterizations. Under this program, a number of important aspects of the technique were investigated including the detailed physics of the dual beam light scattering phenomena, the effects of particle morphology on the light scattering, the effects of the nonuniform illumination of the particle by Gaussian beams, and the consequences of the random trajectories that the particle will take through the Gaussian beams. Failure to properly account for these effects has been demonstrated to result in significant measurement errors. Sampling statistics including the well-known velocity bias from laser Doppler velocimetry and particle number density limitations due to coincident occurrences were also considered.

The ratiometric light scatter detection method was derived to address irregular shaped particles and other particles such as those consisting of inhomogeneous materials such as slurries. This method utilizes the

measurement of the scattered light intensity in the near forward direction to estimate the particle size. The unique feature of the method is the approach to remove the uncertainty due to the particle trajectory through the Gaussian laser beams using an optical deconvolution approach. With this method, two confocal beams are used to determine the particle trajectory through the beam and hence, the incident intensity on the particle. The approach also provides an in situ measurement of the sample volume diameter.

Since the modelling of turbulent two-phase flows generally utilizes the Lagrangian frame description of the particle motion, a method for tracking individual particles in a turbulent environment was investigated. The method utilizes a rapidly swept light sheet to produces a series of images for an individual particle that is identified by, for example, a fluorescent dye. The particle may then be imaged using a high resolution, high speed array detector in three dimensions to obtain its position and velocity in three dimensions. The preliminary studies completed under this program showed that the method is feasible given sufficient laser power and/or a large enough particle.

In order to handle the measurements of drops that are moving at very high speeds, a new approach for implementing the phase Doppler method was considered. This method would use a virtual fringe approach and acousto-optic devices to track the frequency and phase of the scattered light. However, after investigating the light scattering characteristics in some detail, significant limitations were encountered which indicated that the method would not offer advantages over the original approach. Furthermore, important developments were realized in the signal processing for the original phase Doppler approach that advanced the measurement capability of particle size to supersonic speeds.

1.0 Introduction:

The research program focused on the very important problem of simultaneously measuring the particle size and velocity and also the local

number density and volume flux in a variety of applications and environments. The primary application was the characterization of fuel spray drop behavior in the complex turbulent flow fields in both reacting and nonreacting environments associated with gas turbine combustors. These flow fields may be characterized as having from dense to dilute particle fields, a full range of particle trajectories associated with the swirling and recirculating flow, very high levels of gas phase turbulence, reaction with significant turbulence-induced refractive index fluctuations, and soot formation. In addition, there are time-varying fluctuations of the local particle number density and velocities. A major emphasis of this research and development program was to investigate the impact of these flow conditions on the diagnostics, to develop methodologies to overcome the measurement limitations, and to estimate the impact of the flow conditions on the measurement accuracy. Because it was clear that not all of the essential information needed in characterizing these flow fields could be derived from the phase Doppler approach with the existing state of the technology, further development of the phase Doppler method was considered as were other methods that could extract information that could not be acquired with the phase Doppler method.

The phase Doppler method which was first developed by Aerometrics under joint funding from the NASA Lewis Research Center and the AFOSR represented one of the most significant steps forward in spray and two-phase flow diagnostics development. The method is robust and can provide accurate simultaneous measurements of the particle size and velocity in realistic flow environments. Measurements of the gas phase velocity in the presence of both nonburning and burning sprays have been made possible and comparisons to other more basic measurements and to flow field modelling indicate that these data have a high degree of reliability. In addition, the method has the potential for measuring the local number density and volume flux and providing information of the temporal behavior of these quantities. Although the basic principles associated with the method are relatively straightforward, there are some subtleties involved in the dual beam light scattering and the sampling statistics that required more detailed evaluation. Furthermore, in high number density environments, the problem of coincidence (more than one particle passing

the sample volume at one time) can compromise the estimation of the number density and volume flux. These issues were addressed in this report and by others (Edwards and Marx 1991) given in the references. Some very interesting observations on the performance of the instrument have been concluded from these studies.

Originally, the Doppler frequencies to which the phase of the signal could be processed accurately was limited to about 10 MHz. Because of the many practical applications that result in higher velocities, an effort was directed toward the development of the optical and electronic components to extend the range of the system. An interesting signal processing approach has been proposed by Smeets and George, 1981, that offered some potential for application to the phase Doppler method. In addition, the need for a high amplitude dynamic range as well as a large frequency range led to the evaluation of several electronics preamplification schemes. The results of this work carried out in cooperation with a group at Berkeley led to the development of a very high performance detector and preamplifier system. This work will be described.

In many applications, the particles cannot be expected to be spherical and homogeneous. In the analysis of the phase Doppler method, it is required that the particles be spherical and if transparent, they must also be nearly homogeneous. This is not a serious limitation for many spray applications but there is interest in sizing slurries and paints. There is also interest in sizing particles that are the products of combustion. In such cases, it is essential to develop and utilize methods with reduced sensitivity to the particle morphology. It is known that in the near forward scatter region, the light scattering mechanism is dominated by diffraction. Diffractive scattering of light responds to the projected area of the particle. If the light detection is acquired symmetrically about the transmitted beams in the forward direction, the effects of the irregular shape will be integrated out of the response. The proposed ratiometric method uses the scattered light intensity to infer particle size. The ambiguity due to the random trajectories of the particles through the Gaussian beam was eliminated with the use of two confocal beams of different diameters and wavelengths or polarizations. In this way, an optical deconvolution was

possible for eliminating the ambiguity in the incident beam intensity on the particles.

Finally, an imaging method was derived for tracking particles in a Lagrangian reference frame. The method requires the use of a laser beam projected into a light sheet. The sheet is swept through the flow field at up to 10 kHz frequencies, depending upon the particle velocity. The use of special optics and linear array detectors were used to observe the particle trajectories. The study will show that the instantaneous particle velocity and position can be determined in each of the three dimensions as it passes through the field of view.

This report will provide an overview description of the results of the investigations. The details of the studies will be given in either this report or in the papers given in the appendices.

2.0 Research and Development on the Phase Doppler Method

In this section, the developments relating to the phase Doppler instrument will be outlined. Because of the scientific and commercial importance of this method, the greatest effort was expended on this development. With the application of the method to numerous studies in atomization and spray combustion, several areas needing refinement and further development were discovered. These areas were factored into this research program whereas some other areas that were determined to be less important were de-emphasized. Overall, significant progress was made in advancing the method toward acquiring reliable measurements in difficult environments.

2.1 Brief Description of the Method

As a result of approximately 10 years of research and development by Aerometrics and others, the phase Doppler method has been developed into a mature diagnostic for spray measurements and two-phase flow

research. The instrument has been used effectively in a wide variety of applications from gas turbine spray analyses and automotive fuel injector characterizations to the evaluation of medical nebulizers. The instrument has been successful because of the relative insensitivity of the method to the measurement environment and its reliability due to the use of the interferometric approach. In this case, the measurements are dependent upon the laser wavelength rather than the beam intensity. To better understand the results of the present research effort, a brief description of the method will be provided.

The phase Doppler method may be considered to be an extension of the well-known laser Doppler velocimeter (LDV). The differences in the optical configuration are in the receiver wherein at least two and preferably, three detectors are used. In addition, the receiver must be located at certain prescribed angles to the plane of the projected beams and this angle must be carefully defined and used in the calculation of the instrument response to the particle diameter. The very basic optical configuration of the system is given in figure 2.1.1. In this setup, the laser beam is split into two equal intensity beams and focused to the intersection region which will form the measurement volume. The receiver is disposed at a preferred angle to the transmitted beams. Generally, the angle selected is at 30 or 40 degrees with respect to the transmitted beams and in a plane perpendicular to the plane of the transmitted beams. Other angles can be used but the consequences need to be evaluated. This is the subject of the next section.

The receiver aperture serves to complete the delineation of the sample volume. The small slit aperture in the receiver is imaged to the beam intersection and allows light from only a small length of the intersecting beams. Particles passing through this sample volume scatter light to the receiver that passes through the slit aperture. Optics are used to separate the light into three components, each of which passes through a specific segment of the receiver lens (see U.S. Patent 4,540,283).

In the simplest description of the physics, the particle scatters light by refraction (or reflection) from each of the beams. Since the light from each

of the laser beams enters the spherical particle at different angles, light rays from each beam must necessarily pass on different paths through the particle to reach a common point in space, figure 2.1.2. Because of the different path lengths, the light from one of the beams will have a phase shift relative to the light from the other beam. Clearly, the relative phase shift at points in space will depend upon the angle between the beams, the wavelength of light, the particle index of refraction, the dominant light scattering mechanism, the angle to the point of observation, and the angle between the detectors. As a consequence of the phase shift, an interference fringe pattern is formed in the space surrounding the spherical particle. The spatial frequency of this pattern at any prescribed location depends upon the particle diameter as well as the aforementioned parameters. The spacing of the fringe pattern formed by the scattered light may be measured by placing pairs of detectors in the fringe pattern at known separation. Each detector will produce a Doppler burst signal with the same frequency but with a phase shift. The phase shift between the signals can be related to the spacing of the interference fringes and hence the particle diameter through the simple relationship

$$s / L = f / 360 \tag{2.1.1}$$

where s is the spacing between the detectors, L is the local spacing of the interference fringe pattern, and f is the phase angle between the Doppler signals. It remains to accurately describe the scattered light response and the interference pattern formed given specific instrument parameters, drop size and index of refraction. This is the subject of the next section.

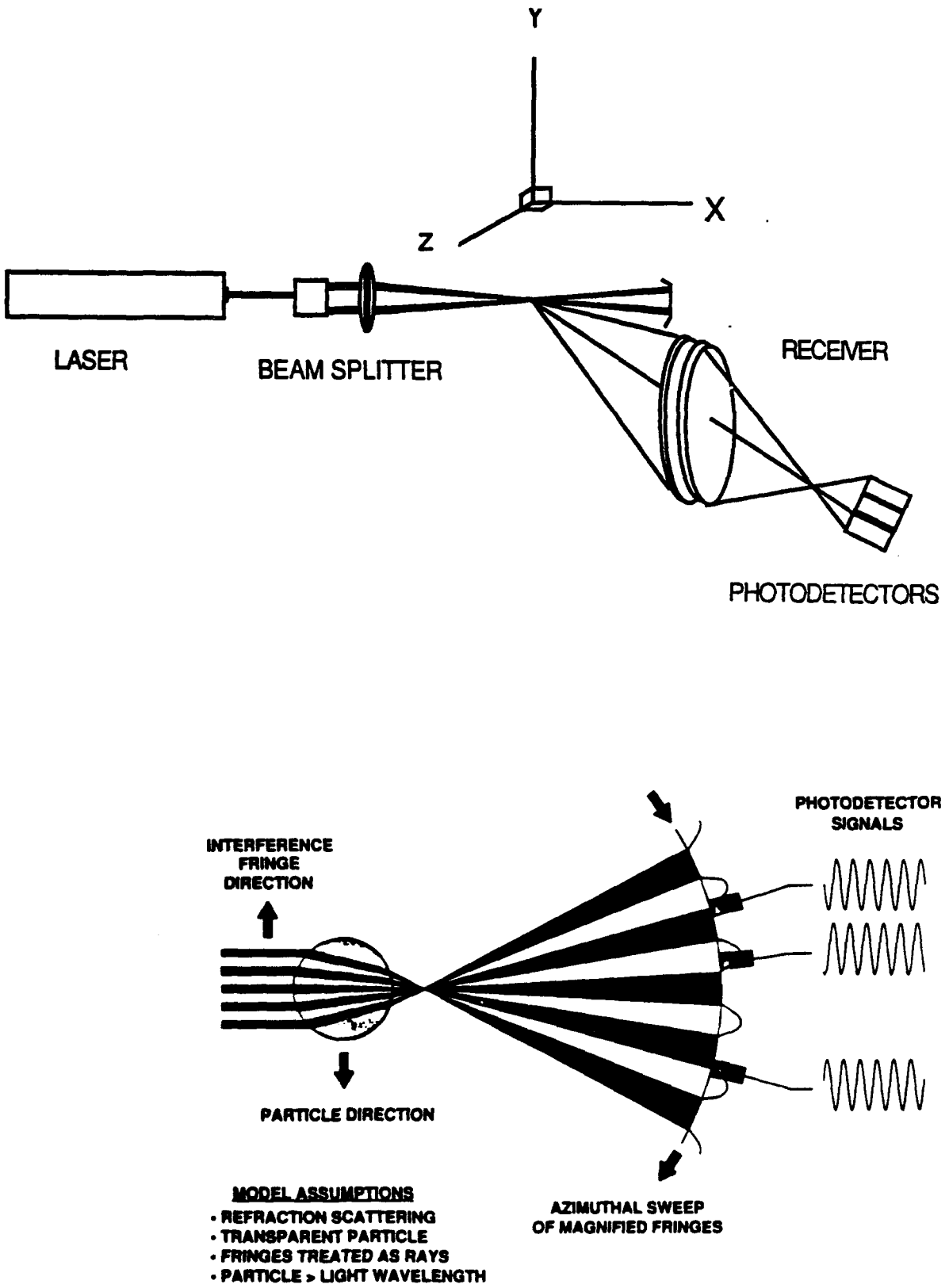

Figure 2.1.1: Basic phase Doppler optical configuration.

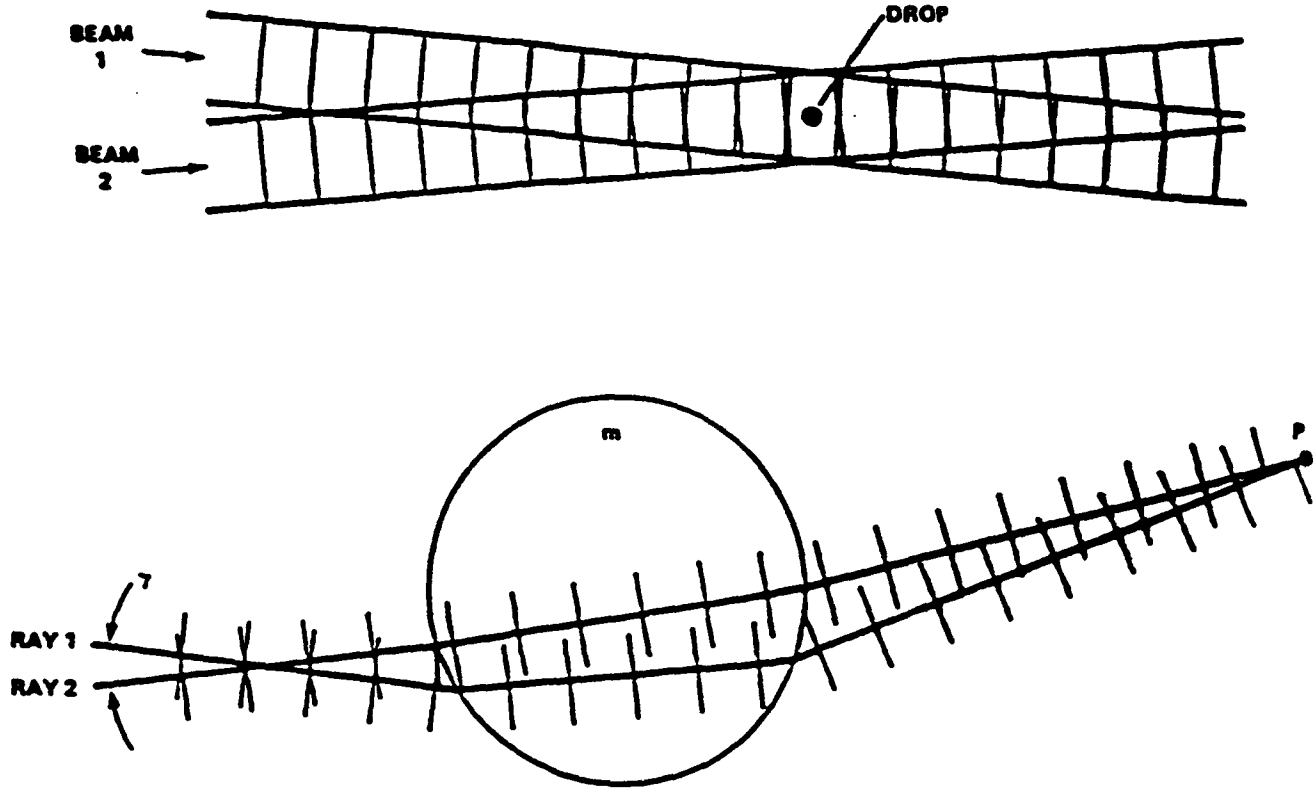

Figure 2.1.2: Dual-Beam ray trace through a sphere showing the phase shift mechanism.

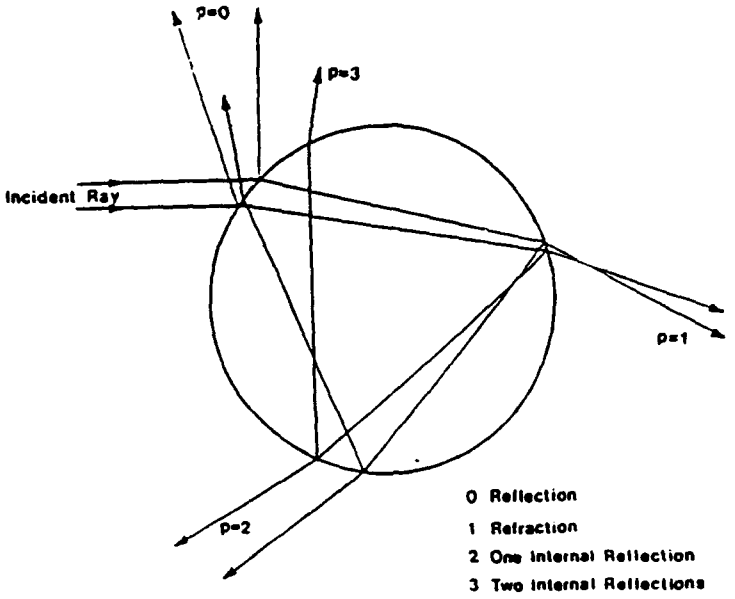

1. Ray trace for a water droplet.

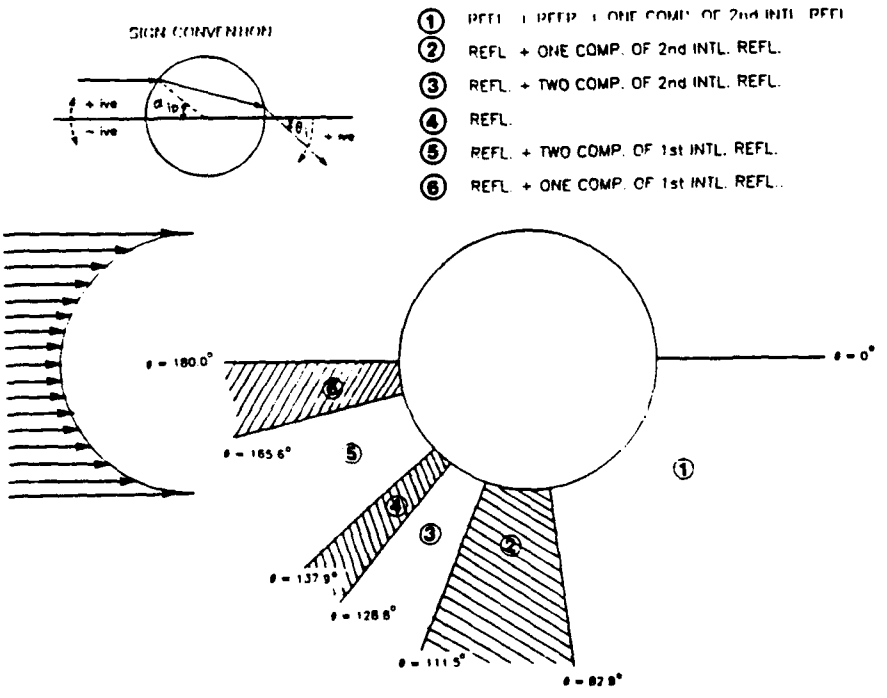

2. Division of scattering angles into scattering regions.

Figure 2.1.3: Light scattering from a Gaussian beam showing how the relative scattered intensities of the different scattering mechanisms depend on the particle trajectory.

2.2 Dual Beam Light Scattering Mechanisms

The original theoretical analysis leading to the development of the phase Doppler method was derived by Bachalo (1980) using the simple geometrical optics theory using the classical reference by van de Hulst (1954). This theory provides an accurate description of the phase shifts produced by light passing through or reflected from a homogeneous sphere situated in a homogeneous environment. The theoretical development assumed that only one light scattering mechanism was present if the appropriate light scatter detection angle was used. This approximation was adequate for the development of the method. However, as the instrument was refined, this simple analytical description proved to be inadequate in describing the details of the performance. Specifically, the contributions from the other scattering components, namely, first surface reflection and internal reflections, could be significant under some optical configurations.

A more refined analysis of the dual beam light scatter detection with off-axis light scatter detection was developed by Pendleton (1982). In this work, the exact Lorenz-Mie theory was used to describe the light scattering. It should be noted that this theory is "exact" only in the special case of a uniformly illuminated homogeneous sphere located in a homogeneous environment. This is not that case when laser light is used with a Gaussian beam intensity profile. Furthermore, in an effort to limit the sample volume size to prevent coincident particle occurrences in high number density environments, the focused beam diameter is often made as small as possible. Typically, the $1/e^2$ diameter of the beam is as small as the largest particle to be measured. Under these conditions, the random particle trajectories through the laser beam will result in a change in the relative scattering intensities by the mechanisms of reflection and refraction, figure 2.1.3.

The consequence of this is to produce significant errors in the measurements. In this section, the details of the light scattering theory will

be discussed. The theory has been developed using both the Lorenz-Mie theory and the geometrical optics approach to calculate the light scattering amplitudes, Bachalo and Sankar, 1988, Sankar and Bachalo, 1991, and Sankar et al., 1991. The geometrical optics theory was developed to include all of the light scattering mechanisms involved; the refraction, reflection, and the internal reflection components. The advantage of the geometrical optics theory is that it can take account of the nonuniform illumination, it can generate the response as the particle is passed on different trajectories through the beams, and it is much more computationally efficient. It has been demonstrated by van de Hulst that this form of the geometrical optics theory is an asymptotic solution to the Maxwell's wave equations and leads to same result as the Lorenz-Mie theory for particles much larger than the wavelength.

Thus, for particles larger than about 5 μm, the geometrical optics approach was appropriate and, in fact, is more reliable than the Lorenz-Mie theory. For particles smaller than 10 μm, the Lorenz-Mie theory is used. This approach is most appropriate since for this size range, the smaller particles can be assumed to be uniformly illuminated because the beam diameter is typically at least 10 times greater than their diameter (>100 μm).

2.3 Sample Volume Definition and Number Density and Volume Flux Measurements

Because the phase Doppler method counts the particles passing through the sample volume and records the elapsed time for the sample accumulation, it is then possible to obtain local particle number density estimations if the sampling cross section is known.

In principle, the PDPA provides sufficient information to produce local drop number density and volume flux (or mass flux if the density is known). However these measurements represent a challenge to the instrument, since not only is it necessary to measure drop size and velocity, but the sampling cross-section of the optical probe must be also accurately characterized. This is a difficult task, due to the typical Gaussian

beam intensity profile, the changes in sampling cross sectional area with drop size, the unpredictable variations in the beam intensity due to light extinction by the drops and intervening windows, reduced signal to noise ratio, and the changes with instrument setup parameters. Nonetheless the critical role that the local drop number and mass flux play in the processes leading to the formation of soot, Nox emissions, air-fuel mixing, and energy release makes very important the ability to measure these quantities locally and with good spatial and temporal resolution.

The light intensity scattered by a particle in a large off-axis scattering mode is proportional to the square of its diameter. It follows that, due to the Gaussian radial intensity distribution of the laser beams, the sampling cross section changes with particle size as well as the measurement conditions and instrument setup parameters. In general, larger particles will exhibit a larger effective sampling probe volume and, as a result, the raw measurements obtained using the phase-Doppler sizing technique are biased towards the largest droplets, since the effective probe area,

$$A_p(d) = \frac{D(d)t}{\sin\theta} \tag{2.3.1}$$

will be bigger for those particles. In expression 2.3.1, $D(d)$ is the effective probe volume diameter for particles with diameter d, and t is the width of the receiver slit apperture as it appears in the object space.

This biasing of the sampling statistics was recognized and documented a number of years ago. Various correction schemes have been devised and implemented to correct the raw measured data to yield unbiased particle size distributions. This is one of the most critical and difficult aspects of the phase Doppler sizing technique. The probe volume correction not only affects the measured number-size distribution, but it is also critical in the computation of all the mean diameters of the distribution and the volume flux. In fact, except for the anemometry measurements, all the parameters computed by the PDPA are influenced by the probe volume correction step.

The determination of the effective probe volume size can be obtained either from a theoretical expression or from a semi-empirical formulation. The most simple correction schemes are based solely upon a theoretical description of the light intensity distribution in the sampling cross section (see, for example, Bachalo et al., 1988). In these scheme, the beam intensity distribution orthogonal to the direction of propagation is given by:

$$I_s = I_o \exp\left(-2\frac{r^2}{b_o^2}\right) \tag{2.3.2}$$

where r is the radial location from the center of the beam and b_o is the diameter at which the intensity falls to $1/e^2$ of the peak intensity. Since particles scatter light in proportion to their diameter squared, and there is a minimum signal amplitude that can be detected, an expression for the sample cross-section diameter $D(d_i)$ can be obtained as a function of the particle diameter, The resulting expression is:

$$D(d_i) = \left\{ D_{\min}(d_i)^2 + \frac{b_0^2}{2} \log\left[\left(\frac{d_i}{d_{\min}}\right)^2 \left(\frac{V+1}{V_0}\right) \right] \right\}^{1/2} \tag{2.3.3}$$

where the subscript min refers to the minimum detectable particle limit, and V is the signal visibility. The amplitude of the high-pass-filtered signals which are detected with the signal threshold detection electronics are affected by the signal visibility.

Semi-empirical procedures are based on the above analysis, assuming that indeed the probe diameter - particle diameter relationship follows the functional law (2.3.3). Instead of calculating directly the coefficients of (2.3.3), which depend on particular experimental conditions and instrument set-up, the semi-empirical procedures developed by Aerometrics estimate these parameters based upon the statistical distributions of the burst lengths or intensities. Essentially, for each data set, the probe diameters for those particle size classes with a number of occurrences higher than a prescribed statistically significant minimum are

computed from the experimental data itself using various methods. These methods are :

1) Fringe Count with Variable Slope

2) Fringe Count with Constant Slope

3) Gate Time * Velocity with Variable Slope

4) Gate Time * Velocity with Constant Slope

5) Intensity with Constant Slope

These methods will be discussed separately and then compared in the conclusions subsection.

2.3.1 Fringe Count with Variable Slope.

The experimental determination of the beam diameter for sizes with high enough statistical representation in the measurement is based on the characteristic histogram distribution of the number of particles that intercept different number of fringes (or equivalently, the particle velocity times transit time, L = v × t) as they cross the probe volume. For particles flowing perpendicular to the fringes, the maximum number of fringe crossings occurs for those particles passing through the beam centerline. On the other hand, a particle intercepting only one fringe crosses the probe almost tangentially. The fraction of particles that intercept n fringes when passing through the probe volume is equal to the fraction of the probe area enclosed by the vertical trajectories that produce n-1 and n fringe crossings (see Figure 2.3.1). This fraction is given by,

$$f(n) = 2\frac{x(n-1) - x(n)}{D(d)} = \left[1 - \left(\frac{n-1}{N_f(d_i)}\right)^2\right]^{1/2} - \left[1 - \left(\frac{n}{N_f(d_i)}\right)^2\right]^{1/2} \qquad (2.3.4)$$

where $N_f(d_i)$ is the number of fringes enclosed by the probe diameter corresponding to the particle class d_i This theoretical distribution is shown in Figure 2.3.2 for N=40. The statistics sharply peak for $n = N_f(d_i)$, immediately before decaying to zero. The beam diameter for that particular size is then given by,

$$D(d_i) = N_f(d_i)\delta_f \tag{2.3.5}$$

The empirical determination of the curve $D(d_i)$ is then as follows:

a) For each of the particle size classes whose number of occurrence is bigger than a prefixed value, obtain the fringe-crossings histogram. If velocity offset (frequency shift) is used, the fringe count is corrected to determine the number of fringe crossings that would have occurred without velocity offset.

b) Find the number of fringe crossings that each particle size class produces more often, $N_{fm}(d_i)$.

c) Determine then the largest number of fringe crossings, N_f^*, whose frequency of occurrence is larger than a specified fraction of the previously determined maximum. The experimental beam diameter is then given by:

$$D_{exp}(d_i) = N_f^*\delta_f \tag{2.3.6}$$

Note that for the theoretical histogram $N_f^* = N_{fm}$. In a real experimental situation, some broadening of the expected peak in the distribution occurs due to experimental imperfections. These imperfections introduce uncertainty in the location of the peak. However, the decay to zero after the maximum is still sharply defined, and N_f^* approaches closely N_{fm}.

Once the probe-volume diameters have been determined for those particle size classes with statistically significant representation in the sample, least squares can be used to find the constants k_1 and k_2 that would fit these to the theoretical expression,

$$D(d) = k_1 \log\left(\frac{d}{d_{\min}}\right) + k_2 \tag{2.3.7}$$

The constants are obtained from the following system of equations:

$$\frac{\partial}{\partial C_1} \sum_{d_j} \left[w_j \left(D^2_{\exp}(d_j) - k_2 - k_1 \log\left(d_j / d_{\min}\right) \right)^2 \right] = 0$$

$$\frac{\partial}{\partial C_2} \sum_{d_j} \left[w_j \left(D^2_{\exp}(d_j) - k_2 - k_1 \log\left(d_j / d_{\min}\right) \right)^2 \right] = 0 \tag{2.3.8 a,b}$$

The weights w_j used in the least squares fit are chosen as the number of samples with diameter d_j, i.e. inversely proportional to the statistical uncertainty of the determination of $D(d_j)$. Other choices could incorporate the noise sensitivity of the different particle size classes, the effects of changes in the signal-to-noise ratio, and the thresholding noise sensitivity.

Since there is a minimum number of fringe crossings required for signal processing (when velocity offset is not used), the actual width $w(d_i)$ of the measurement cross section which forms the sampling area is:

$$w(d_i) = \left[D(d_i)^2 - \left(N_{\min}(d_i)\delta \right)^2 \right]^{1/2} \tag{2.3.9}$$

where $N_{\min}$ is the minimum number of fringe crossings required for accepting signals.

The correctness of the above determination of the probe diameter-particle size relation hinges upon the validity of the following hypothesis:

a) The beams are Gaussian and circular.

b) The laser light intensity is constant throughout the measurement.

c) The signal processor is capable of perfect thresholding.

d) The particle trajectory is normal to the fringe pattern.

e) The extinction coefficient through the spray remains constant.

Figure 2.3..3 shows typical histograms for the different particle size classes and the resulting fit to the log distribution.

This method has the advantage of not requiring a priori knowledge of the optical parameters and instrument setup conditions corresponding to each particular measurement. Its main limitation is that the flow must be orthogonal to to the fringe pattern. In cases where the flow angle is unknown (and it might be different for the different particle size classes), the flow direction must be measured, i.e. a two or three component system is required depending on the application.

2.3.2 Fringe Count with Constant Slope

In the fringe count method presented in the previous section, the slope k_1 of the curve fit D^2 vs d theoretically equals half of the beam waist squared (compare equations 2.3.3 and 2.3.7). After analyzing many data sets and their curve fits, it is apparent that for most applications in which optical access and signal to noise ratios are good, the calculated slope falls very close to the actual beam waist relation.

In situations where the particle size distribution is very narrow, small experimental errors can propagate into large errors in the slope determination. However, if it is assumed that the slope is equal to half of the beam waist squared, the only unknown left is the minimum (or,

alternatively, the maximum) probe diameter, which can be determined very accurately.

In order to achieve this goal, the fringe count histograms for the different size class particles can be converted to an equivalent fringe count for the smallest particle size class through the relation:

$$D^2_{\min,equiv.} = b_0^2 \log(d / d_{\min}) + D^2 \tag{2.3.10}$$

When these equivalent distributions are added, a single histogram, similar to those obtained before for each particle size results. From this single distribution, $N_f(d_{\min})$ can be easily obtained, using the same algorithm used in the previous section.

2.3.3 Gate Time * Velocity with Variable Slope

This method is very similar to the fringe count method, with the Gate Time multiplied by the Velocity replacing the Fringe Count. The (Gate Time)(Velocity) value, however, is not discrete and has to be divided into distance bins. These distance bins can be preset by taking advantage of the knowledge of the approximate size of the probe volume, the number of validations and the size distribution, to maximize the accuracy of the method. The distances could be sorted for each diameter size and the percentage method could be used to determine diameter probe paths.

The main advantage of this method is that it would offer improved resolution for situations in which only a small number of fringes (say less than 10) is present in the probe volume.

This method is still trajectory dependent since the velocity value is needed to determine the path length traversed by the particles. However, in situations were the trajectory is unknown or is varying, accurate results can be obtained by employing two component or three component velocimetry in conjunction with this algorithm.

2.3.4 Gate Time * Velocity with Constant Slope

This method is similar to the Fringe Count with Constant Slope except that the product (Gate Time)(Velocity) replaces the fringe count. Again, a continuous distribution is obtained and has to be binned into a single distribution for the smallest size class. This method offers the advantages of less sensitivity to noise and improved resolution, as discussed above.

2.3.5 Intensity

All of the methods presented above have the disadvantage of being trajectory-dependent, In this section, a novel idea, involving measuring the maximum intensity of the light scattered by the particles as they traverse the probe volume, is presented.

Figure 2.3.4 shows a schematic of a particle traversing the cross-section of the probe volume. The maximum light intensity seen by the particle will depend on how far the particle trajectory is from the center of the probe volume and will be reached as the particle crosses the diametral line orthogonal to the particle trajectory.

When this occurs, the light intensity seen by the particle will be given by the relation,

$$I_s = I_o \exp\left(-2\frac{r^2}{b_o^2}\right) \tag{2.3.11}$$

The intensity of the light scattered by a particle traversing the probe volume is proportional to the incident light intensity and to the particle diameter squared. For a given particle size class, light intensity histograms can be obtained. These are obtained by discretizing (binning) the continuous intensity readings provided by the instrument (as in the gate time*velocity method). Since the probability of a particle crossing anywhere in the probe volume is the same, the probability of a particle scattering in an intensity range $[I - \Delta I/2, I + \Delta I/2]$ will be proportional to the

traverse diametral distance where this intensity range exists. This, in turn, is proportional to the inverse of the first derivative of the light intensity distribution and is be given by the relation,

$$f(r) = \frac{b_0^2}{4r\exp\left(-2r^2/b_0^2\right)}\Delta I \qquad (2.3.12)$$

This distribution is shown in Figure 2.3.5. Again, as for the fringe counting method, the distribution sharply peaks at the maximum scattered intensity before falling to zero. This makes it easy to identify the maximum scattered intensity for a given particle size class, corresponding to those particles crossing through the center of the probe volume. The distribution also peaks at the minimum detectable scattered intensity, corresponding to those particles traversing through the edge of the probe volume.

Once the maximum intensity has been determined for each particle size class, these maxima can be plotted against their respective particle diameters. Theoretically, these should follow the relation,

$$I_{s,\max} = kI_0 d^2 \qquad (2.3.12)$$

A simple linear curve fit is used to determine the value of kI_0, which, in turn, can be used to determine the maximum probe radius for each particle size from the Gaussian intensity relation and the peak on the distribution at the minimum detectable intensity. By setting a maximum allowable radius for the probe volume, the software can throw out any particles which pass outside the imposed limit. Once the probe volume size for each particle size is known, correction factors for each particle size class can be obtained, as with any of the methods previously mentioned.

One of the major advantages of the intensity method is that the measurement of the probe volume size is using the intensity distribution itself, so that any factors affecting the light arriving at the detector will be accounted for in the correction factors. Also, and most important, the

method is trajectory independent., i.e. and does not require knowledge of the trajectory angle or particle velocity vector.

2.3.6 Discussion.

As part of this study, Bachalo et al. (1988) conducted mass flux measurements of high number density sprays to test the validity of the fringe counting probe volume correction scheme. Comparison of his data to those obtained with sampling probes and beam light extinction techniques showed agreement within 10 and 20%, respectively. This shows that, when corrected for probe volume size effects, the phase Doppler method is a reliable instrument, capable of measuring the mass flux and number density in sprays with number densities characteristic of those found in gas turbine combustors and liquid-fueled rocket engine injectors.

More recently, Lazaro (1991) also performed measurements of sprays employing a PDPA monitoring the estimated value of the probe volume diameter vs. the particle size. He also concluded that the experimentally obtained fringe statistics corresponded almost exactly to those expected experimentally.

A table of some of the advantages and disadvantages of each method are listed below.

Method	Advantages	Disadvantages
Fringe Count with Variable Slope	Relatively quick.	- Requires a wide size distribution. - Trajectory dependent
Fringe Count with Constant Slope	Doesn't need wide size distribution.	- Trajectory dependent.

Velocity * Gate Time with Variable Slope	- Better resolution than fringe-count methods.	- Requires a wide size distribution. - Trajectory dependent.
Velocity x Gate Time with Constant Slope	- Doesn't need wide size distribution. - Better Resolution	- Trajectory dependent.
Intensities	- The probe diameter can be set to any size. - Trajectory independent. - Gate time independent.	- Relies on an accurate peak light intensity detection.

The fringe count and gate time methods are similar in concept, but the gate time method also can be applied to frequency domain processors, which have no fringe count.

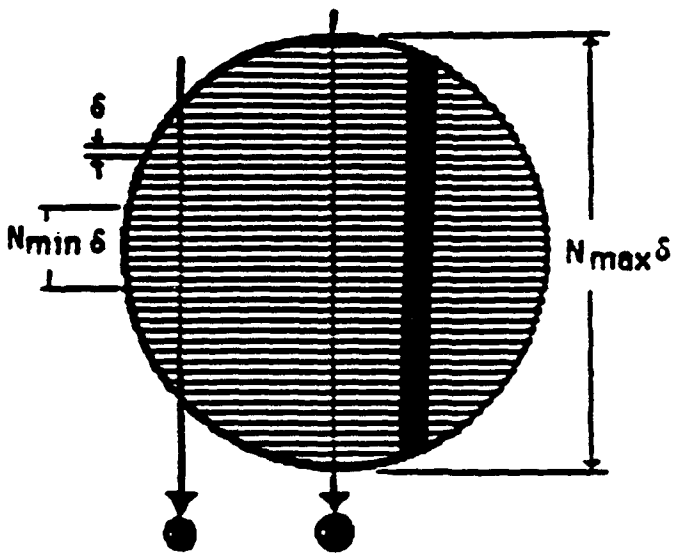

Figure 2.3.1: Schematic drawing of the cross-section of the probe volume. The plane of the cross section is orthogonal to the optical axis. The figure shows the region where a particle traveling orthogonal to the fringe pattern will produce a given number of fringe crossings.

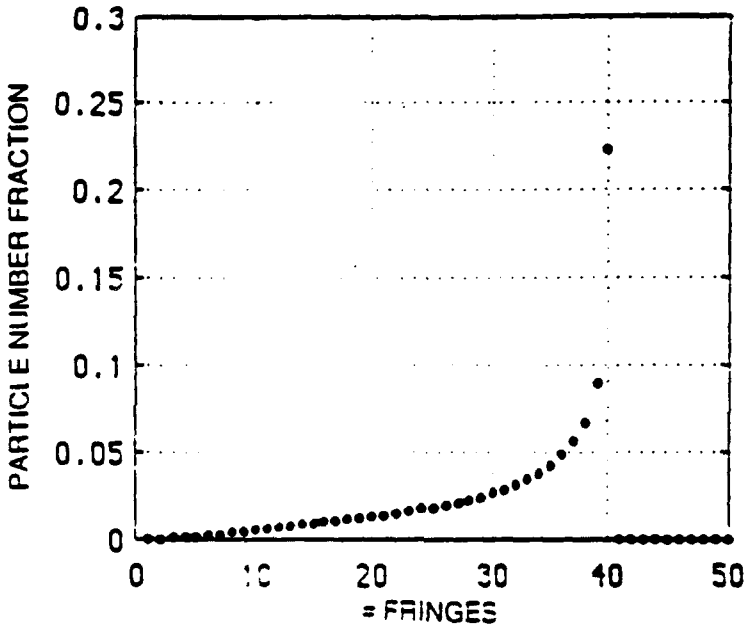

Figure 2.3.2: Theoretical particle fringe crossing histogram. The curve gives the fraction of particles that will cross a certain number of fringes when passing through the probe volume.

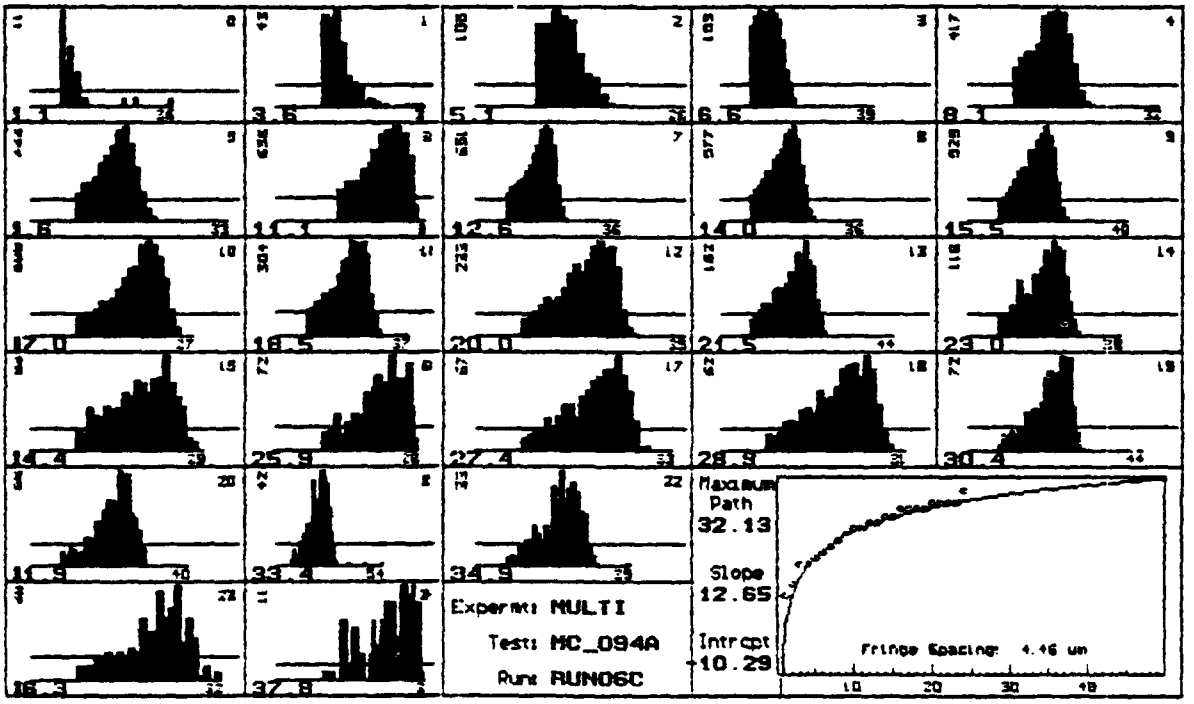

Figure 2.3.3: Typical fringe crossing histograms, and fit of the D_{exp} vs d to the expected theoretical curve.

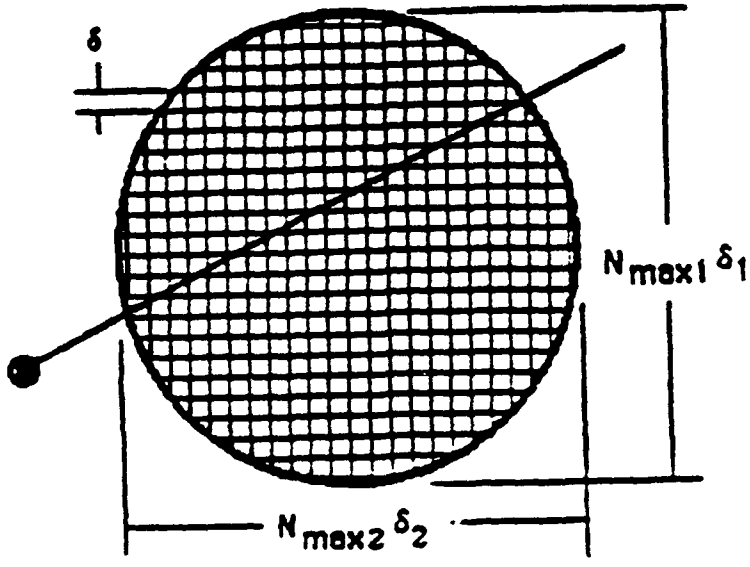

Figure 2.3.4: View of the Probe Volume, showing an arbitrary particle path.

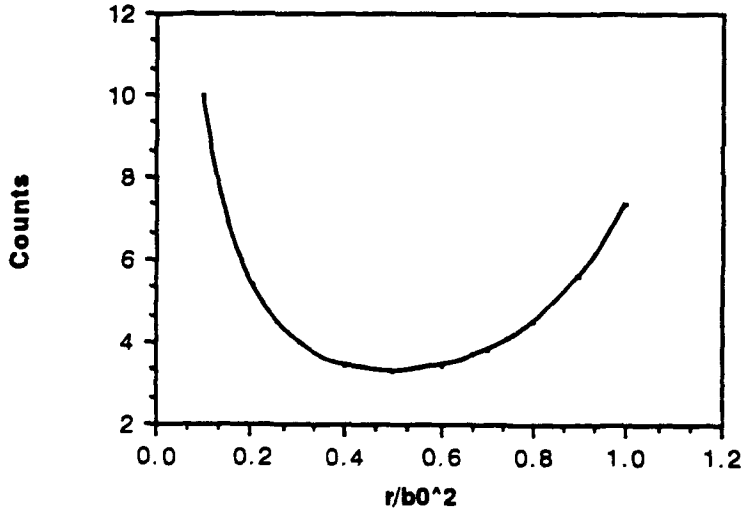

Figure 2.3.5: Theoretical maximum intensity histogram.

2.4 Signal Processing Considerations and Hardware Development

The critical component in the performance of the phase Doppler method is the signal conditioning and the signal processing means used. There are a number of possible schemes that may be used to measure the frequency and phase of the Doppler burst signals. The first approach used by Aerometrics was a dedicated counter type signals processor. Another approach used a transient recorder to record the signals and to perform either an autocorrelation analysis or Fourier transforms on the result to determine the frequency and phase. The more reliable concepts will be described along with the advantages and some of the limitations with the methods discussed.

A special consideration needed in the phase Doppler application is the very large signal amplitude dynamic range that needs to be covered. For example, a particle size range of 35 to 1 implies the the signal amplitude range must be approximately 1000 to 1. To extend the particle size range that can be measured at one instrument setting, the instrument must be capable of measuring signals with this amplitude range. That is, signals from 5 millivolts to 5 volts must be detected and measured. This is possible when the SNR is high but in dense sprays, combustion environments, etc. the SNR will deteriorate and so will the effective dynamic range of the instrument. The goal of this task of the program was to define, evaluate, and test methods that may serve to extend the dynamic range and the maximum Doppler frequencies that may be measured.

2.4.1 Counter Processor

The counter processor has been the standard method used for LDV signal processing for about two decades. The method has the advantage of being relatively easy to implement and is very accurate when the signal to noise ratio is sufficient (greater than about 5 dB). The counter processor, illustrated in figure 2.4.1 requires that the Doppler burst signal be high

pass filtered to remove the low frequency pedestal component and is low pass filtered to remove the high frequency noise. This requirement limits the frequency range that may be processed at one filter bandpass setting unless frequency shifting is used.

The phase shift is determined by timing the zero crossing of signal 1 to the zero crossing of signal 2, figure 2.4.2. The phase measurements using the counter method are somewhat more robust than the signal period measurements since extra zero crossings produced by noise are not as serious as in the period measurements. A three-level threshold and zero crossing detector is used in the instrument to detect and count each cycle in the Doppler burst. The first cycle in the Doppler burst passing the three-level detection logic starts a gate counter to time the duration of the burst signal. A high speed clock (400 MHz) is used to time the gate signal. The gate time is then divided by the number of cycles in the burst to determine the average signal period. This method has the advantage of processing the entire Doppler burst signal irrespective of the length. The measurements are independent of the previous signals, the processing is very fast, the instrument can handle a high dynamic range, and the measurements are very accurate as long as the signal to noise ratio is high.

The performance of the counter has been carefully analyzed using the classical treatments provided in the signal processing literature, Ibrahim et al, 1989. It was shown in that study how the counter processor will show a bias in the frequency estimate and the variance in the phase estimate will increase as the SNR deteriorates. For example at an SNR of 3 dB, the counter is predicted to show a frequency bias error of up to 10% and a a phase rms error of up to 3.5 degrees.

2.4.2 Optical Fourier Transform Processor

The need to increase the size range of the instrument requires the improvement of the detector and preamplifier dynamic range and the ability to process lower signal to noise ratios. Several methods were considered and evaluated, including the heterodyne concept to be

discussed in another section. It is well known the the Fourier transform method provides the optimum frequency and phase estimation, especially for low SNR signals. However, in the early part of this program, the suitable electronics necessary to implement the approach, including high speed analog to digital converters (ADC) and digital signal processors (DSP), were not available. Because of these limitations in the electronics technology, the possibility of using an optical Fourier transform was considered.

Optical spectrum analyzers were successfully used for radar signal processing, and the preliminary evaluation suggested that they may be suitable for laser Doppler and phase Doppler applications. This signal processing approach was attractive because of its simplicity, response speed, and the availability of the inexpensive optical components. The high frequency response of these devices, along with a relatively large bandwidth when using 40 and 80 MHz Bragg cells, made them an attractive candidate.

To better understand the approach and why it may be attractive, a simple description of the method will be provided. The schematic of the proposed optical spectrum analyzer for velocity measurements is shown in figure 2.4.3. A low power helium neon or solid state laser is used as the coherent monochromatic light source. The laser beam is collimated (after spatial filtering) and is directed into the Bragg cell (an acousto-optic device). The electronic input to the Bragg cell acoustic driver is the amplified burst signal from the photomultiplier. This signal drives the piezoelectric pressure transducer attached to the Bragg cell which, in turn, sets up a travelling acoustic wave within the Bragg cell crystal. The presence of the travelling acoustic wave within the crystal leads to optical index modulation across its optical aperture causing it to behave as a diffraction grating. The collimated laser beam, upon passing through the Bragg cell, undergoes diffraction and gives rise to several collimated beams (different order beams), each emerging from the Bragg cell at a different angle. For example, an input signal of frequency f would cause the first order diffracted beam to emerge at an angle θ to the incident beam. This angle is

related to the acousto-optic cell parameters and the signal frequency by the well-known Bragg law:

$$\theta = 2\sin^{-1}\left[\frac{\lambda f}{2nV_s}\right] \tag{2.4.1}$$

where λ is the wavelength of light in air, n is the refractive index of the Bragg cell crystal, and V_s is the acoustic wave speed. From this expression it can be observed that, to a first order approximation, the diffraction angle is proportional to the input signal frequency.

The diffracted light from the Bragg cell is then imaged onto a high speed linear CCD (Charge Coupled Device) sensor by means of a converging Fourier transform lens. It is well-known that at the back focal plane of such a lens, the 2-D light intensity distribution corresponds to the 2-D power spectrum of the electric field distribution at the object plane (the Bragg cell aperture, in this case). This result is true because the electric field in the Fourier transform plane can be expressed in terms of the electric field in the object plane as

$$E_f(x_f, y_f) = \frac{\exp\left[j\frac{k}{2f}\left(1-\frac{d_o}{f}\right)\left(x_f^2+y_f^2\right)\right]}{j\lambda f}\int_{-\infty}^{\infty}\int_{-\infty}^{\infty}E_o(x_o,y_o)\exp\left[-j\frac{2\pi}{\lambda f}\left(x_o x_f + y_o y_f\right)\right]dx_o dy_o \tag{2.4.2}$$

where E_o, and E_f are the electric field distribution in the object plane and transform plane, respectively, d_o is the distance of the lens from the object plane, f is the focal length of the lens and, x_o, x_f, y_o, and y_f, are the coordinates of the optical system. The term within the integrals is the Fourier transform of $E_o(x_o, y_o)$. The Fourier transform relation between the object and the focal plane amplitude distributions is not exact because of the appearance of a phase factor before the integral. However, if the intensity distribution is measured in the transform plane then the phase factor is no consequence and, furthermore, this intensity distribution corresponds to the power spectrum of the object. That is,

$$I_f(x_f, y_f) = \frac{1}{\lambda^2 f^2}\left|\int_{-\infty}^{\infty}\int_{-\infty}^{\infty} E_o(x_o, y_o)\exp\left[-j\frac{2\pi}{\lambda f}(x_o x_f + y_o y_f)\right]dx_o dy_o\right|^2 \qquad (2.4.3)$$

where $x_f/\lambda f$, $y_f/\lambda f$ are the frequencies of the Fourier components.

The method was tested and proved to be promising for frequency estimation over the frequency bandwidths of the Bragg cells. Unfortunately, although the method could handle high frequencies (centered around 40 or 80 MHz) the frequency bandwidth was not as wide as was desired or deemed necessary. A more serious limitation was that no possible means could be found to obtain the phase of the signals. The method could have been combined with the counter approach for phase measurement but it was concluded that this would not provide an advantage over the current method. For example, at 80 MHz signal frequencies, a time resolution of 1 nanosecond is necessary for 3 degrees of phase resolution. Unfortunately, this is pushing the limits of even a very high speed counter processor.

2.4.3 Discrete Fourier Transform Processor

Several strategies were considered in the initial evaluation of the signal processing requirements under this program to meet the stated goal of increasing the frequency and size range of the phase Doppler method even while operating in difficult environments. The first was to conduct extensive development on the detectors and preamplifiers. Research into both photomultiplier tubes (PMT's) and avalanche photodiodes was conducted. It was found that the PMT's did not have the frequency response as stated by the manufacturers. The PMT's tested showed a significant loss in the high frequency response which manifested as a loss in the signal visibility, and consequently, the SNR of the signals. Working with the PMT manufacturers, modifications were made to bring the performance up to handle signal frequencies to 100 MHz. Avalanche photodiodes (APD's) were also evaluated for their performance at high frequencies and over a large amplitude dynamic range. The quantum efficiency of these devices is much greater than that of the PMT's and the

frequency response is also better. The only disadvantage of the APD's is their small active area. This makes the design and alignment of the optical system more critical.

The PMT or APD current output is converted to a voltage and amplified with a preamplifier. It is essential to have a preamplifier that has a relatively flat gain response over the bandwidth of from about 400 kHz to 200 MHz and a dynamic range of approximately 10,000 to 1 in order to handle a size range of up to 50 to 1. A common approach to achieving wideband performance in a PMT preamplifier is to employ 50 ohm wideband amplifiers such as those commonly used in RF work. These amplifiers, while exhibiting a low noise level in a 50 ohm system, are not the best choices when used in conjunction with a high source impedance, such as, a PMT. It is, however, possible to decrease the noise level with the use of a transimpedance preamplifier. The noise advantage of the transimpedance amplifier was investigated in detail with the help of a mathematical analysis under this program as well as under a NASA Marshall Space Flight Center Phase I SBIR contract. Specifically, the various noise sources used in the analysis have been examined and the conditions for optimum noise performance have been considered.

Without going into detail on the preamplifier design, the current program and subsequent support led to the development of a transimpedance preamplifier with exceptional performance. The input device is an RF gallium arsenide (GaAs) FET, which is enclosed in a feedback loop. The circuit is dc-coupled to allow accurate measurement of the unipolar pedestal signal used for peak detection and additional particle size validation. The preamplifier has a transimpedance gain of approximately 1600 ohms, the bandwidth is dc to 150 MHz, +/-2 dB, and an output swing of 1.0 volt peak into 50 ohms.

Following the preamplifier and the high pass filter, the signal is further amplified with a logarithmic amplifier. The log amplifier with a gain of 75 and a clipping amplitude level of about 600 mv pp serves to compress the signal amplitude dynamic range before sampling.

Advances in the electronics over the past five years have made the possibility of developing a high speed signal processor based upon sampling the signals and processing them using the discrete Fourier transform (DFT) with the fast Fourier transform (FFT) algorithm.

After the analog conditioning, the signal is down mixed with a quadrature mixer to form both a real and imaginary signal component. This allows the extension of the frequency range by a factor of two compared to that when only using real sampling. The amplified signal is digitized by a high speed ADC and the digitized signal is stored in a first in, first out (FIFO) buffer. After some extensive research and evaluation, it was decided to sample the signal using a 1-bit ADC. This removes the dependence on the signal amplitude and turns the signal into a simple square wave. A description of the performance of 1-bit sampling will be given in a later section.

To ensure that the recorded samples are centered around the peak of the Doppler burst signal, a circular buffer is utilized. The signals are digitized continuously (whether a burst is detected or not) and stored in the buffer. When a Doppler burst signal is detected, the peak detection circuit is enabled. When the peak amplitude of the signal is detected, 50 % of the samples preceding the peak and 50 % after are transferred to the next FIFO before being processed. This method known as "pre-triggering" ensures that only the central part of the Doppler burst with the highest SNR is used in the estimation of the signal frequency and phase.

The DFT given as

$$f(n) = \frac{1}{N}\sum_{k=0}^{N-1} x(k)\left[\cos\frac{2\pi nk}{N} - i\sin\frac{2\pi nk}{N}\right] \qquad (2.4.4)$$

where n is the discrete frequency, N is the total number of samples, x(k) is the complex sampled data from the ADC's, and i is the imaginary number, is applied to the complex sampled data using the FFT algorithm.

The phase is computed using the complex amplitude coefficients at the signal frequency, f(s) determined from the DFT with interpolation:

$$f(s) = \frac{1}{N}\sum_{k=0}^{N-1} x(k)\left[\cos\frac{2\pi sk}{N} - j\sin\frac{2\pi sk}{N}\right] \qquad (2.4.5)$$

where s is the signal frequency and the x(k) are the discrete samples of the continuous signal. The x(k) are complex. The phase of the signal relative to the sampling frequency is simply

$$\phi(s) = \arctan\left(\frac{\sum_{k=0}^{N-1} x(k)\sin\frac{2\pi sk}{N}}{\sum_{k=0}^{N-1} x(k)\cos\frac{2\pi sk}{N}}\right) \qquad (2.4.6)$$

This process is carried out for each of the three signals used in the phase Doppler method. The phase differences ϕ_{12} and ϕ_{13} that are proportional to the particle size are then obtained as:

$$\phi_{12} = \phi_1 - \phi_2 \quad \text{and} \quad \phi_{13} = \phi_1 - \phi_3 \qquad (2.4.7\ \text{a,b})$$

where ϕ_i are the phase angles for each of the three detectors.

The work initiated under this program, namely, the investigation of other possible processing methods for the phase Doppler instrument to increase the frequency and size dynamic range lead to the subsequent development of the Aerometrics Doppler Signal Analyzer (DSA) as well as the transimpedance amplifier for phase Doppler applications. The development of this instrument was furthered by a NASA Marshall Space Flight Center SBIR Phase I contract to carry the method into the characterization of rocket injectors, a NASA Lewis Research Center contract for the development and delivery of such an instrument, and by Aerometrics internal funding. The performance of the phase Doppler instrument was improved from a limit of 10 MHz to 150 MHz maximum signal frequency. The earlier counter processor could only operate to a SNR as low as 5 dB whereas the DSA can operate down to a SNR of -10 dB. Thus, the size range was also extended from a factor of 35 to 1 up to a factor of 50 to 1.

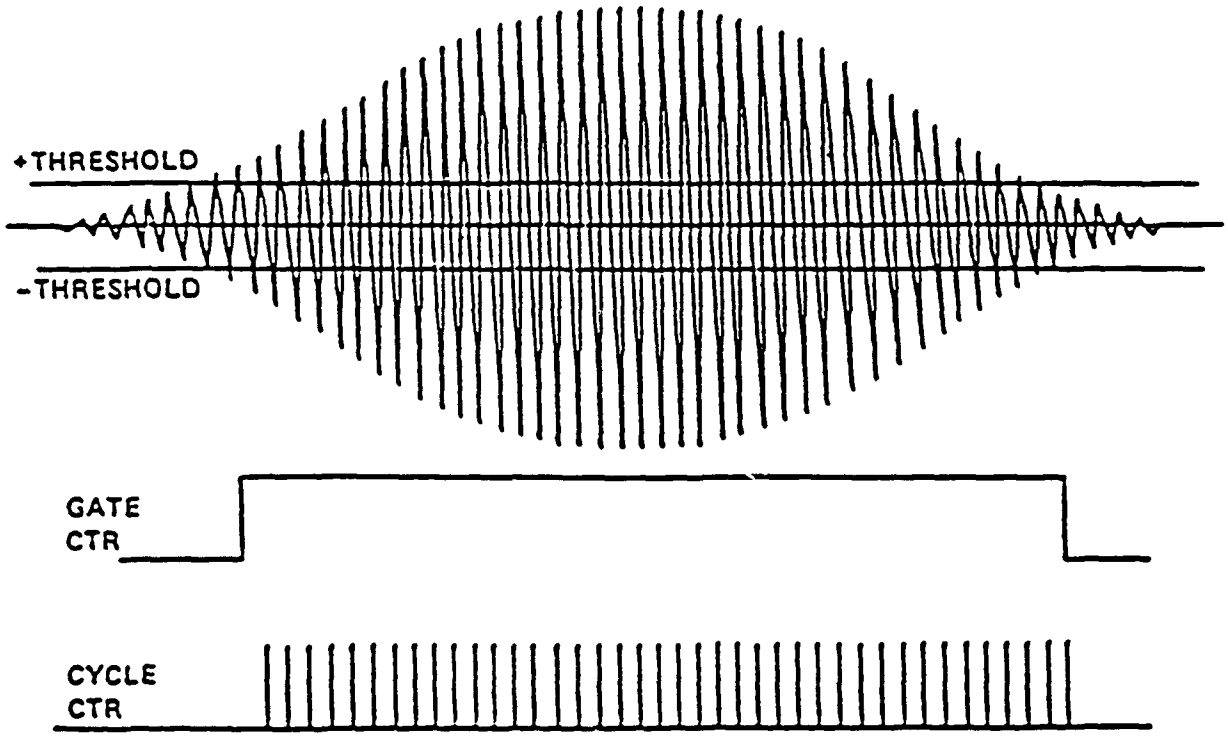

Figure 2.4.1: Schematic showing the counter processor for frequency estimation.

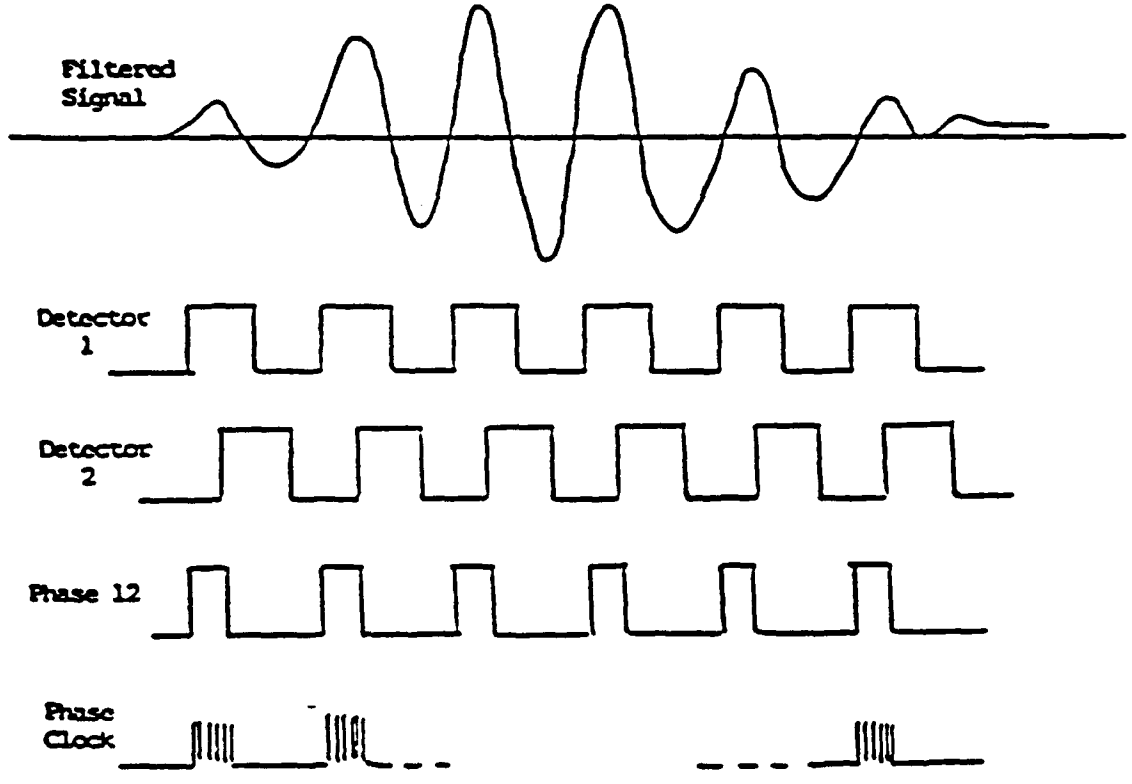

Figure 2.4.2: Method for phase measurement using the counter processor.

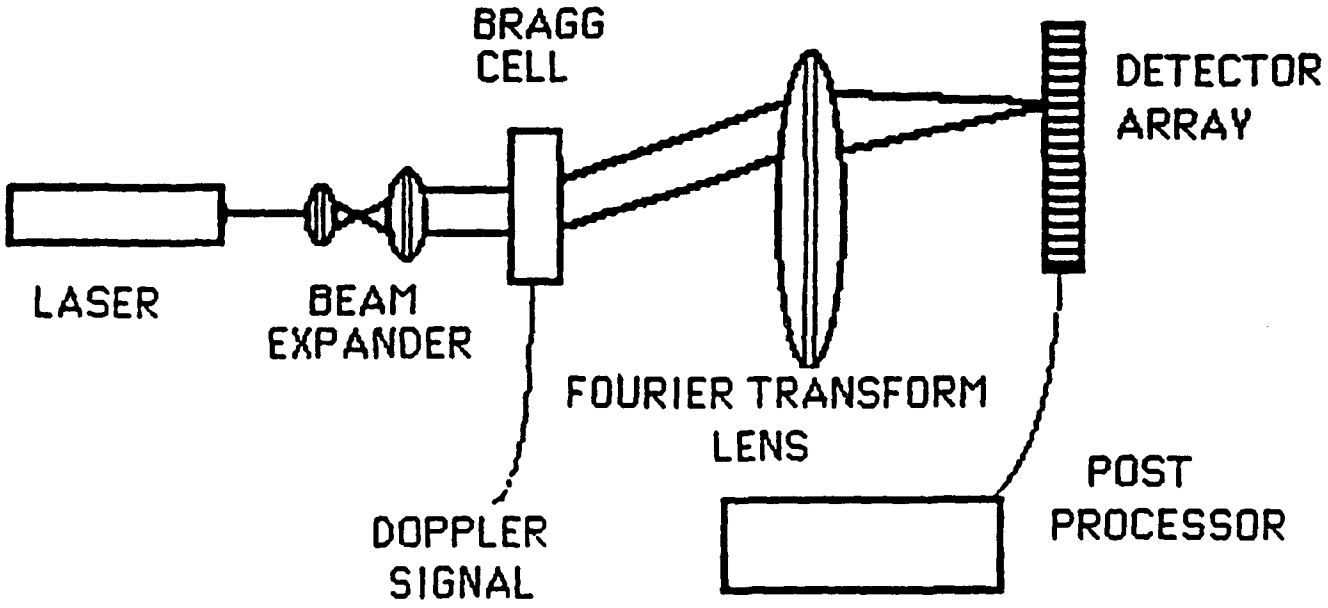

Figure 2.4.3: Schematic of the optical spectrum analyzer.

2.5 Particle Number Density Limitations On The Measurement Accuracy

The phase Doppler method is a single particle counter-type instrument which means that if more than a single particle passes the sampling volume at a time, a measurement error can occur or the samples may be rejected resulting in a loss in accuracy of the number density and volume flux determinations. In general, realistic applications of sprays are in environments wherein the number density is high, at least near the point of injection. In the past, single particle counters were considered to be unsuitable for relatively dense spray because of this limitation and because it was believed that direct forward scatter light detection was necessary, resulting in a relatively large sampling volume. With off-axis light scatter detection (Bachalo, 1980), the sampling volume was significantly reduced. However, a limit still exists on the performance of the instrument in high number density environments. This issue will be discussed in terms of the light scattering and interference response when more than one particle exists in the sampling volume and what the probability is of more than one particle residing in the sampling volume, given the sample volume size and number density.

Another limitation on the number densities in which the instrument will function properly is determined by the beam extinction. If the beams and the scattered light must pass through a long path with high particle number density, the signal will not reach the photodetectors with sufficient signal to noise ratio. The beam extinction is given by the well-known Beer's law expression as

$$I = I_0 \exp\left(-\frac{3\bar{Q}C_v L}{2D_{32}} \right) \tag{2.5.1}$$

where, $\bar{Q}$ is the scattering cross-section, C_v is a constant depending on the medium, L is the path length, and D_{mn} is a mean diameter, defined as,

$$D_{mn} = \left(\frac{\sum_N d_i^p}{\sum_N d_i^q} \right)^{\frac{1}{p-q}} \qquad (2.5.1a)$$

This problem isn't as restrictive as the problem of coincidence since in the worst case, the beam paths can be shielded, at least allowing semi-intrusive measurements. Under very dense conditions, the coherence of the beam will be degraded, resulting in a reduction of the signal to noise ratio (SNR). This condition of multiple scattering has been investigated by Felton, et al., 1984, for the application of the Fraunhofer diffraction method.

It is important to first define the conditions of a "dense spray", a "spray" or moderately dense spray, and a "dilute spray". This must be done in terms of a dimensionless parameter involving the mean drop diameter. In this case, D_{10} can be used since the number of particles is of interest. In a dense spray, the mean particle separation is assumed to be on the order of 10 mean diameters, e.g. $T/D_{10} = 10$. In a moderate spray, the mean drop separation is assumed to be on the order of 30 and in a dilute spray, 100 drop diameters or more. For example, a spray with $D_{10} = 20\ \mu m$, the number density would be 100,000/cc, giving an approximate mean drop spacing of 10 diameters. For a moderate density spray, the number density would be 10,000/cc, giving a mean drop spacing of about 25 diameters, and in the dilute spray of 1,000/cc, the mean drop spacing is 50.

Another important consideration that was analyzed was the response of the method and the instrument hardware to the occurrence of more than one particle in the sample volume at one time. The assumption has been made that two particles passing the sample volume would lead to two separate Doppler burst signals of different phase, frequency and amplitude. This assumption was undoubtedly based on the simple fringe model (or Rudd Model) of the LDV description. That is, it is assumed that a fringe pattern is produced at the intersection of the two beams. Particles passing through this volume scatter light in proportion to the spatially varying light of the fringe pattern. However, this simplified model is not

always accurate, and it appears that it will fail in the description of the multiple particle scattering.

The correct approach to use is to treat the light scattered from each beam by the particle as being independent of the other beam and then producing the interference in the plane of the receiver. When two particles pass the sample volume at one time, the light scattered from each beam by each particle must be described and used in the description of the interference fringe pattern. Even if the scattered light is only due to one scattering component, namely refraction, the interference fringe pattern still will not be a simple sinusoidal wave as for a single particle. Light scattered by particle 1 from beam 1 will mix and interfere with light scattered from beam 2 by particle 1, with beam 1 by particle 2 and with beam 2 by particle 2. The further complications to the interference will result from the relative sizes of the two particles and the the relative positions of the particles within the Gaussian intensity distribution of the sample volume. In addition, the relative motion of the two particles as they pass the sample volume will result in time-varying changes to the resulting interference patterns produced by the scattered light. The light scattering theory based on the detailed geometrical optics approach is continuing development to describe this complex phenomena. The geometrical optics approach developed under this program has been shown to be accurate when compared to the Lorenz-Mie theory and has the flexibility in handling these more complex situations, (Sankar and Bachalo, 1991).

The characteristics of the resultant interference fringe pattern and the corresponding signal characteristics are of importance since they determine whether or not such occurrences will produce not only errors in the number density and volume flux measurements but also in the size distributions. The previous assumption that the resultant signals would be a simple superposition of two Doppler burst signals may have led to misconceptions on the logic required to reject these occurrences. It is necessary to have both experimental and theoretical information on the resulting interference fringe pattern and the corresponding signals. Tests were conducted on a limited number of parametric conditions using the

Aerometrics monodispersed drop generator (MDG). The understanding and observation of the resulting signals have led to some innovations in the development of the signal processing approach.

The probe volume used in the PDPA technique, although small, introduces constraints in the number density of the suspended phase that can be characterized within known error bounds. The effective probe volume size can be characterized by the aperture of the slit in the receiving optics, the collection angle, the beam waist diameter, and the size of the particle being measured. When two particles are simultaneously present in the probe volume, the signal detected by the photomultipliers is a combination of the scattering patterns of both particles. In consequence, the phase difference between the signals captured by the three sizing detectors will differ from the expected values when only one particle is crossing the probe volume and, as a result, the compound burst is expected to be rejected by the signal processor, although this might not be the case. Further investigations are being conducted on the rejection criteria and there effectiveness on rejecting one, both, or neither of the particles.

The probability of finding two or more particles in the probe volume will then give the fraction of droplets that are going to be rejected. Since this probability depends on the size of the probe volume, different diameters will be affected in different ways by this effect, due to the dependence of probe volume size in particle diameter. Since larger particles have a larger effective probe volume size, it may be anticipated that particles of larger sizes will be rejected more often in high number density flows (this may not be true since the larger particles will have dominant signals). In consequence, not only the volume flux will be affected by the coincidence of several particles in the probe volume, but the number-size distribution will be biased as well.

When either photomultiplier gain or beam intensity is increased, two effects connected to the performance of the instrument in a high density environment occur. First, the effective probe volume diameter for each of the different particle sizes becomes larger, thus increasing the probability of multiple particle coincidences. In addition, a higher number of very

small particles produce signals above the threshold, resulting in an increase in the detected number density.

A review of the literature has revealed two detailed studies on the performance of the PDPA instrument when measuring high number density flows. Edwards and Marx (1991) explored the effects of particle statistics on the ability of a phase-Doppler system to make accurate measurements of complex particle flows. This was accomplished by analyzing the response of an ideal phase-Doppler system to a postulated particle flux. The ideal system they defined was postulated to be capable of sensing particles of all sizes and velocities with perfect accuracy, subject to one constraint: a measurement to be considered valid only when one particle crossed the probe volume at that time.

The analysis of Edwards and Marx showed that, as a consequence of the constraint of a single particle in the probe volume, the measured flux of particles is similar to the true flux, but reduced by passage of two sets of filters, whose characteristics are specified by spatial and temporal Poisson processes.

The first stage filter is formed by a spatial Poisson process. Since a particle can only be measured if it is the only one in the probe volume, then at the instant of entry of any particle into the probe volume there must be sufficient inter-particle separation that the previous particle has already left the probe volume. If the separation is not sufficient, the particle will be invalidated.

In a system containing multiple size classes, each denoted by the index i Edwards and Marx show that the probability that the composite probe volume is empty at the time a test particle first enters is,

$$P_e = \prod_i P_{ei} = \prod_i \left\{ 1 - \int_0^{\Delta V_i} p_{ei}\left(\tilde{V}_i\right) d\tilde{V}_i \right\} \tag{2.5.2}$$

where P_{ei} is the probability that the particle of size class i enters the probe volume when it is empty, $p_{ei}(V)$ is the probability that the inter-particle

volume , $\tilde{V}_t$, is greater than the probe volume ΔV_i for particles that belong to the class i.

Once the particle has passed through this spatial Poisson filter - that is, it has an empty probe volume at the time of its entrance - the particle must still pass through another Poisson filter before it can be validated. This filter corresponds to the particle being able to exit the probe volume before another particle enters the probe volume and therefore invalidates it. The probability that the test particle will be able to do this will depend both upon its residence time in the probe volume and upon the distribution of inter-particle arrival times at the probe volume. Edwards and Marx show that, for a system containing multiple size classes, the probability that the test particle is able to exit before some other particle enters the composite probe volume is,

$$P_t = \prod_i P_{ti} = \prod_i \left\{ 1 - \int_0^{\tau} p_{ti}(\hat{t}_i) d\hat{t}_i \right\} \tag{2.5.3}$$

where P_{ti} is the probability of passage of the test particle before another one enters for a single particle size class i, $p_{ti}(t)$ is the probability density distribution of inter-particle arrival times at the probe volume for class i, and t is residence time of the test particle in the probe volume.

Figure 2.5.1 illustrates the serial nature of these filters. The true flow of particles through the region of space considered to be the probe volume is first reduced by the spatial filter (where particles are rejected for insufficient spacing) and then by the temporal filter (where particles are rejected for excessive residence time). The flow of particles measured by the ideal phase-Doppler instrument then corresponds to the true flow of particles, but is reduced by the losses through the filters. Since the filters represent independent (and serial) processes, the probability of passage through the composite filter (spatial and temporal) is given by the product of the probabilities, $P_s P_t$. Edwards and Marx determined the distribution functions $p_{si}(V)$ and $p_{ti}(t)$, needed to complete the statistical description, by applying homogeneous Poisson statistics to the point particle flux, that is,

the probe volume was considered to be small in comparison to the length and time scales in the system. Also, the mean particle flux was considered to be constant.

In sum, the assumptions leading to a Poisson process are:

a) Independent inter-particle separation: The separation of the particles at one point is independent of the separation of the particles at other different points.

b) Local isotropy: Although in different areas of the flow the number density can vary, it is assumed that within the measuring volume there is isotropy in the inter-particle separation statistics.

c) In the infinitesimal volume dV, the probability of finding one particle is finite. The probability of finding two or more particles is a higher order in $dV$and can be neglected.

With these assumptions,

$$p_t(\bar{t}) = \lambda_t(\vec{x})\exp\left(-\lambda_t(\vec{x})\bar{t}\right) \tag{2.5.4}$$

$$p_t(\bar{V}) = \lambda_x(t)\exp\left(-\lambda_x(t)\bar{V}\right) \tag{2.5.5}$$

where $\lambda_x(t)$ and $\lambda_t(x)$ are the temporal and spatial process intensities. Edwards and Marx considered only the special case of λ_t and λ_x constant. Note that λ_x is the number density of the spray, ρ. On an ideal system, P_x and P_t reduce to.

$$P_x = \exp\left(-\bar{\rho}\,\Delta V_x\right) = \exp\left(-\lambda_t''\overline{\Delta V_x}/\overline{S_x}\right) \tag{2.5.6}$$

$$P_t = \exp\left(-\lambda_t''\overline{A_{pt}}\,\tau\right) = \exp\left(-\lambda_t\tau\right) \tag{2.5.7}$$

These filters perform essentially the same function. Whenever a particle enters the probe volume while a particle is already present in it, both particles have to be discarded by this ideal processor. Suppose a particle has entered the probe volume, while no other particles were in it. Then it passes filter I. Suppose further that, while the first particle is in the probe volume, a second particle enters the probe volume. At this point, the first particle (already in the probe volume) will be discarded by virtue of the second filter. By the same token, the second particle entering the probe volume is thrown out by virtue of the first filter. Since two particles have to be discarded by a single event, two filters have to be considered.

Lazaro (1991) performed a similar analysis and concluded that the critical parameter that characterizes the accuracy of the measurement of particles of diameter d for high number density flows is,

$$\eta = N_{dt}\frac{D(d^*)D(d)t}{\sin\theta} \tag{2.5.8}$$

where d^* is the size where the distribution peaks, N_{dt} is the total number density of all particles in the spray that can trigger the burst detector, t is the effective slit apperture, D is the probe volume size, and θ is the collection angle. Based on experimental evidence, he concludes that $\eta < 0.1$ is probably a good criterion to ensure error free operation.

Besides the problem of coincidence of two or more particles in the probe volume, beam extinction plays a major role in hindering the ability of the PDPA when measuring high density spays, since the range of light extinction levels to which the laser beams are subjected before reaching the probe volume vary widely. For example, in the periphery of the spray, the attenuation is minimal, and the probe volume features a very uniform illumination. On the other hand, in the core of the spray the beams have to propagate over regions where substantial attenuation and scattering take place: the portions of the spray located between the transmitter and the probe volume produces random intensity fluctuations of both laser beams crossing at the measurement point. These fluctuations are characterized by

an rms level that increases with the attenuation. The fluctuations of the beam intensities at the probe volume are generally uncorrelated.

As a result of these fluctuations, the spectral distribution of these fluctuations in time is very wide, and substantial laser power variations can occur even during an individual burst time. In addition, lower frequency fluctuations associated with the spray's turbulent structure result in variations of laser power for different droplet bursts. Furthermore, the presence of spray between the probe volume and the receiving optics can produce further modifications in the collection of the burst generated at the measurement point.

If the oscillations in light intensity at the probe volume are high enough, it becomes likely that the burst corresponding to a single particle is triggered more than once. Since the highest particle residence time occurs when they have a diametrical trajectory, these trajectories will be the ones that exhibit the maximum probability of being split. This has a double effect towards the measurement results: a) a fraction of the particles is counted twice, and b) the effective probe volume diameter is underestimated, since the fringe statistics tend to shift towards lower number of crossings. Both effects produce an overestimation of the volume flux. In addition, since burst splitting occurs preferentially for larger-sized particles (given their larger effective probe volume size), not only the volume flux, but also the mean diameters of the distribution become affected.

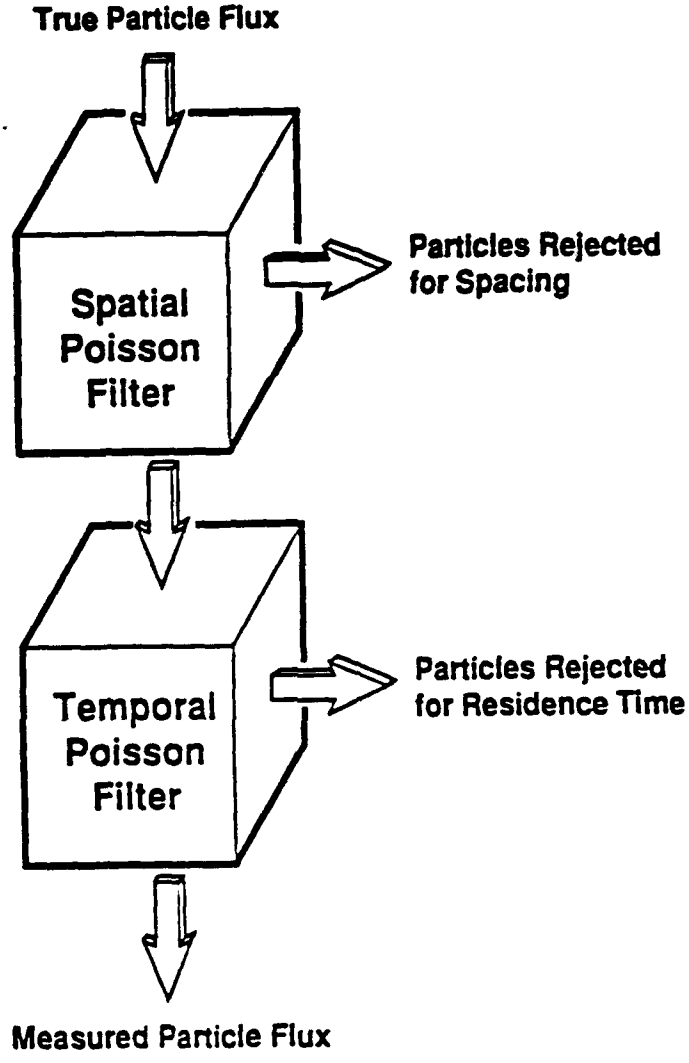

Figure 2.5.1: Illustration of the serial nature of the Poisson filters. The particle flux measured by the ideal phase-Doppler system corresponds to the true particle flux, but reduced by losses throught the two filters.

2.6 Performance In Measuring Quasi-Spherical Particles and Inhomogeneous Particles

2.6.0 Introduction

Initial tests relating to this topic utilized a a monodispersed drop generator to form spheroidal drops. This work was done in conjunction with Dr. D. Alexander's group at the University of Nebraska, Lincoln. In that study, the drops exiting a monodispersed drop generator were found to be oscillating, passing from oblate to prolate spheroids. Under carefully selected conditions, the phase of the oscillations in the drops would remain stationary. The drops were imaged with the high quality imaging system developed at UNL at the same location that they were measured with the PDPA. Based upon the operating conditions of the monodispersed drop generator, the diameter of the spherical drop was known. The results of the comparisons to the imaging system showed that the error in sizing the drop increased with aspect ratio of the drops. For example at an aspect ratio of 1.1, the error was 10%, and at an aspect ratio of 1.3, the error was 15%.

Because of the difficulty in forming drops with a stable and known spheroidal shape, bubbles in water were considered as an alternative. This work was also of interest to other agencies where research in bubble formation and cavitation occurs. Bubbles have some different scattering characteristics than drops but are the same as drops of opaque and inhomogeneous materials such as slurries and coal water mixtures. These fluid are most often difficult to atomize and form quasi-spherical particles. Bubbles have the added advantage of being relatively easy to form at nearly a monosize and with predictable deformation.

2.6.1 The Light Scattering of Bubbles

Mie's solution to the problem of scattering efficiency and pattern of a dielectric sphere is given as a function of the ratio $m = n_i / n_o$, where n_i and n_o are the refractive indices of the inner and outer media, respectively, and is usually expressed in terms of the scattering parameter $x = 2\pi r / \lambda_0$ where r is the sphere radius and λ_0 is the wavelength in the outer dielectric. In the case where the refractive index of the sphere exceeds that of the surroundings, forward scattering, the rainbow, and the glory are the regions in which light scattering is important, van de Hulst (1957). In the case where the refractive index of the sphere is less than that of the surroundings, for example in air bubbles, refraction in the rainbow region is not present, however, a new region, which is known as the critical scattering region appears, Marston (1979), Marston et al (1981). Scattering is important in this region due to an abrupt change in the amplitude of the reflected wave as the local angle of incidence, β, of the ray changes from $\beta < \beta_c$ for small impact parameters to $\beta > \beta_c$ for large ones. Here $\beta_c = \arcsin(m^{-1})$ is the critical angle for a plane surface and $\psi_c = \pi - 2\beta_c = 82.82°$ is the critical scattering angle for an air bubble in water. Marston (1981), has proposed a model for the light scattering of bubbles which adopts the geometrical optics approximation. Marston's important investigation suggests that the reflective component might be the dominant light scattering mode at some scattering angles for air bubbles (a more complete discussion of Marston's investigation has been provided by Breña de la Rosa et al. 1989). This last point is paramount from the standpoint of bubble sizing using the phase Doppler approach, the diagnostic technique used in the present investigation, since Bachalo and Houser (1984) showed that the scattered light is phase-shifted by an amount directly proportional to the diameter of the spherical scatterer and that if any one of the scattering components, namely reflection or refraction, is dominant then the phase relationship is exact.

2.6.2 The Lorenz-Mie Theory versus the Geometrical Optics Theory

Two independent light scattering models of the phase Doppler technique have been developed and implemented at Aerometrics using the Lorenz-Mie theory and the geometrical optics theory, each having their individual advantages and disadvantages. The Mie theory is exact, and it completely describes the scattering of plane electromagnetic waves by spherical particles. It is based on the solution of the complete electromagnetic wave equations along with the appropriate boundary conditions (van de Hulst, 1957, and Born and Wolf, 1975). On the other hand, geometrical optics (or ray optics) is approximate and its solutions asymptotically approach those of the Mie solutions for particles very much larger than the incident light wavelength. van de Hulst has shown that for $\pi d / \lambda >> 1$ it is possible to approximate the Mie scattering by the interference of diffracted, refracted, and reflected rays which is the fundamental basis for the geometrical optics approach.

The geometrical optics approach, though approximate, provides much greater physical insight into the complex problem of light scattering than does the Mie theory, where one tends to get lost within the mathematics. Furthermore, the computational efficiency of the geometrical optics method is far superior to that of the Mie theory which is based on series solutions where the number of terms required for convergence is directly proportional to the size of the particle. This implies that the computational time increases with particle size. On the other hand, the computational time of the geometrical optics theory is independent of the particle size. The higher computational speed of the geometrical optics theory, therefore, makes it economically viable to compute the amplitude and phase of the scattered light over a fine grid on the receiver aperture, especially for large sized particles.

In several practical applications of the phase Doppler technique, the laser beam diameters at the probe volume are required to be of the order of the particle diameter itself. In such situations, the non-uniform (Gaussian) illumination of the laser beam cannot be ignored. The geometrical optics

approach possesses a significant advantage over the Mie theory in handling such cases. The non-uniform illumination, on the other hand, violates a fundamental assumption of the Mie theory and, therefore, the theory needs modification. Recently, such modifications to the Mie theory have been made by some researchers (Gouesbet et al., 1988).

The geometrical optics theory, in spite of all its advantages over the Mie theory, does have certain disadvantages. It, for instance, is not valid for the analysis of light scattering by small particles, and the predictions of the theory, when used for such purposes, is open to question. Furthermore, the geometrical optics theory solutions fail near the regions of the rainbow and the glory angles and, therefore, are generally not very suitable for backscatter angles. After careful consideration of the advantages and disadvantages of the two approaches, analytical models of the phase Doppler technique were developed based on both approaches. Of these two, the Mie theory based model was generally used for small sized particles (<20 μm), and the one based on the geometrical optics approach was used for larger particles. The models basically differ only in the way the scattering amplitudes functions $S_1(m,\theta,d)$ and $S_2(m,\theta,d)$ are computed for each of the incident beams.

In order to demonstrate, theoretically, the creation of spatial fringe patterns by the interference of scattered light, the developed models were used to map out the light intensity distribution as seen by the receiver lens (the interested reader is referred to Bachalo and Sankar (1988) for a detailed analysis and discussion on this topic).

Figure 2.6.1 shows a computer generated spatial fringe pattern that is formed on the receiving lens due to the scattering of light by a 40 μm water droplet. The assumption of pure refraction (p=1 only) has been made in the calculations. The circle in Figure 2.6.1 delineates the receiving lens. This lens collects the scattered light, and a system of optics image the collected light from three different areas of the lens onto three separate photodetectors. The parallel vertical lines in Figure 2.6.1 show the three areas of the receiving lens. Figure 2.6.2 is a schematic of the receiving apertures showing the three areas from which light is collected. Apart

from the presence of distinct fringes in the x'-direction, see Figure 2.6.2, a gradual intensity variation in the z'-direction can also be seen in this figure. These secondary fringes are responsible for causing oscillations in the calibration curves, and their presence can be physically understood as due to the interference of one scattering order with another, for example, refraction with reflection. Also observed in the figures is a certain randomness in the intensity distributions which also contributes to oscillations. These undesirable contributions can be treated as "noise", and the receiving lens performs a reasonable job of integrating them out and yielding linear calibration curves for certain optical configurations.

The wavelength of the spatial intensity variation in the x'-direction is directly and linearly related to the size of the particle. Furthermore, it is this wavelength that we are attempting to measure indirectly by determining the phase differences between the outputs of the different detectors.

The simultaneous presence of external reflection, refraction, and second internal reflection at 30° results in a degradation of the fringe pattern. This effect can be seen in Figure 2.6.3, which is a computed fringe pattern assuming interference by reflection, refraction and second internal reflection. It is clear from this figure that the presence of the additional scattering components, namely reflection and second internal reflection, has led to a modulation of the intensity in the z' direction. Note, however, that the intensity variation in the x' direction remains distinct and therefore still carries particle size information which can be easily retrieved.

Results similar to those discussed above were obtained for various scattering angles between 20° and 80°. For all angles that were investigated in this forward scatter region, it was possible to obtain useful linear calibration curves by integrating the fringe pattern over the lens surface.

Backscatter angles ($\approx$ 150°) provide another region of significant practical applications. For water droplets, however, this region corresponds to the

main rainbow region where external reflection and two components of first internal reflection are present. Our experimental investigations at the backscatter (150°) angles have resulted in good agreement with the forward scatter (30°) data.

Calibration curves were initially generated using just three points on the receiver lens for two different cases, namely, first internal reflection (p=2) only and combined external and internal reflections (p=0 and p=2). The interference of external reflection with the first internal reflection gives rise to high frequency oscillations with phase varying from 0° to 360°.

The effect of performing spatial and temporal integrations is shown in Figure 2.6.4 An integration mesh of size 100x20 was used for these spatial integrations, and 5 time steps were used to perform the time averaging. It is very interesting to note that the process of integration has indeed been able to damp out the high frequency oscillations, especially for the larger particles, leaving behind only small oscillations in the region of small particles (<10 μm in diameter). Comparing the integrated calibration curves with the linear regression fits presented in Figure 2.6.4, it is clear that light scattering collection at 150° is certainly adequate for sizing water droplets using the phase Doppler method.

The small oscillations seen in the calibration curves for the smaller sized particles could be due to the fact that the mesh size used for performing the spatial integrations was not sufficiently fine. A more probable cause is that the geometrical optics is not a good approximation of the Mie theory for very small particles, especially near the rainbow region. It remains to be seen whether integration of the Mie scattering solutions over the receiver surface can remove these oscillations.

2.6.3 Mathematical Analysis of the Light Scattering of Bubbles

The analysis begins by selecting the coordinate system, shown in Figure 2.6.6, for the theoretical model. Two incident laser beams *beam1* and *beam2* lying in the x-y plane intersect at an angle γ to form a probe volume. Spheroidal air bubbles moving through the probe volume in the x-direction scatter the incident light beams, and the scattered light interferes to form spatial fringe patterns (as discussed earlier). The receiving lens of the phase Doppler instrument is placed at a distance R from the probe volume at an angle Θ from the x-y plane and at an angle Φ from the y-z plane. The coordinate system (x',y',z') which describes the receiving lens is such that it can be obtained by performing two coordinate transformations on the (x,y,z) system. First, the x-y plane is rotated about the z-axis by an angle Φ to yield the (x'',y'',z'') coordinate system. Next, the y''-z'' plane is rotated about the x''-axis by an angle Θ to yield the (x',y',z') coordinate system, Figure 2.6.6. As mentioned earlier, the receiving aperture is divided into three areas and the total light collected by each of these areas is imaged onto three separate photodetectors located within the receiving assembly of the PDPA.

In order to generate calibration curves that relate the phase differences between the detector outputs, namely, θ_{12} and θ_{13}, to the diameter of the bubble, it is necessary to perform spatial integration of the scattered light over the different collection areas of the three detectors. The first step towards this is to compute the scattering amplitude functions $S_{mn}(\theta_n)$ at several points on a fine rectangular mesh placed on the receiving lens. The first subscript m stands for the direction of electric field polarization where, m=1 implies perpendicular polarization and m=2 implies parallel polarization. The second subscript n identifies the two incident laser beams and, therefore, can either be 1 or 2. The amplitude function $S_{mn}(\theta_n)$ is complex and is related to the complex electric field, E_{mn} by (assuming that the amplitude of the incident electric field is 1 and that it is linearly polarized)

$$E_{1n} = \frac{i}{k_n r}\exp(-ik_n r + i\omega_n t)\cos(\phi_n)S_{1n}[\theta_n] \tag{2.6.1}$$

and

$$E_{2n} = \frac{i}{k_n r}\exp(-ik_n r + i\omega_n t)\sin(\phi_n)S_{2n}[\theta_n] \tag{2.6.2}$$

In Eqs.(1) and (2), k_n and ω_n are the wave number and frequency, respectively, of the scattered light of the n_{th} incident beam, and r is the distance of the point (x',z') from the probe volume. Furthermore, the scattering angles θ_n and ϕ_n are defined in Figure 2.6.6. For each point (x',z') on the receiving aperture, it is possible to calculate θ_1, θ_2, ϕ_1, and ϕ_2, the scattering angles for *beam1* and *beam2*. As mentioned earlier, at each of these points on the receiver surface, the scattered light interferes to yield a light intensity which varies temporally at the Doppler difference frequency, $\omega_D = \omega_1 - \omega_2$.

The mathematical expressions for the scattered light intensity are subsequently derived and integrated over the collection areas of each of the three photodetectors, from which the phase difference between the photodetectors can be determined. By performing these calculations for a range of bubble sizes, calibration curves (i.e., phase difference versus bubble diameter curves) can be generated for any assumed optical configuration.

2.6.4 Computing the Scattering Amplitude Functions Using the Geometrical Optics Theory

The fundamental assumption of the geometrical optics approach is that the light scattered by large spheres can be adequately described by considering the scattered light to consist of diffracted, refracted, and reflected light rays. In the analysis of light scattering by spheroidal bubbles, contributions from scattering components up to and inclusive of the second internal reflection will be accounted for. Figure 2.6.7 shows the

ray trace for a spherical air bubble in water. Diffraction effects were neglected in the analysis, and this was found to be a reasonable approximation for angles greater than about 20°. This approach, though valid for any refractive index, is discussed here from the point of view of sizing air bubbles in water (m = 0.75). The light rays incident upon the bubble emerge from it at different angles depending, in turn, upon the incident region and angle. In the case of a spherical bubble, the symmetry simplifies the analysis and the classification of scattering regions. In the case of spheroidal bubbles, the analysis is much more complicated, since the bubble can be oriented in many directions in its trajectory through the probe volume. However, as a first approximation, the spheroid will be considered with one of its main axes oriented parallel to the reference coordinate system.

Figure 2.6.8 shows schematically, for a spherical air bubble in water, the broad classification of the various scattering angles into two regions depending upon the type and number of scattering components present. The notation of van de Hulst has been adopted in representing the different scattering orders by p. It is important to realize that the multiple components of the same order of scattering p arise due to contributions from light incident on different regions of the bubble.

For such a system, the scattering amplitude function $S_{mn}(\theta_n)$ is the sum of all possible individual contributions $s_{mnp}(\theta_n)$. That is,

$$S_{mn}(\theta_n) = \sum_{p=0}^{3} s_{mnp} \qquad (2.6.3)$$

where the subscripts m and n, as before, stand for the polarization and incident beam number, whereas, p stands for the type of scattering component. The derivation then follows with the determination of the Fresnel coefficients for perpendicular and parallel polarization and, finally, the determination of the phase shift due to optical path length which carries the bubble size information.

The measurement of bubble diameter using the phase Doppler technique consists of determining the local radius of curvature of the object which traverses the control volume. The intensity of light scattered by a particle depends upon the angular deflection of the collimated light incident upon the sphere which, in turn, depends upon the diameter of the sphere. In light scattering interferometry, sizing of the particles can be obtained by measuring the relative phase shifts in the incident plane waves. The angular deflection of the scattered light in any plane depends upon the radius of curvature of the particle in that plane, Figure 2.6.9. In the case of the phase Doppler method, the radius of curvature is measured in the plane of the intersecting beams.

2.6.5 Computer Simulations of the Light Scattering of Spheroidal Bubbles

The overall theoretical approach adopted for the spheroidal bubble case is similar to the one described in the previous section for studying spherical bubbles. However, unlike the latter, the determination of a mathematical equation to describe the relationship between the light incident angles and the scattering angles turns out to be quite complex for spheroidal bubbles. Furthermore, the mathematical complexity increases significantly with higher values of p, i.e., with reflection, refraction, etc. The reason for this complexity can, of course, be traced to the fact that while analyzing light scattering by spheroidal bubbles, different points on the receiver aperture give rise to different scattering cross-sections. Specifically, these scattering cross-sections (formed by the intersection of the scattering plane and the bubble) are ellipses with varying size, asphericity, and orientation. In stark contrast, scattering by spherical bubbles always gives rise to circular cross-sections with their radii being the same as that of the spherical bubble.

In order to simplify the development of the theoretical model, only reflected light has been accounted for in the present analysis. This simplification is justified based upon the results of the spherical bubble model which showed that only the reflection component is dominant in the

forward scatter angles. Furthermore, the model showed that the predicted response of the phase Doppler instrument was insensitive to whether all the light scattering modes were accounted for or only the reflection component was used.

In the theoretical model developed, as in the case of the spherical bubble model, the resulting phase and amplitude of the intensity oscillations are calculated at several points on the receiving aperture. The computed light intensities are then integrated over the collection areas of each of the three separate detectors to yield the phase difference between them. For each point on the receiver and for each of the two incident laser beams, the model first determines the corresponding light scattering plane which is dependent upon the direction of the incident laser beam, the receiver location, and the location of the point-of-interest on the receiver. The model then computes the size and orientation of the resulting scattering cross-section which, in turn, is determined by the intersection of the light scattering plane and the spheroidal bubble. Typically, an elliptic equation for the scattering cross-section is sought in the following form,

$$\alpha\xi^2 + 2\gamma\xi\eta + \beta\eta^2 = 1 \tag{2.6.4}$$

where α, β, and γ are dependent upon the direction of the incident laser beam and the scattering angle, and ξ and η are coordinate directions. Having determined α, β, and γ, the relationship between the scattering angle θ_s and the incident angle θ_i can be expressed as,

$$\theta_i = \arctan\left[\frac{\alpha + \gamma\tan(\theta_s/2)}{\beta\tan(\theta_s/2) + \gamma}\right] \tag{2.6.5}$$

Furthermore, the phase difference δ, as a result of the phase shift between the reflected beam and a hypothetical reference beam passing through the center of the bubble, can be expressed as,

$$\delta = C^*\left\{1 + \sec\theta_i \cos\left[\pi - 2\arctan\left(\frac{\alpha - \gamma\tan\theta_i}{\beta\tan\theta_i - \gamma}\right) - \theta_i\right]\right\} \tag{2.6.6}$$

where C^* is given by

$$C^* = \frac{2\pi m}{\gamma\sqrt{\alpha - 2\gamma \tan\theta_i + \beta \tan^2\theta_i}} \qquad (2.6.7)$$

The remaining procedure for determining the response of the phase Doppler instrument is identical to that of the spherical bubble case, explained in the earlier section.

2.6.6 Special Cases Considered in the Modelling of Spheroidal Bubbles

For the simulation of the light scattering of spheroidal bubbles, two shapes of particles were considered: firstly, an oblate spheroidal bubble with the shape similar to that of a pill and, secondly, a prolate spheroidal bubble with the shape of a football. The circular cross section of these two bubbles is considered in the vertical plane, i.e., in the plane of the two green laser beams.

Figures 2.6.10 and 2.6.11 show a plot of the phase response ϕ_{13} of photodetectors 1 and 3 for both receivers as a function of the diameter of the circular cross section A and of the parameter η (η=0.6 and η=1.4), which represents the aspect ratio of the two axes of the spheroid. By keeping η constant, the second axis $B = \eta \times A$ was determined, and, using the geometrical optics approximation, the light scattering of the resulting spheroidal bubble was obtained. In this case, the circular dimension of the bubble was considered in a plane of the green laser beams.

The orientation of the spheroid inside the probe volume was also kept constant since in the experimental phase of the program the bubbles maintained a fixed orientation as observed from the photographs. Figures 2.6.10 and 2.6.11 show that this response is linear for bubbles up to 1000 μm in diameter. Larger sizes of spheroids up to 3500 μm were also studied

but are not plotted because when the phase ϕ_{13} of the photodetectors reaches 360°, it shifts back to a phase of 0°, showing a discontinuity in the figure. This is, obviously, only an aesthetic issue in the plots, as the response of the photodetectors was found to be linear over the range from 0.5 - 3500 μm in diameter.

Figures 2.6.12 and 2.6.13 are similar to the plots obtained in Figures 2.6.10 and 2.6.11, except that the circular dimension was considered in a plane perpendicular to the green laser beams. The eccentricity of the spheroid was also studied for η=0.6 and η=1.2. The results show that the response of the photodetectors is linear and that the sizing of spheroids is possible under the conditions considered here.

Figures 2.6.14 and 2.6.15 depict the phase response of pairs of photodetectors ϕ_{12} and ϕ_{13} for five conditions of eccentricity η and for the circular dimension in the plane of the green laser beams. This is the orientation of the bubbles which was found during the experimental phase of the program. Figures 2.6.16 and 2.6.17 show similar curves for those spheroids having their circular dimension in a plane perpendicular to the plane of the green beams.

2.6.7 Conclusions from the Computer Simulations

From the previous numerical modelling of the light scattering of spheroidal bubbles, the following conclusions can be drawn:

- It is feasible to measure spheroidal bubbles or drops using light scattering interferometry. The phase response of the photodetectors yielded a linear behaviour up to diameters of 3500 μm.

- To keep the simulations to tractable proportions, the spheroids were restricted to travel fixed orientations within the probe volume defined by the intersection of the two laser beams. This restriction was appropriate for the experimental setup for all but the largest spheroids ≈ 3500 μm,

since the bubbles were not observed to rotate or oscillate but, rather, kept a fixed orientation through most of their trajectory.

- Oblate and prolate spheroidal bubbles were considered in the study, ranging from very flat discs (which in the limit collapsed into a circle) to elongated prolates (which in the limit attained the shape of a cylinder). Within the large range of sizes considered, the eccentricity of the spheroid was kept constant.

- From the numerical simulations, it seems possible to configure, experimentally, a multiangle detection system to measure the curvature of spheroids or other shapes of bubbles and drops. The detection system can be set up to measure two or three dimensions of the bubbles.

2.6.8 Experimental Setup

In its standard configuration, the PDPA is composed of a transmitter unit and a receiver unit. However, to measure the dimensions of two orthogonal axes of a spheroidal bubble, a multiangular detection system was set up where two receiver units were located in two different detection planes, see Figure 2.6.18. The collection angle for both receivers was set at 60° in the forward scatter direction (Figure 2.6.19) which, as determined from analytical modelling of the light scattering of bubbles using the Lorenz-Mie theory, rendered a linear relationship between phase difference and the diameter of the scatterer (Kerker, 1969).

An Argon-ion laser was used for the two-component PDPA transmitter which separated the source beam in two green beams (λ=0.5145 μm contained in a vertical plane and two blue beams (λ=0.488 μm) contained in the horizontal plane to measure the minor and major axes of the spheroid, respectively. With the interference fringes lying in the horizontal and vertical planes, respectively, and the fringes sweeping in the corresponding orthogonal directions, the system was set up to measure two dimensions of the spheroidal bubbles.

The output from each of the receivers was fed to a separate processor and computer terminal for subsequent data reduction. Hence, for each measurement which consisted of 10,000 bubble samples, two histograms of particle size, one for the major axis and one for the minor axis of the spheroid, and two histograms of bubble velocity were obtained. Notice that for the first receiver, the velocity histogram shows positive velocities only because the bubbles were moving upward, i.e., in the positive direction. However, the second receiver yielded velocity histograms which are centered approximately around zero velocity. This is because large bubbles wobbled and oscillated from side to side. Since the second receiver measured the horizontal component of velocity, the oscillatory nature of the flow is reflected as positive and negative velocities in the histogram.

2.6.9 Experimental Results

Several spherical monosize air bubbles in the range between 300 μm and 700 μm were generated, and their diameters were measured with both receivers. Figures 2.6.20-2.6.23 show the results obtained with the PDPA system in the measurement of the spherical bubbles. Also included in this set is the measurement of a polydispersion consisting of three streams of nearly monosize bubbles which was produced coincidentally when a fine thermocouple wire of 125 μm was introduced inside the micropipette, Figure 2.6.23.

The first and second receivers yielded results which agreed to within ± 5%. Direct photography was used in this part of the study to verify the sizes predicted by the PDPA instrument. The phase Doppler technique and the photographs agreed to within ± 6%. The discrepancies are mainly attributed to a slight departure from sphericity of the bubbles and a nonuniform generation of monosize bubbles with the syringe pump.

A reasonable confidence was obtained in the multiangular light scattering detection system, and subsequently, monosize spheroidal bubbles of eighteen different sizes were generated yielding major axis dimensions in the range from 750 μm to 3500 μm. The bubbles were produced with a

syringe pump feeding a micropipette of 200 μm ID by varying the air flow rate until a bubble having the desired approximate dimensions was obtained. With this method of producing bubbles the repeatibility of bubble sizes for the same air flow rate was within ± 30%. Producing a steady stream of monosize spheroidal bubbles usually required a long time, since small variations in the air flow rate or possible convection effects inside the water tank seemed to have an adverse effect on the stability of the bubbles. The stream of spheroidal bubbles was oriented such that a vertical cross-section of the bubble showed its major axis contained in a horizontal plane and its minor axis in a plane orthogonal to it. The bubbles appeared to have the shape of a pill, that is, a top view of the bubble would depict, approximately, a circular cross section while a side view would depict an ellipse.

Direct photography was used to assess the accuracy of the measurements with the PDPA. A Nikon N8008 camera with a bellows and an inverted wide angle 28 mm Nikkor lens (to produce a magnification of approximately 20 times) were used to photograph the bubbles. Twelve photographs were obtained for each set of 10,000 spheroidal bubbles measured with the PDPA system. The results show that the discrepancy in the major and minor axes between the measured PDPA values and those produced by the photographic images increased with larger spheroidal bubbles. In spite of the controlled flow conditions and an apparent stability in the generation of the bubbles, the results reported by the PDPA showed much wider size distributions for larger bubbles, whereas for bubbles in the size range of 1000 μm, the histogram of bubble sizes was much narrower. This is due to the fact that larger bubbles oscillated and rotated significantly, such that their orientation became random within the control volume. Moreover, for a steady stream of spheroidal bubbles the PDPA does not report a narrow distribution of sizes either. This is because the radius of curvature of the bubble varies as the rays of light pass through the bubble and scatter light along the scattering plane which is formed by the direction of the incident laser beam, the point of incidence on the bubble, and the incidence point on the receiver unit. In other words, the PDPA reported values which represent an average of the curvatures of the major and minor axes of the spheroids. Figures 2.6.24-

2.6.28 show selected results from the measurements of large spheroidal bubbles. The different sizes of bubbles resulted from varying the air flow rate in the syringe pump from 0.5 ml/minute to 6 ml/minute, approximately.

2.6.10 Summary and Conclusions of the Experimental Phase

The experimental phase of the project consisted in the design and testing of a multiangular detection system using light scattering interferometry to measure two orthogonal dimensions of spheroidal bubbles. This would give an indication of the error that may be expected as a spheroidal particle passes at varying orientations through the sample volume. A modified phase Doppler system consisting of two receiver units located at different planes collected the light scattered by the bubbles to measure their size. The system used an Argon-ion laser, with the green beams used for sizing one of the axes of the spheroid and the blue beams used for sizing an orthogonal axis.

Two different signal processor units and data processors were used to determine histograms of size and velocity of the bubbles measured from the two planes. Eighteen different sizes of spheroidal bubbles, covering major axis dimensions in the range of 750 μm to 3500 μm, were generated using a syringe pump and a micropipette. The size of the spheroidal bubbles was controlled with the syringe feeding air to the micropipette. Typical air flow rates varied from 0.05 ml per minute to 3.00 ml per minute. The repeatibility of bubble sizes from day to day at a particular setting of the syringe pump was about ± 30 %. Direct photography was used to assess the accuracy of the measurements with the PDPA system.

Even if the bubbles did not oscillate, the phase Doppler instrument determines the sphericity of the particle along the scattering plane. Since the sphericity measured by the instrument varies depending on the orientation of the bubble with respect to the beams inside the probe volume, the reported diameter reflects these changes in curvature.

Smaller bubbles of the order of 1500 μm show a more stable elliptical shape which can be predicted with an accuracy of $\pm$ 10-15 %. Since these smaller bubbles have a shape closer to spherical, the eccentricity is closer to one, and the instrument reported diameters which have less uncertainty with respect to the actual value of the major and minor axes.

Thus, the error due to asphericity can be significant, depending on the aspect ratio, for individual particle measurements. However, whether measuring drops or bubbles, the random oscillations of the particle shape and orientation will inevitable serve to mitigate this error, and the instrument will output the correct mean size but with a increase in the width of the size distribution.

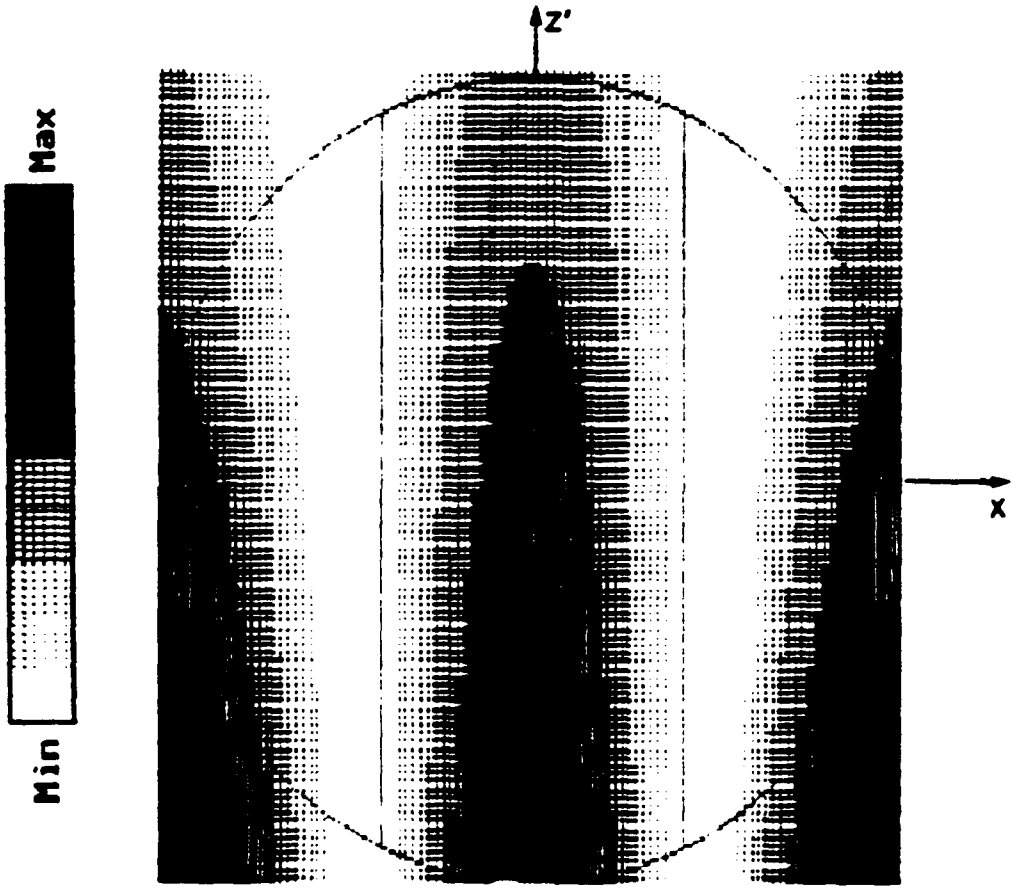

Figure 2.6.1: Computer generated spatial fringe pattern formed on the receiving lens due to the scattering of light by a 40 μm water droplet. Ideal case of pure refraction (p=1 only) at a mean scattering angle of 30 °. The circle delineates the receiving lens.

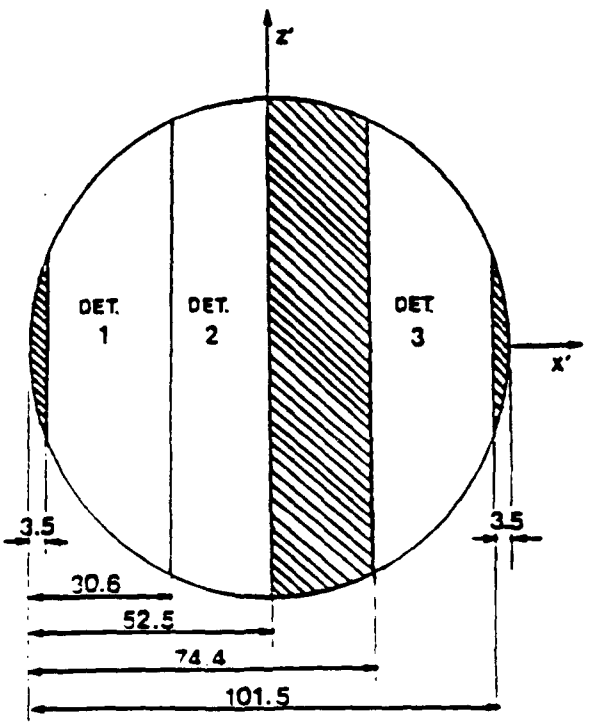

Figure 2.6.2: Schematic of the receiving apertured showing the areas from which light is collected. The dimensions are in mm.

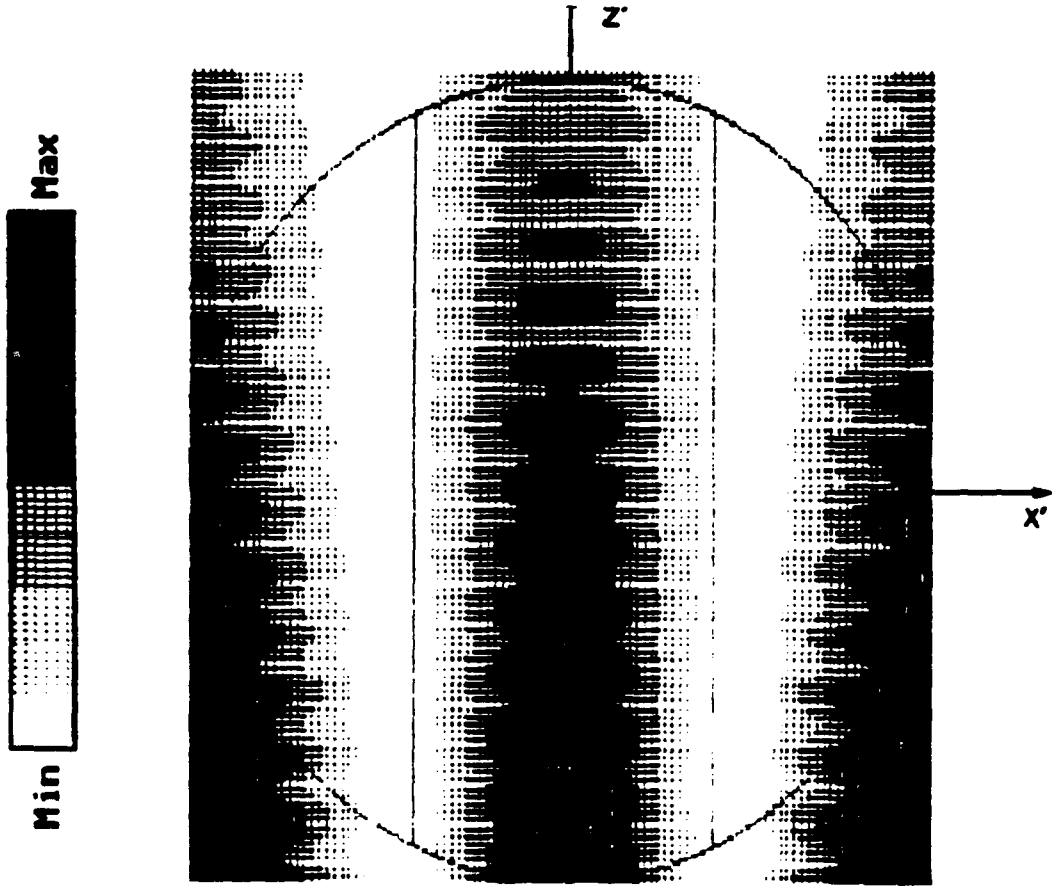

Figure 2.6.3: Computer generated spatial fringe pattern for a 40 μm water droplet. Simultaneous presence of external reflection, refraction and second internal reflection at a mean scattering angle of 30°.

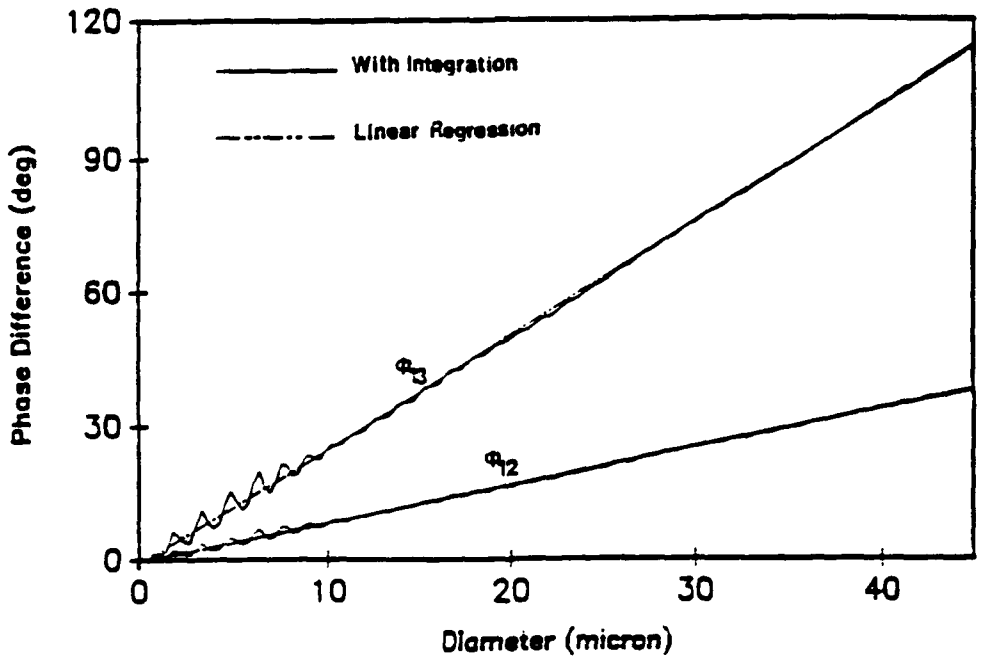

Figure 2.6.4: Computed calibration curves for 150° mean scattering angle showing the effect of performing spatial and temporal integration of the spatial intensity pattern.

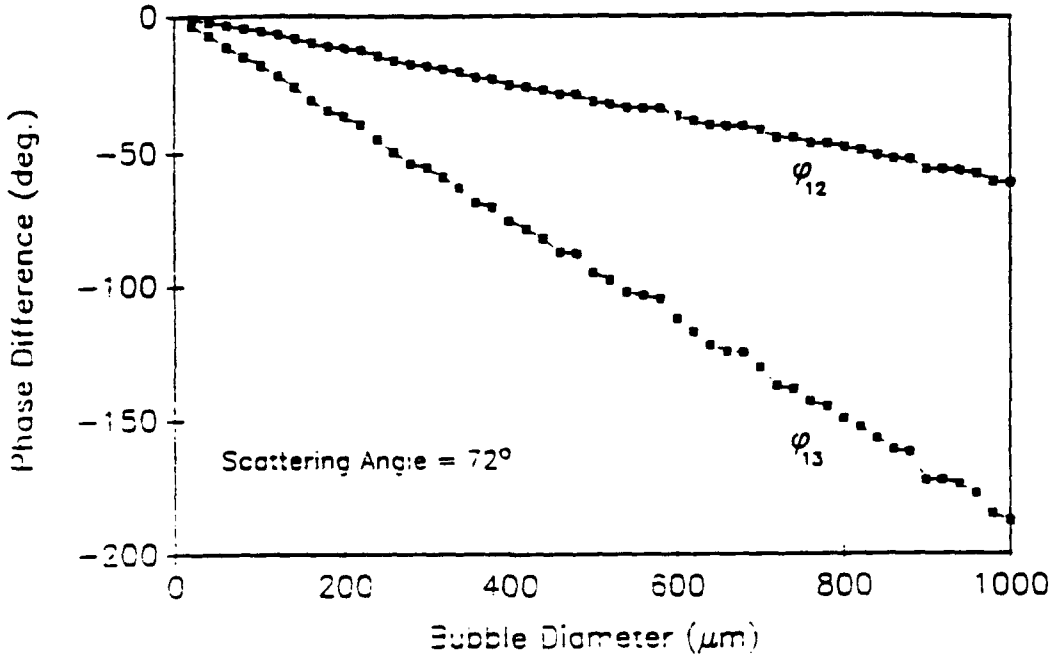

Figure 2.6.5: Computed calibration curves for 72° mean scattering angle for spherical bubbles in the range of 0.5 μm to 1000 μm in diameter.

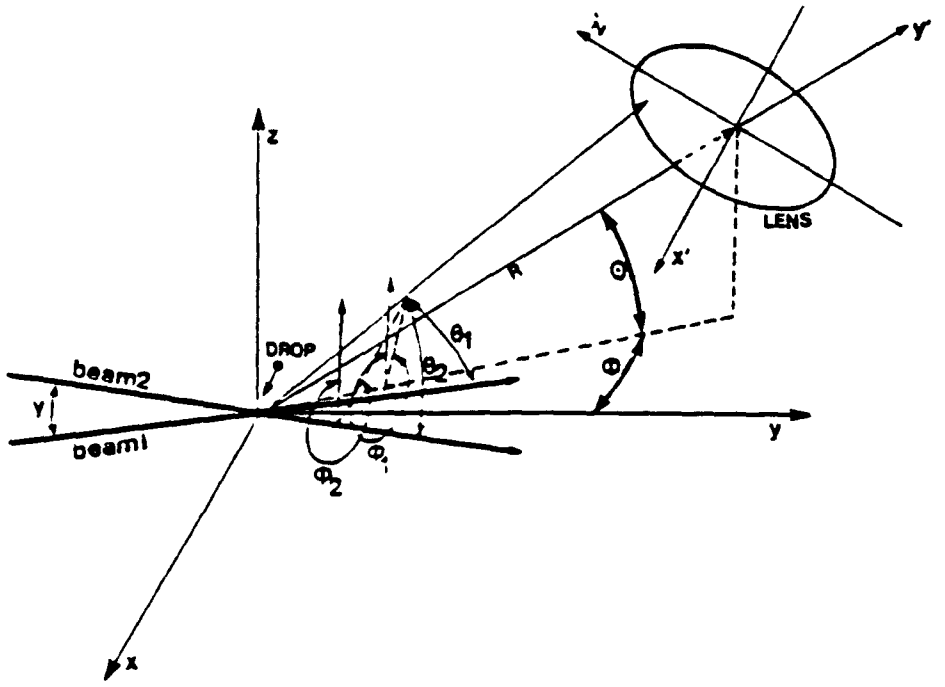

Figure 2.6.6: Coordinate system chosen for the theoretical analyses.

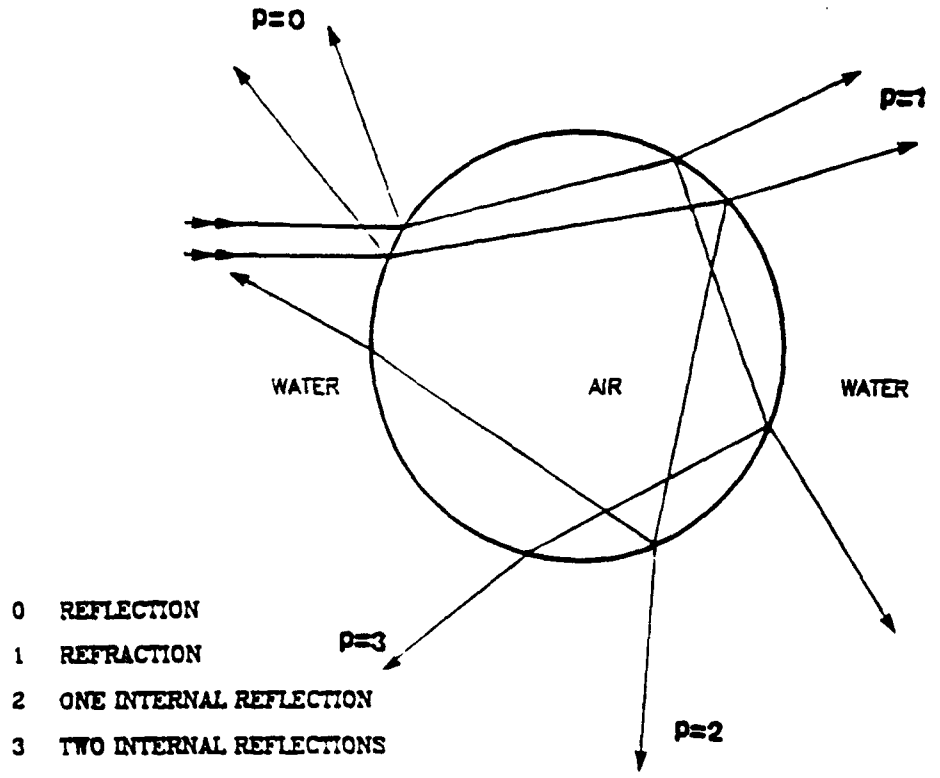

Figure 2.6.7: Ray trace for a spherical air bubble in water.

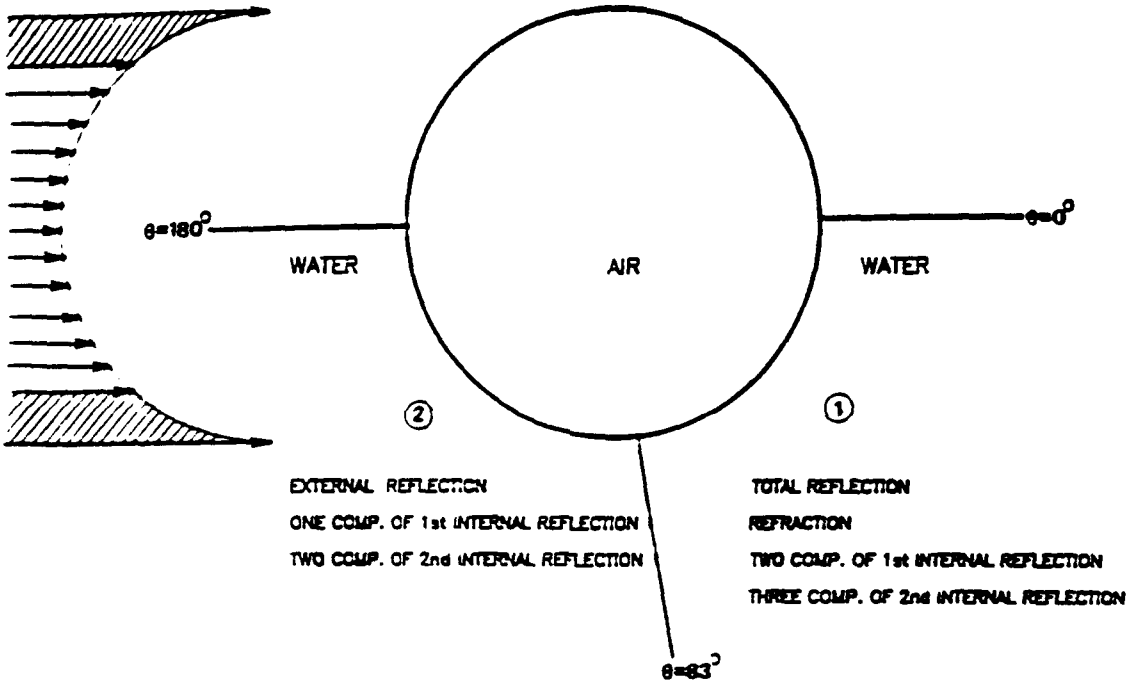

Figure 2.6.8: Divison of scattering angles into scattering regions.

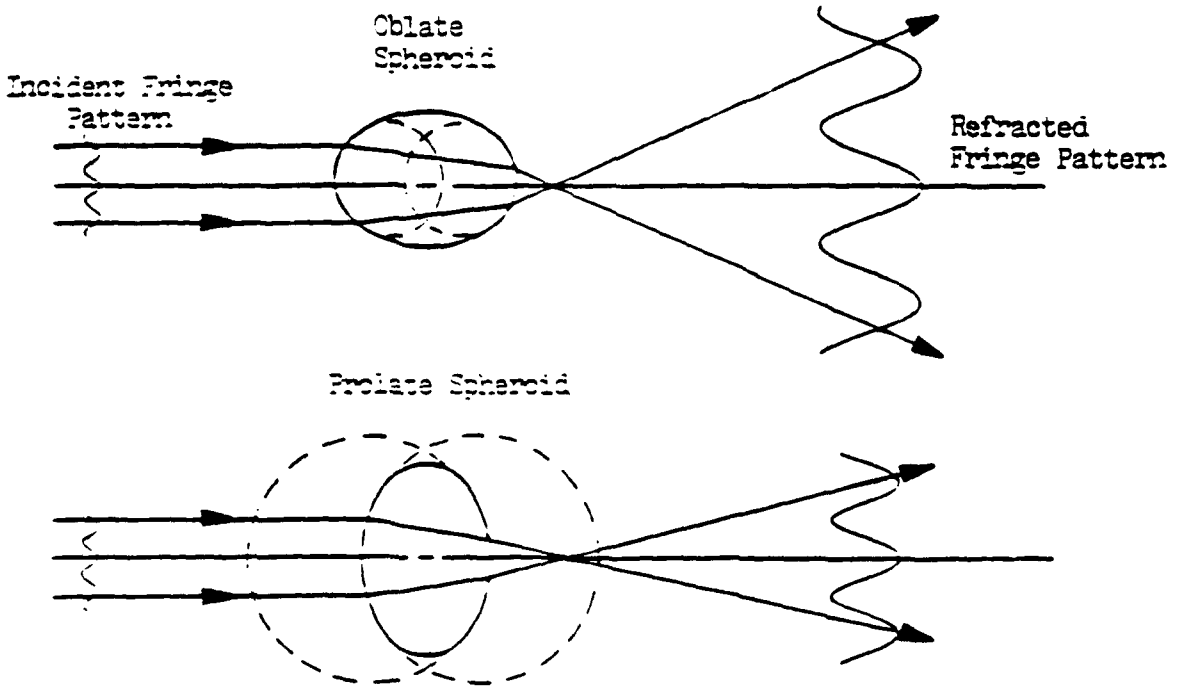

Figure 2.6.9: Schematic showing the effect of the radius of curvature on the scattered interference fringe pattern.

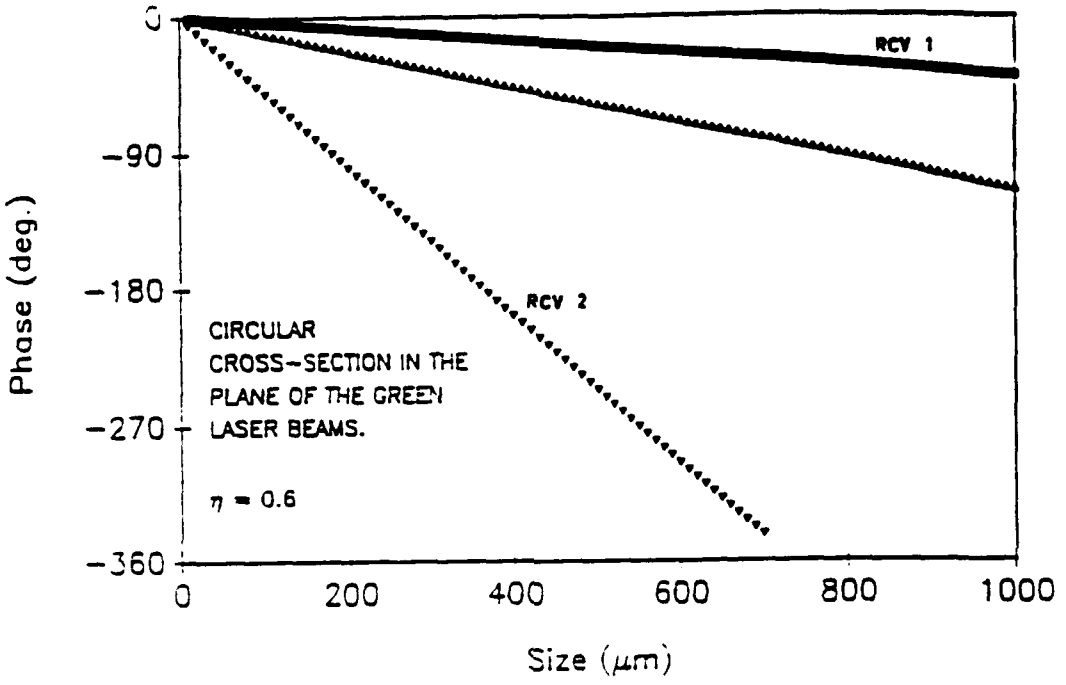

Figure 2.6.10: Phase response of detectors 1-3 ϕ_{13} versus the diameter of a bubble for receivers 1 and 2 (on stands) for η=0.6. The third line denotes the response if the bubbles were spherical.

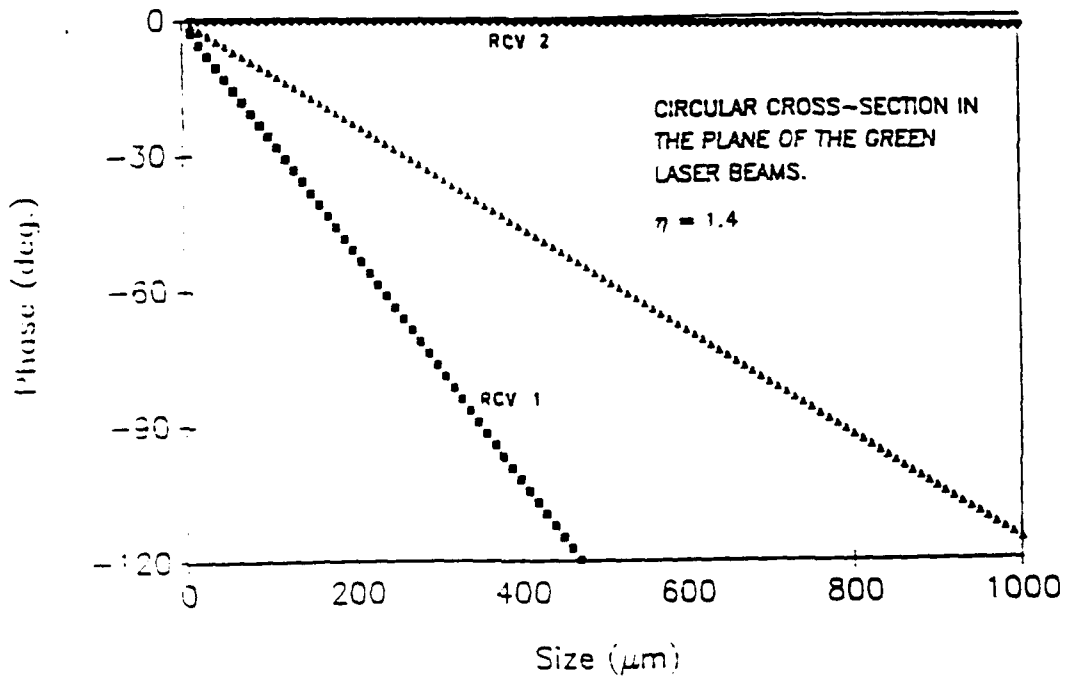

Figure 2.6.11: Phase response of detectors 1-3 ϕ_{13} versus the diameter of a bubble for receivers 1 and 2 (on stands) for η=1.2. The third line denotes the response if the bubbles were spherical.

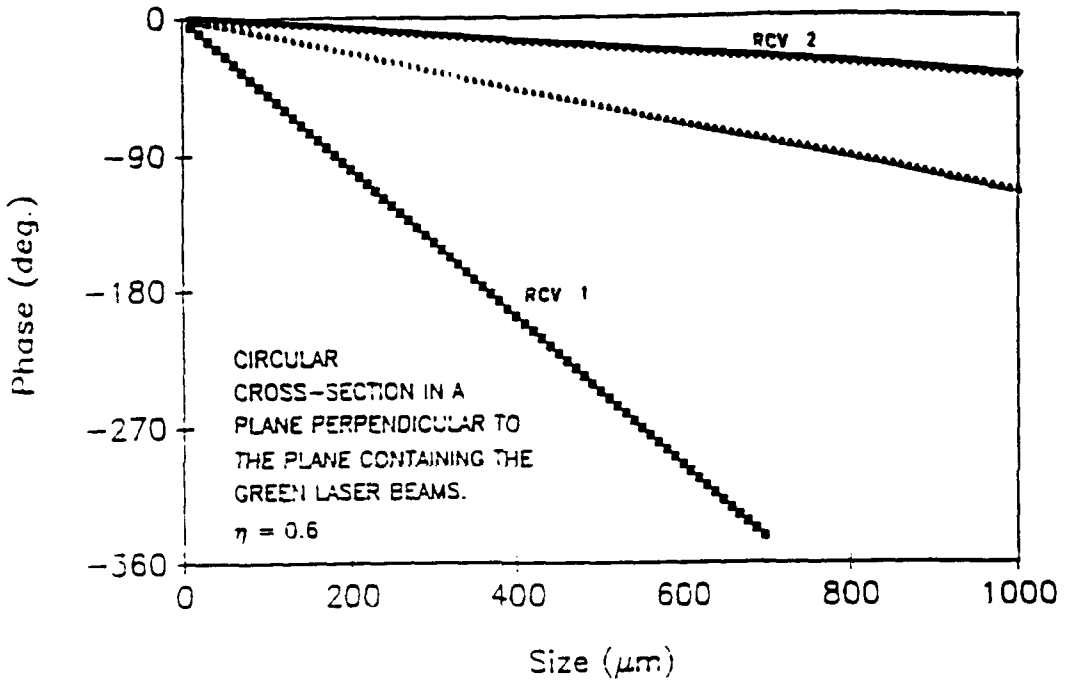

Figure 2.6.12: Phase response of detectors 1-3 ϕ_{13} versus the diameter of a bubble for receivers 1 and 2 for η=0.6. The third line denotes the response if the bubbles were spherical.

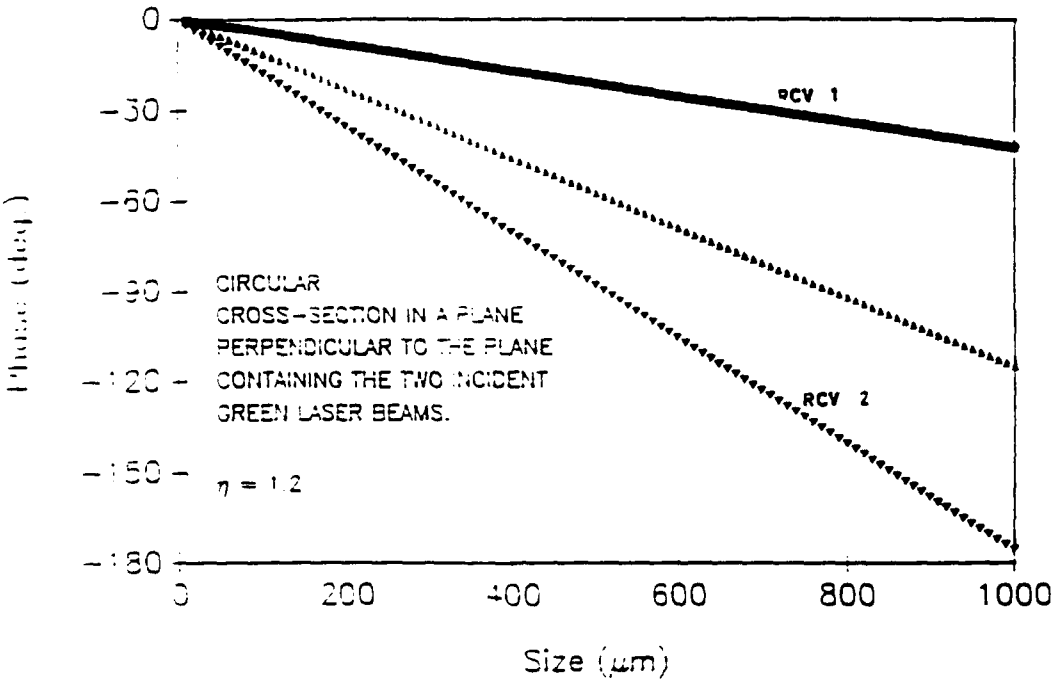

Figure 2.6.13: Phase response of detectors 1-3 ϕ_{13} versus thediameter of a bubble for receivers 1 and 2 (on stands)for η=1.2. The third line denotes the response if the bubbles were spherical.

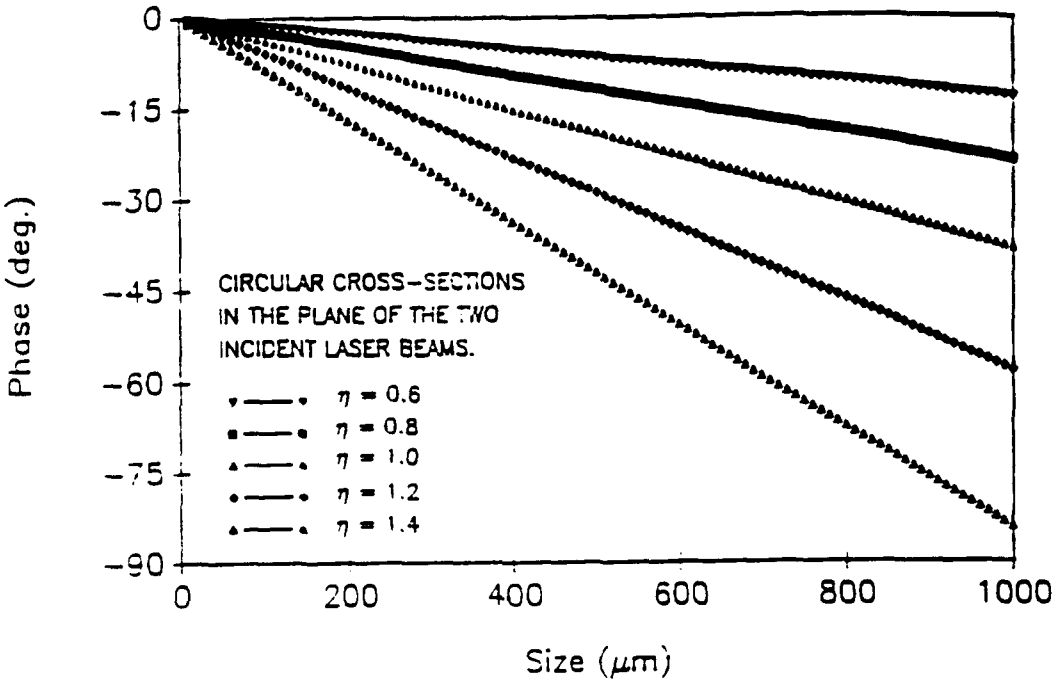

Figure2.6.14: Phase response of detectors 1-2 ϕ_{12} versus the diameter of a bubble for five conditions of eccentricity. The circular dimension is in the plane of the green beams.

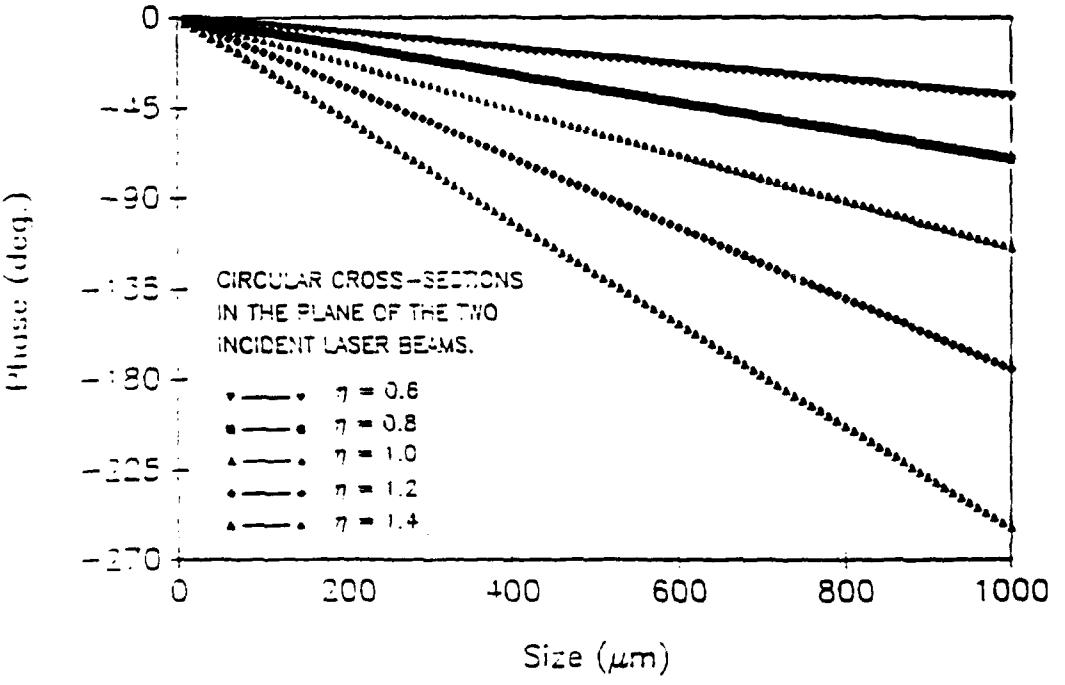

Figure 2.6.15: Phase response of detectors 1-3 ϕ_{13} versus the diameter of a bubble for five conditions of eccentricity. The circular dimension is in the plane of the green beams.

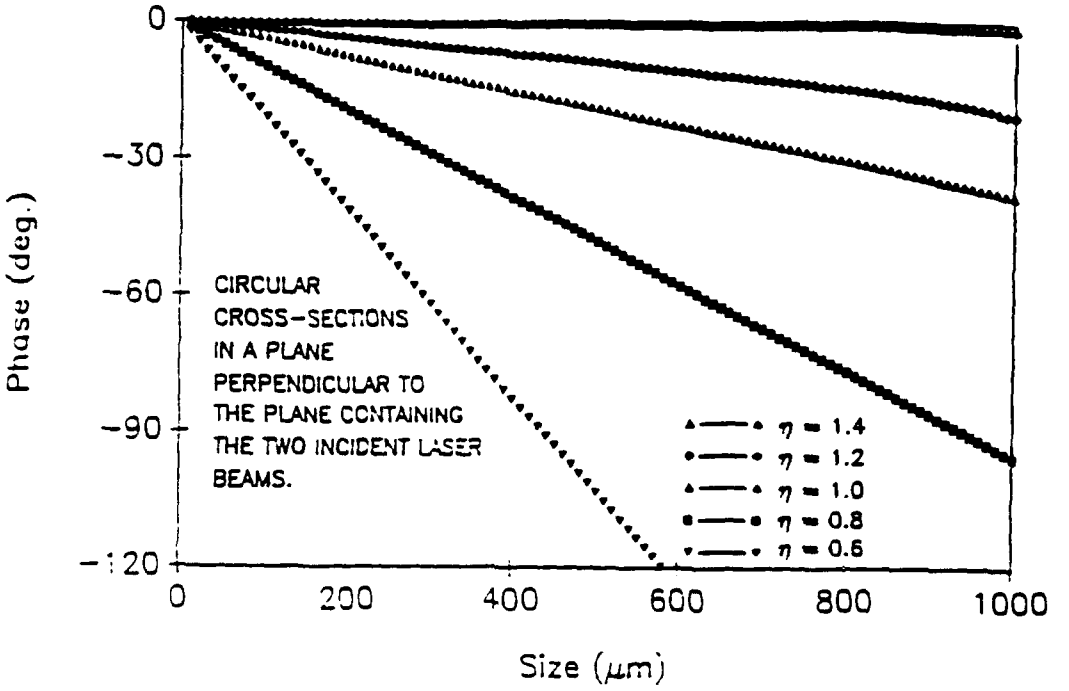

Figure 2.6.16: **Phase response of detectors 1-2 ϕ_{12} versus the diameter of a bubble for five conditions of eccentricity. The circular dimension is in a plane perpendicular to the green beams.**

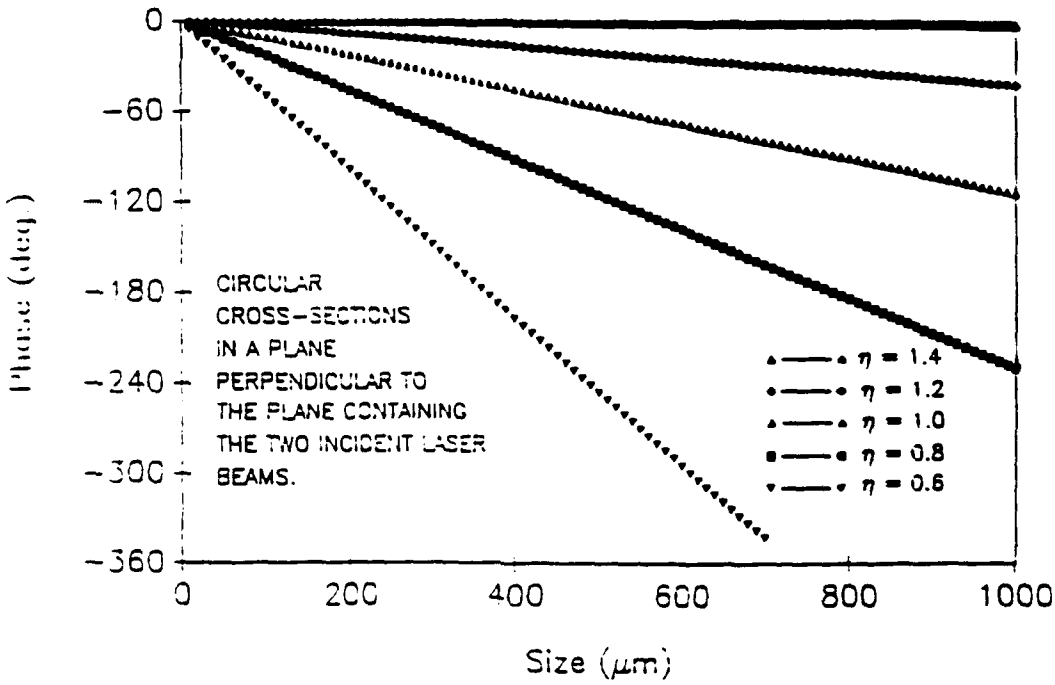

Figure 2.6.17: Phase response of detectors 1-3 ϕ_{13} versus the diameter of a bubble for five conditions of eccentricity. The circular dimension is in a plane perpendicular to the green beams.

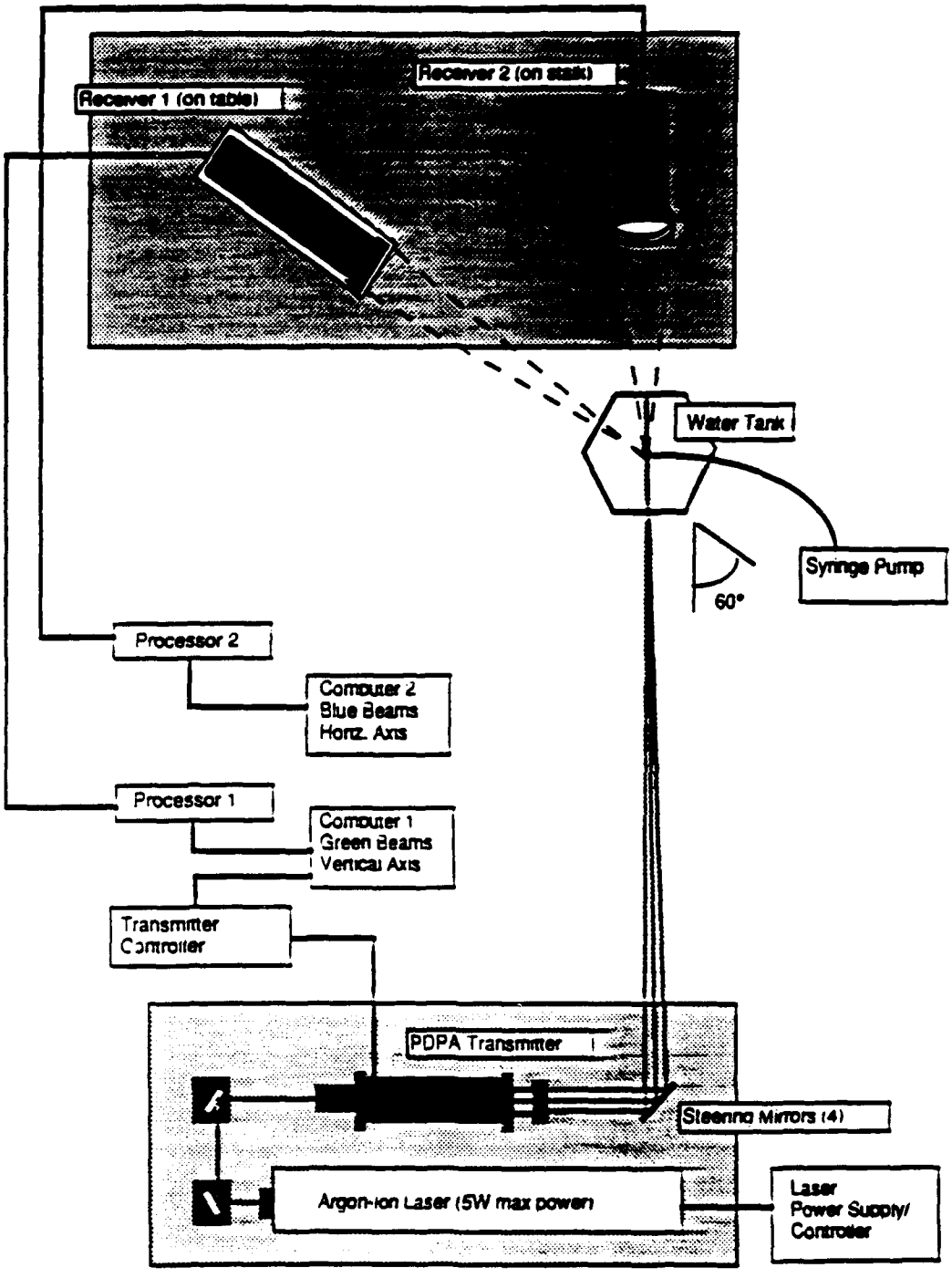

Figure 2.6.18: A second receiver unit was added to the standard PDPA system to measure two orthogonal axes of the spheroids.

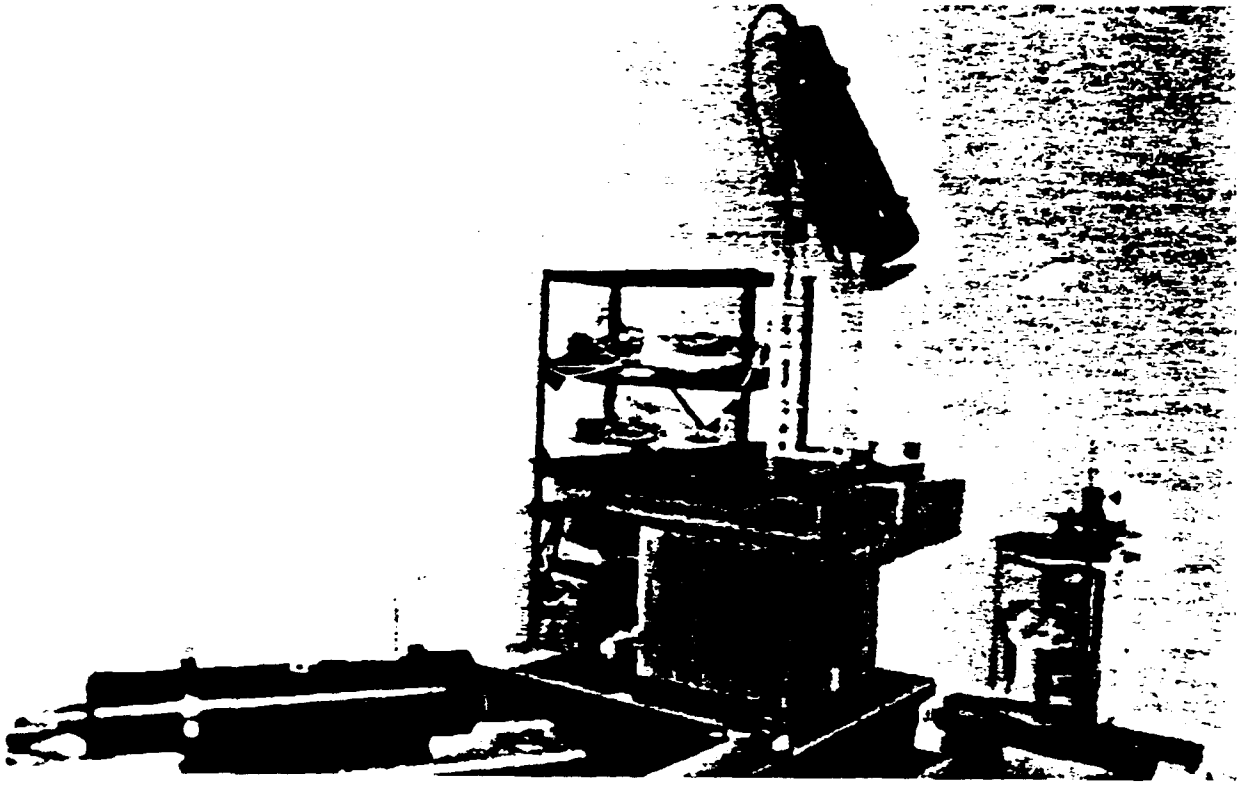

Figure 2.6.19: The two receiver units were located at 60° off-axis in the forward scatter direction.

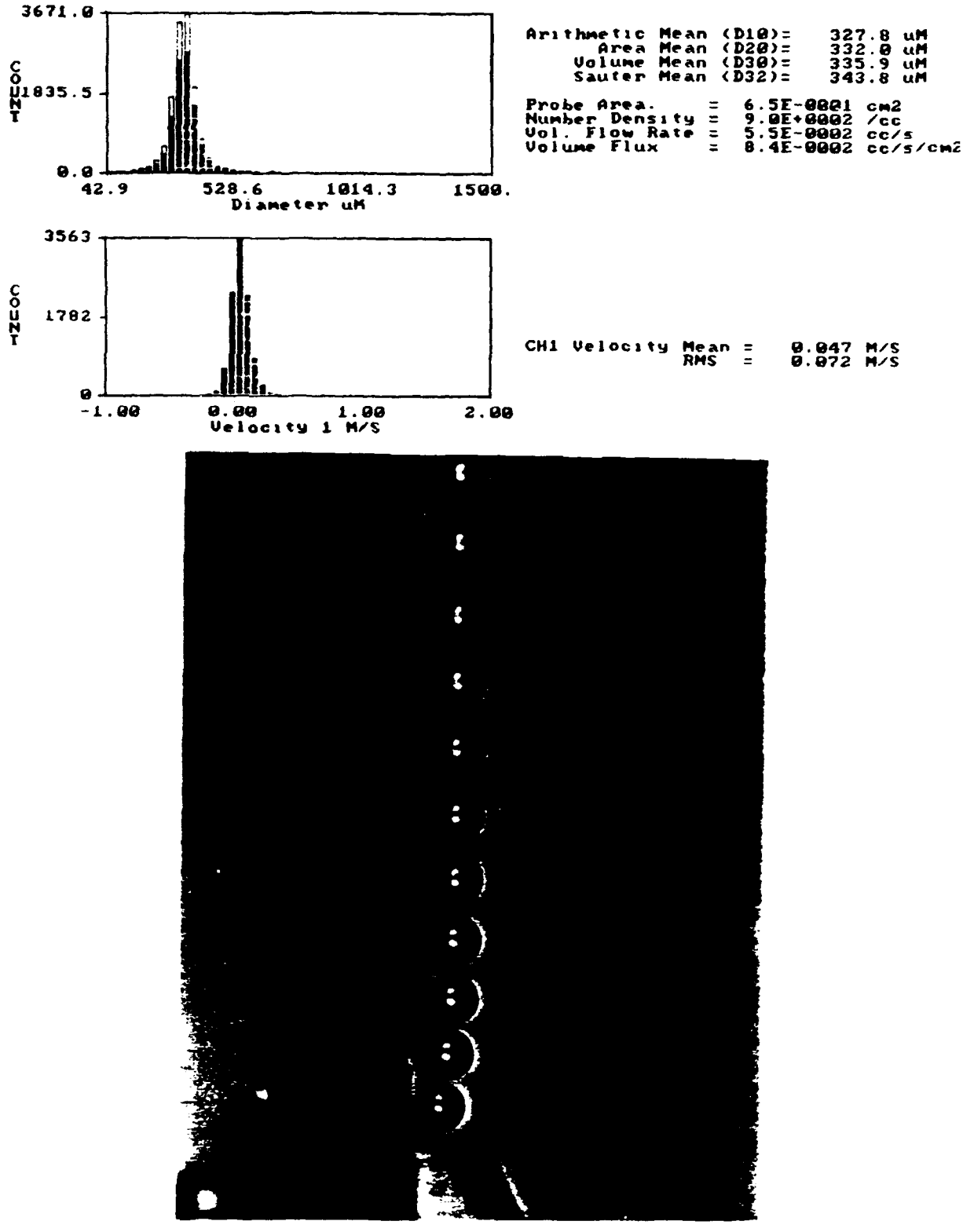

Figure 2.6.20: Results obtained with the PDPA multiangular detection system in the measurement of spherical bubbles. Top: results from the first receiver. Photograph yielded D_{10}=350 μm. Void fraction = 0.018.

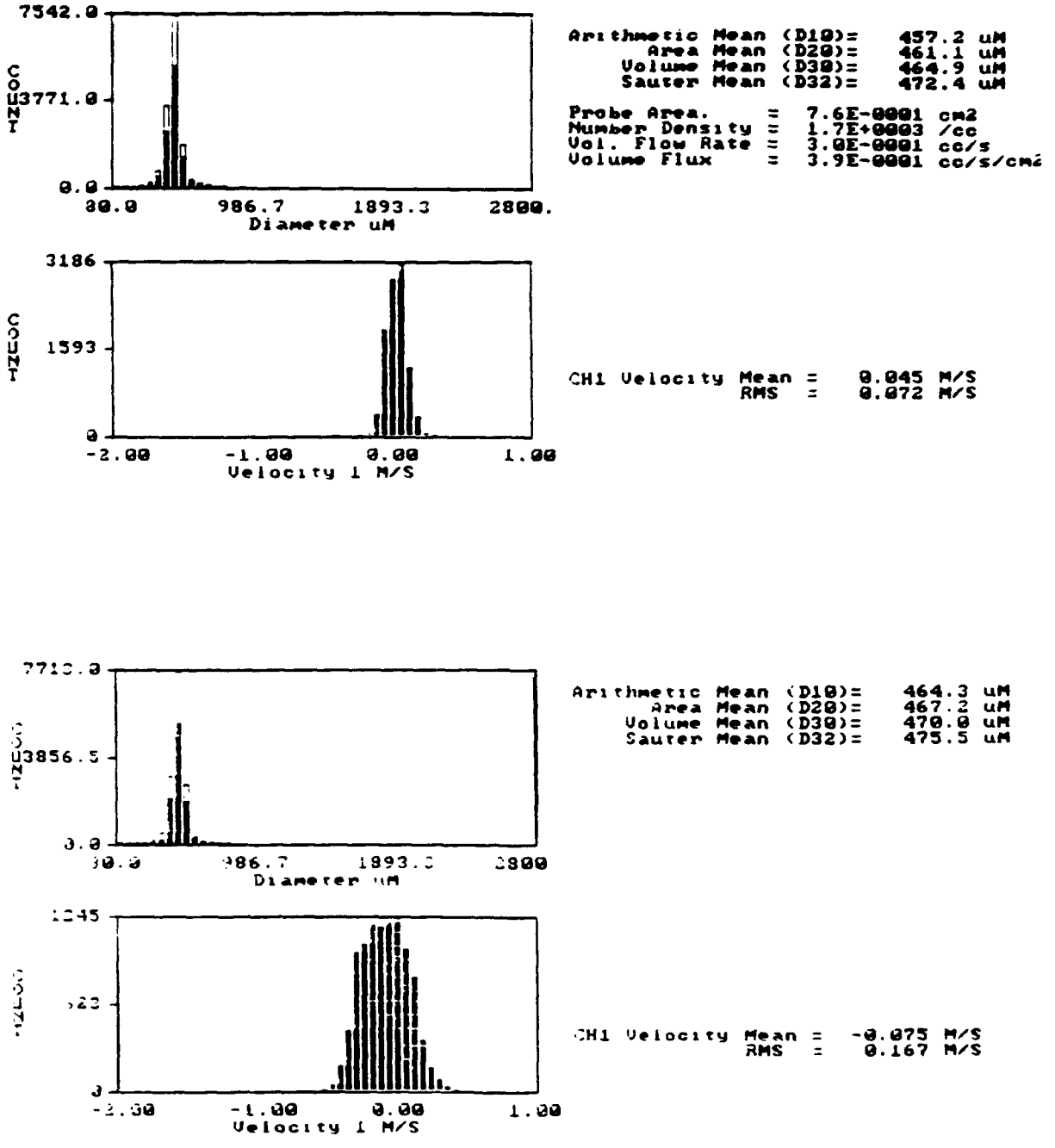

Figure 2.6.21: Results obtained with the PDPA multiangular detection system in the measurement of spherical bubbles. Top: results from the first receiver; bottom: results from the second receiver. Photograph yielded D_{10}=470 μm. Void fraction = 0.089.

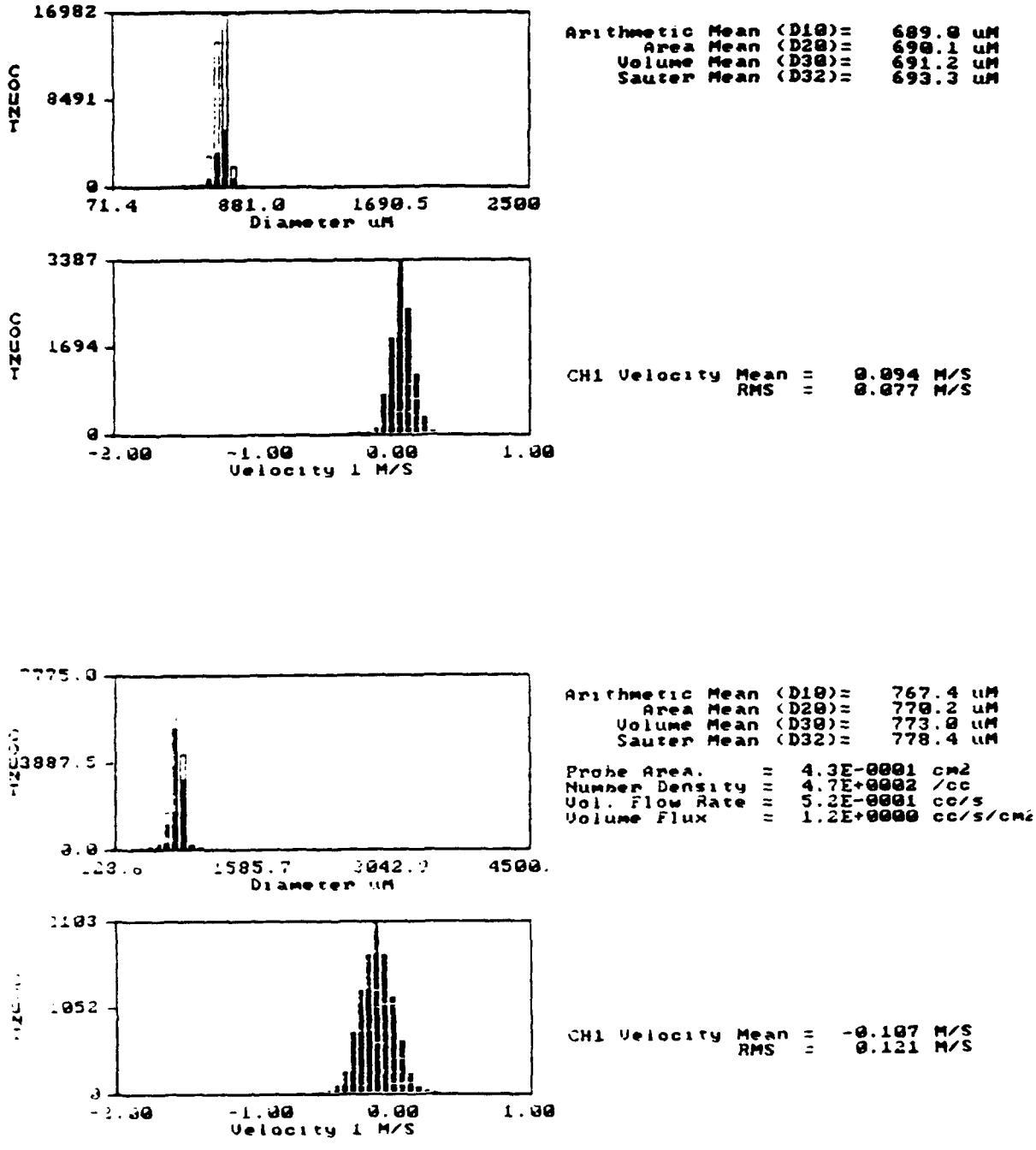

Figure 2.6.22: Results obtained with the PDPA multiangular detection system in the measurement of spherical bubbles. Top: results from the first receiver; bottom: results from the second receiver. Photograph yielded D_{10}=730 μm Void fraction = 0.114.

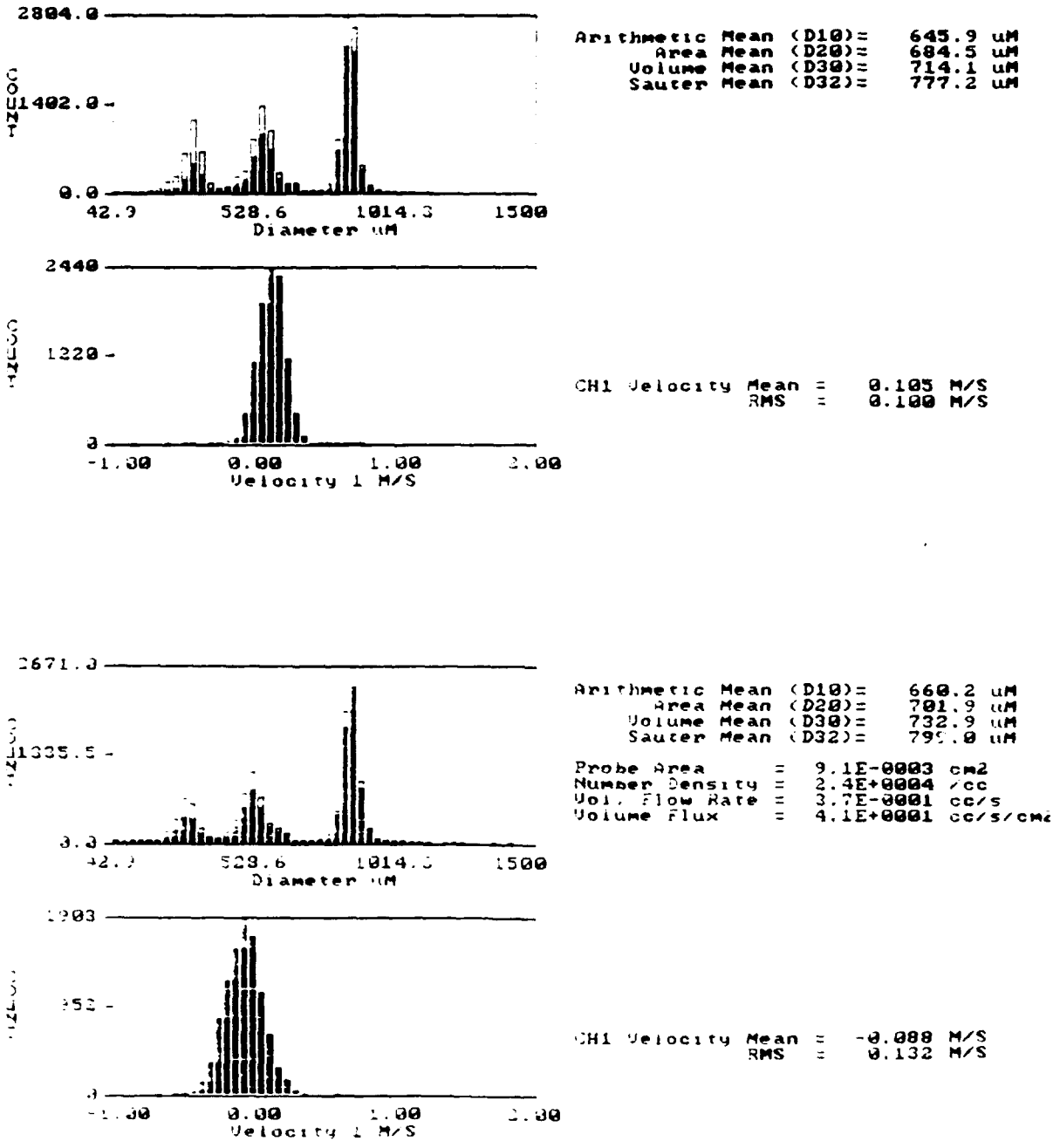

Figure 2.6.23: Measurement of a polydispersion of bubbles consisting of three streams of nearly monosize bubbles. The mean value of each peak in the size histogram is D_{10}=310 μm, D_{10}=550 μm, and D_{10}=875 μm, respectively.

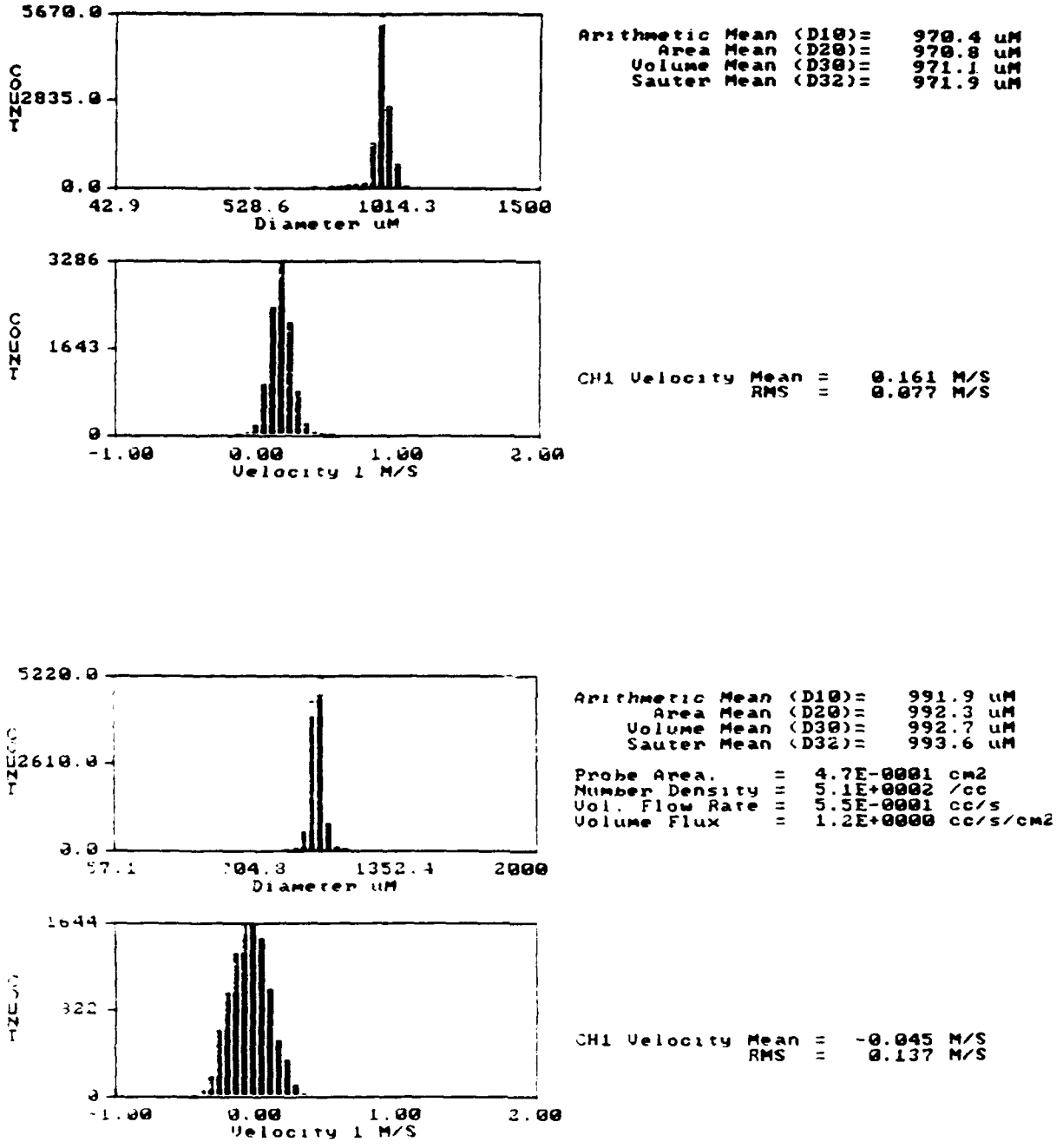

Figure 2.6.24: Results obtained with the PDPA multiangular detection system in the measurement of spheroidal bubbles. Top: results from the first receiver; bottom: results from the second receiver. Photographs yielded major axis: 1200 μm, minor axis: 1050 μm. Void fraction = 0.261.

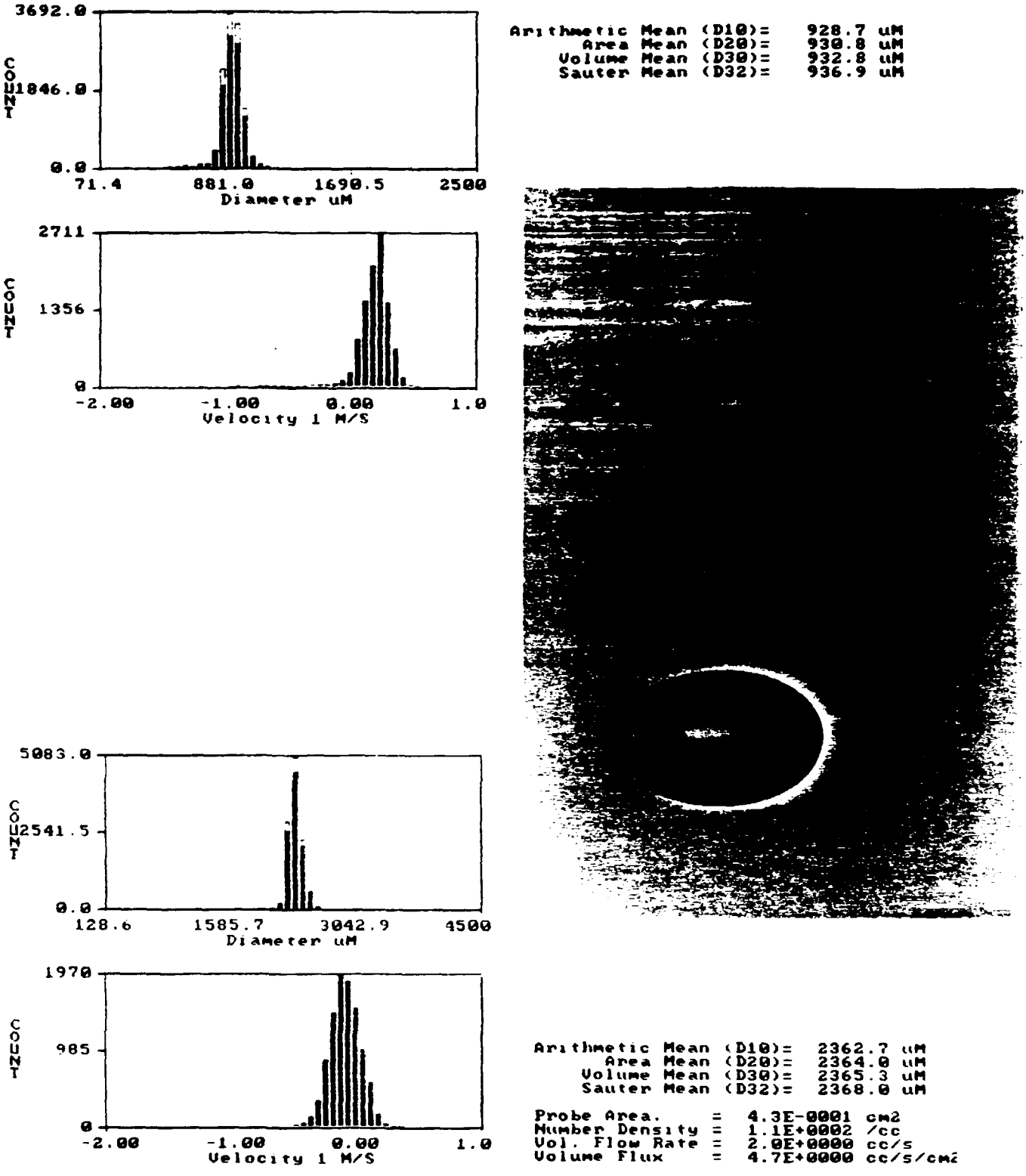

Figure 2.6.25: Results obtained with the PDPA multiangular detection system in the measurement of spheroidal bubbles. Top: results from the first receiver; bottom: results from the second receiver. Photographs yielded major axis: 2050 μm, minor axis: 1350 μm. Void fraction = 0.762.

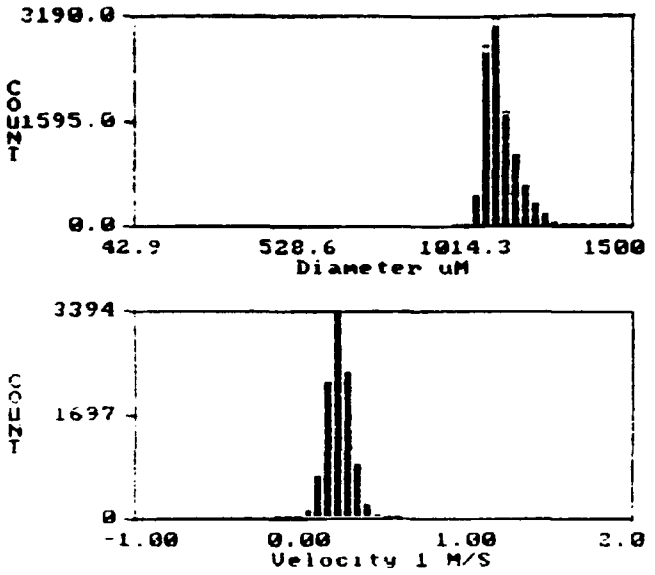

Arithmetic Mean (D10)= 1127.0 uM
Area Mean (D20)= 1128.0 uM
Volume Mean (D30)= 1129.1 uM
Sauter Mean (D32)= 1131.3 uM

Probe Area. = 6.5E-0001 cm2
Number Density = 3.6E+0001 /cc
Vol. Flow Rate = 4.1E-0001 cc/s
Volume Flux = 6.2E-0001 cc/s/cm2

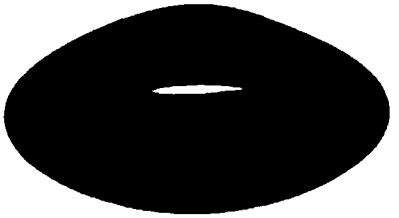

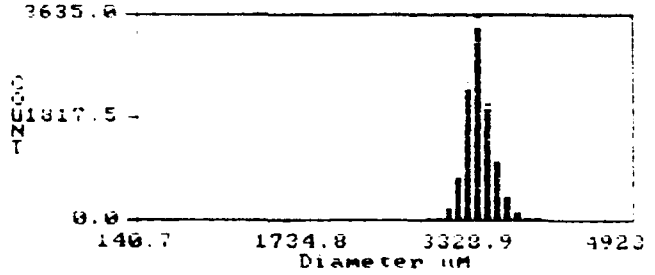

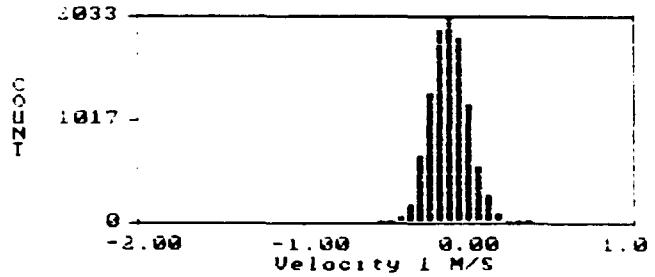

Arithmetic Mean (D10)= 3470.1 uM
Area Mean (D20)= 3472.6 uM
Volume Mean (D30)= 3475.0 uM
Sauter Mean (D32)= 3479.8 uM

Figure 2.6.26: Results obtained with the PDPA multiangular detections system in the measurement of spheroidal bubbles. Top: results from the first receiver; bottom: results from the second receiver. Photographs yielded major axis: 2800 μm, minor axis: 1500 μm.

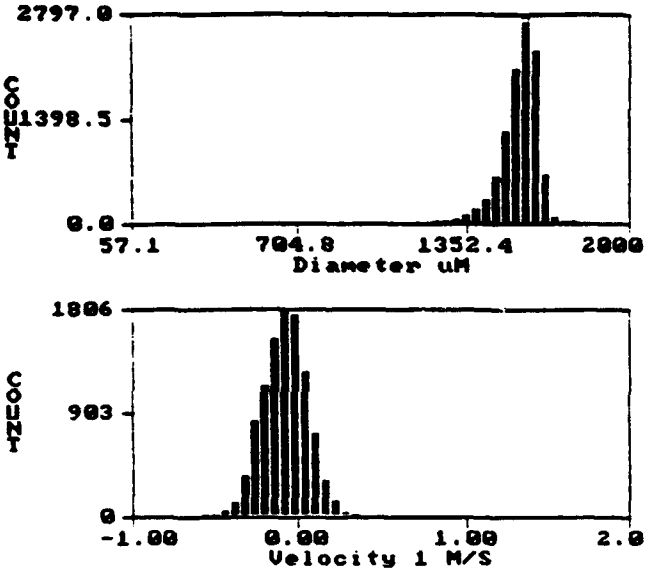

Arithmetic Mean (D10)= 1583.2 uM
Area Mean (D20)= 1584.6 uM
Volume Mean (D30)= 1585.9 uM
Sauter Mean (D32)= 1588.6 uM

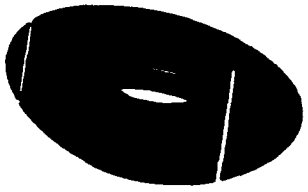

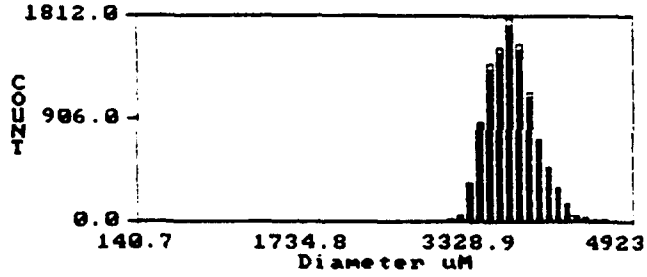

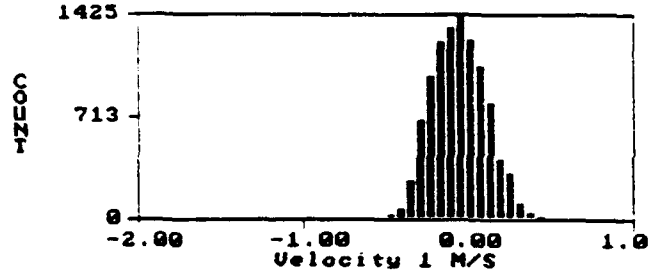

Arithmetic Mean (D10)= 3772.2 uM
Area Mean (D20)= 3779.1 uM
Volume Mean (D30)= 3786.1 uM
Sauter Mean (D32)= 3800.2 uM

Probe Area. = 4.3E-0001 cm2
Number Density = 4.9E+0002 /cc
Vol. Flow Rate = 2.9E+0001 cc/s
Volume Flux = 6.7E+0001 cc/s/cm2

Figure 2.6.27: Results obtained with the PDPA multiangular detection system in the measurement of spheroidal bubbles. Top: results from the first receiver; bottom: results from the second receiver. Photographs yielded major axis: 3300 μm, minor axis: 1800 μm.

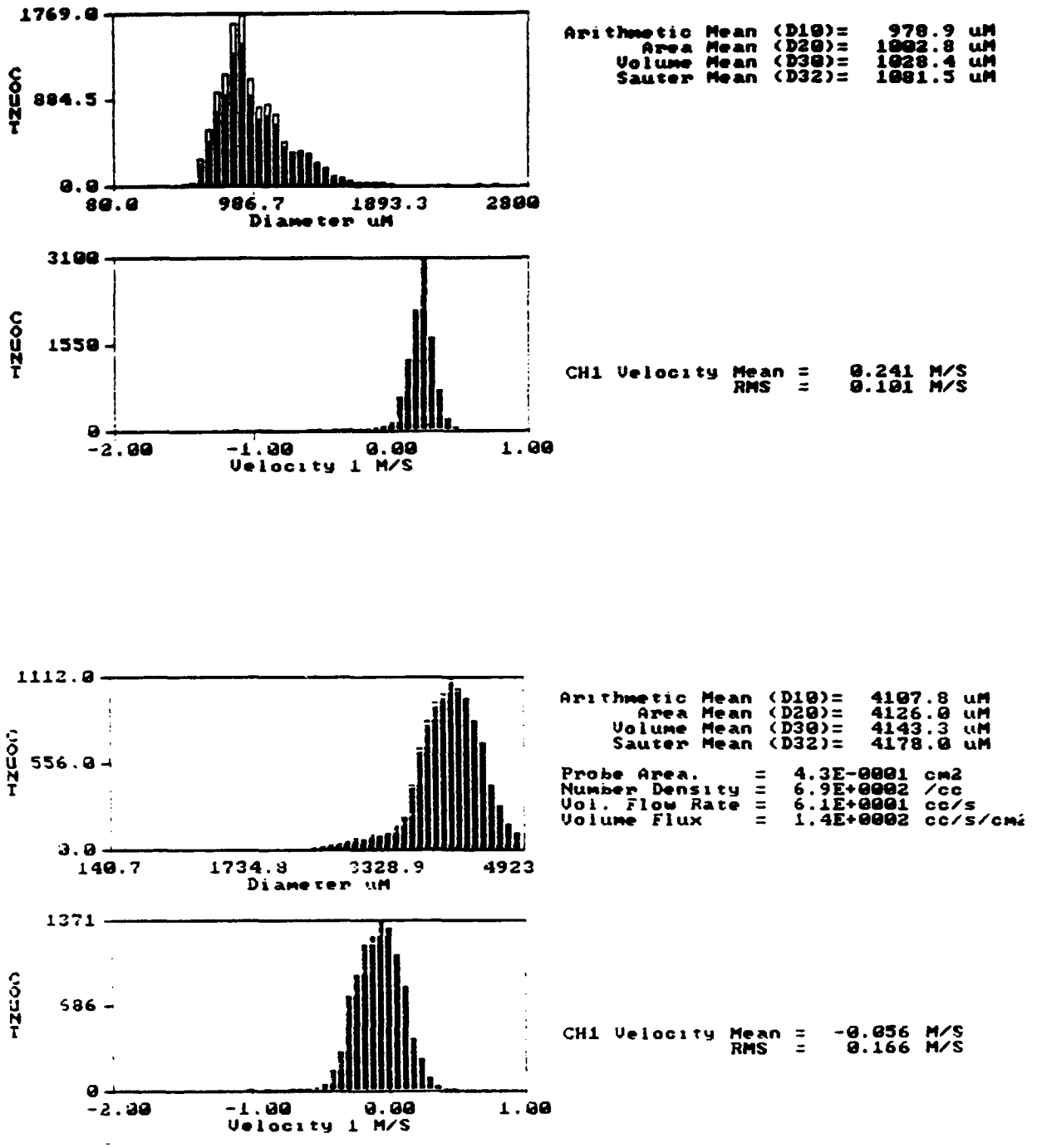

Figure: 2.6.28: Results obtained with the PDPA multiangular detection system in the measurement of spheroidal bubbles. Top: results from the first receiver; bottom: results from the second receiver. No photographs were obtained of this particular set.

2.7 Velocity Bias Considerations

2.7.1 Introduction

A primary *systematic* error source that affects the accuracy of laser Doppler velocimetry measurements in highly turbulent flows is velocity or statistical bias: velocity data are obtained at unequal time intervals as controlled by random particle passages through the probe volume. Since more particles per unit time pass through the probe volume during time intervals when the velocity is high, the mean velocity calculated by simple averaging of the data is higher than the true time mean. Of course, turbulence intensity estimates and higher order statistical moments are also affected. It is important to stress that in the limit of zero statistical error, bias error remains. Various correction methods have been proposed in the past to obtain statistically correct averages and moments from biased velocity distributions. The purpose of the research conducted under this phase was to summarize and compare these methods, evaluate their suitability under realistic measurement conditions, and incorporate the most suitable methods into the phase Doppler instrument.

2.7.2 History

The analytical prediction and computer simulations of McLaughlin and Tiederman (1973) showed the existence of velocity bias. Since then, many investigators have conducted experiments to verify its existence. Others have conducted experiments in highly turbulent flows and employed various correction schemes in their data reduction.

Durao and Whitelaw (1975) proposed random sampling of the data from burst type processors. Although computer predictions supported their argument, measurements on the center line of a free jet at 25 %, 40 % and 100 % turbulence intensity levels proved inconclusive.

Johnson, Bachalo and Modarress (1976) reported measurements in a Mach 2.9 separated boundary layer and in transonic flow past an airfoil. They found no evidence of velocity bias. They claimed that velocity bias will not occur if the particle arrival rate is much less than the turbulence frequencies.

Quigley and Tiederman (1977) applied McLaughlin and Tiederman's one-dimensional correction scheme to their velocity measurements. The corrected velocities agreed well with the profiles obtained from pressure drop measurements. However, subsequent measurements by Bogard and Tiederman (1979) in the same water channel did not agree with the predicted velocity profiles. One of their findings was that, apparently, the particle arrival rate did not affect the velocity measurements. This is in direct contradiction with Johnson et al. (1976), and with Barnet and Bentley (1974), who suggested the use of the time between validated data to correct the velocity histograms.

Hoesel and Rodi (1977) proposed a particle separation time correction for non-uniformly seeded flows when the average separation is small compared with the time scale of turbulence. For uniformly seeded flows, they suggest a probe volume residence time correction. They applied this correction to the measurements made across a free jet. Near the jet axis, their corrected velocities agreed well with those using McLaughlin and Tiederman's correction equations but deviated toward the edge. It is interesting to note that the difference between the corrected and uncorrected velocities was negligible near the outer edge of the jet.

Buchhave (1979) and Buchhave et al. (1979) also claim, based on analytical and experimental evidence, that the complete time statistics of the velocity field can be recovered from the random burst signal if the particle residence time is measured along with its velocity.

Giel and Barnett (1979) questioned the existence of bias, based mainly on the lack of experimental verification in their own velocity measurements in a jet very similar to that of Hoesel and Rodi.

Dimotakis, Collins, and Lang's (1979) measurements of turbulent boundary layer profiles over a flat plate showed that only after bias correction did LDV and pitot tube measurements agree well. Simpson and Chew (1979) suggested the use of a constant time-interval data sampling for elimination of velocity and density bias.

In other studies, such as Stevenson et al. (1980, 1982), Johnson et al. (1981), the bias was experimentally verified but seemed to depend on the particle concentration and vanished in the limit of high particle densities. Edwards (1979) described this effect qualitatively and showed that it was due to the fact that the data-handling system was saturated, leading to uniform time interval sampling. Similar saturation effects were obtained by Erdmann and Tropea (1981) in their detailed computations on "controlled" processors.

Edwards (1981) analyzed the measurement statistics when the velocity is sampled at a constant rate and showed that the product of the particle density and the sample interval is the controlling parameter for the statistical description of the measurements. He also presented the asymptotic forms of the analysis for low and high particle density-sample time products.

Craig and Nejad (1984) further developed the approach of Simpson and Chew and established an easily measurable data collection time interval to indicate when an acceptable ratio of seeding and sampling rates has been achieved.

Edwards and Jensen (1983) performed a rigorous analysis of the influence of the data-handling algorithm on the measurement statistics of a laser Doppler velocimeter, first for a sample-and-hold system and then for a rate limiting device. They showed that the measured statistics can differ from those of the flow statistics and from the particle arrival statistics.

Craig and Nejad (1985) have shown that velocity bias may even occur in flows with low turbulence. This problem usually arises when one is measuring second or third components of the velocity, where its mean

value is small and the turbulence is nearly isotropic. Nejad and Davis (1982) performed a study on velocity bias in two component individual realization LDV. They show that measurements with a narrow coincidence window and/or a low coincidence seeding rate result in velocity measurements which are larger than the true local average and that standard statistical bias correction techniques yield unsatisfactory results for this case.

Gould, Stevenson and Thompson (1986, 1989) performed LDV measurements of the turbulent flow past a sudden expansion in a circular tube. They compared the results of ensemble average statistics for fixed gate sampling with McLaughlin and Tiederman's two dimensional correction and Barnett and Bentley's time between data scheme. They claim that ensemble average statistics yield the true velocity average only when two conditions are met simultaneously: that the counter's data validation rate be three times larger than the inverse of the turbulent Taylor microscale, and that the effective sampling rate be less than 10% of the data validation rate. Furthermore, their results indicate that neither McLaughlin and Tiederman's nor Barnett and Bentley's method is effective in correcting adequately for velocity bias.

Edwards (1986) presents a review of the theory of particle measurement statistics in laser anemometry. By performing a rigorous derivation analysis of the uncertainties present, he identifies and clarifies several sources of confusion about the measurement statistics. Also, he presents an alternate method to determine the measurement statistics and extract Eulerian velocity information. Also, Edwards (1987) presents the conclusions of the special panel that met during the Second International Laser Anemometry Symposium at the 1985 ASME meeting. The panel evaluated the most common bias detection/correction algorithms, giving for each case a recommendation, but did not conclude which correction, if any, to use. The algorithms will be presented below, along with a description of the techniques involved.

For a long time, a high degree of controversy existed and still exists on this subject, and care should be exercised when reviewing and evaluating the

literature. The controversy arises because it is difficult to verify the existence of the bias experimentally. *Significant* biasing only occurs when the turbulence intensities are quite high. In these cases, there are no other measurement techniques to use as a standard for comparison. Measurement devices such as pitot pressure probes and hot wire anemometers have their own limitations at these levels of turbulence. However, it is clear now that bias always exists in the particle arrival rate, even for non-uniform particle concentrations. Why is it that it has not always been seen when it has been looked for? According to Edwards (1986), many factors may have contributed, among them:

- The precision of the measurement is not high enough to discriminate between bias and no-bias.

- The measurement probability of a velocity v is not proportional to the particle arrival rate due to some parts of the instrumentation compensating for the effect .

- The inappropriate statistics were measured.

- Velocity gradient effects affected the measurements, due to insufficient spatial resolution.

- Particle lag effects may have also affected the measurements.

- The signal-to-noise ratio was too low for accurate signal-processing.

- The detector response was poor.

If extreme care is not taken, spurious conclusions can be drawn regarding sampling bias which are really due to some other element in the experiment.

2.7.3 Statement of the Problem

The problem to be dealt with is that, in a sparsely seeded flow, the probability of recording a measurement of a velocity v depends on (Edwards, 1986):

- The probability of the velocity v appearing in the measurement volume.

- The probability of a particle arriving at the measurement volume when the velocity is v.

- The probability of detecting a velocity from a particle of velocity v, even if it passes through the volume.

- The probability of recording a measurement.

In general, all these effects depend on the velocity itself. As mentioned above, for a *flow with uniform spatial seeding, the higher speeds* will carry more particles per unit time through the measurement region than will the lower speeds. In addition, the electronics may have a lower probability of recording a higher speed particle than a lower speed one (Durao and Whitelaw, 1979, Durao et al., 1980). Biasing can occur when bursts are discarded because of low signal amplitude, when the counters have a relatively long reset time, when the fixed gating method is used, and when dual-counter validation circuits are used.

Several studies have assumed that velocity bias is dependent on turbulence intensity and scales and on particle arrival and measurement rates. However, a lot of confusion regarding the particle statistics arises from imprecise terminology in the field. In the following discussion, the terminology defined in Edwards (1987) will be adopted:

Measurement Rates

- $\dot{N}_0$, *Particle arrival rate*. This is the rate that measurable particles pass through the measurement volume. It is calculated using the particle number density, the laser power, the optical setup, and the particle size distribution. It reflects the number of particles that could be measured by an ideal laser anemometer. This rate does not depend on the processor settings.

- $\dot{N}_1$, *Trigger rate*. Rate of events that trigger the burst processor. This rate depends on the processor threshold setting. Note that every particle that triggers the processor will not result in a successful measurement. The measurement may be rejected by the processor validation circuit.

- $\dot{N}_2$, *Validation rate*. Rate that a free running burst processor measures particles. This is the number that appears on some counters as the validation rate. The validation rate does depend on the burst processor settings. If only one measurement is made per particle, $\dot{N}_1$ is the upper limit for this rate. For various reasons, it is possible that not all of the successful measurements are stored or used on subsequent algorithms, so that one more rate definition is necessary. In general, $\dot{N}_2$ is a function of velocity.

- $\dot{N}_3$, *Stored data rate*. Rate that measurements are stored in memory or used by algorithms inside a computer. This rate can differ from $\dot{N}_2$ for many reasons. If the validation rate is higher than the rate that the measurements can be stored for processing, some measurements from the burst processor will be missed. Also, the system may set so that it only stores velocity measurements made at regular time intervals; this is the so-called "controlled processor".

Turbulence Scales

- T_λ, *Taylor Time Microscale.* It is a measure of the time that the flow needs to change one standard deviation. In terms of the flow Eulerian flow parameters,

$$T_\lambda = \sigma_v / \left(< \left(\frac{dv}{dt} \right)^2 > \right)^{1/2} \tag{2.7.1}$$

The brackets, <>, denote the expected value of the enclosed expression. There is an implicit assumption that stationary systems are being discussed so that no distinction is made between time averaging and ensemble averaging. The parameter σ_v is the flow r.m.s. variation. The Taylor microscale has also been described as the time scale over which there is no significant change in the energy of an eddy.

- T_u, *Flow integral time scale.* Flow memory time,

$$T_u = \int_0^\infty R_{uu}(\tau) d\tau \tag{2.7.2}$$

where $R_{uu}(\tau)$ is the normalized Eulerian fluctuation autocorrelation function.

- L_λ, *Taylor micro-length scale.*

- L_u, *Integral length scale.*

Adrian (1983) and Edwards (1987) point out the importance of employing a dimensionless data rate parameter, called data density, by normalizing the dimensional data rate using the Taylor microscale. The following convention, proposed by Edwards (1987) will be used throughout this document:

- High data density: $\dot{N}_2 T_\lambda > 5$

- Intermediate data density: $5 \geq \dot{N}_2 T_\lambda \geq 0.05$

- Low data density: $0.05 \geq \dot{N}_2 T_\lambda$

In general, a histogram of measured velocities at a fixed point, $p_m(v)$ is related to the Eulerian velocity probability density function $p(v)$ by an equation of the form:

$$p_m(v) = N\, p(v) h_m(v) \tag{2.7.3}$$

where N is the total number of measurements, and $h_m(v)$ is the conditional probability of recording a measurement if the velocity is v. $h_m(v)$ is sometimes also interpreted as the relative measurement rate for the velocity v.

$$h_m(v) = \frac{\dot{N}_2(v)}{< \dot{N}_2 >} \tag{2.7.4}$$

Under the ideal conditions of uniform random particle spatial distribution and all particles measured, the relative conditional probability of measurement of a velocity, if it occurs, changes with velocity. This can be shown by considering the equation for particle arrival rate, $\dot{N}_0(v)$:

$$\dot{N}_0(v) = \rho\, A(\vec{v}) \tag{2.7.5}$$

where $A(\vec{v})$ is the measurable volume carried through per unit time, ρ is the particle number density, and, in general, $A(\vec{v})$ is proportional to $\vec{v}$. If the particles are uniformly spread in space, more particles per unit time will arrive at the probe volume for higher values of $\vec{v}$. On the other hand, if the particles are not uniformly distributed, the instantaneous rate of arrival will still be proportional to the local particle density and the instantaneous volumetric rate. Thus, according to this argument, bias will always be present in the particle arrival rate, even for ideal measuring

conditions, i.e. $\dot{N}_0(v) = \dot{N}_2(v)$. The aim of a biasing correction is to remove this bias from the measured density function so that the correct mean and rms of the velocity in the flow can be determined.

One can estimate whether particle bias is of concern in a particular instance, by using the formula derived by Buchhave (1975), using McLaughlin and Tiederman's (1973) theory:

$$\bar{v}_m \cong \bar{v}\left(1 + \sigma_v^2 / \bar{v}^2\right) \tag{2.7.6}$$

where the m subscript denoted the measured mean velocity, $\bar{v}$ is the true mean velocity and σ_v^2 is the flow variance. This expression states that the bias is on the order of the square of the turbulence intensity. However, the bias encountered in practice can be higher or lower than this (Edwards, 1981), and this expression should be used only to estimate the magnitude of the possible problem.

Some bias correction methods attempt to generate weighting factors for each of the individual velocity measurements used to compute the mean flow quantities. For example, these methods compute the corrected mean and r.m.s. as,

$$\bar{v} = \frac{\sum_N \frac{v_i}{h(v_i)}}{\sum_N \frac{1}{h(v_i)}} \tag{2.7.7}$$

$$\left(\overline{v'^2}\right)^{1/2} = \left(\frac{\sum_N \frac{(v_i - \bar{v})^2}{h(v_i)}}{\sum_N \frac{1}{h(v_i)}} \right)^{1/2} \tag{2.7.8}$$

where $h(v_i)$ is interpreted as an estimate of the probability of realization i. It is important to note that this is not the same as the relative sampling probability, $h_m(v)$ defined above. Equation (2.7.5) shows that the arrival

rate is not a function of the measured velocity component, but a function of the velocity vector. Therefore, different realizations which have the same v_i will usually have different realization probabilities $h(v_i)$, so that the relative sampling probability $h_m(v)$ is an average probability for all realizations with the same v_i.

Under the best of circumstances, both $h(v_i)$ and $h_m(v)$ are very difficult to estimate. Worse, the assumptions made to compute $h_m(v)$ are often not valid. For example, many times the seeding particle density is not uniform. In such cases, any bias correction applied to eliminate the effect of $h_m(v)$ may actually bias the data more!

2.7.3.1 Measurement Accuracy

In order to appropriately assess the presence of bias in a velocity record, the magnitude of the bias should be greater than the measurement error. The variance in the estimation of the mean in a turbulent flow is proportional to the flow variance, and inversely proportional to the number of *independent* samples of the mean (Edwards, 1986). The estimation of the number of independent samples is complicated by the fact that the laser anemometer signal is a random sample of random turbulence. Edwards (1986) shows that an estimate of the measurement error, independent of any bias present, is given by

$$\sigma_{\bar{v}}^2 = \frac{\sigma_v^2}{N}\left(1 + 2 < \dot{N}_2 > T_u\right) \tag{2.7.9}$$

provided that N is large. Comparing this with Buchhave's estimate of the bias error, Equation 2.7.6, the condition that the measurement error in the mean must be smaller than the bias yields,

$$N \geq \frac{\bar{v}^2\left(1 + 2 < \dot{N}_2 > T_u\right)}{\sigma_v^2} \tag{2.7.10}$$

The number of required measurements is a function of the turbulence intensity and the number of measurements per correlation time. Many of the reported measurements on velocity bias ignored or did not measure the flow correlation time and the mean data rate, so that it is impossible to estimate if they could detect bias. However, in many of the papers, the scatter in the plotted data is larger than the expected bias.

2.7.4 Other sources of bias

2.7.4.1 Filter Bias

This error occurs because of the tendency of real systems to have a measurement efficiency that is dependent on the speed of the measured particle. The experimenter must insure that the frequency response of his system is flat in the range of measurement. All velocities present in the flow must be measurable. No correction scheme can reasonably correct missing velocities.

2.7.4.2. Angle Bias (Fringe Bias)

This error is caused by the fact that real processors cannot measure all speeds at all angles. For instance, counters are usually set so that a preset number of fringes must be encountered by a particle before a measurement is considered valid. Even if a Bragg cell is used, there can exist particle trajectories that do not satisfy the processor's preset criteria. In a properly set system, there should not be velocities present that are outside of the measurable range. Buchhave et al. (1979) presents and extensive discussion of this problem. In order to provide uniform angular response, Buchhave et al. recommend that the effective fringe velocity should be at least twice the maximum Doppler shift. Also, reducing the number of required fringe crossings or using a variable number of fringes may help reduce the problem.

2.7.4.3 Gradient Bias

This error occurs if there is a mean gradient in the flow. The measurement volume is always finite in size and thus several velocities can be present in it at the same time. Like the case of velocity bias, the measurement rate for a given velocity can be correlated with that velocity, and the arithmetic average of the measurements will not be the same as the average in the measurement volume.

2.7.5 The Bias Correction Relation of McLauglin and Tiederman

McLaughlin and Tiederman (1973) were the first to recognize that the probability of the individual velocity measurements is biased. They proposed a simple correction method based on the following three assumptions:

- $|\vec{v}|$ is proportional to the magnitude of the instantaneous measured velocity component v.

- The flow is uniformly seeded.

- The probe volume is a sphere.

With these assumptions, the particle arrival rate becomes directly proportional to the magnitude of the measured velocity component $|\vec{v}|$. Therefore, we have,

$$h_m(v) = h(v_i) = |v_i| \tag{2.7.11}$$

and, from Equations 2.7.7 and 2.7.8,

$$\bar{v} = \frac{\sum_N \frac{v_i}{|v_i|}}{\sum_N \frac{1}{|v_i|}} \tag{2.7.12}$$

$$\overline{(v'^2)}^{1/2} = \left(\frac{\sum_N \frac{(v_i - \bar{v})^2}{|v_i|}}{\sum_N \frac{1}{|v_i|}} \right)^{1/2} \qquad (2.7.13)$$

These are the one-dimensional correction relations proposed by McLaughlin and Tiederman. They are extremely easy to employ, since the relative sampling probability need not to be measured separately. However, because of the assumptions introduced, the linear relation between h and v is strictly valid only for flows that are uniformly seeded and in which the flow direction is constant. These severe restrictions make the McLauglin-Tiederman correction formula inapplicable to general, three-dimensional, turbulent flows. Hoesel and Rodi (1977) and Gould et al. (1989) show that the McLaughlin and Tiederman correction does not give accurate mean velocities when the turbulence level is above 30% and that its ability to correct the rms values is doubtful at a turbulence level of 20%, even when measuring the main flow direction in boundary layer flows. Furthermore, problems arise when v_i is measured as zero within the experimental accuracy, since it appears in the denominator of Equations 2.7.12 and 2.7.13.

McLauglin and Tiederman also proposed a more elaborate correction method, in which assumption (1) above is removed and the magnitude of the measured (two or three component) velocity vector is employed to compute $h(v_i)$. This is equivalent to substituting $|v|$ by $|\vec{v}|$ in Equations 2.7.12 and 2.7.13. The three-dimensional version of this correction method is extremely cumbersome to implement, since few LDV systems record all three components of velocity simultaneously, and for three dimensional systems, coincidence bias has also to be taken into consideration. The assumptions of uniform seeding and a spherical probe volume make the correction doubtful.

The 1985 panel on Statistical Particle Bias Problems in Laser Anemometry could not agree to recommend any version of this correction method. The

McLaughlin and Tiederman correction can sometimes increase the error over that obtained in applying no correction.

2.7.6 Residence Time Weighting.

This method was proposed independently by Hoesel and Rodi (1977) and by Buchhave (1979), and Buchhave et al. (1979). The amount of time that a particle spends in the measurement volume is measured in addition to the particle's velocity. The arguments presented by Hoesel and Rodi differ from those presented by Buchhave et al. The former, being more intuitive, will be presented first.

For uniformly seeded flows, based on Equation (2.7.5), Hoesel and Rodi argue that the number of particles passing through the probe volume per unit time, $\dot{N}_0(v)$ is a constant proportion of the measurable volume flow $A(\vec{v})$. They also assume ideal measuring conditions, that is, $\dot{N}_2(v) = \dot{N}_0(v)$, and thus $h(v_i) \cong A(\vec{v})_i$, where $A(\vec{v})_i$ is the volume flow at the time of each realization i. To estimate $A(\vec{v})_i$, they propose to use the *average* "residence time" that particles of velocity $\vec{v}$ spend within the probe volume, $\overline{\Delta t(\vec{v})}$, together with the relation,

$$A(\vec{v}) = V_p / \overline{\Delta t(\vec{v})} \tag{2.7.14}$$

that is, the volumetric flow when the velocity is $\vec{v}$ is inversely proportional to the *average* particle residence time.

Hoesel and Rodi show that the probe volume V_p does not depend on the velocity vector $\vec{v}$. If the residence time were only a function of $\vec{v}$, then $A(\vec{v}) = A(\vec{v})_i$. However, residence time depends also on the trajectory of the particle through the probe volume. Fortunately, since all the averaging process is linear, $\overline{\Delta t(\vec{v})}$ can be replaced by $\Delta t(v_i)$ in Equation 2.7.14 to obtain an estimate of $A(\vec{v})_i$, and thus, the weighting function $1/h(v_i) \cong \Delta t(v_i)$. This

substitution can be performed provided that the number of samples is very large. The bias free estimates are then obtained using the relations,

$$\bar{v} = \frac{\sum_N v_i \Delta t(v_i)}{\sum_N \Delta t(v_i)} \tag{2.7.15}$$

$$\overline{(v'^2)}^{1/2} = \left(\frac{\sum_N (v_i - \bar{v})^2 \Delta t(v_i)}{\sum_N \Delta t(v_i)} \right)^{1/2} \tag{2.7.16}$$

In an alternate derivation, Buchhave et al. (1979) formally writes the measured velocity as

$$v_m(t) = \int w[\vec{x}(\vec{a},t)] v(\vec{a},t) g(\vec{a}) d^3\vec{a} \tag{2.7.17}$$

where v is the velocity of the particle that was at $\vec{a}$ at $t=0$, $g(\vec{a})$ is a function that accounts for the presence (or absence) of a particle at $\vec{a}$, and the function w is defined such that $w(0)=1$ and can be taken to specify the spatial extent of the probe volume, i.e.,

$$V \equiv \int w(\vec{x}) d^3\vec{x} \tag{2.7.18}$$

and $d^3\vec{x}$ is the volume differential. Equation 2.7.17 reproduces the instantaneous velocity of the scattering particle only while it is in the scattering volume, that is $v_m = v$ only while there is a particle in the probe volume. Mapping from the Lagrangian frame to the Eulerian frame,

$$v_m(t) = \int w(\vec{x}) v[\vec{x}(\vec{a},t)] g_1(\vec{x},t) d^3\vec{x} \tag{2.7.19}$$

where,

$$\vec{x} = \vec{a} + \int_0^t \vec{v}(\vec{a},t_1) dt_1 \tag{2.7.20}$$

and $g(\vec{a}) \rightarrow g_1(\vec{x},t)$. The statistics of $g_1(\vec{x},t)$ for statistically uniform seeding to second order can be shown to be given by (Buchhave, 1979),

$$\overline{g_1(\vec{x},t)} = \rho \tag{2.7.21}$$

$$\overline{g_1(\vec{x},t)g_1(\vec{x},t)} = \rho\, p(\vec{x},t|\vec{x}',t') + \rho^2 \tag{2.7.22}$$

where $p(\vec{x},t|\vec{x}',t')$ is the probability that the particle at $\vec{x}$ has moved to $\vec{x}'$ at time t' and ρ is the expected number of particles per unit volume. An excellent approximation to $p(\vec{x},t|\vec{x}',t')$ is:

$$p(\vec{x},t|\vec{x}',t') = \Delta(\vec{x} - \vec{x}' - \vec{v}\tau) + \rho^2 \tag{2.7.23}$$

Substitution of these relations in Equation 2.7.19 and taking the average yields,

$$\overline{v_m(t)} = \int \overline{v(\vec{x},t)} w(\vec{x}) d^3\vec{x} \tag{2.7.24}$$

For the simple case of $\overline{v(\vec{x},t)}$ independent of $\vec{x}$ and $w(\vec{x}) = 1$ within the volume and zero outside,

$$\overline{v_m(t)} = \rho V \overline{v(\vec{x},t)} \tag{2.7.25}$$

Assuming that averages are determined by time averaging,

$$\overline{v_m(t)} = \frac{1}{T}\int_0^T v_m(t)dt = \frac{\rho V}{T}\int_0^T v(\vec{x},t)dt \cong \rho V \overline{v(\vec{x},t)} \tag{2.7.26}$$

Thus,

$$\overline{v(\vec{x},t)} \cong \frac{1}{\rho VT}\int_0^T v_m(t)dt \tag{2.7.27}$$

ρVT is exactly the fraction of time that the signal $v_m(t)$ is nonzero. Thus, the correct mean is given by averaging only during those periods where there is a signal. Most processors measure the average velocity during the burst. Since there is only a single realization during each particle passage, then the realization must be weighted by the time the particle would contribute to the integral, that is the residence (or transit) time. Thus, Equation 2.7.15 is recovered. A similar argument for the r.m.s. yields Equation 2.7.16.

In general, residence time correction methods are very difficult to implement since the total length of each Doppler burst must be recorded. When frequency shifting is used -as will always be the case at high turbulence levels - most processors will exhibit fringe count overflows, which make accurate residence time determinations impossible (Gould, et al., 1989). Most off-the-shelf counters do not always give accurate burst times.

This method has a qualified recommendation of the 1985 special panel on statistical particle bias problems in laser anemometry. The limitations are that the particle seeding density has to be spatially uniform, that filter bias is not present and that the processor gives an accurate estimate of the residence time.

For non-uniformly seeded flows, Hoesel and Rodi also employ Equations 2.7.15 and 16, but $\Delta t(v_i)$ is interpreted as the time between a high quality burst (validated) and the next detectable low quality burst (usually not validated). This implicit assumes that the concentration of particles generating the high quality bursts is proportional to the concentration of particles generating the low quality bursts, and that the velocity of the fluid is constant in the time between the two realizations. This method was not reviewed by the 1985 panel.

2.7.7 The Controlled Processor

Erdmann and Tropea (1981) and Edwards (1981) show that if the detector attempts to make measurements in regular intervals, the statistical bias is a function of the product of the particle density, ρ, and the sample interval T - in strong contrast to the predicted behavior of systems that make a measurement for every particle the detector sees. Edwards shows that the statistical bias is a minimum when the detector obtains a measurement every sample period. His argument will be presented below.

Let L be the length of the probe region. A particle must traverse it completely in order to be measured. Consider a processor that attempts one velocity measurement every time interval T. The particles have a Poisson distribution in space, so that the expected number of particles in a volume L' is $\rho L'$. Thus, the probability of there being at least one particle in a volume L' is $1-\exp(-\rho L')$. The available volume to be sampled during each measurement is $|\vec{v}|T-L$ since a particle must traverse L before it is measured. The probability that there was at least one particle present in that volume is

$$1-\exp\left(-\rho(|\vec{v}|T-L)\right) \tag{2.7.28}$$

The probability of measuring a velocity v during any one T is thus

$$\begin{cases} p(v)\left(1-\exp(-(\rho|\vec{v}|T-L)\right)dv, & |\vec{v}| \geq L/T \\ 0, & 0 \leq |\vec{v}| < L/T \end{cases} \tag{2.7.29}$$

$p(v)$ is the velocity probability density function. The two regions of v reflect the fact that no measurement is made if the particle does not cross at least a distance L. The probability density merely shows the fact that the larger the volume swept through the sample region L, the higher the probability of finding at least one particle in it. Note that it predicts a decreased bias in the limit $\rho \to \infty$, independent of the turbulence field described by $p(v)$, since the probability density tends to just $p(v)dv$ in this

limit. Furthermore, the error tends to zero as the ratio of the average velocity to the minimum measurable velocity, $\bar{v}t/L$, increases.

The controlled processor divides time into equally spaced intervals of T seconds. Only the first particle measured during each time interval is stored and used in the subsequent algorithms. When the time interval T is small compared to the flow microscale $T << T_\lambda$ and the data density is high for all velocities of interest ($\dot{N}_2 T > 5$), the procedure approaches that of uniform sampling of a continuous data record with time interval T. Hence, one can construct a time series whose statistics are indistinguishable from those of the flow. Essentially, the rate is high enough that a measurement is obtained for every measurement interval, making the sampling procedure independent of the velocity. Of course, any flow information above a frequency of $(2T)^{-1}$ is lost because of the sampling procedure.

This method was recommended by the 1985 special panel on statistical particle bias problems in laser anemometry for situations in which there are high data rate densities. With the proviso that the filters are set so that the data density for all velocities present in the flow exceed the requirements set above, the processor is also insensitive to the distortions caused by filter bias errors.

The measurements performed by Gould et al. (1989) of the turbulent flow past a sudden expansion in a circular tube provide experimental confirmation for this technique. They show that bias can be reduced if two conditions are met simultaneously: that the counter's data validation rate be three times larger than the turbulent Taylor microscale and that the effective sampling rate be less than 10% of the data validation rate.

2.7.7.1 Controlled Processor in Low and Intermediate Seeding Rate Systems

Erdmann and Tropea (1981) claim that the controlled processor can eliminate velocity bias at any data density, if the sampling time is increased so that the probability of getting a measurement every interval

is high. This claim has never been experimentally verified. Further work in this area is needed.

2.7.8 The Saturable Processor

The data logger will record no additional measurements for a time T after a measurement is recorded. This system attempts to store all the measurements for processing, but contains a rate limiting device. Because of this device, some measurements may be lost when the particle rate is high. A finite speed computer buffer behaves this way. It can only record another reading when the buffer is "ready".

Edwards (1983) presents an expression to approximate the conditional probability of recording a measurement if the velocity is v, $h_m(v)$, when using this processor. They show that

$$h_m(v) = \frac{\dot{N}_2(v)}{<\dot{N}>} = \frac{\dot{N}_0(v)}{<\dot{N}>} \frac{\left(1+<\dot{N}>T\right)}{\left(1+<\dot{N}>\left(T-T_u(T)\right)+\dot{N}_0 T_u(T)\right)\omega} \qquad (2.7.30)$$

where $T_u(T) = \int_0^T R_{uu}(\tau)d\tau$, (that is, $T_u(\infty) = T_u$), and ω is a normalization constant.

For $T << T_u$ and $\dot{N}_0 T >> 1$ (many particles arrive during the reset time), Equation 2.7.30 predicts that this processor will generate a time series that has statistics identical to those of the flow ($h_m(v) = 1$).

This method was recommended by the 1985 special panel on statistical particle bias problems in laser anemometry for situations in which there are high data rate densities. Again, given that all velocities present in the flow are measured at the appropriately high rate, this method is also insensitive to filter bias errors.

2.7.9 Sample and Hold

In this method, a continuous analog signal is created by holding the last measurement until a new measurement is obtained. Variations of this scheme include interpolating between measuring points by a trapezoid or other spline fit, and the use of a backward step algorithm. When the data density is high ($\dot{N}_2 T_\lambda > 5$) the statistics of the reconstructed signal are identical to those of the flow up to a frequency of $1/\dot{N}_2$ (Dimotakis, 1976, Edwards and Jensen, 1983, Adrian and Yao, 1987). In this case, the approximate integration schemes are good approximations to the continuous integrals.

This method places less stringent conditions on the particle rate than does attempting to saturate the system. Saturation requires both $T << T_u$ and $\dot{N}_2 T >> 1$, whereas the sample and hold method only requires $\dot{N}_2 T >> 1$.

This method was recommended by the 1985 special panel on statistical particle bias problems in laser anemometry for situations in which there are high data rate densities. Again, given that all velocities present in the flow are measured at the appropriately high rate, this method is also insensitive to filter and bias errors.

2.7.10 Rate Measurements

Here the measurement rate corresponding to each velocity is either computed or measured. The computational method consists of consists of computing $\dot{N}_0(v_i)$ (Dimotakis, 1976), the expected arrival rate for the ith velocity realization v_i from the theoretical model. One then assumes that the measurement rate for each velocity is proportional to $\dot{N}_0(v_i)$. The corrected mean and r.m.s. are found from Equations 2.7.7 and 2.7.8 setting $h(v_i)$ equal to $\dot{N}_0(v_i)$.

An alternate method is given by Edwards (1986). He argues that one cannot measure $\dot{N}_2(v_i)$ (and thus $h_m(v)$) by measuring mean particle

interarrival times. However, *estimates* for $r_m(v)$ can be obtained by examining the data rate for times that are small compared to the Taylor microscale.

In a turbulent flow the probability of getting two or more measurements of the same velocity is very small. Thus, in order to estimate the measurement rate, a histogram of velocities has to be constructed using a finite number (say H) of non-overlapping velocity ranges Δv_H. These ranges can be arranged so that each range contains at least two measurements. Roughly, if N_h is the total number of measurements in any given interval h, the relative error in the estimated rate is $1/\sqrt{N_v}$, if each measurement is independent.

In the worse case, an estimate of the worse fractional change of the rate over a velocity range Δv_H is $\Delta v_H / v_h$, where v_h is the average velocity of the interval. This result is obtained assuming a rate proportional to the velocity, following McLaughlin and Tiedermann's one dimensional model (see Equation 2.7.5). Most other models yield a weaker dependence on velocity. Let Δv_R be the entire range of measured velocities, or four standard deviations, whichever is larger. The change in rate in each interval compared to the change across the entire velocity range is then roughly $\Delta v_H / \Delta v_R$.

For a real data set with a finite number of measurements, the above considerations place contradictory requirements on the selection of Δv_H. An accurate estimation of the rate within each range demands a large number of sample measurements, and thus a Δv_H as large as possible. On the other hand, accurate resolution of the change of rate across the measurement range requires a small Δv_H. Based on experimental results, the compromise value of $\Delta v_H / \Delta v_R = 1/9$ is recommended by Edwards.

In order to determine rates, a time interval T has to be selected. Edwards recommends to choose T to be the average time the velocity stays within a histogram velocity interval. To determine this value, pick a velocity from the data set and then search successive data points until the first velocity

value lying outside the initial velocity's histogram interval is found. Record the time of this interval. Repeat this procedure, starting with the velocity that was outside the interval. After the whole data set is scanned in this fashion, average the recorded time intervals.

Given Δv_H and T, the measured rate $\dot{N}_2$ is estimated using the following procedure:

- Pick a velocity v_i.

- Assign it to the appropriate histogram interval v_h.

- Measure and record the number of measurements that occur within T seconds after that measurement. Keep a separate sum for each v_h.

- Skip to the next measurement occurring over T seconds later.

- Repeat the above procedure until the data set is exhausted.

Let N_h be the total number of measurements for the histogram interval h, and let l_h be the number of times that the interval h was encountered in the above procedure. Then, the average measurement rate $\dot{N}_2(v_h)$ is given by $N_h/(l_h t)$.

The corrected velocity distributions can be computed using Equations 2.7.7 and 2.7.8, setting $h(v_i) = \dot{N}_2(v_h)$, where h is the velocity interval corresponding to v_i. Alternately, a corrected histogram $p(v_h)$ can be computed from the measured histogram $p_m(v_h)$,

$$p(v_h) = \frac{p_m(v_h)/\dot{N}_2(v_h)}{\sum_N p_m(v_h)/\dot{N}_2(v_h)} \tag{2.7.31}$$

This corrected histogram can be used to compute an unbiased estimate of the Eulerian flow statistics.

Dimotakis' method had the qualified recommendation of the 1985 panel on statistical particle bias problems in laser anemometry. The qualifications are that a uniform spatial particle seeding must be assured and that filter bias effects are negligible. Edwards' method was recommended for high and intermediate data densities $\dot{N}_2 T_\lambda > 0.05$. Provided that all velocities present in the flow are measured with a high enough rate, this method is insensitive to filter bias effects.

2.7.11 Additional recommendations of the 1985 panel (Edwards, 1987).

All relevant parameters must be known, recorded and reported in order to assess the reliability of the measurements.

Seeding Parameters: The uniformity of the seeding and the average particle number density should be reported. The mean measurement rates, $\dot{N}_{2,3}$, should be reported along with estimates of T_λ. The effective particle size distribution must also be reported, as well as the method used to estimate it.

System Parameters: The properties of the data recorder, such as speed and capacity, should be reported. The processor settings, such as number of fringes required for a successful measurement, the Bragg cell frequency, the filter settings and the deadtime should also be reported. The type of processing scheme should also be reported.

2.7.12 Discussion

Velocity bias is still an important fundamental issue in laser Doppler velocimetry. Although this survey has revealed many inconsistencies in the published literature, in recent years efforts have been made to try to standardize notation and terminology in order to avoid confusion. Several reliable techniques exist to deal with the velocity bias problem in cases where data densities are high. For moderate and low data densities, there

are no comparable techniques to adequately process the data. Work is needed in resolving related issues, like filter, gradient and angle bias. Experimental testing of existing techniques and development of new ones are needed for cases in which the data density is low.

In the measurement of turbulent two phase flows, the velocity of each size class must be corrected for velocity bias. However, the number density of each size class of the dispersed phase is such that the uniform time sampling method cannot be used to effectively eliminate or even mitigate the velocity bias error. It is also difficult to achieve sustained high seeding rates as required by the uniform time interval sampling even when measuring the velocity of the continuous phase. Thus, the rate measuring techniques and simple, empirical-based corrections are of considerable interest.

Software has been developed for the Aerometrics PDPA to enable investigations along the approaches of Gould et al., (1986) and Edwards (1986). The PDPA signal processor can acquire data at up to 100 KHz and store the particle size, velocity, and time of arrival of each particle.

Knowing the data validation, any selected sampling rate can be used to reprocess the data to obtain information on velocity bias. This is accomplished by selecting a sampling interval and a window over which samples will be selected and averaged. The advantage of the present software is that the same data can be processed using different sampling criteria.

The issue of velocity bias and bias corrections remains open. Despite the somewhat extensive efforts that have been expended on this question, the experts in this field openly admit that no conclusions or recommendations can be made on which bias correction, if any, that should be used. It has been suggested by Edwards (private communication) that with the advanced signal processing and the available software, the Aerometrics DSA could be used in some carefully designed experiments to resolve some of the remaining discrepancies in the previous results. However, there are some issues which will be difficult to overcome. For example, to have a

mean particle rate that meets the requirement of resolving even the integral length scales of the turbulence will lead to significant coincidence rejections. This can be overcome by accepting measurements from only a selected small segment of the signal which is now possible with the DSA. Furthermore, the DSA electronics have been designed to measure the burst length accurately irrespective of how much of the signal is processed.

Thus, many of the concerns with the application of the residence time weighting approach have been eliminated. Another uncertainty is the change in the burst length with particle size. Although the seed particle size range may be small (0.5 to 3 μm), the light is scattered approximately as d^4, so the amplitude range is approximately 1000 to 1. As is known from the discussion on sample volume characterizations, the sample volume and hence, the transit time, will vary significantly with particle size. This problem can be examined by simultaneously measuring the seed particle size to determine whether this phenomenon has a significant effect on the results.

Experiments were conducted using the controlled processor or uniform time interval sampling approach. However, these tests were conducted with the counter processor since the DSA was still under development. At seeding rates that were high enough to resolve the small scale velocity fluctuations, the gate times and the inter-particle arrival times became uncertain. At lower seeding rates, there was no apparent difference in the results for turbulence intensities up to 20 %. These results were by no means conclusive.

Future work is planned to extend the axisymmetric jet measurements to not only cover the particle response to turbulence but also to aid the understanding of the velocity bias question. Some final features of the software and hardware, initiated in part under this program, need to be incorporated into the system and tested. The parameters to be varied are the particle seeding rate, the flow velocity, and turbulence intensity. Each of the methods described will be used to examine the same data sets, and the results will be compared to the classical jet flow data and the mean flow velocity calculated from the jet flow parameters.

2.8 Gas Phase Turbulence Measurements In Two-Phase Flows

Extensive work was carried out in the development and application of the phase Doppler method to turbulent two-phase flows and specifically, spray interaction with complex turbulent flows. This has been a very significant capability made possible by the development of the phase Doppler method. In exercising this capability, a number of areas needed to be examined to minimize the errors in the application of the method. Many of the considerations are similar to those experienced in the application of the standard LDV. These include the need to have sufficient fringe crossings to process all signals irrespective of the angle of trajectory. This problem also affects the sample volume characterization which is discussed in another section. Also, the problems of biasing of the turbulence measurements due to particle concentration gradients needed to be addressed. Concentration gradients can bias the sampled velocities toward that part of the flow field having the highest particle concentration. This problem is more likely in turbulent two-phase flows because of the local injection of the spray and the difficulty of uniformly seeding these flows.

The questions addressed were as follows: can the gas phase turbulence be measured simultaneously with the dispersed phase, what can be done to address the affects of the inevitable particle concentration gradients, and can the particle drag coefficient be derived in complex turbulent flows. An important study that relates to the first question is how large can the particles be and still respond adequately to the gas phase mean velocity accelerations and the turbulence fluctuations? This question has a much broader interest to the general application of the LDV in turbulent flow measurements. Thus, a good deal of effort was expended on this topic under this program and a related contract with the NASA Lewis Research Center.

The problem of measuring the gas phase turbulence simultaneously with the dispersed phase is that the particles that will track or represent the

gas phase turbulence have been assumed to be 1 μm or less in diameter. The dispersed phase particles can be as large as 200 μm or larger. This represents a very large signal amplitude dynamic range. Furthermore, particles on the order of 1 μm scatter light in proportion to the diameter to the fourth power. Thus, it is all but impossible to simultaneously detect the seed particles and measure the dispersed phase. The obvious question was whether or not larger particles (eg. particles as large as 10 μm) would track the flow and if so, under what conditions. If larger particles would represent the turbulence parameters, this would significantly reduce the dynamic range requirements of the instrument. To establish the largest particle that would adequately track the gas phase turbulence, a series of studies were conducted. These studies included the measurement of the particle velocity response (mean velocity and rms velocity) under flow conditions representative of gas turbines and other combustor flow conditions.

The early studies conducted consisted of generating a spray behind a bluff body in our wind tunnel. The bluff body produced a highly turbulent flow with a significant mean flow accelerations and re-circulation. A range of drop sizes was available, and, in some instances, the flow was also seeded with micron-sized particles. Thus, the turbulence could be well-characterized by the small particles (O(1 μm). The response of the larger particles could then be assessed by simultaneously measuring their size and velocity and comparing the mean and rms velocities. This investigation showed that particles as large as 5 μm would track the turbulence fluctuations and mean velocity accelerations (Rudoff et al., 1987). Furthermore, studies of the drop drag coefficient were conducted to verify the established drag correlations and to determine whether the correlations were valid in polydispersed particle fields and in turbulent flows (Rudoff et al. 1991). These studies led to the further observation that it may be possible to use larger particles to infer the gas phase mean and turbulence parameters by using the response of a range of particle size classes. This concept will be described in the following paragraphs along with the analyses and results.

The question of particle lag arises in both single phase flows using the LDV and, more critically, in two-phase flows using the phase Doppler instrument. It must be accepted that particles will lag the gas phase flow if there are flow accelerations and turbulence present unless the particles are neutrally buoyant. This statement is true because it is the relative velocity between the particle and the flow that produces the restoring drag force on the particles. The degree of this particle lag depends upon the particle size and density as well as the particle Reynolds number. Anticipating the need to obtain measurements in high speed flows, the analyses were carried out for flows from low speed to sonic velocity.

The approach used to examine the behavior of particles in a turbulent flow involved the use of a turbulent jet in which a polydispersion of particles was entrained, figure 2.8.1. The size and velocity of the particles were measured, figure 2.8.2, using the DSA which was, by now, highly developed. The particles in the size class of 0.5 to 1 μm were considered to accurately track the mean velocity and turbulent fluctuations. A parallel analysis was conducted to describe the expected response of the particles to the turbulent flow. The measurements would then be used to evaluate the analysis and determine whether or not the behavior of the larger particles can be extrapolated to establish the actual gas phase mean and turbulence intensity.

It is first necessary to establish the particle response criteria. This can be obtained from the paper by Hinze, 1972. The momentum balance equation is used with the velocity difference $U = u - v$ where u is the particle velocity and v is the local velocity of the gas. The drag of an unsteady or turbulent flow on the particle is assumed to consist of a steady flow condition and a relaxation term which accounts for the unsteady change in the flow. This latter component is normally disregarded. The steady flow drag is described as

$$D = f(Re_d)\, d\, \mu\, U \qquad (2.8.1)$$

where d is the particle diameter and μ is the dynamic viscosity. For very low Reynolds number, the Stokes drag law , $f(Re_d)$ = Const holds. In

general, the drag correlation, $C_d = 24/Re_d + 0.44$ is an adequate estimation. With this resistance law, the momentum equation is used to arrive at the particle characteristic response as

$$\tau = \frac{d_p^2}{3\nu}\left(\frac{2\rho_p + \rho}{3\rho}\right) \tag{2.8.2}$$

where ν is the kinematic viscosity, ρ is the fluid density, ρ_p is the particle density, and d_p is the particle diameter. This relationship also assumes that the ratio of the fluid to particle density is small.

The bounds on the particle response requirements in a turbulent flow can be estimated. It is well-known that the turbulence consists of a continuum of scales from the small scale or Kolmogorov scales to the large scale eddies. For the high wave number part of the turbulence energy spectrum, the basic parameters describing the turbulence are the kinematic viscosity, ν and the viscous dissipation per unit mass, ε. The Kolmogorov time scale is then given as

$$\tau_k = \left(\frac{\nu}{\varepsilon}\right)^{\frac{1}{2}} \tag{2.8.3}$$

For an axisymmetric free jet, Friehe, Van Atta, and Gibson, 1971, provide the following correlation for the turbulent dissipation rate

$$\varepsilon\frac{D}{U^3} = 48(x/D)^{-4} \tag{2.8.4}$$

where D is the jet diameter. Using this expression with the above characteristic times leads to the expression

$$\frac{\tau}{\tau_k} = 0.38\,Re_D^{\frac{3}{2}}\left(\frac{x}{D}\right)\left(\frac{d_p}{D}\right)^2\left(\frac{\rho_p}{\rho}\right) \tag{2.8.5}$$

As stated by Hinze, 1972, for the particle to respond to the small scale eddies, $d_p/\eta < 1$ where

$$\eta = \left(\nu^3/\varepsilon\right)^{\frac{1}{4}} \tag{2.8.6}$$

is the Kolmogorov microscale. Hinze also notes that for large values of ρ_p/ρ, the particles should be an order of magnitude smaller than the Kolmogorov microscale length. In the present case, τ/τ_k will be set equal to 1 which leads to the following expression base on the above equations

$$\frac{d_p^m}{D} = 1.6\left(\frac{x}{D}\right)\left(\frac{\rho}{\rho_p}\right)^{\frac{1}{2}}\left(Re_D\right)^{\frac{-3}{4}} \tag{2.8.7}$$

where x is the axial distance from the jet exit. This expression provides a means of estimating the response of particles to the small scale turbulence but more important, it illustrates the parameters that influence the particle response.

In the case of the large energy-containing eddies, the characteristic time scale can be estimated (Hinze, 1972) Λ/u' with Λ being the integral length scale. With the appropriate viscous drag law, Hinze arrives at the following expression

$$\frac{d_p^m}{\Lambda} = \left[\frac{u'\Lambda}{\nu}\left(\frac{\rho_p}{\rho}+\beta\right)\right]^{-\frac{1}{2}} \tag{2.8.8}$$

where u' is the rms velocity fluctuations and $\beta = 1 + \rho/\rho_p$. Since ρ/ρ_p is small, $\beta = 1$ is a reasonable approximation. For a subsonic jet of exit diameter, D, emanating into still air at exit velocity v, the above expression reduces to

$$\frac{d_p^m}{D} = \left[\frac{C}{\frac{u'}{v} Re_D (1 + \frac{\rho_p}{\rho})} \right]^{\frac{1}{2}} \qquad (2.8.9)$$

where C is an empirical constant equal to 0.4, u'/v is the actual turbulence intensity and Re_D is the jet exit Reynolds number.

Using the above equations, the estimates for the largest particles that will respond adequately to the Kolmogorov and the integral length scales of the turbulent eddies respectively. These values are tabulated for the jet velocities considered in the experiments and presented in Table 2.8.1.

U (m/s)	d_p (μm) Kolmogorov	d_p (μm) Large Scales
42	0.42	5.4
55	0.34	4.7
64	0.30	4.4
84	0.25	3.8
104	0.21	3.4
135	0.17	3.0
150	0.16	2.9
182	0.14	2.6
191	0.13	2.5
221	0.12	2.4
254	0.11	2.2
273	0.1	2.1
300	0.1	1.9

Table 2.8.1

Before discussing the approach as applied to turbulence intensity measurements, the results for the mean velocity correction will be

discussed. A number of experiments have been conducted at Aerometrics relating to particle lag. The results of these studies showed that the simultaneous measurement of the particle size and velocity could be used to correct for the particle lag and obtain the actual gas phase velocity, (Jones, et al. 1990). The method involved the measurement of the particle velocity at a number of axial stations in a decelerating flow, figure 2.8.3. By measuring the particle response and size as well as knowing the particle density and the fluid density, this information could then be used with the particle drag coefficient and equation of motion to establish what the velocity of the gas was at each location. Applying this method showed that excellent results describing the fluid flow could be obtained for particles that otherwise showed a large lag.

The method also worked in high speed flows. More work was required in evaluating the drag coefficient when the the drop Reynolds number, Re_d is larger than the values for which the original correlations were generated. This work was completed by Rudoff et al., 1991 (see appendices), and showed good agreement with the correlation equation.

A similar concept for correcting the turbulence intensity measurements was the object of this study. Thus, the mean velocity and turbulence intensity was measured for a range of jet velocities. The rms velocities for each exit velocity condition were recorded. Although the analysis provides an idea of the parameters that affect the particle response to the turbulence and may even provide bounds to the particle response, the requirement of the particle in responding to the turbulent fluctuations is, in fact, not well-known. The particles are moving with the turbulent eddies whereas the turbulence measurements are made in an Eulerian frame using stationary probes. Thus, the results of these studies will provide the much needed information on the particle dynamics requirements in turbulent flows.

Figures 2.8.4 through 2.8.8 show the size-velocity correlation plots at representative jet exit velocities. These results are interesting in that they show the sizes of the particles that appear to stop tracking the larger velocity excursions. Although the data are not conclusive, the results

suggest that there is agreement with the response estimated from the analysis. For example, at an exit velocity of 42 m/s, the largest particles estimated to track the flow is 5.4 μm. Looking at figure 2.8.6, the velocity spread for each particle size class appears to decrease between 5 and 6 μm. This is especially true of the high velocity excursions. At 84 m/s, the estimated largest particle to track the velocity fluctuations was 3.8 μm. Figure 2.8.7 shows that the velocity excursions begin to decrease at about 4 μm. At 182 m/s, the largest responsive particle was estimated to be 2.6 μm whereas figure 2.8.8 shows that the velocity excursions appear to start dropping at around 3 μm. Unfortunately, in this case, the population of small particles was not high enough to provide a good distribution to properly show the response.

The bulk turbulence intensities were plotted in figure 2.8.9 estimated from each size class for a range of jet exit velocities. Although there is some considerable scatter in these preliminary data, there are clear trends in the particle response to the gas phase turbulence intensity. At high jet exit velocities, only the particles of less than 1 μm in diameter could respond adequately to the gas phase turbulence fluctuations. Focusing one's attention on the case for an exit velocity of 273 m/s, as an example, it is easy to see that there is a monotonic decrease in the reported turbulence intensity with increasing particle size. The question is whether the actual turbulence intensity (which is reported by the 0.7 μm particles) can be predicted from the rms velocities of the larger particles but with a correction procedure. These data will be used to attempt to derive a correlation equation to describe the particle response to the turbulence.

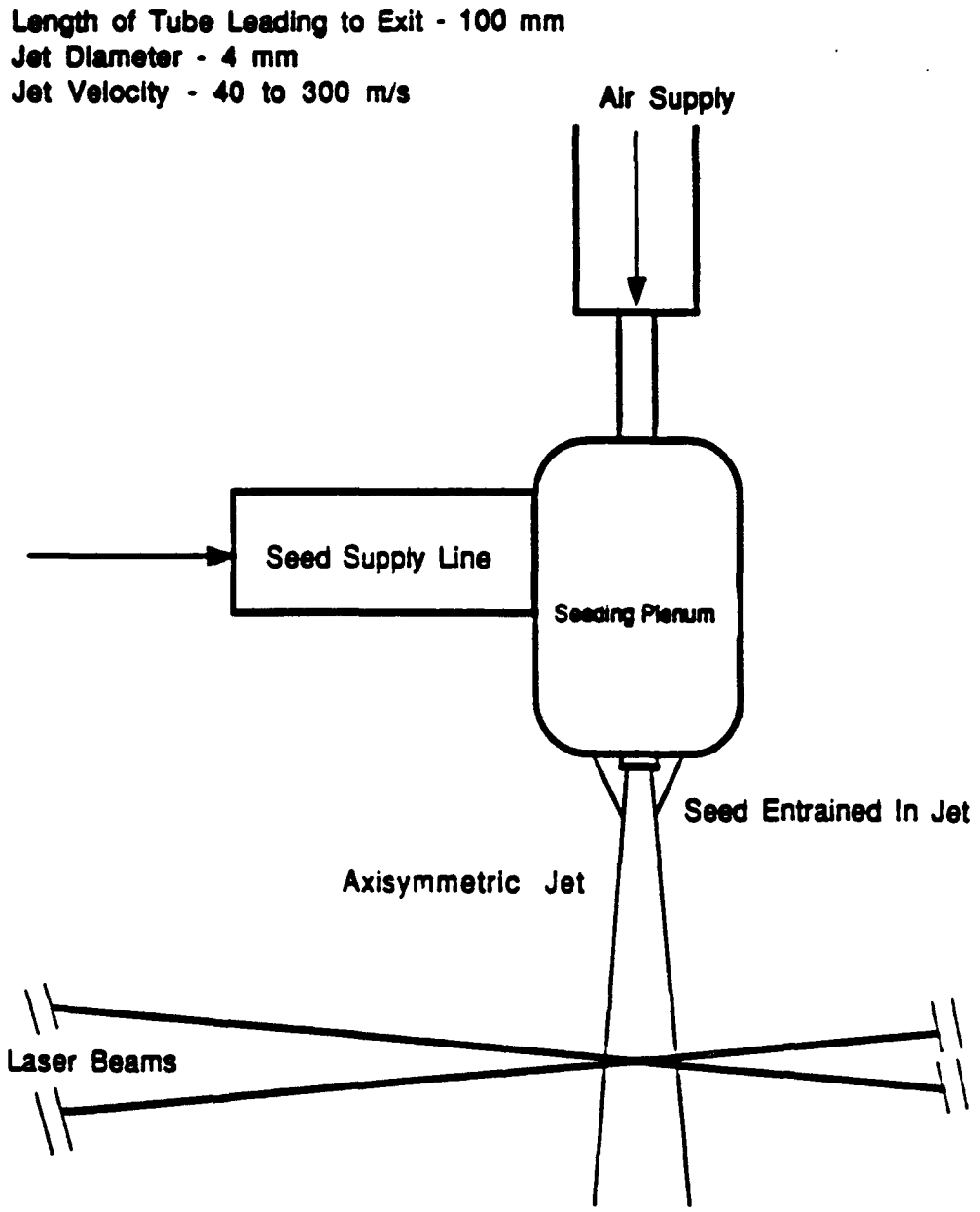

Figure 2.8.1: Schematic of the particle response study using a turbulent axisymmetric jet flow.

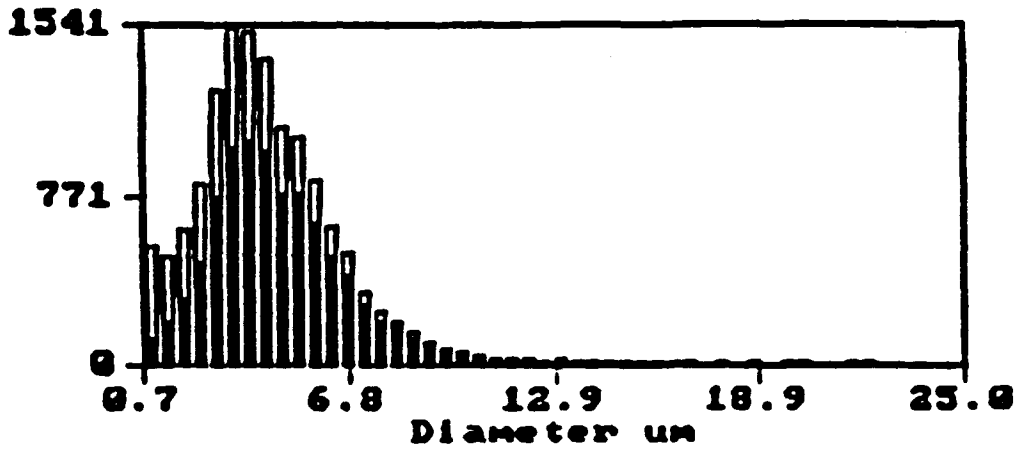

Figure 2.8.2: Size distribution of seed particles.

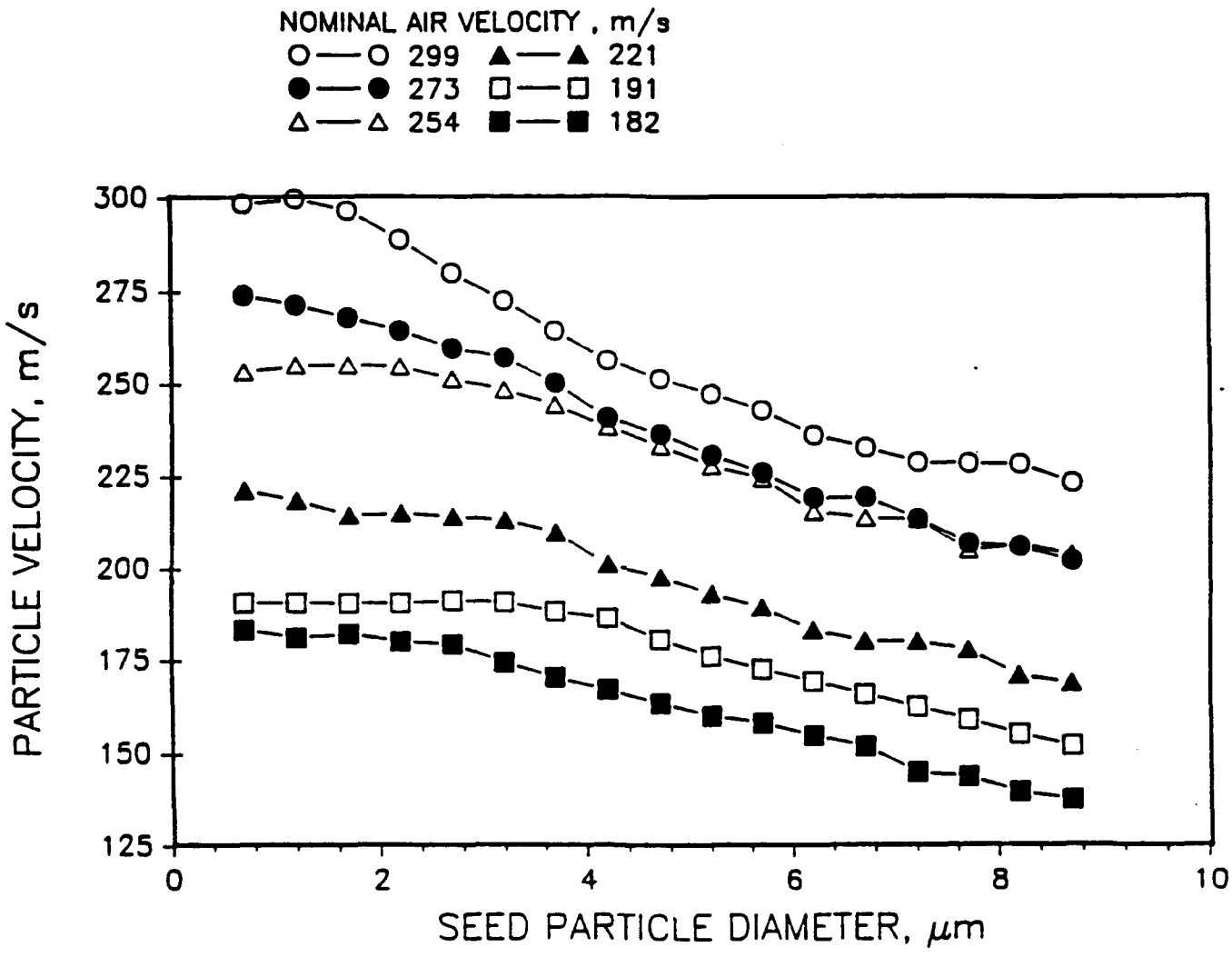

Figure 2.8.3: Example of size-axial velocity response in a turbulent flow.

Size - Velocity Correlations

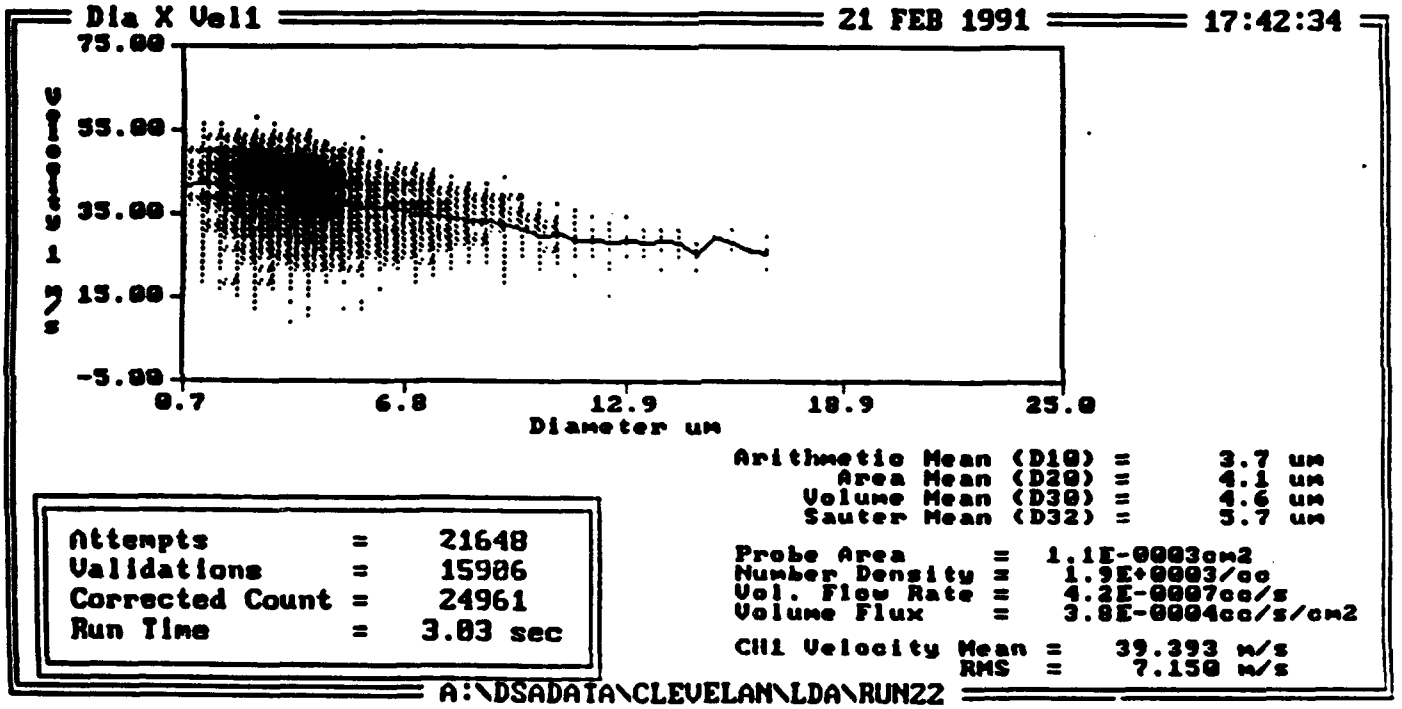

Figure 2.8.4: Particle size-velocity correlation at x/D = 2.0 and a jet velocity of 42 m/s.

Size - Velocity Correlations

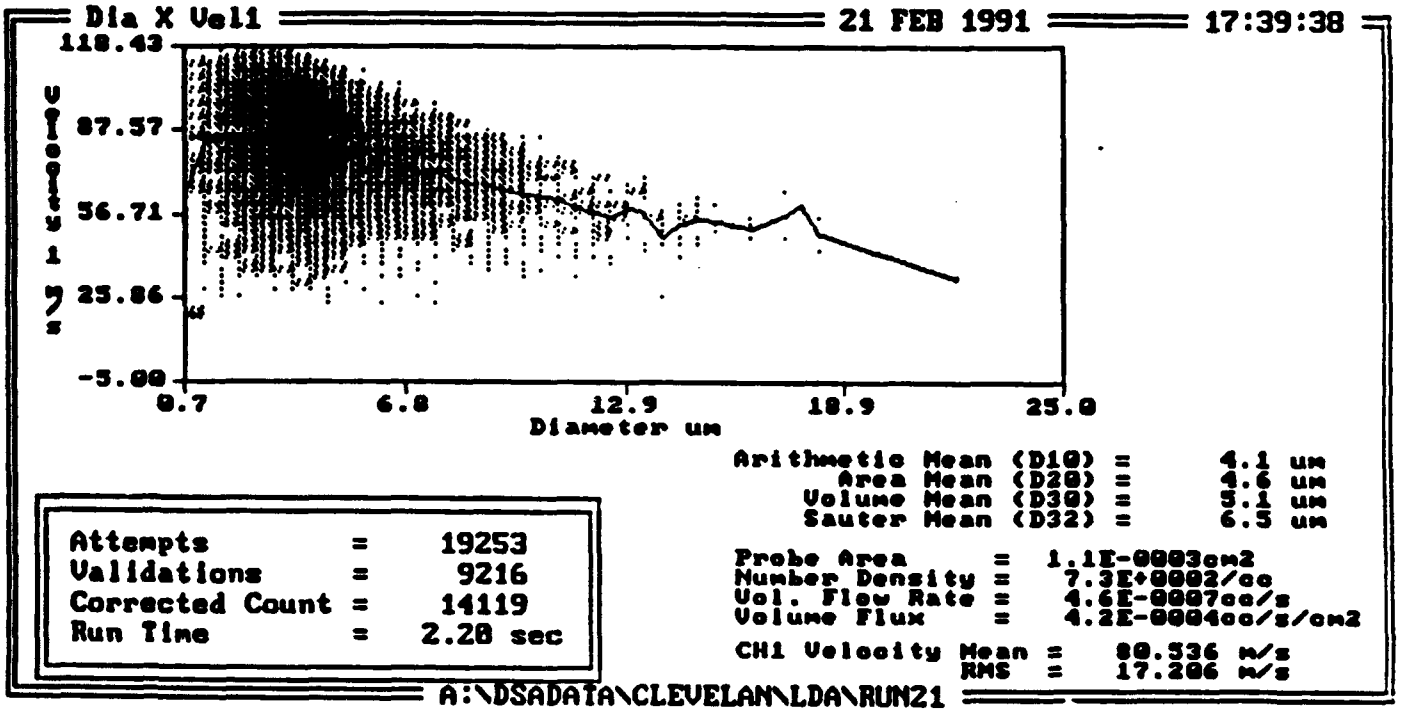

Figure 2.8.5: Particle size-velocity correlation at x/D = 2.0 and a jet velocity of 84 m/s.

Size - Velocity Correlations

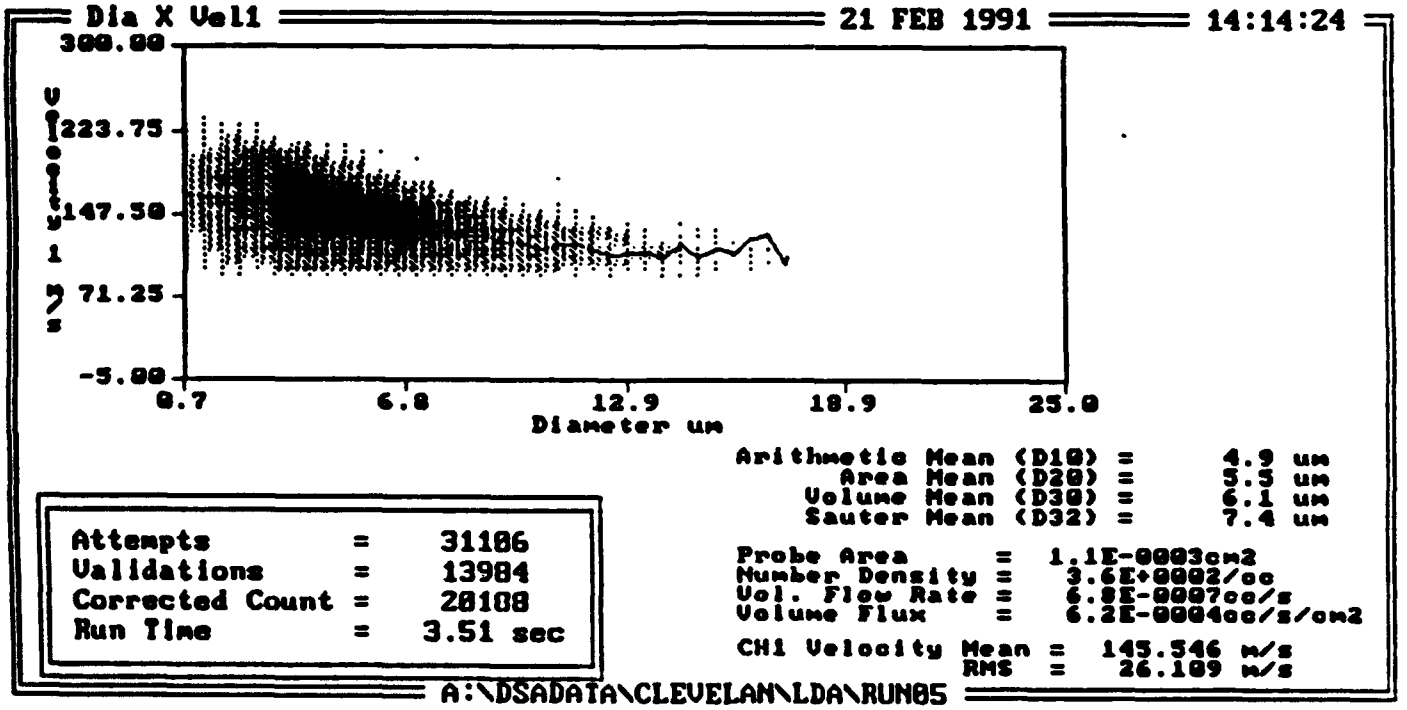

Figure 2.8.6: Particle size-velocity correlation at x/D = 2.0 and a jet velocity of 150 m/s.

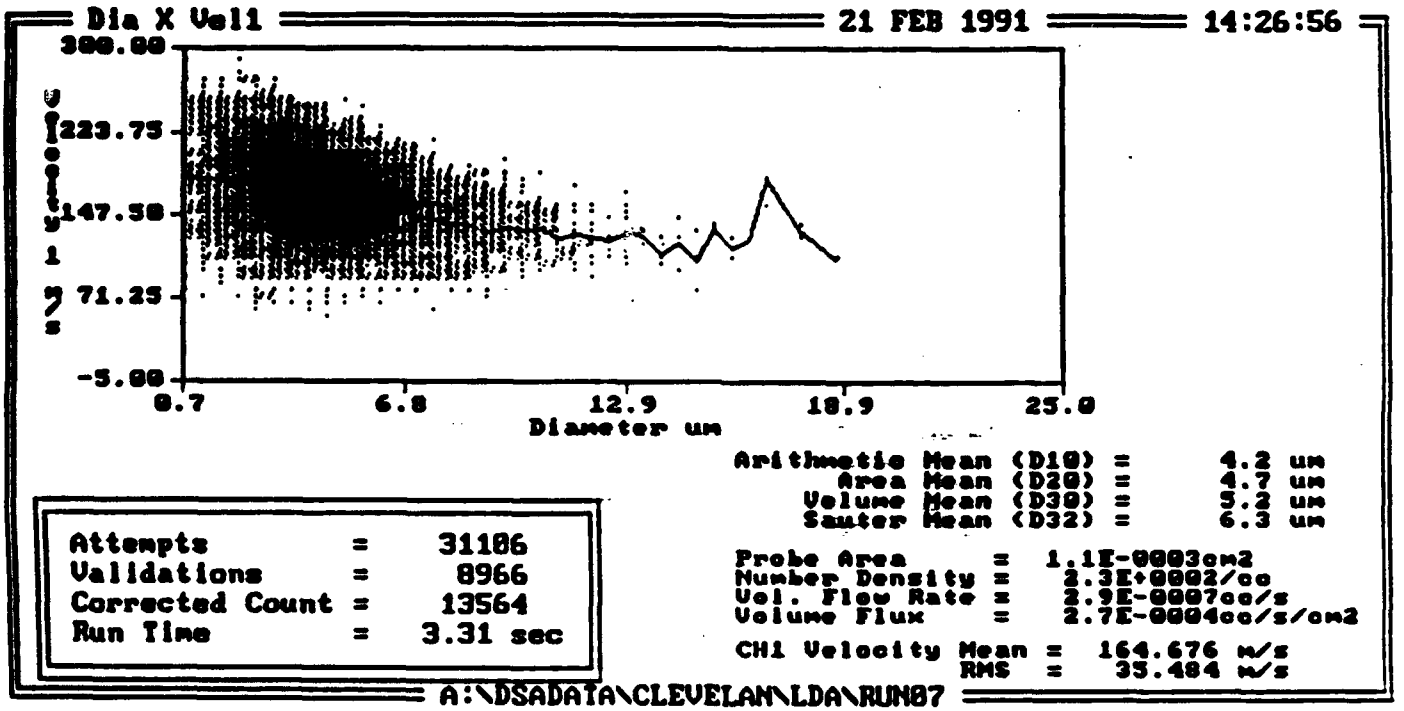

Figure 2.8.7: Particle size-velocity correlation at x/D = 2.0 and a jet velocity of 182 m/s.

Size and Velocity Distributions for the Seed Particles

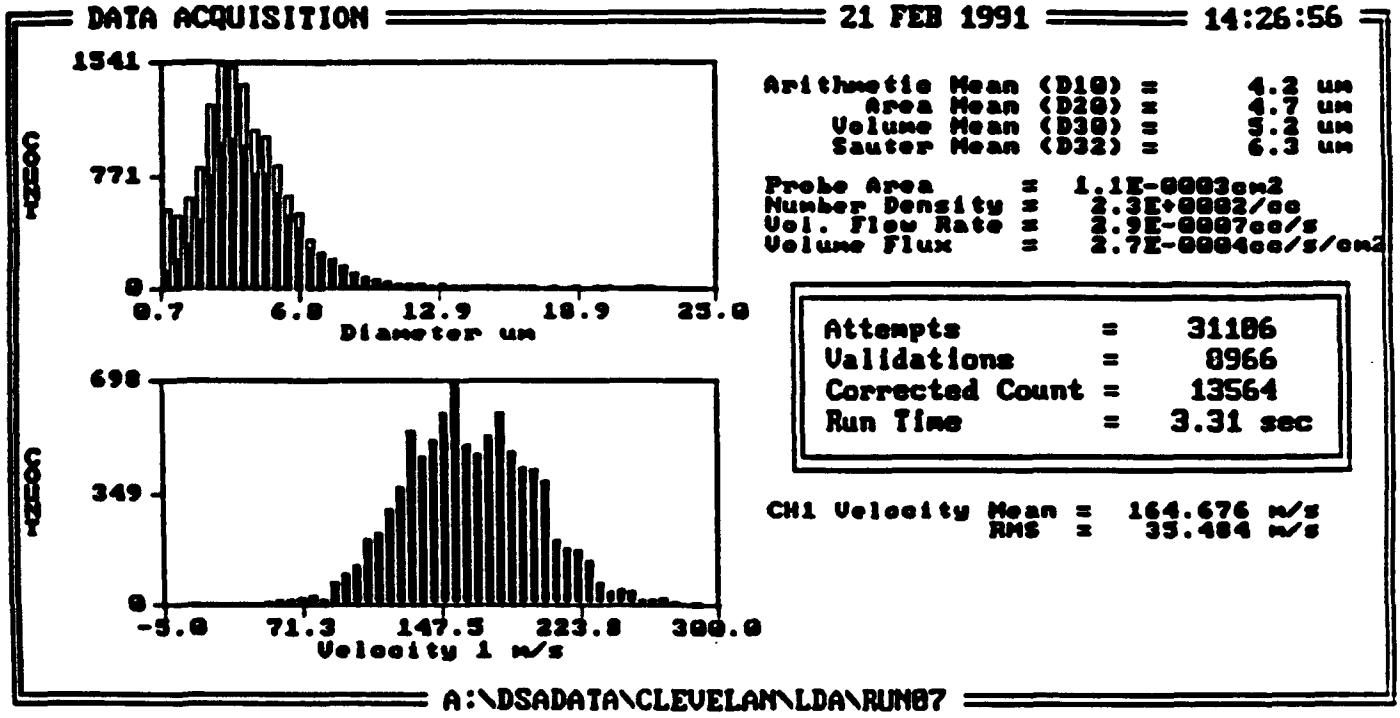

Figure 2.8.8: Size and Velocity Distfibutions for the seed particles, x/D= 2.0 and a jet velocity of 182 m/s.

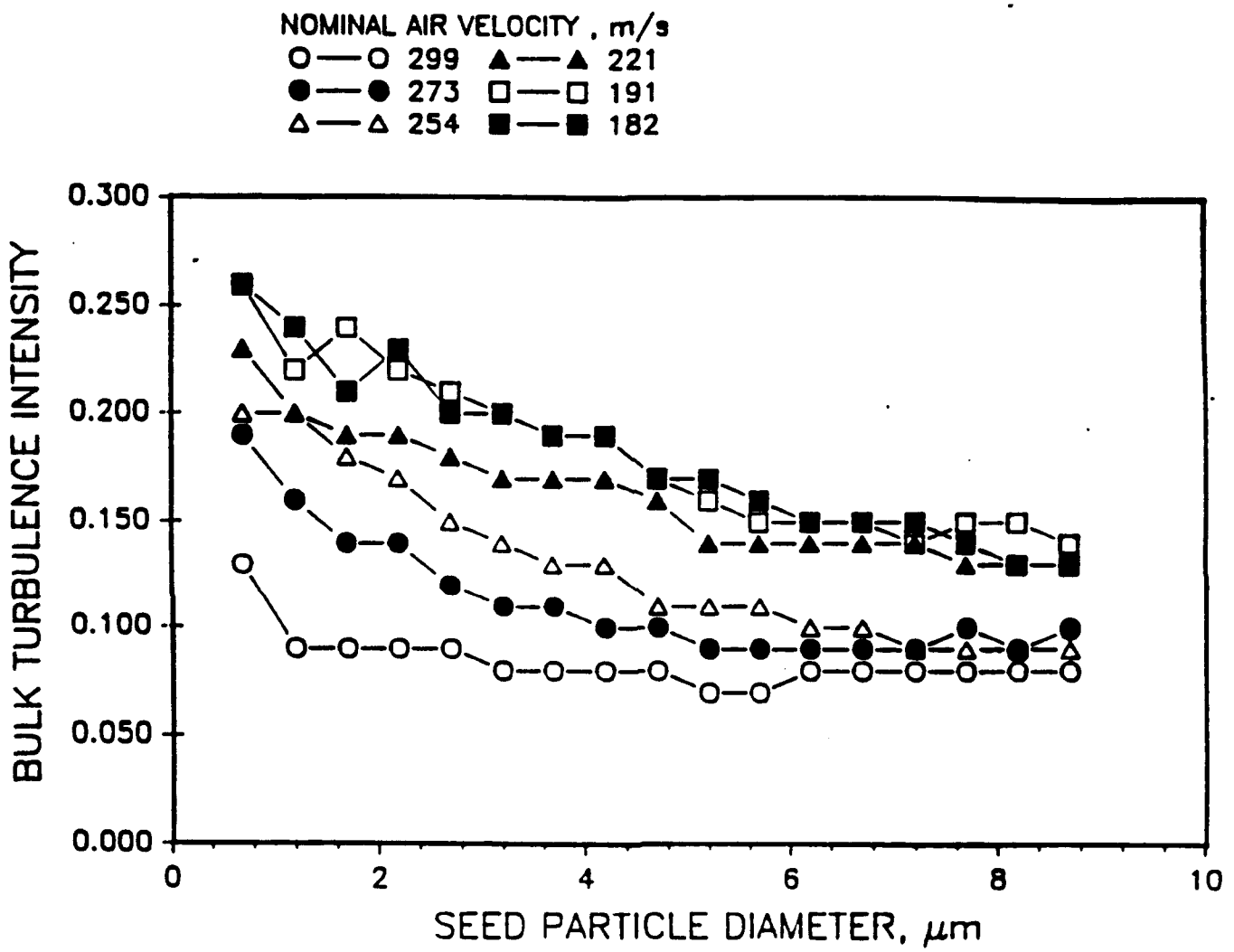

Figure 2.8.9: Distribution of the turbulence intensity versus particle size for the range of jet velocities.

2.9 Measurements in Turbulent Spray Flames

A number of experiments have been conducted under the present research program, as well as under related programs. The original work on the evaluation consisted of some basic experiments to evaluate the effects of the turbulence induced refractive index fluctuations and the local flame fronts around the drops. The experiments then evolved to spray combustion measurements of both open and enclosed spray combustors. Some detailed examinations were also made of the particle arrivals in a swirl stabilized spray flame. These data showed the formation of drop clusters and locally high luminosity apparently due to the higher soot formation associated with the cluster formation. Finally, a detailed set of measurements was obtained of a spray flame in a cooperative effort with Dr. Chris Edwards of the Sandia National Laboratories (Edwards et al. 1990).

In the first stage, turbulent gaseous flames were introduced in the beam path between the transmitter and the measurement volume while measuring a monodispersed stream of drops of known size. The flame caused some beam steering and spreading, as observed at a distant point. However, the size measurements were not significantly affected. In the worst case, a spread in the size distribution of approximately +/- 5 % was observed, but the mean value remained within the expected error bounds of +/- 2 %. However, at high turbulence levels, there was an intermittent loss of signal as the beam intersection moved off the image of the receiver aperture. The flame was then introduced into the receiver cone of light collection. Aside from causing a small amount of aberration to the image of the particle at the receiver aperture, the flame had no effect upon the measurements.

Subsequent to these studies, the instrument was tested at the NBS (now NIST) on an open swirl stabilized spray flame. The objective of this test was to evaluate the performance of the instrument on spray flame measurements by comparing the case of a burning and nonburning spray.

The radial distribution of the Sauter mean diameter, D_{32}, of the burning and nonburning spray is shown in figure 2.9.1, taken at an axial distance of 5 cm from the atomizer exit. At the center of the spray flame, where little or no burning takes place, the D_{32} values were approximately equal in the two cases. However, nearer to the periphery of the spray flame, the D_{32} values were smaller in the case of the nonburning spray. This was to be expected, since the evaporation and burning reduce the relative population of the smaller drops, which initially cause an increase in the value of D_{32}.

The phase Doppler instrument signal processor and software were further developed to analyze the temporal behavior of sprays. This required the accurate recording of the particle time of arrival. A resolution of 0.8 μs over a duration of approximately 30 minutes was achieved. The software was then developed to plot the time history of the particle arrivals, figure 2.9.2, to observe selected time increments and size and velocity subranges. A FFT algorithm was used to estimate the frequency content, if any, in the particle time of arrival record. This was done by breaking the time record into fixed time increments and taking the average of the parameter of interest (velocity, size, etc.) in each time increment. This approach could be used to investigate the behavior of spray drops in highly turbulent flows and flows with large scale vortex shedding.

Experiments were conducted to evaluate the discrete Fourier transform with the FFT algorithm before using the method to determine if there were characteristic frequencies present in sprays in a turbulent flow environment. The first studies involved the observation of sprays interacting with the wake of a cylinder aligned orthogonal to the flow direction. The cylinder shed large scale vortices at a predictable frequency based on the Reynolds number. The spray drop time of arrival data was recorded for this flow field, and the Fourier analysis was used on the particles of diameters less than 10 μm to determine if the vortex shedding frequency could be recovered. The results showed that the procedure for computing the frequency spectrum was satisfactory and produced an accurate representation of the shedding frequency.

Investigations of the behavior of a spray emanating into a swirling flow were conducted. In this case, the response of various drop size classes was investigated to first determine if the aerodynamics produced the drop cluster formation and how the various size classes were affected by the interaction with the large scale shedding in the flow field. The time of arrival data was used to analyze the power spectrum of a discrete number of size classes. Using the smallest drops in the distribution, the dominant frequency in the flow was identified, figure 2.9.3. The discrete Fourier transforms (DFT) of the larger size classes were then compared to that representing the air flow. It was found that for this particular flow, drops as large as 25 μm followed the large scale eddies. However, drops larger than 50 μm showed little or no indication of a specific frequency in the time of arrival record. These drops apparently passed ballistically through the vortices. The DFT was also calculated based on the particle counts in each time increment. The frequency detected in the particle arrival rates correlated with the frequency determined from the velocity power spectrum. Thus, it was concluded that the drop clustering was a result of the collection of drops into the vortices before being shed.

A similar study was conducted on a commercial burner which consisted of a swirl vane, a central coaxial flow about the atomizer, and radial dilution air injection from a cylindrical housing. The time of arrival measurements showed a significant degree of drop clustering, figure 2.9.4. Visualization of the flame, figure 2.9.5, showed packets of flame indicating local burning of clusters of drops. The DFT approach was applied to the time records and produced some indication of a coherent frequency of 55 Hz in the spray. This frequency was in agreement with the Strouhal number calculated using the 30 mm diameter hole surrounding the atomizer and the flow speed of 5 m/s measured coming out of the hole (Bachalo et al. 1988). These results clearly illustrated the additional information that can be obtained with the phase Doppler instrument after the extensive development that was a part of this research program.

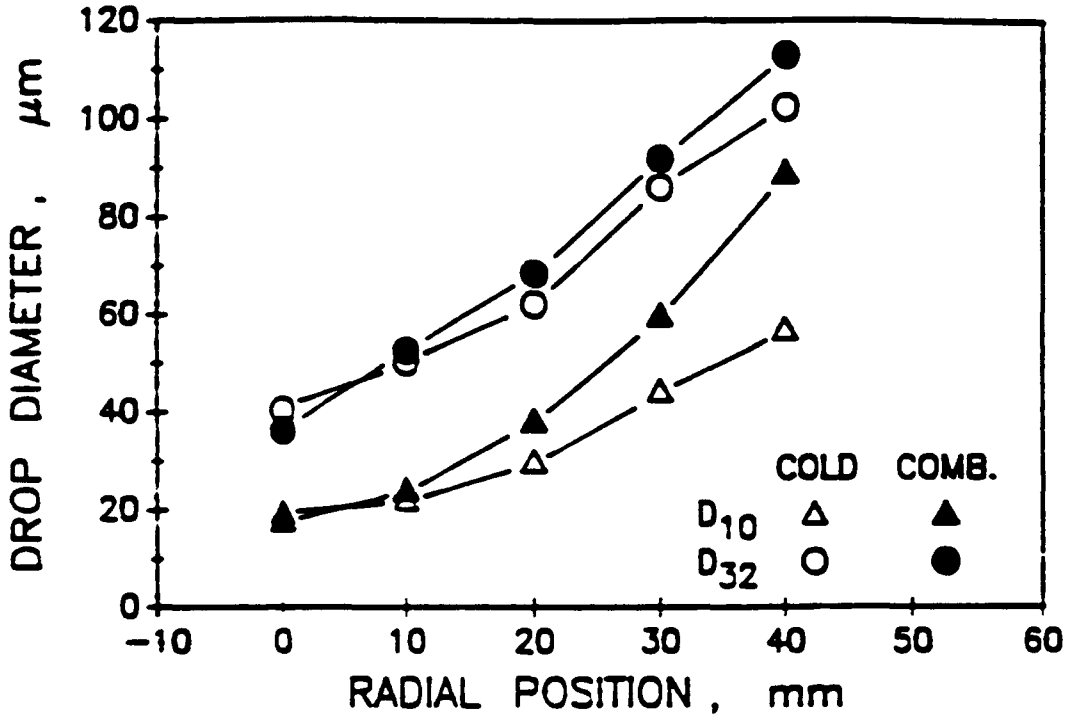

Figure 2.9.1: Comparison of the Sauter mean diameter for the burning and non-burning spray.

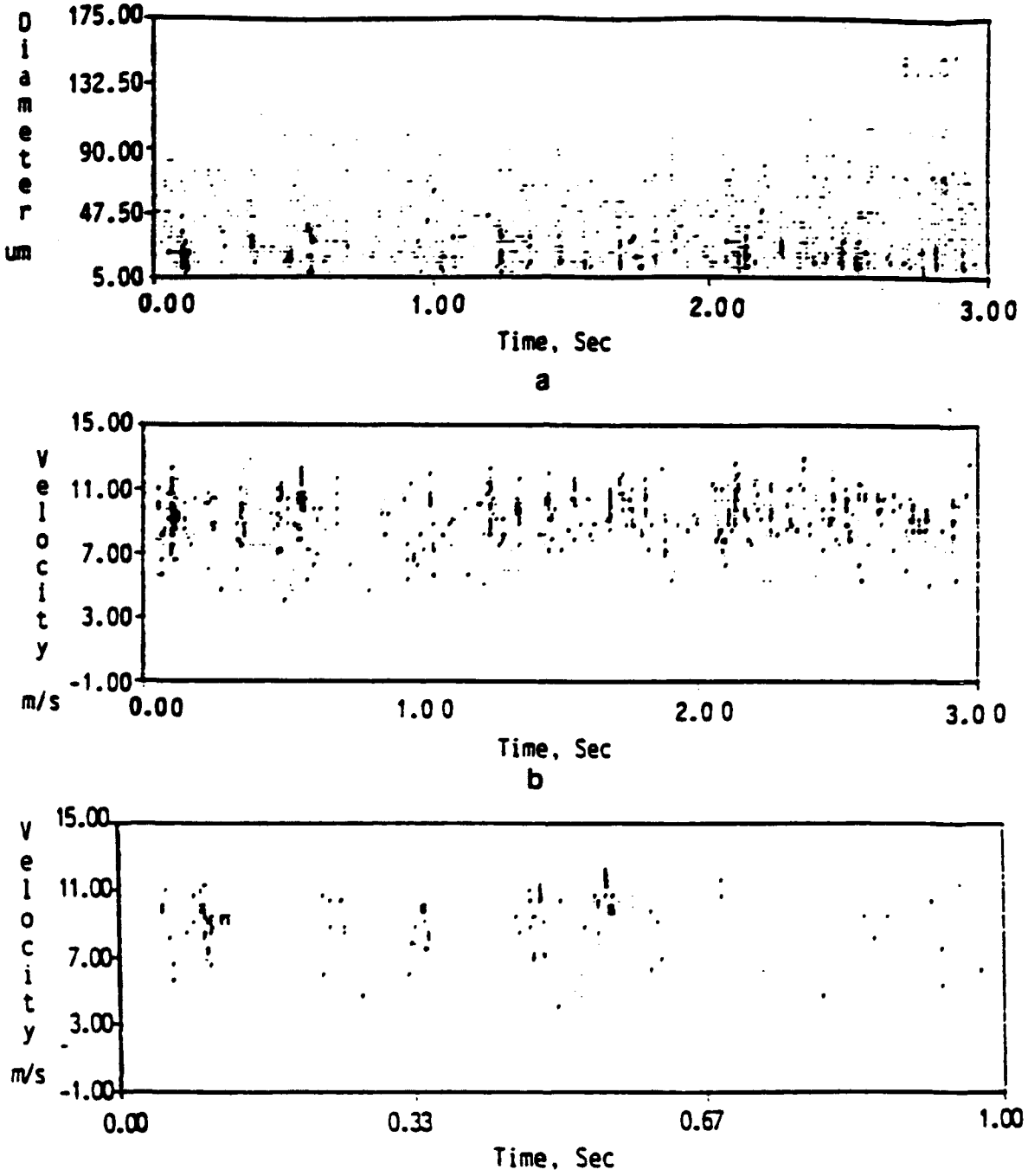

Figure 2.9.2: Example of the particle time of arrival for spray drops.

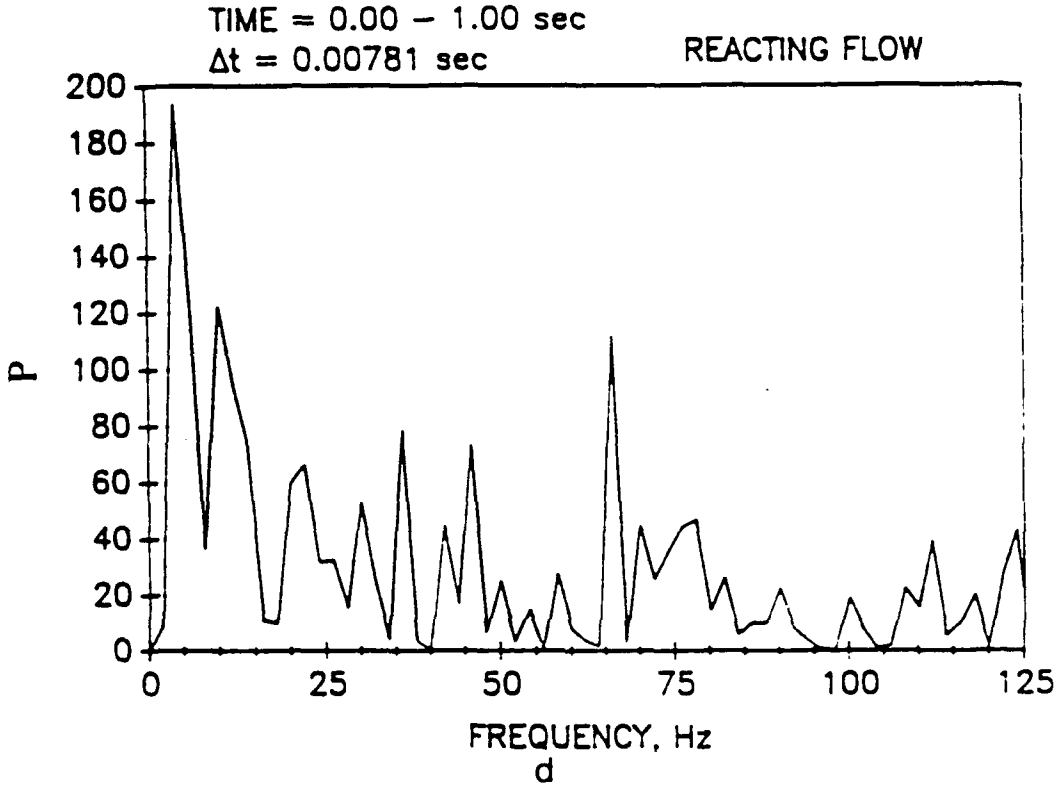

Figure 2.9.3: Spectral analysis of the time of arrival of the small drops in the spray injected behind a bluff body. P is the power spectral density of drop arrival.

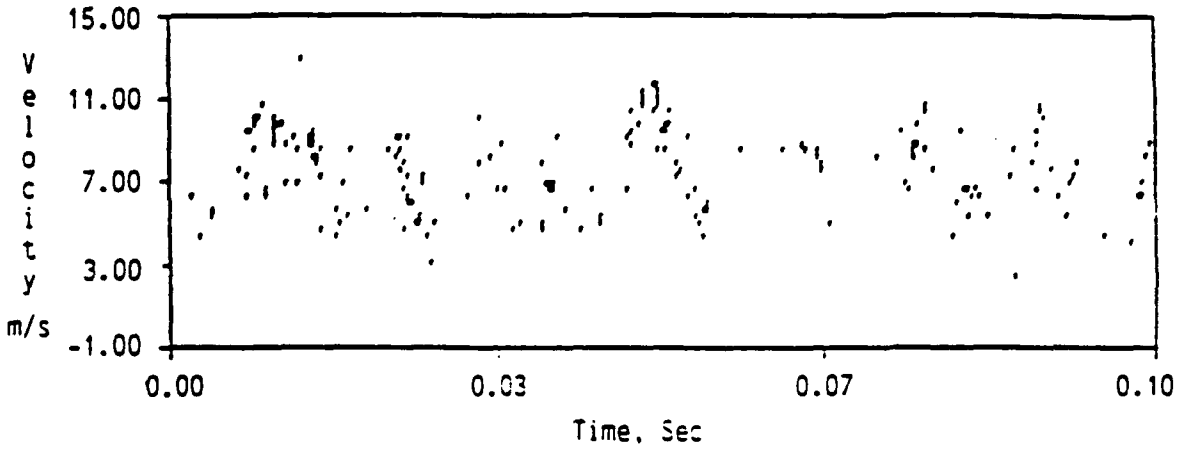

Figure 2.9.4: Time of arrival plot for the spray from a commercial burner showing drop clustering.

Figure 2.9.5: Photograph of the spray flame showing packets of flames due to drop clustering.

3.0 Scattered Light Heterodyne Interferometry

This extension or alternative approach to the phase Doppler approach was investigated to determine if the method is feasible and has any advantages over the present approach. The heterodyne method which follows from the approach of Agrawal and McCullough, 1981, for LDV applications, utilizes a single transmitter beam to illuminate the particles. Light is detected by a single receiver and then partitioned into three or more segments and mixed to form the necessary interference. Because the light reaching the different detectors has travelled on different paths through the drop, there will be a relative phase shift imparted to the detected light. The phase shift can then be related to the drop size and the beat frequency to the velocity. Although the receiver optics become more complicated, the transmitter is very simple.

An advantage of the heterodyne approach is that a different scheme may be used in detecting the phase, leading to better immunity to noise on the signal and to very high signal processing speeds. A problem with the dual beam approach is that drops passing outside the sample volume will extinguish the individual beams, producing an additional modulation to the Doppler signal and apparent spurious phase shifts. With a single beam the beam extinction pulses may lead to momentary loss of signal in high number density environments but should not produce measurement error. The receiver acquires light over a relatively large solid angle of collection so that individual extinction pulses in the optical path will not affect the interference. When using fiber optics on the transmitter of a two beam system, the problem of phase shifts due to vibrations in the fiber can occur. This problem is essentially eliminated in the single beam approach.

Work on this method has been primarily analytical and has covered the effects of such phenomena as aperture broadening and the expected sensitivities as a function of optical parameters. It has been determined (Agrawal and McCullough, 1981) that with beam splitting and a second

detector system oriented orthogonal to the first, two components of velocity can be measured.

In the description by Agrawal and McCullough, figure 3.1, the system for velocity measurements consisted of a laser beam, a focusing lens, and the receiver optics. The confocal receiver consisted of a large aperture lens

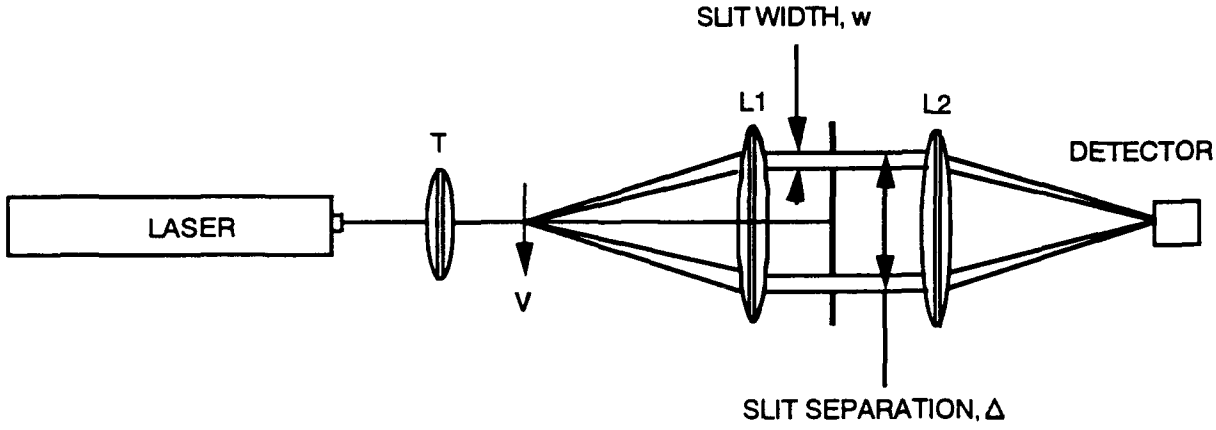

Figure 3.1 Schematic Showing the Basic Optical System Required When Using a Virtual Fringe System (Agrawal and McCollough)

with a slit aperture stop and a second lens to focus the collected light to the aperture in front of the photodetector. Light scattered by a particle passing through the focused beam scatters light which is collected by the first receiver lens. The collected light is collimated and falls on a mask with two horizontal slits. Light passing through the two slits is focused with a second lens to an intersection at the back focal plane (Fourier transform plane). The scattered light forms Young's fringes at the focus of the second lens. If the scattering particle is moving with a velocity component perpendicular to the slit apertures, the light passing through each slit is Doppler shifted. The interference fringe pattern will thus moves at the Doppler difference frequency, given as

$$f_c = \vec{v} \bullet \vec{n} \Delta / \lambda f_1 \qquad (3.1)$$

where f_c is the center frequency (center to center of the slits), $\vec{v}$ is the velocity vector, $\vec{n}$ is the unit vector orthogonal to the beam direction and

to the slit direction, λ is the light wavelength, Δ is the width of the slits, and f_1 is the focal length of the first collecting lens. Because the apertures must have a finite width, w, there will be an aperture broadening effect on the frequency. The bandwidth of this frequency broadening is given by

$$f_B = 2\vec{v} \bullet \vec{n} w / \lambda f_1 \tag{3.2}$$

The aperture broadening has been one of the reasons that this method has not been adopted for general LDV applications. It may be possible to mitigate the effects of aperture broadening by reconfiguring the receiver optics as shown in figure 3.2. In this case, the light scattered to the upper slit is folded over so that rays reaching the upper part of the upper slit mix with rays reaching the upper part of the lower slit. This serves to keep a similar scattering angle difference across the slit. The focused light will then have a nearly uniform spatial distribution but will be modulated in time at the Doppler difference frequency.

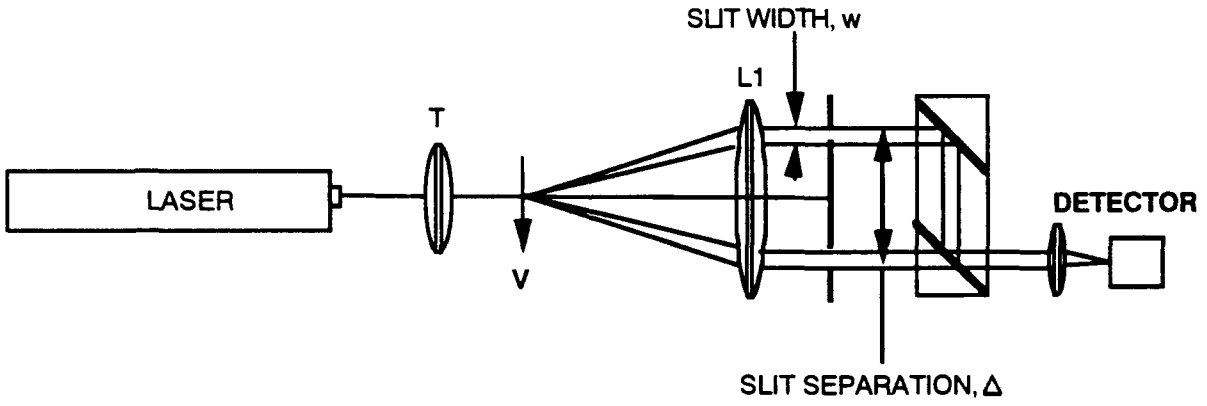

Figure 3.2 Possible Configuration For Limiting the Effects of Spectral Broadening Due to a Finite Aperture Width.

Phase shift response to particle size is another matter. The optics must be rearranged as shown in figure 3.3 to accept only light scattered by the mechanisms of refraction or reflection. For simplicity, only two detectors were considered. One design concept was to adjust the collection angles of the light entering the receiver and direct it through the four lens segments such that the Doppler difference frequency was equal for both detectors.

In this case, the phase shift between the signals could be measured reliably. Using the assumption of simple light scattering by the mechanism of refraction, the size can be recovered (the more detailed analysis using the complete light scattering developed under this program would be used after the feasibility of the method is illustrated).

Considering the light scattering by a sphere, the collected light will have an average phase shift centered over each detector pair given by the relationship

$$\phi_c = \frac{3\pi}{2} + 2\alpha(\sin\tau - m\sin\tau')$$
$$\theta = 2(\tau - \tau')$$
$$\sin\tau = m\sin\tau' \qquad (3.3.\ a,b,c)$$

where $\alpha = \pi d/\lambda$ is the size parameter, τ and τ' are measured to the surface tangents of the sphere, and θ is the light scatter detection angle, in this case, measured to the centers of the collection apertures.

The phase shift between the signals could then be measured in the usual way. However, to reach the goal of measuring the size of very fast moving particles, the fast wave tracking method was considered as a potential means for phase measurement. This approach was introduced by Smeets and George, 1981. Their device used a Michelson interferometer configuration along with a glass block to introduce a finite optical path difference (or a fixed phase shift) into one of the legs of the interferometer. This produces a sensitivity of the interference to changes in the light wavelength. A pair of detectors was used with a feedback system to a Pockels cell that served to change the phase shift to keep $\Delta\phi/\lambda$ a constant. The optical configuration used for this purpose is shown in figure 3.3 The voltage required to maintain the phase shift is proportional to the phase change, and this phase tracking may have the potential of being adjusted with time response on the order of 10 nanoseconds. For the maximum sensitivity setting, the method was potentially able to achieve a resolution limited by the photon shot noise.

The question was whether or not this means of tracking the phase of the scattered light could be used for phase Doppler applications. After studying the numerous possible configurations, the basic arrangement in figure 3.3 shows that two sets of interfering beams can be obtained. These interfering beams can be described as

$$I_1(t,\varphi) = E_{01}^2 + E_{02}^2 + 2E_{01}E_{02}\cos(\Delta\varphi + \omega_D t) \tag{3.4}$$

$$I_2(t,\varphi) = E_{01}^2 + E_{02}^2 + 2E_{01}E_{02}\cos\left(\Delta\varphi + \frac{\pi}{2} + \omega_D t\right) \tag{3.5}$$

where $\Delta\phi$ is the phase introduced by the particle, ω_D is the Doppler difference frequency, the I's represent the intensity distributions in the fringes, and the E's represent the electric field of the light passing through the slits. The problem that emerged is that in the general case of a particle moving in a trajectory perpendicular to the slit apertures the Doppler frequency will make the subtraction of the phase with the feedback loop difficult. It is possible that the Doppler difference frequency could be filtered out of the phase signal, but this raises other complication. This would not meet the goal of being able to process Doppler difference frequencies to 100 MHz.

Other complications were that the system could not be easily aligned to the infinite fringe condition since the phase object is not always present in the sample volume. The particles also pass through the probe volume, spending only a short residence time there. The phase shift changes instantaneously as soon as the particle is detectable. This makes tracking the phase shift with the fast wave tracking electronics extremely difficult. Finally, the phase shifts will vary over several cycles, so some additional complex electronics, along with another pair of detectors, would be needed to accomplish this. Thus, the fast wave tracking approach was abandoned in favor of the development of the discrete Fourier transform approach, DSA. After some significant development, this latter approach has proven to be the most satisfactory solution, as it is now capable of making frequency and phase measurements to 150 MHz and at SNR levels as low as -10 dB.

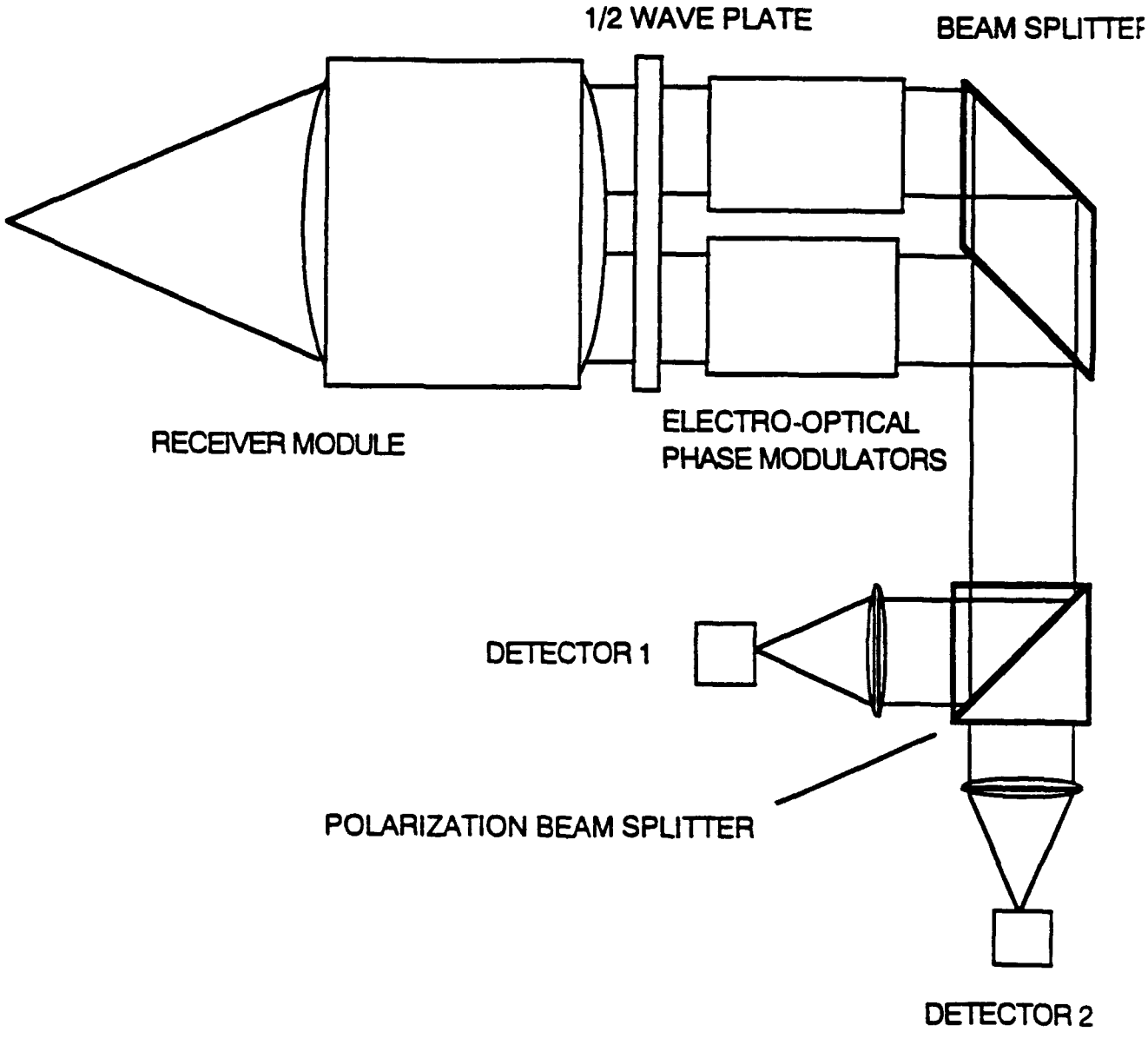

Figure 3.3 Optical Configuration For Obtaining Phase Measurements Using the Virtual Fringe Approach.

4.0 Ratiometric Particle Analyzer

In order to size irregularly-shaped particles, light scatter detection at confocal forward scatter or small off-axis angles is necessary. The validity of this approach has been demonstrated by Jones (1987), Gebhart and Anselm (1987), Killinger and Zerrull (1987), and others. At small off-axis angles the light scattering by particles greater than the wavelength may be described by Fraunhofer diffraction, which treats the particle as an opaque disk. The angular distribution of the scattered light is inversely proportional to the dimension of the particle. If the light scatter detection is symmetric about the transmitted beam, the measured average size tends to be equal to the equivalent spherical diameter, since the particles pass the beam at random orientations. This is true if the aspect ratio of the particles is not too large. For smaller particles, the distribution of the scattered light tends to be less dependent upon the shape (see Killinger and Zerrull, 1987).

The ratiometric method utilizes the measurement of the scattered light intensity to infer the particle size. As such, near forward scattering light can be used for measuring irregular-shaped quasi-spheres and off-axis detection can be used when measuring spheres. A key feature of the method is that a relatively straightforward and practical means is used to remove the incident intensity ambiguity due to the Gaussian beam.

Basically, (as first proposed by Bachalo, US Patent #4,854,705) the ratiometric technique for particle characterization consists of a laser beam which is split into two beams having approximately equal intensities. One of the beams is passed through a beam expander while the second one is directed to a polarization rotator. Subsequently the two beams are focused into a common point. Particles passing through the probe volume scatter light which is collected by the receiver lens and focused onto photodetectors which are coupled to a signal amplitude detection device for further analysis and data reduction.

In the original concept the waist of one of the beams was a factor of 5 to 10 greater in diameter than the other. This large beam ratio was found to be inefficient in data acquisition and was limited to relatively low particle number densities due to the necessary beam size. In LDV applications the large beam resulted in an unnecessary reduction of signal-to-noise ratio. The present approach employs a beam ratio from 2 or 4 to 1, which is a significant improvement.

The two coaxial laser beams which are focused into a common point establish two confocal beam diameters, as is shown in Figure 4.1. The particles that pass through the focused beams will scatter light with an intensity that is a function of their diameter, of their index of refraction, and of the intensity of the incident light, which depends on the trajectory of the particles through the beams.

A particle passing on an arbitrary path through the probe volume, as illustrated in Figure 4.2, will produce a signal from detectors 1 and 2. In order to determine the incident intensity on the particle, the trajectory defined by the distance x_p from the center of the beam must be known.

The Gaussian intensity distribution of the incident beams is given by

$$I_{\xi} = I_{0,\xi} \exp\left(-2x_{\xi}^2 / b_{\xi}^2\right) \tag{4.1}$$

where the subscript ξ refers to either beams 1 or 2, I_0 is the peak intensity of the beam which may be measured, x is the radial coordinate of the beam, and b is defined, by convention, as the radius wherein the intensity I is equal to $1/e^2$ of the peak intensity, I_0. The radius b can be measured also for each beam.

The energy scattered by a particle crossing beams 1 and 2 can be specified as a function of the scattering parameters Q_1 and Q_2, which may be computed if the characteristics of the particles, such as shape and material, are known or can be determined by previous calibration with samples which have known sizes and refractive indices. The scattering coefficients

depend on the diameter, index of refraction, and shape of the particles, wavelength and polarization of the incident light, and angle of collection. These coefficients are generally calculated or obtained by calibration as a function of the size of the particle and subsequently integrated into a look up table, such that if Q can be determined, a diameter d can be read off the table. $Q(d)$ will, therefore, be specified as a function of d.

For an arbitrary particle path x_p measured from the center of the beams and shown schematically on Figure 4.2, the scattered peak intensities may be expressed as,

$$I_{sc.1} = I_{01} Q_1(d) \exp\left(-2x_p^2 / b_1^2\right) \tag{4.2}$$

and

$$I_{sc.2} = I_{02} Q_2(d) \exp\left(-2x_p^2 / b_2^2\right) \tag{4.3}$$

Taking the ratio of the two equations yields,

$$\frac{I_{sc.1}}{I_{sc.2}} = \frac{I_{01} Q_1(d)}{I_{02} Q_2(d)} \exp\left(-2x_p^2\left(1/b_1^2 - 1/b_2^2\right)\right) \tag{4.4}$$

Solving for x_p results in the following expression,

$$x_p = \left\{ \frac{1}{2}\left(\frac{b_1^2 b_2^2}{b_1^2 - b_2^2}\right) \log\left[\frac{I_{sc.1}}{I_{sc.2}} \frac{I_{02}}{I_{01}} \frac{Q_2(d)}{Q_1(d)}\right] \right\}^{1/2} \tag{4.5}$$

In Equation 4.5, the ratio $Q_2(d)/Q_1(d)$ can be determined by calculating the light scattering of a spherical particle for the respective polarizations, which is the only parameter that is different between the two quantities. In the case where beams of different wavelength are used, the scattered intensities by a particle in the probe volume are proportional, to a first approximation, to the square of the diameter of the particle. Preliminary computer modeling has shown that the ratio of the scattering coefficients

will remain constant over the particle size range of interest if the incident polarization of the two different laser wavelengths (colors) is the same; that is, to a first approximation Q_2/Q_1 is not a function of d. The ratio of the scattering coefficients is expected to change with a different set of physical parameters and has to be calculated and incorporated into the look up tables.

The incident beam intensities, I_{01} and I_{02}, in Equation 4.5 are determined a priori by calibration of the system. Measurements of $I_{sc,1}$ and $I_{sc,2}$ are obtained for each particle based on the signal amplitude measurements. Thus, x_p can be calculated explicitly from the measured quantities for each particle size and trajectory. With x_p determined, Equations 4.4 and 4.5 may be rearranged as,

$$Q_1(d) = \frac{I_{sc,1}}{I_{01}} \exp\left(2x_p^2 / b_1^2\right) \tag{4.6}$$

and

$$Q_2(d) = \frac{I_{sc,2}}{I_{02}} \exp\left(2x_p^2 / b_2^2\right) \tag{4.7}$$

to obtain $Q_1(d)$ and $Q_2(d)$. The values of $Q_1(d)$ and $Q_2(d)$ are subsequently used with the respective look up tables to obtain the values of the diameter of the particles. Even in those cases when the Lorenz-Mie theory is used to generate the scattering parameters, calibration is still required to determine the constants that describe the collection efficiencies and gains of the system. The Lorenz-Mie theory must be used with some reservation, since it does not apply to nonspherical particles. With certain light scatter detection geometries, the theory does offer a good approximation.

For irregular shaped particles the light transmission through the particle will not be the same as for spherical particles. The oscillations in the response curves (i.e., scattering coefficients) which arise from the interference between the refractive and diffractive light scattering will be significantly damped.

In order to determine whether the approach could give satisfactory results, preliminary tests were run in the computer using Lorenz-Mie theory to obtain a calibration curve for the particle range which covers the sizes of special interest in flue gas streams. Figure 4.3 depicts the relative scattering efficiency versus particle diameter for particles which have a complex refractive index. The reference scattering coefficient was determined for a particle of 0.1 μm diameter. This value was chosen to cover relative intensities of four orders of magnitude (10,000).

Particles scatter light in relation to their diameter. For particles that are much larger than the wavelength of light, the light scattering intensity is approximately proportional to their diameter squared. Since a scattered light level above a given threshold must be attained before the particle is detected, this constraint sets a maximum radial dimension of the probe volume within which the particle must pass before it is detected. The other dimension of the sample volume is set by the image of the receiver aperture on the probe volume. Because of the Gaussian intensity distribution falling on the particle, the maximum radius for detection will be a function of the particle size. This topic has been discussed by Bachalo and Houser (1984) and is the subject of other sections in this report. This change in the sampling cross section must be accounted for to prevent biasing the measured size distribution towards the large particles, which have an effectively larger target for detection.

4.1 Particle Statistics

Once the particles are measured over a sampling time τ, they are classified into bins of nominal size class i to form the size histogram. Using the technique described in the previous paragraphs for determining the radial coordinate, x_p, of the particle trajectory, it is possible and desirable to have a statistical distribution of such radii for the particles of size class i. From such a statistical distribution, the maximum value of the radius $x_{i,\max}(d)$ is determined for each size class i. The set of maximum radii defines the sample cross section for each size class i. Biasing of the drop size distribution towards the large particles is suppressed by weighting

proportionately the number of particles $n_i(d)$ in each size class i. This is accomplished by multiplying each $n_i(d)$ by the ratio of the overall largest sample cross section to the largest sample cross section of the corresponding size class i. For every size class the corrected number of particles is given by,

$$n(d)_{i,new} = n_i(d)\frac{x_{\max}(d_{\max})}{x_{i,\max}(d)} \tag{4.8}$$

where $x_{\max}(d_{\max})$ is the peak value of the statistical distribution of probe volume radii corresponding to the particle trajectories of the largest size class i obtained in the particle size distribution. The average radius for each size class may also be used for this purpose and, in fact, may be more reliable, considering the statistics. This correction is very similar to that employed in the PDPA instrument.

Knowledge of the radii of particle transit also provides the necessary information for obtaining the speed of the particle. Since the focused beam is circular, the path length through the beam, as shown in Figure 4.2, is known. The intensity of the threshold level is given by,

$$T = Q_1(d)I_{01}\exp\left(-2x_T^2/b_1^2\right) \tag{4.9}$$

where x_T is the beam radius at the intensity level that produces a signal to the threshold level. Based on the previous analyses, $Q_1(d)$, b_1, and I_{01} are known. Therefore, the equation can be used to solve for x_T, that is,

$$x_T = b_1\left[\frac{1}{2}\log\left(\frac{T}{Q_1(d)I_{01}}\right)\right] \tag{4.10}$$

Referring back to Figure 4.2, the particle path length is equal to the distance measured from the point where the signal exceeds the threshold to where it falls below it,

$$L = 2\left(x_T^2 - x_P^2\right)^{1/2} \tag{4.11}$$

where x_P and x_T are obtained from the preceding equations. A counter and a fixed frequency clock are used to measure the time, t, taken for the signal to exceed the threshold and fall below the threshold again. The particle speed is obtained from,

$$U = \frac{L}{t} \tag{4.12}$$

Once the values for the speed of the particle, sampling cross section, and number of particles counted per second are calculated, the particle number density can be obtained. This is done by determining a swept volume and using the cross-sectional area defined by the sampling cross section and a length given by $\mathcal{L} = U\tau$, where τ is the sampling time. Strictly, the sample volume and speed must be determined for each particle size. The number density is then given by,

$$N = \sum_{i=1}^{m} \frac{n_i(d)}{A_i(d)U_i(d)\tau} \tag{4.13}$$

where $n_i(d)$ is the number of particles in each size class i of which there are a total of m size classes, $A_i(d)$ is the corresponding sampling average cross-sectional area for particle size d, and $U_i(d)$ is the average speed of the particle of size class i. Other useful parameters such as mass flux, particle size-velocity correlations, and turbulence parameters of the flow could be extracted from the above information.

4.2 Relative Scattering Coefficient Calculations

Numerical simulations have been performed by Holve and Self (1982) to determine the intensity of scattered light by spherical particles. The calculations were obtained at various collection angles and for different indices of refraction by integrating the intensities over the collection solid angle. The results show that when intensity is plotted versus diameter of

the particle the oscillations decrease with such integration. Because of the interference between the diffractive and refractive light scattering for irregular particles, it is believed that the oscillations in the scattering coefficients $Q_1(d)$ and $Q_2(d)$. will be significantly damped, resulting in a ratio of these two parameters which is basically constant over the particle size range of interest.

For the generation of the scattering coefficients, existing Lorenz-Mie scattering computer codes at Aerometrics were further developed for the specific application in question. Lorenz-Mie theory of light scattering was used for the determination of the scattering coefficients. An example is shown in Figure 4.3. The results show that for absorbing particles the relative scattering efficiency grows monotonically with particle size.

4.3 The Breadboard System

A breadboard optical system has been constructed for testing the ideas presented in this section. It consists of a laser, a beamsplitter, a beam expander, a beam recombination means, and a receiver unit, see Figure 4.4. A detailed description of the optical configuration is now given.

The laser beams used are generated by a single laser producing linearly polarized light. The generated beam is partitioned into two beams using a beamsplitter, and subsequently one of the beams is increased in diameter using a beam expander. The second beam reflected by the beamsplitter is directed to a polarization rotation device to rotate the polarization by 90°, then reflected to a second beamsplitter, and finally made coaxial with the first beam. The coaxial beams are then focused at a common point. In the configuration just described, the beams have orthogonal polarizations and the intensities of the beams are approximately equal. In those cases where the light scattered by the particles produce significant depolarization, different wavelengths of light will be required.

As was previously mentioned, the focused beams establish two confocal beam diameters, see Figure 4.1, and the particles that pass through the

focused beams will scatter light with an intensity that is a function of their diameter, of their index of refraction, and of the intensity of the incident light, which depends on the trajectory of the particles through the beams. The amplitude of the light scattered simultaneously from both beams contains the required information to determine the particle size.

The collection system of the instrument is composed of the receiver lenses which collect the scattered energy onto the aperture, a collimating lens, and a polarizing beamsplitter (or dichroic beamsplitter if different wavelengths are used), see Figure 4.5. Sometimes additional lenses may be used to focus the light onto the photodetectors.

The lenses in the receiver unit define a solid angle of collection extending into the focused beams, i.e., into the probe volume. The light scattered within the solid angle by the particles passing through the probe volume is collected and focused by the receiver lenses onto an aperture. This aperture serves to admit only light scattered by the particles crossing the laser beams in the appropriate region where they are completely focused. The intersection or overlap of the image of the aperture in the collection system and the focused laser beams serves to define the sample volume.

The receiver optics selectively separate the energy scattered from the small and large beams by their polarizations or wavelengths and direct the scattered light to their respective photodetectors, which are coupled to a fast transient recorder and peak detection circuit.

The receiver system produces two signals, with peak amplitudes proportional to the particle diameter and to its trajectory through the large and small beams. These signals have nominal Gaussian shapes and are coupled to linear preamplifiers that preserve the amplitude information. Two simultaneous signals will only be accepted when the particle passes within the diameter of the small focused beam.

Signal processing electronics have been developed to handle data rates up to 100,000 particles per second moving at up to 500 m/s.

4.4 Particles of Irregular Shape

In a recent work by Killinger and Zerull (1988) the scattering functions of rough spheres oriented in 36 different ways were compared to those of smooth spheres and found to be well described by Lorenz-Mie calculations for smooth spheres.

Fraunhofer diffraction may be employed as a measuring tool in the relatively high number density environments. Scattering in the near forward direction tends to be less dependent upon shape and properties of the particle. In a recent paper, Jones (1988) developed a statistical model for Fraunhofer diffraction by random irregular particles. The model is described in terms of a distribution function for radii and a correlation function in the surface of the particle. Electron micrographs of quartz, cement, and sand particles were obtained. The model was compared to the Airy function for spheres. His results show that the forward peak of the diffraction pattern is not sensitive to shape, although it was estimated that particles could be oversized by up to 10%.

In another work, Gebhart and Anselm (1988) studied the effect of particle shape on the response of single particle optical counters. In this work, theoretical approximations for the limiting cases $d << \lambda$ and $d >> \lambda$ are compared with experiments performed with optical counters using nonspherical particles. Gebhart and Anselm conclude that for irregularly shaped particles with dimensions above the wavelength of light, the effect of the particle shape on light scattering is lowest if the flux of scattered light is a function of the projected area of the particle. Their suggestion is either to collect only diffracted light (i.e., at low scattering angles) or to collect almost all reflected and refracted light. The projected area of the irregular particle obviously depends on its orientation on the sample volume.

Based on the above findings and on other similar investigations, and because the range of particle sizes is wide and the scattering properties of the particles in this size range may vary considerably, it seems necessary to divide the overall range of particle sizes into small subranges which

may require different small off-axis detection angles. The following points will be considered in the strategy to handle irregularly shaped particles.

-For small particles with higher number densities, it is possible to use larger off-axis collection angles since the diffraction lobe is broader.

- It is feasible to consider using two sampling probes to ensure a small enough sampling volume for single particle signals and for signal to noise ratio considerations.

- For very large particles with lower number densities it is desirable to use smaller off-axis angles and size them using diffraction theory.

Tentative settings for the measurement range of particle sizes which can be measured at any one particular setting are as follows:

- First collection angle, 0.3 - 5 μm diameter particles.

- Second collection angle, 3 - 30 μm diameter particles.

- Third collection angle, 20 - 400 μm diameter particles.

The measurement ranges are limited by the signal to noise ratio. For the particle sizes considered, the scattered intensity is roughly proportional to their diameter squared. For a typical particle size setting the maximum dynamic range in particle sizes is approximately 40. The lower and upper limits of particle size, 0.3 μm and 400 μm, respectively, that can be detected with the new diagnostic technique are imposed by the ability to detect signals from small particles and by the small scattering angle by diffraction of large particles.

4.5 Comparisons with Other Instruments.

There are currently two instruments which may be applied with severe limitations to size irregular particles: Fraunhofer diffraction based instruments and particle counters based on intensity deconvolution techniques. Both approaches suffer the limitation of being unable to measure mass flux.

Fraunhofer based instruments can not determine the velocity of the particles; a parameter which is important in studying the dynamic properties of two-phase flow streams and in determining deposition velocities.

The current in situ particle counters based on intensity measurements use a sophisticated intensity deconvolution algorithm to relate the light scattering signals to particle size and concentration, [12]. There are several problems with this approach. These problems include:

-The solution of Fredholm integrals of the first kind to perform the deconvolution is based on an inversion scheme which brings instabilities to the system of equations since the inversion matrix is ill-conditioned (Holve and Davis, 1982). Therefore, the convergence to a unique solution may sometimes be very difficult.

- The method is more dependent on the variations of the intensity distribution in the sample volume than the interferometric and Fraunfoffer diffraction techniques. Due to the numerical deconvolution of the scattered intensity measurements, the entire distribution of particle sizes is affected when distortions of the beam intensity are present in the probe volume. In contrast, the ratiometric technique is likely to give erroneous results only for those particles going through the edges of the probe volume when intensity distortions are present in it.

- The sample volume cross section is affected by the distortions in the intensity field in the probe volume. This would seriously affect volume flux calculations (if they were feasible).

- The instruments using the mathematical deconvolution need to be calibrated using several different size classes. The ratiometric method needs only one size class for calibration.

- No speed is obtained for each individual particle, and the maximum velocity of the flow can not exceed 200 m/s.

- The measurement range is 0.3 μm - 200 μm.

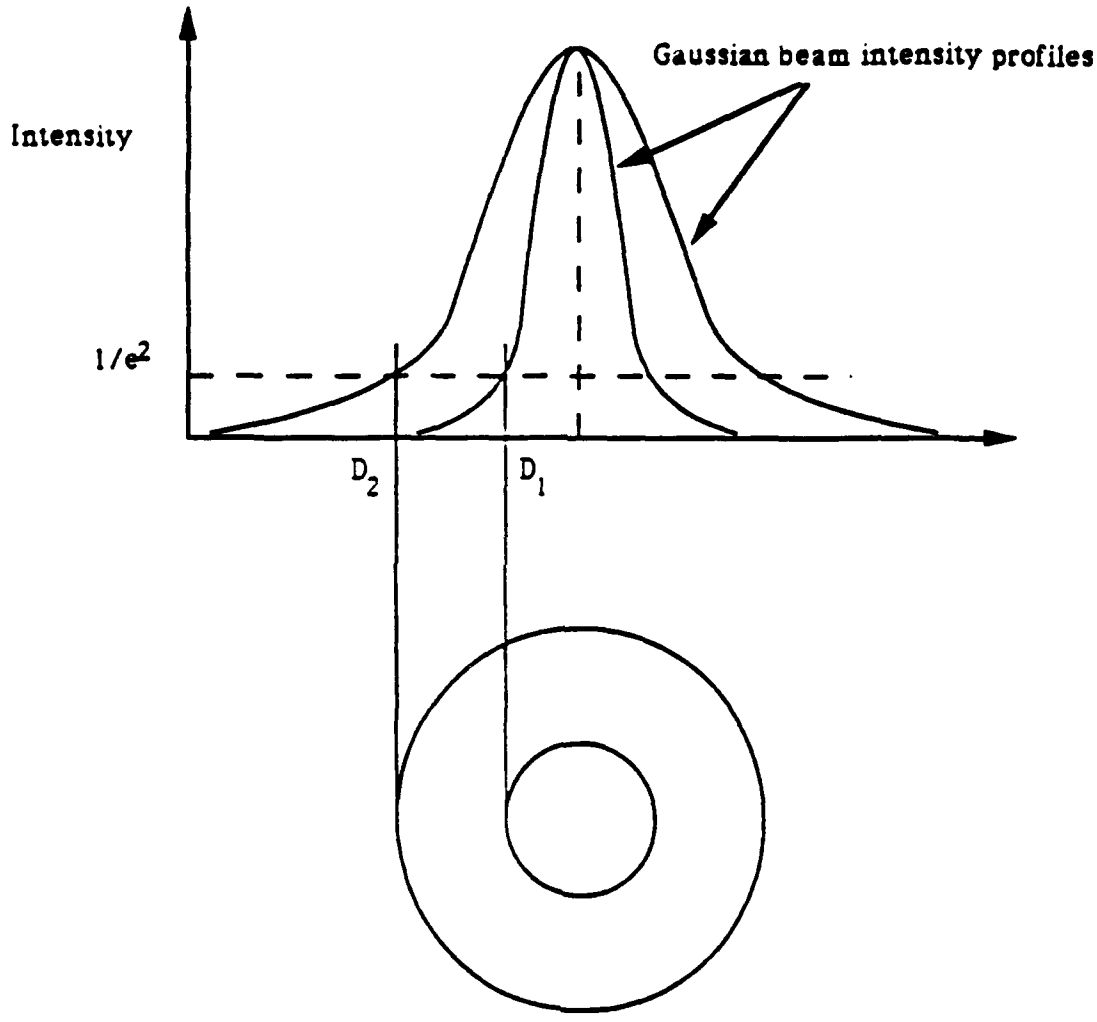

Figure 4.1: Top: Gaussian Intensity Distribution of the Laser Beams. Bottom: End View of the Concentric Laser Beams.

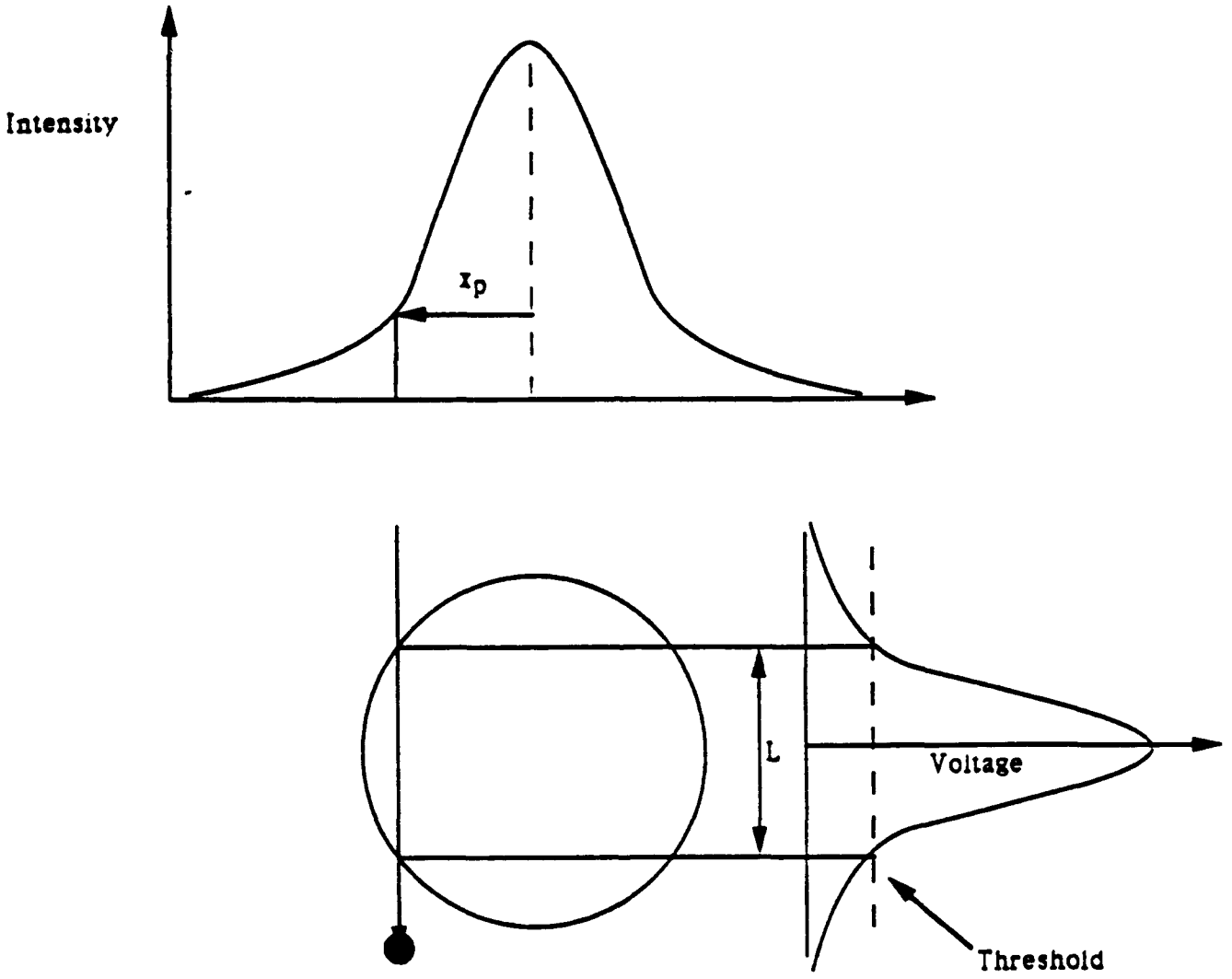

Figure 4.2: View of the Probe Volume Showing an Arbitrary Particle Path, x_p

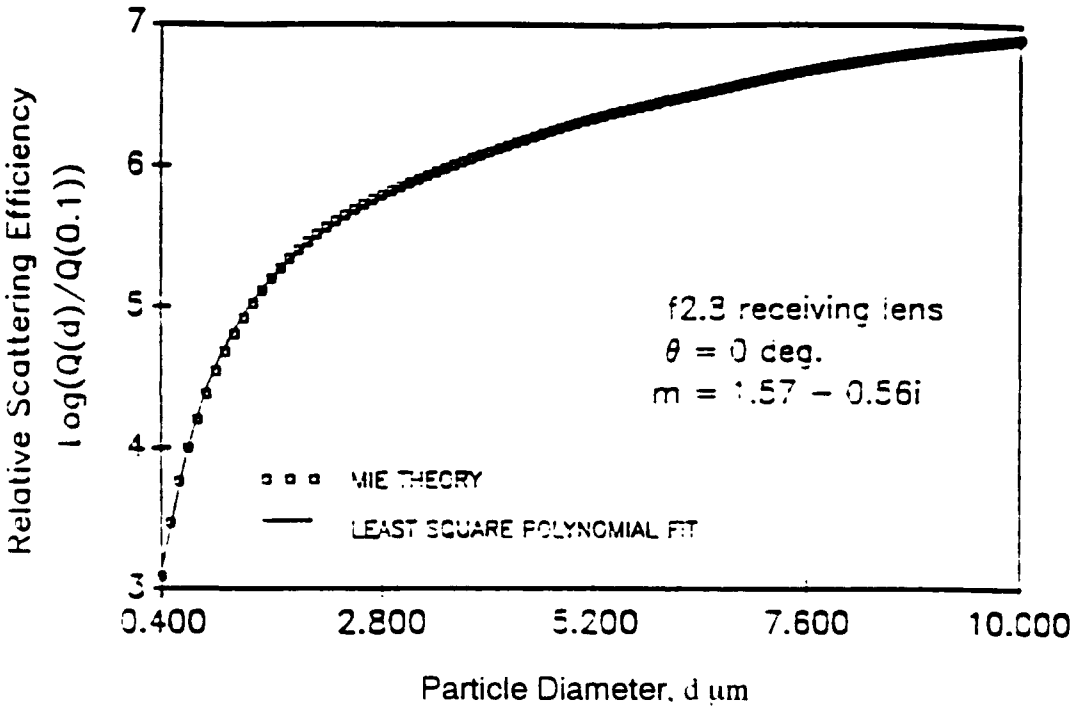

Figure 4.3: Relative scattering efficiency versus particle diameter for the proposed diagnostic technique determined from Lorenz-Mie scattering theory.

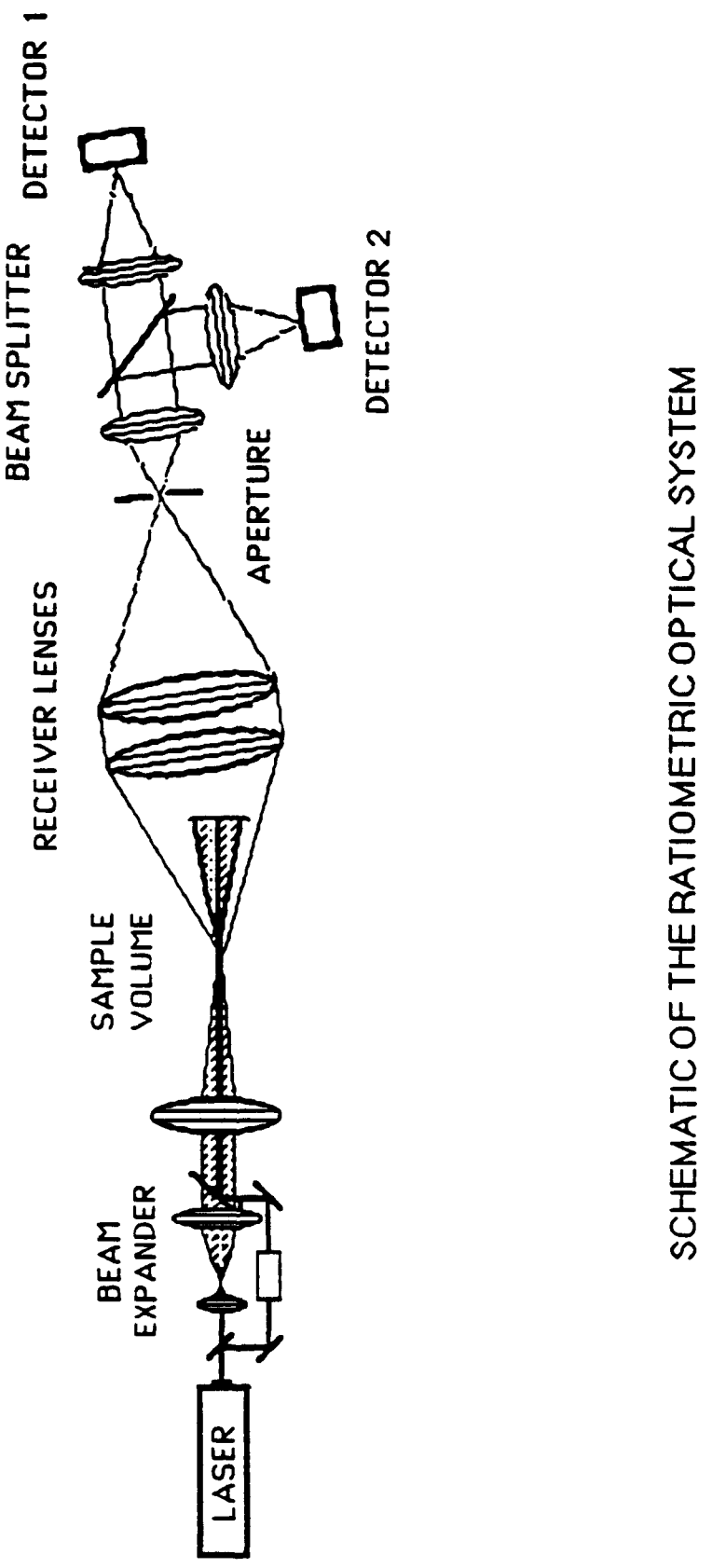

Figure 4.4: Optical Configuration of the Ratiometric Laser Diagnostic Technique for Particle Analysis.

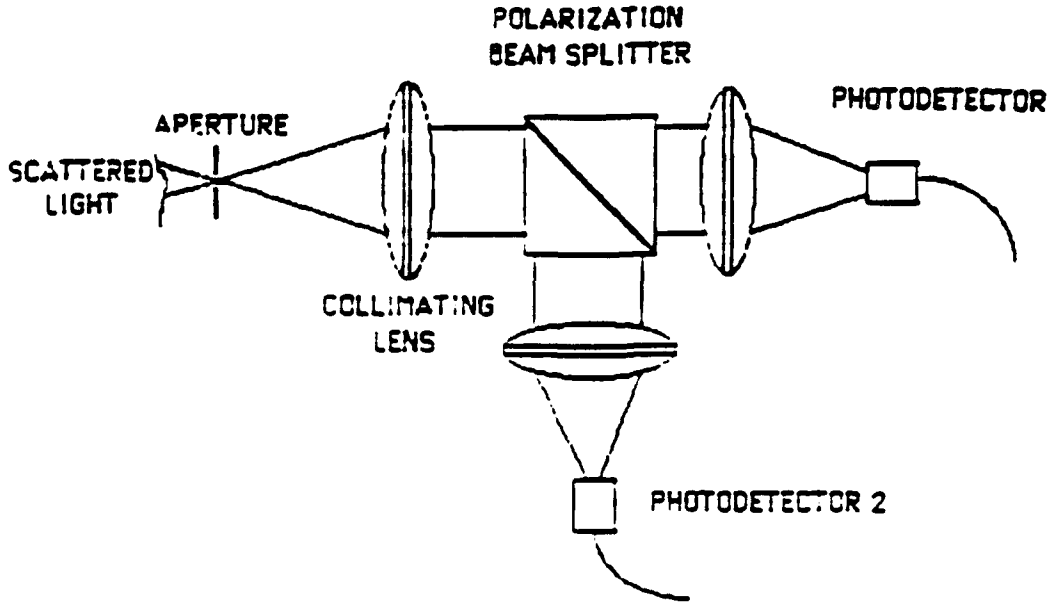

Figure 4.5: Schematic of collection system for the proposed particle size diagnostic technique.

5.0 Lagrangian Frame Particle Dynamics Analyzer

The Lagrangian frame method was conceived to allow the investigation of individual drop behavior in sprays. Such studies are of importance to drop drag measurements, evaporation studies, and drop interactions with turbulent flows. Most of the early research on sprays relied on studies of single drop evaporation and combustion because these phenomena are generally regarded to be of fundamental importance to the understanding of the principles of spray combustion. Much of this early research was also restricted to single drop combustion because of the limited instrumentation available to perform practical diagnostics of actual sprays.

With the advent of laser based diagnostics, the emphasis on single drop combustion has been now restricted mainly to numerical modelling of such mechanisms as evaporation, internal circulation and heating, and diffusion under steady and transient conditions. Little experimental work has been done lately on single drop evaporation and combustion; one of the reasons being that new experimental techniques have not evolved to obtain the more sophisticated and challenging information required for the current numerical codes.

New critical experimental data can be obtained if a diagnostic system is designed which can follow the same particle along its trajectory. This goal is a very challenging one since a fuel drop interacts with its environment and is subjected to fluctuations in its velocity and influenced by the turbulent eddies in the flow. The information which could be obtained from such measurements is of paramount importance, since in CFD codes the velocity, size, temperature, drag coefficients, and evaporation rates of the drops must be given to the model either as boundary conditions or as submodels to be used during the computations.

The possibilities for acquiring particle velocity (and possibly size) data in a Lagrangian frame general involve some sort of imaging techniques. The particle field could be illuminated with laser light or even incoherent light

and the particles imaged with a fast framing rate camera. This approach does not make very efficient use of the available laser light and would not be feasible when using the dye-tagging approach to identify the target particle. The use of "white" light strobes would provide enough power but again, would not work with the dye-tagging approach. Laser light sheets have been used in particle image velocimetry (PIV) to obtain an instantaneous mapping of the particle velocities in a plane. Presumably, multiple images of a dye-tagged particle could be used to obtain its velocity in a Lagrangian frame. Unfortunately, the particle will also move in a direction normal to the sheet and will be lost from the illuminated region. Hence, a hybrid method was proposed to overcome these difficulties, and it will be shown that the particle size can also be measured simultaneously.

The method consists simply of a laser light sheet that is swept through the region of interest at a rate appropriate to the flow velocities present and the resolution in position and velocity that is needed, figure 5.1. However, at high sweep rates, the particle residence time in the beam is reduced as is the signal to noise ratio. By locating three linear CCD array detectors with cylindrical lenses in the proper orientations, three components of the velocity and position of the particle can be measured for each sweep. Furthermore, with the lateral position of the particle in the laser sheet known, the incident intensity on the particle is known, so the scattered light intensity can be used to size the particle at each sweep. This will give the rate of change of the particle size.

Before attempting to design and test a technique capable of tracking a single particle in an actual spray environment, the present work was restricted to studying the feasibility of obtaining one and two components of velocity from a stream of liquid drops. The points that this task addressed are the following:

- Design the optical layout for a one and two-dimensional Lagrangian Particle Tracker (LPT), i.e., one that provides one or two components of velocity from a stream of liquid drops.

- Investigate the feasibility of "tagging" the drops with a dye, for example, fluorescein dye, to distinguish these drops from untagged ones in a spray.

- Determine the laser power requirements of the LPT system to detect drops having sizes typical of spray combustion systems using low grade fuels.

- Investigate the use of charge coupling device (CCD) arrays to detect the particles.

- Investigate the use of area CCD arrays for this application.

- Determine the feasibility of coupling the LPT with a light scattering technique to determine the temperature of the drops.

Investigations on the feasibility of using the LPT system for the diagnostics of single drop evaporation and combustion were carried out. A breadboard system has been built, and data has been obtained, which has shown the potential of the method. This breadboard system is shown schematically in Figure 5.1. The transmitter system consists of an Argon-ion water-cooled laser, spatial filtering means, optical lenses to provide a collimated beam, a rotating polygon mirror assembly, and a lens to create a collimated scanning beam.

In the receiver end of the system, light is collected at right angles to the scanning beam by a set of lenses to produce a real image which is subsequently focused onto a linear, 1024 element CCD array. Dedicated circuitry was designed at Aerometrics to provide the different clocks necessary for the digitizer and the motor controller of the rotating polygon mirror. The CCD array has a readout rate of 20 MHz. The array can be read into the Tektronix model 2430A digital oscilloscope or into the Compaq 386/20 computer.

The principle of operation of the LPT is as follows: as the collimated beam hits the rotating decahedron mirror assembly, the beam is reflected from one of the mirrors and onto the collimating lens, which is positioned at the

lens' focal distance. As each mirror rotates into the beam path, the reflected beam sweeps from top to bottom of the collimating lens. At a sufficiently high rotating speed of the mirrors, the reflecting beam appears as a continuously illuminated vertical sheet of light which is incident on the stream of drops. This stream was generated with the Drop on Demand (DoD) instrument designed at Aerometrics to provide, via a piezoelectric device, a specified number of liquid drops per second. The DoD can be fitted with nozzles having different pinholes to produce drops of different sizes. In addition, the signal voltage to the piezoelectric disc can be varied, as well as the slew rates (volts/μs) of the rise, dwell, and fall portions of the voltage signal. The use of a Berglund Liu monosize drop generator would not have been suitable for these preliminary studies because this instrument typically operates at relatively high frequencies and generates many particles per second.

The scanning frequency of the mirror assembly was synchronized with the digitizer frequency, such that a full sweep of the CCD linear array (length of CCD=25 mm) by the laser beam would correspond to a single horizontal line on the video display. Therefore, a drop passing through the illuminated sheet of light, which was fixed at 50 mm, was seen on the video monitor as a series of small dark lines, each occupying one horizontal line on the monitor. The relative intensity of the light falling on the pixel elements of the CCD array covered a range from 0 (maximum) to 255 (minimum). Individual analysis of the video lines containing information revealed the relative intensity of the light and the pixel location. With this information and the scanning frequency, along with the ratio of the length of the illuminated sheet to the length of the image, R_i=50/25, the velocity of the drop at each location along its path can be obtained.

Figure 5.2 shows some preliminary results obtained with the breadboard LPT system. Using a 100 μm pinhole in the nozzle of the DoD instrument, drops of 212 μm were generated, moving with a velocity which varied from 1.2 to 1.5 m/s (measured with the Aerometrics PDPA system). What is observed in Figure 5.2 is the individual hits of the scanning beam on one drop along its trajectory through the light sheet.

These preliminary measurements show that the technique might have the potential to perform velocity measurements in a Lagrangian frame of reference for a simple stream of drops and that the method should be explored to measure two components of velocity.

By using a second cylindrical lens and a linear array detector oriented orthogonal to the first, in principle a second velocity component in the plane of the beam sweep may be obtained. An additional receiver and a third linear array looking down the sweep direction can be used to locate the particle in the direction normal to the sweep and, hence, provide information on the third component of velocity.

The question of accurately detecting and locating out of focus particles arises when attempting to cover a larger field of view. A method referred to as sub-pixel imaging can be used. With this method, the blur spot produced by the out of focus particle spans several pixels. The blur spot is then fit with a parabola, or other polynomial, which allows the peak or center of the image to be located with better resolution than if the drop were in focus on a single pixel. Thus, a much greater field of view can be covered than with in-focus imaging.

Ultimately, this method is intended to track individual tagged particles of known diameter that are injected into the spray. The injection rate has to be controlled, so that there is no confusion as to which particle is being observed during its transit through the flow field. Particles can be tagged with fluorescent dye, and a line filter can be used in front of the detector to limit the signals detected to only the tagged particles. A major concern is the detectability of the dye drops. The preliminary tests show that scattered light at approximately 45 degrees produced a very good signal to noise ratio, but the fluorescent signal was marginal. This was due to a rather large noise level, apparently from the pixel readout. There appeared to be an error in the array sampling electronics. This problem needs to be addressed.

Further work on the method will require the use of more sensitive CCD arrays and greater laser power. Our research and development in drop

temperature measurements is being considered in conjunction with this approach to obtain drop size, velocity and temperature in a Lagrangian frame, as it passes through a turbulent flame.

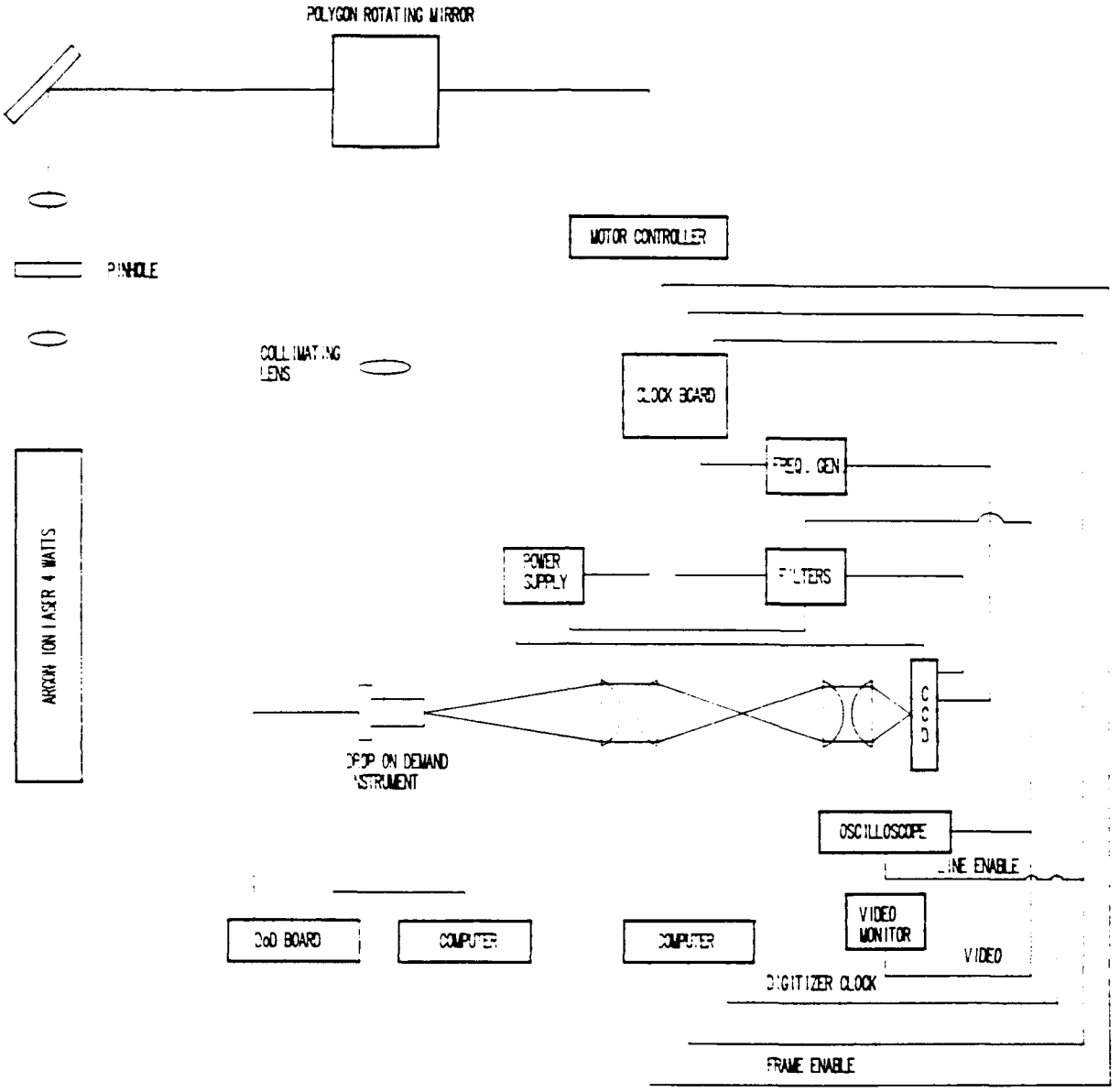

Figure 5.1: Schematic of the proposed Lagrangian Particle Tracker.

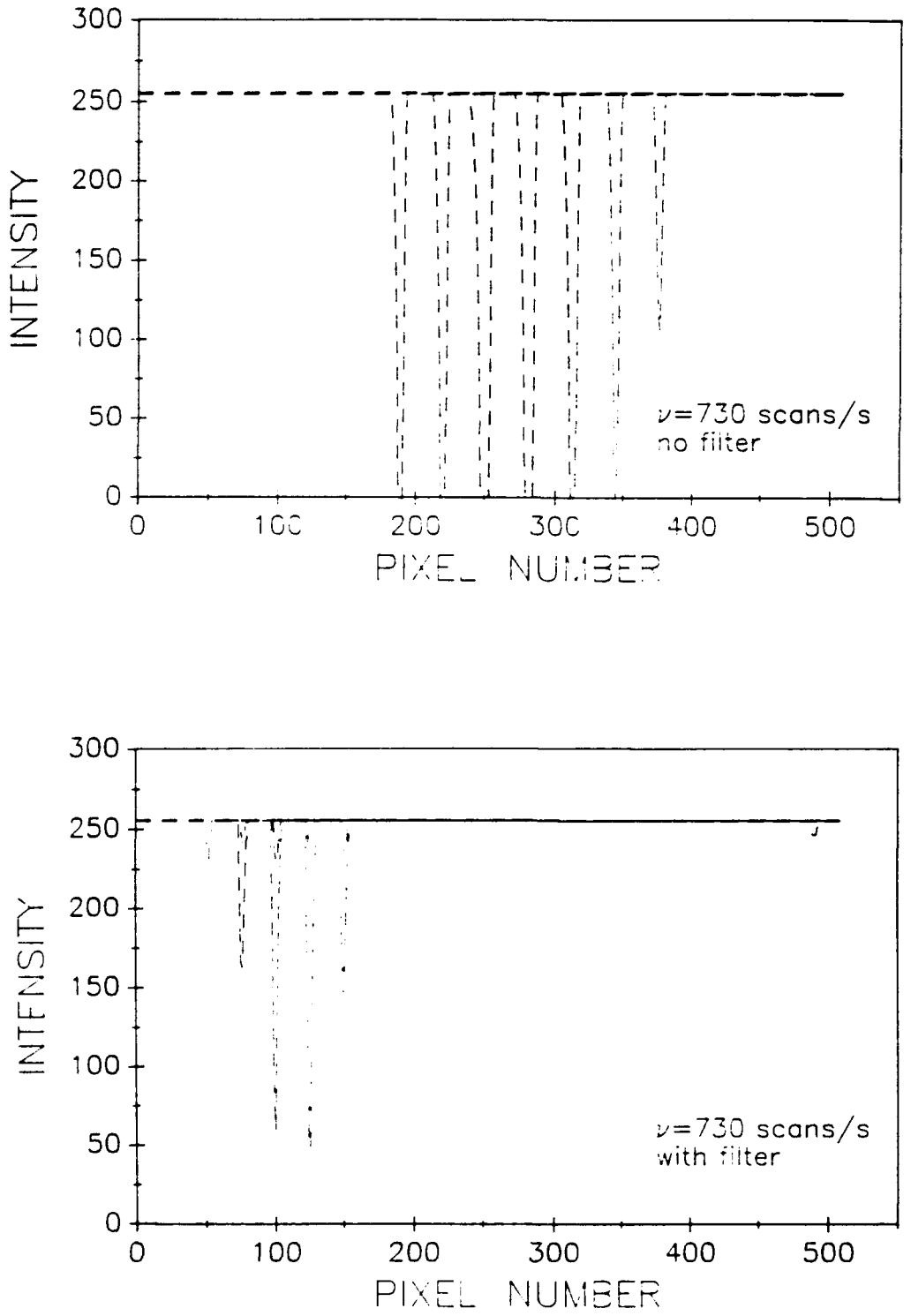

Figure 5.2: Preliminary results with the Lagrangian Particle Tracker showing individual images of a single drop along its trajectory on the CCD array.

References

Agrawal Y.C., and McCullogh J.R. (1981) "Directional pedestal-free laser Doppler Velocimetry without Frequency Biasing, Part 1", Applied Optics, vol. 20, p 1553.

Alexander D.R., Wiles J.J., Schaub S.A., and Seeman M.P. (1985) "Effects of Non-Spherical Drops on a Phase Doppler Spray Analyzer", SPIE Particle Sizing and Spray Analysis, vol 573, pp. 67-72.

Asano, S., (1979) "Light Scattering Properties of Spheroidal Particles", Applied Optics, Vol. 18, No. 5, March, pp. 712-723.

Bachalo W.D. (1980) "Method for Measuring the Size and Velocity of Spheres by Dual-beam Light-Scatter Interferometry" Applied Optics, vol 19, pp. 363-370.

Bachalo W.D., and Houser M.J., (1984) "Development of the Phase Doppler Spray Analyzer for Liquid Drop Size and Velocity Characterization," AIAA-84-1199,

Bachalo W.D., Rudoff R.C., and Brena de la Rosa A. (1988) "Mass Flux Measurements of a High Number Density Spray System Using the Phase Doppler Particle Analyzer" AIAA 26th Aerospace Sciences Meeting, Jan 11-14, Reno, NV.

Bachalo, W. D., and Sankar, S. V., (1988) "Analysis of the Light Scattering Interferometry for Spheres Larger than the Light Wavelength", Paper presented at the 4th International Symposium on Applications of Laser Anemometry to Fluid Mechanics, Lisbon, Portugal, July 11-14.

Bachalo, W.D., (1980) "Methods for Measuring the Size and Velocity of Spheres by Dual-Beam Light-Scatter Interferometry}, Applied Optics, Vol. 19, No. 3.

Barber P. W., and Hill S. C., (1988) "Effects of Particle Nonsphericity on Light Scattering, Optical Particle Sizing: Theory and Practice," Ed. by G. Gouesbet and G. Grehan, Plenum Press, pp. 43-53.

Barnett, D. and Bentley, H.T. III (1974) "Statistical Bias of Individual Realization Laser Velocimeters", proc. of the 2nd International Workshop on Laser Velocimetry, Purdue University, vol. 1, pp. 438,442.

Billet, M.L.,(1985) "Cavitation Nuclei Measurements- A Review," Presented at the ASME Cavitation and Multiphase Flow Forum, Albuquerque, New Mexico, June 24-26.

Bogard D. and Tiederman W. (1979) "Experimental Evaluation of Sampling Bias in Naturally Seeded Flows" in Laser Velocimetry and Particle Sizing, Hemisphere Pub., pp. 86,-.

Born, M. and Wolf, E., (1975) "Principles of Optics.} Fifth Edition, Pergamon Press.

Bradshaw, P., Ed. (1978), Turbulence, Topics in Applied Physics, Volume 12, Springer-Verlag,

Breber, G., (1988) "Agitated Vessels: Onset of Cavitation Near Mechanical Impellers}, Presented at the AIAA First National Fluid Dynamics Congress, Cincinnati, Ohio, July 24-28.

Breña de la Rosa, A., Sankar, S. V., Weber, B., Wang, G., and Bachalo, W. D., (1989) "A Theoretical and Experimental Study of the Characterization of Bubbles Using Light Scattering Interferometry," Presented at the Third International Symposium on Cavitation Inception, San Francisco, U. S., December 10-15

Buchhave P. (1975) "Biasing Errors in Individual Particle Measurements with the LDA Counter Signal Processor", Proc. LDA Syposium, Copenhagen, pp. 258,278.

Buchhave P. (1979) "The Measurement of Turbulence with the Burst-Type Laser Doppler Anemometer - Errors and Correction Methods" Technical

Report # TRL-106 Turbulence Research Laboratory, State University of New York at Buffalo.

Buchhave P., George W., and Lumley J.L. (1979) "The Measurement of Turbulence with the Laser Doppler Anemometer", Ann. Rev. of Fluid Mech., vol. 11, pp. 443,503.

Chahine, G. L., and Bovis, A. G., (1983) "Pressure Field Generated by Nonspherical Bubble Collapse", Journal of Fluids Engineering, Vol. 105, Sept. 1983, pp. 356-363.

Clift, R., Grace, J. R., and Weber, M. E., (1978) "Bubbles, Drops, and Particles}, Academic Press Inc., New York.

Craig, R.R and Nejad A.S. (1985) "Velocity Biasing of Two-Component LDV Data in Low-Turbulence Flows", AIAA Journal, vol. 23, no. 6, pp. 973,-.

Craig, R.R. Nejad, A.S. and Hahn E.Y. (1984) "A General Approach for Obtaining Unbiased LDV Data in Highly Turbulent Non-reacting and Reacting Flows", AIAA Paper 86- 0366.

Damp S., (1991) "Miniature Laser Doppler Anemometer for Sensor Concepts," Proceedings of the SPIE International Symposium of High Power Lasers, Part of OE LASE '91, Los Angeles, USA, Jan 20-25.

Dimotakis P.E. (1976) "Single-Scattering Particle Laser Doppler Measurements of Turbulence" AGARD Conference No. 193, Applications of Non-Intrusive Instrumentation in Fluid Flow Research, paper 10.

Dimotakis P.E., Collins, D.J., and Lang, D.B. (1979) "Laser Doppler Velocity Measurements in Subsonic, Transonic and Supersonic Turbulent Boundary Layers" in Laser Velocimetry and Particle Sizing, Hemisphere Pub., pp. 208,-.

Dopheide D., Faber M., Reim, G., and Taux G., (1988) "Laser and Avalanche Diodes for Velocity Measurement by Laser Doppler Anemometry," Experiments in Fluids, Vol. 6, pp. 289-297.

Dopheide D., Pfeifer H., Faber M., and Taux G., (1989) "The Use of High-Frequency Pulsed Laser Diodes in Fringe Type Laser Doppler Anemometry," Journal of Laser Applications, Vol. 1, No. 4, October, pp. 40-44.

Durao D.F.G. and Whitelaw J.H. (1975) "The Influence of Sampling Procedures on Velocity Bias in Turbulent Flows", Proc. of the LDA-symposium, Copenhagen, Technical University of Denmark, pp. 138-.

Durao D.F.G. and Whitelaw J.H. (1979) "Relationship Between Velocity and Signal Quality in Laser- Doppler Anemometry", Journal of Physics E: Scientific Instruments, vol. 12, pp. 47,-

Durao D.F.G., Laker J., and Whitelaw J.H. (1980) "Bias Effects in Laser Doppler Anemometry", Journal of Physics E: Scientific Instruments, vol. 13, pp. 442,445.

Edwards C.F., Rudoff, R.C., and Bachalo, W.D. (1990) "Measurement of Correlated Droplet Size and Velocity Statistics, Size Distributions, and Volume Flux in a Steady Flame," Proceedings of the Fifth International Symposium on the Applications of Laser Techniques to Fludi Mechanics, Lisbon, Portugal, 1990.

Edwards C.F. , and Marx K.D. (1991) "Analysis of the Ideal Phase-Doppler System: Limitations Imposed by the Single-Particle Constraint", Sandia Report SAND91-8560, June.

Edwards R.V. (1981) "A New Look at Particle Statistics in Laser Anemometry Measurements", Journal of Fluid Mechanics, vol. 105, pp. 317,-.

Edwards R.V. (1987) "Report of the Special Panel on Statistical Particle Bias Problems in Laser Anemometry", Journal of Fluids Engineering, vol. 109, pp.89,93.

Edwards R.V. and Jensen, A.S. (1983) "Particle Sampling Statistics in Laser Doppler Anemometers: Sample-and-Hold and Saturable Sysyems", Journal of Fluid Mechanics, vol. 133, pp. 397,411.

Edwards R.V. and Meyers J.F. (1984) "An Overview of Particle Sampling Bias", Proc. of the 2nd Symposium on Applications of Laser Doppler Velocimetry to Fluid Dynamics, Lisbon, Portugal, pp. 2.1.1, 2.1.5.

Erdmann J.L. and Tropea C.D. (1981) "Statistical Bias in Laser Anemometry" SBF 80/ET/198, Universitat Karlsruhe Report

Erdmann J.L. and Tropea C.D. (1981) "Turbulence - Induced Statistical Bias in Laser Anemometry", 7th Biennial Symposium on Turbulence, Rolla, MO.

Felton, P.G., Hamidi, A.A.,and Aigal, A.K., (1984), "Multiple ScatteringEffects on Particle Sizing by Laser Diffraction", University of Sheffield Report No. 431 HIC, August.

Franc, J. P., and Michel, J. M., (1988) "Unsteady Attached Cavitation on an Oscillating Hydrofoil", Journal of Fluid Mechanics, Vol. 193, pp. 171-189.

Fraser, S. M., Carey, C., and Wilson, (1984) "Investigation by LDA of the Fluid Behaviour Downstream of a Mixed-Flow Impeller", Presented at the Second International Symposium on Applications of Laser Anemometry to Fluid Mechanics, Lisbon, Portugal, July.

Friehe, C., Van Atta, C.W., and Gibson, C.H., (1971), "Jet Turbulence Dissipation Rate Measurements and Correlations", NATO AGARD, pp18-1 to 18-7.

Gebhart J., and Anselm A., (1988) "Effect of Particle Shape on the Response of Single Particle Optical Counters, Optical Particle Sizing: Theory and Practice," Ed. by G. Gousbet and G. Grehan, Plenum Press, pp. 393-409.

Giel T. and Barnett D. (1979) "Analytical and Experimental Study on Statistical Bias in Laser Velocimetry" in Laser Velocimetry and Particle Sizing, Hemisphere Pub., pp. 86.-.

Glantschnig, W. J., and Chen, S.,(1981) "Light Scattering from Water Droplets in the Geometrical Optics Approximation", Applied Optics, Vol. 20, No. 14, p. 2499, July 15.

Goldstein R.J. (1983) Flid Mechanics Measurements, Hemisphere Pub.

Gouesbet, G., Maheu, B., and Gréhan, (1988) "Light Scattering from a Sphere Arbitrarily Located in a Gaussian Beam Using a Bromwich Formulation", Journal of the Optical Society of America, Vol. 5, p. 1427, September.

Gould R.D., Stevenson W.H. and Thomspson H.D. (1986), "A Parametric Study of Statistical Velocity Bias", Procs. of the 5th International Congress on Applications of Lasers and Electro-Optics, Arlington, VA, Nov. 10,13.

Gould R.D., Stevenson W.H., and Thompson H.D. (1989) "Parametric Study of Statistical Bias in Laser Doppler Velocimetry", AIAA Journal, Vol. 27, no. 8, pp. 1140,1142.

Graham L.J.W., Winter A.R., Bremhorst K., Daniel B.C. (1989) "Clock-Induced Bias Errors in Laser Doppler Counter Processors", Journal of Physics E-Scientific Instruments, Vol. 22, No. 6, pp. 394,397.

Hinze, J.O. (1972) "Turbulent Fluid and Particle Interaction", Progress in Heat and Mass Transfer, vol. 6, Pergamon Press, New York.

Hodkinson J. P., and Greenleaves I., (1963) "Computations of Light Scattering and Extinction by Spheres According to Diffraction and Geometrical Optics," Journal Optical Society of America, Vol. 53, p. 577,

Hoesel W. and Rodi W. (1977), "New Biasing Elimination Method for Laser-Doppler Velocimeter Counter Processing", Rev. Sci. Instrum., vol. 48, no. 7, pp. 910,919.

Holve D. J., and Davis G. W., (1982) "Analysis of a Single Particle Counter for Application to General Aerosol Environments," Presented at the 1982 Fall Meeting of the Western States Section of the Combustion Institute, Sandia National Laboratories, Livermore, CA, October 11-12.

Holve D., and Self S. A., (1978) "An Optical Particle-Sizing Counter for In-Situ Measurements, Project" SQUID, Technical Report SU-2-PU, Purdue University, West Lafayette, Indiana.

Ibrahim K.M., Wertheimer G.D., and Bachalo W.D. (1991) "Signal Processing Considerations for Low Signal to Noise Ratio Laser Doppler and Phase

Doppler Signals", presented at the Fourth International Conference on Laser Anemometry, Cleveland, OH, August 5-9.

Jackson, T. A., and Samuelsen, G. S., (1987) "Droplet Sizing Interferometry: A Comparison of the Visibility and Phase Doppler Techniques", Applied Optics, Vol. 26, No. 11, pp. 2137-2143

Johnson D.A. and Bachalo W.D. (1980) "Transonic Flow About a Two-Dimensional Airfoil - Inviscid and Turbulent Flow Properties", AIAA Journal, vol. 18, pp. 16-24.

Johnson D.A., Bachalo W.D., and Modarres D. (1976) "Laser Velocimetry Applied to Transonic and Supersonic Aerodynamics", AGARD Conference Proc. No. 193 of Applications of Non-Intrusive Instrumentation in Fluid Flow Research.

Johnson D.A., Modarres D., Owen F.K. (1981) "An Experimental Verification of Laser Velocimeter Sampling Bias and its Elimination in Highly Turbulent Shear Flows" Proc. of the 3rd Syposium on Turbulent Shear Flows, U.C. Davis, Sept. 9-11.

Johnson D.A., Modarres D., Owen F.K. (1982) "An Experimental Verification of Laser Velocimeter Sampling Bias Correction" Proc. of the Syposium on Engineering Applications of Laser Velocimetry, ASME Winter Annual Meeting, Phoenix, AZ.

Jones A. R., (1988) "Fraunhofer Diffraction by Random Irregular Particles, Optical Particle Sizing: Theory and Practice," Ed. by G. Gouesbet and G. Grehan, Plenum Press, pp. 301-310.

Jones, G.S., Kamemoto, D.Y., and Gartrell, L.R.,(1990), "An Investigation of the Effects of Seeding in Laser Velocimeter Systems", AIAA Paper 90-0502, 28th Aerospace Sciences Meeting, Reno, Jan.

Kamiyama, S., and Yamasaki, T., (1986) "Critical Condition of Cavitation Occurrence in Various Liquids", Journal of Fluids Engineering, Vol. 108, December, pp. 428-432.

Kerker, M., (1969) "The Scattering of Light," Academic Press.

Killinger R. T., and Zerull R. H., (1988) "Effects of Shape and Orientation to be Considered for Optical Particle Sizing, Optical Particle Sizing: Theory and Practice, " Ed. by G. Gouesbet and G. Grehan, Plenum Press, pp. 419-429.

Kuiper, G., (1978) "Scale Effects on Propeller Cavitation Inception - Variation of Roughness and Nuclei", Presented at the Twelfth Symposium on Naval Hydrodynamics, Washington, D. C.

Kuiper, G., (1982) "Some Experiments with Specific Types of Cavitation on Ship Propellers", Journal of Fluids Engineering, Vol. 104, March 1982, pp. 105-114.

Lazaro B.L. (1991) "Evaluation of Phase Doppler Particle Sizing in the Measurement of Optically Thick., High Number Density Sprays" Unitet Technologies Research Center, August 1991.

Marston, P. L., (1979), "Critical Angle Scattering by a Bubble: Physical-Optics Approximation and Observations", Journal of Optical Society of America, vol 69, No. 9, September.

Marston, P. L., Langley, D. S., and Kingsbury, D. L., (1981), "Light Scattering by Bubbles in Liquids or in Glass", Technical Report No. 1, Department of Physics, Washington State University,

McDonell, V. G., Cameron, C. D., and Samuelsen, G. S.,(1987) "Symmetry Assessment of a Gas Turbine Air-Blast Atomizer", AIAA/SAE/ASME/ASEE 23rd Joint Propulsion Conference, San Diego,

McLaughlin D.K. and Tiederman W.G. (1973), "Biasing Correction for Individual Realization of Laser Anemometer Measurements in Turbulent Flows", Physics of Fluids, vol. 16, no. 12, pp. 2082,2088.

Meyers J.F. and Clemmons J.I., Jr. (1979) Processing Laser Velocimeter High-Speed Burst Counter Data" in Laser Velocimetry and Particle Sizing, eds., H.D. Thompson and W.H. Stevenson, Hemisphere Pub., pp. 300,-.

Meyers J.F. and Hepner T.E. (1984) "Velocity Vector Analysis Using a three Component Laser Velocimeter", Proc. of the 2nd Symposium on

Applications of Laser Doppler Velocimetry to Fluid Dynamics, Lisbon, Portugal, pp. 3.1.1, 3.1.5.

Meyers J.F. and Wilkinson S.P. (1982) "A Comparison of Turbulence Intensity Measurements Using a Laser Velocimeter and a Hot Wire in a Low Speed Jet Flow", Proc. of the International Symposium on Applications of Laser-Doppler Anemometry to Fluid Mechanics, Lisbon, Portugal.

Naude, C. F., and Ellis, A. T., (1961) "On the Mechanisms of Cavitation Damage by Non-hemispherical Cavities Collapsing in Contact with a Solid Boundary", ASME Journal of Basic Engineering, Vol. 83, 1961, pp. 648-656.

Nejad A.S. and Davis D.L. (1982) "Velocity Bias in Two Component Individual Realization Laser Doppler Velocimetry", Exact reference missing. Report from the Aero-Propulsion Laboratory, Wright-Patterson Air Force Base, Dayton, OH 45433.

Pendleton, J. D., (1982), " Mie and Refraction Theory Comparison for Particle Sizing with the Laser Velocimeter", Applied Optics, Vol. 21, Part 1, pp. 684-688.

Quigley M.S. and Tiederman W.G. (1977) "Experimental Evaluation of Sampling Bias in Individual Realization Laser Anemometry", AIAA Journal, vol. 15, no. 2, pp. 266,268.

Roesler T., Stevenson W.H., and Thompson H.D. (1980) "Investigation of Bias Errors in Laser Doppler Velocimeter Measurements", AFWAL-TR-80-2108.

Rudoff R.C., Houser M.J., and Bachalo W.D. (1987) "Two Phase Measurements of a Spray in the Wake if a Bluff Body" ISABE 87-7017.

Sankar S.V., Bachalo, W.D. (1991) "Response Characteristics of the Phase Doppler Particle Analyzer for Sizing Spherical Particles larger than the light wavelength" Applied Optics, vol. 30, No. 12.

Sankar S.V., Weber B.J., Kamemoto D.Y., and Bachalo W.D. (1991) "Sizing Fine Particles with the Phase Doppler Interferometric Technique",

Presented at the 2nd International Congress on Optical Particle Sizing, Tempe, AZ, 1990.

Schmidt, R., (1972) "Acoustic Properties of Wakes", NUSC TR 4096.

Simpson R.L. and Chew Y.T. (1979) "Measurements in Steady and Unsteady Separated Turbulent Boundary Layers" in Laser Velocimetry and Particle Sizing, Hemisphere Pub.

Smith W. B., and Wilson R. R., (1978) "Development and Evaluation of a Five-Stage Cyclone System," Report EPA-600/7-78-226, Nov.

Smeets, G. and George, A.(1981), "Michelson Spectrometer for Instantaneous Doppler Velocity Measurements", J. Phys. E. Sci. Instrum., Vol. 14.

Sparks L. E., (1984) Handbook of Air Pollution Technology, Ed. by S. Calvert and H. M. Englund, Wiley-Interscience, New York,

Stevenson W.H., Thompson H.D., and Gould R.D. (1983) "Laser Velocimeter Measurement and Analysis in Turbulent Flows with Combustion", AFWAL-TR-82-2076, Part II.

Stevenson W.H., Thompson H.D., and Luchik T.S. (1983) "Laser Velocimeter Measurements and Analysis in Turbulent Flows with Combustion", AFWAL-TR-82-2076, Part I.

Stevenson W.H., Thompson H.D., and Roesler T.C. (1982) "Direct Measurements of Laser Velocimeter Bias Error in a Turbulent Flow", AIAA Journal, vol. 20, no. 12, pp. 1720,1723.

Stevenson W.H., Thompson H.D., Bremmer, R., and Roesler, T. (1980) "Laser Velocimeter Measurements in Turbulent and Mixing Flows - part II" Air Force Tech. Rep. AFAPL-TR-79-2009.

Stewart, M. B., (1988) "Bubble Dynamics in a Turbulent Ship Wake", Paper No. AIAA-88-3630, Presented at the First National Fluid Dynamics Congress, Cincinnati, Ohio, July 25-28.

Thompson H.D. and Stevenson W.H. (editors) (1979) "Laser Velocimetry and Particle Sizing", Proc. of the 3rd International Workshop on Laser Velocimetry, Purdue University, Hemisphere Pub.

Tomita, Y., Shima, A., and Takahashi, K., (1983) "The Collapse of a Gas Bubble Attached to a Solid Wall by a Shock Wave and the Induced Impact Pressure", Journal of Fluids Engineering, Vol. 105, Sept., pp. 341-349.

Twomey S., (1962) "On the Numerical Solution of Fredholm Integral Equations of the First Kind by the Inversion of the Linear System Produced by Quadrature," Journal Association of Computing Machinery, Vol. 9, No. 1, Jan, pp. 84-97.

van de Hulst, (1981) Light Scattering by Small Particles, Dover Publications.

van de Hulst, H. C., Light (1957) " Scattering by Small Particles", Dover Publications, Inc., New York.

Williamson S. J. (1973) Fundamentals of Air Pollution, Addison-Wesley, Reading, MA,

Winter A.R., Graham L.J.W., Bremhorst K. (1991) "Effects of time scales on velocity bias in LDA measurements using sample and hold processing", Experiments in Fluids, Vol. 11, no. 2 pp. 147-152.

United States Patent [19]

Bachalo

[11] **Patent Number: 4,854,705**

[45] **Date of Patent: Aug. 8, 1989**

[54] **METHOD AND APPARATUS TO DETERMINE THE SIZE AND VELOCITY OF PARTICLES USING LIGHT SCATTER DETECTION FROM CONFOCAL BEAMS**

[75] Inventor: **William D. Bachalo, Los Altos Hills, Calif.**

[73] Assignee: **Aerometrics, Inc., Sunnyvale, Calif.**

[21] Appl. No.: **177,630**

[22] Filed: **Apr. 5, 1988**

[51] Int. Cl.[4] **G01N 15/14; G01N 21/47**

[52] U.S. Cl. **356/336; 356/338**

[58] Field of Search 356/336, 338; 250/574

[56] **References Cited**

U.S. PATENT DOCUMENTS

3,915,572	10/1975	Orloff	356/106
3,941,477	3/1976	Schodl	356/28
4,140,395	2/1979	Kreikebaum	356/336
4,179,218	12/1979	Erdmann et al.	356/336
4,329,054	5/1982	Bachalo	356/336
4,348,111	9/1982	Goulas et al.	356/336
4,387,993	6/1983	Adrian	356/336
4,444,450	4/1984	Flinsenberg et al.	356/336
4,492,467	1/1985	Drain et al.	356/336
4,537,507	8/1985	Hess	356/336
4,540,283	9/1985	Bachalo	356/336
4,636,075	1/1987	Knollenberg	356/336
4,701,051	10/1987	Buchhave et al.	356/336

OTHER PUBLICATIONS

Heterodyne and Quasi-Heterodyne Holographic Interferometry; Dandliker & Thalmann, 24 Opt. Eng. 824, (1985).

Heterodyne Holography Applications in Studies of Small Components, Pryputniewicz; 24 Opt. Eng. 849, (1985).

Phase/Doppler Spray Analyzer for Simultaneous Measurements of Drop Size and Velocity Distributions; Bachalo & Hauser; 23 Opt. Eng. 583, (1984).

(List continued on next page.)

Primary Examiner—Davis L. Willis
Assistant Examiner—Matthew W. Koren
Attorney, Agent, or Firm—Blakely, Sokoloff, Taylor & Zafman

[57] **ABSTRACT**

An apparatus for sizing particles, droplets, bubbles, or the like employing laser light scattering is disclosed. A laser is used for generating two beams of light having different wavelengths or polarizations. The beams with different wavelengths may be generated by an argon ion laser or by two different lasers (e.g., Helium Neon and Helium Cadmium). Two beams with orthogonal polarizations may be produced by partitioning a single linearly polarized beam and rotating the polarization of one by 90°. One of the beams is then expanded using a conventional beam expander and then redirected to be coaxial with the first beam. The beams are then focused to a common focal region. One beam is from two to four times larger in diameter than the other. An optical collection apparatus for sensing the light scattered caused by the particles, droplets, bubbles or the like passing through the focused beams has an axis extending into the focused beams. The axis of the collection apparatus may be aligned with the transmitted beams in the forward or backward direction (on-axis detection) or at some suitable angle to the beams (off-axis detection). The collection apparatus includes receiver lenses which focuses the scattered light through the beam splitter onto a first photo-detector, and light reflected from the beam splitter is directed onto a second photo-detector. The photo-detectors sense the scattered light from the beams with separate wavelengths or polarizations and produce proportionate voltage amplitudes. The peak voltages are determined from the information sensed by the light collection apparatus. A mathematical formulation is used with the known beam diameters and intensities along with the two measured signal voltage amplitudes to determine the particle trajectory through the beams and hence, particle size. The technique also allows for the determination of the sample volume cross-section and particle speed, thus allowing the determination of particle number density and volume flux.

28 Claims, 6 Drawing Sheets

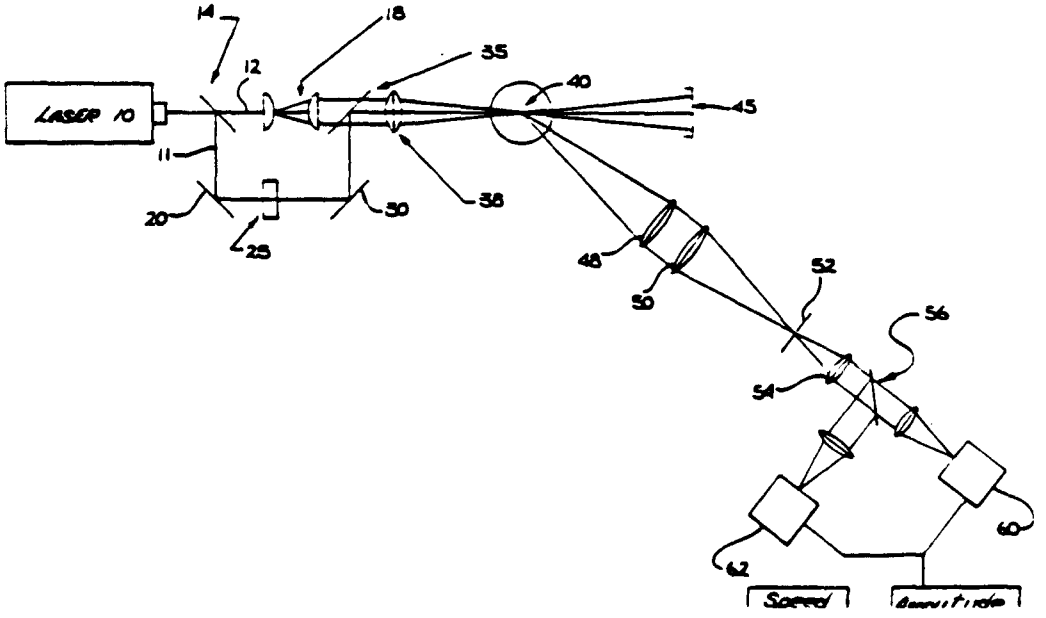

OTHER PUBLICATIONS

Development of the Phase/Doppler Spray Analyzer for Liquid Drop Size and Velocity Characterizations; Bachalo & Houser; AIAA/SAE/ASME 20th Joint Propulsion Conf., (1984).

MIE and Refraction Theory Comparison for Particle Sizing with the Laser Velocimeter; Pendleton; 21 App. Opt. 684, (1982).

Method for Measuring the Size and Velocity of Spheres by Dual-Beam Light-Scatter Interferometry; Bachalo; 19 App. Opt. 363, (1980).

Particle Sizing Using Laser Interferometry; Roberds; 16 App. Opt. 1861, (1977).

Scattering from a Moving Spherical Particle by Two Crossed Coherent Plane Waves; Chu & Robinson; 16 App. Opt. 619, (1977).

Laser Doppler Measurements in Two-Phase Flows; Durst & Zare; Proc. of the LDA-Symposium Copenhagen 403, (1975).

Diffraction Analysis of Doppler Signal Characteristics for a Cross-Beam Laser Doppler Velocimeter; Robinson & Chu; 14 App. Opt. 2177, (1975).

High Resolution Hologram Interferometry by Electronic Phase Measurement; Dandliker, Ineichen & Mottier; 9 Opt. Comm. 412, (1973).

Interference Phase Measurement; Crane; 8 App. Opt. 538, (1969).

Heterodyne Holographic Interferometry; Dandliker; Progress in Optics, vol. XVII, (E. Wolf ed. 1980).

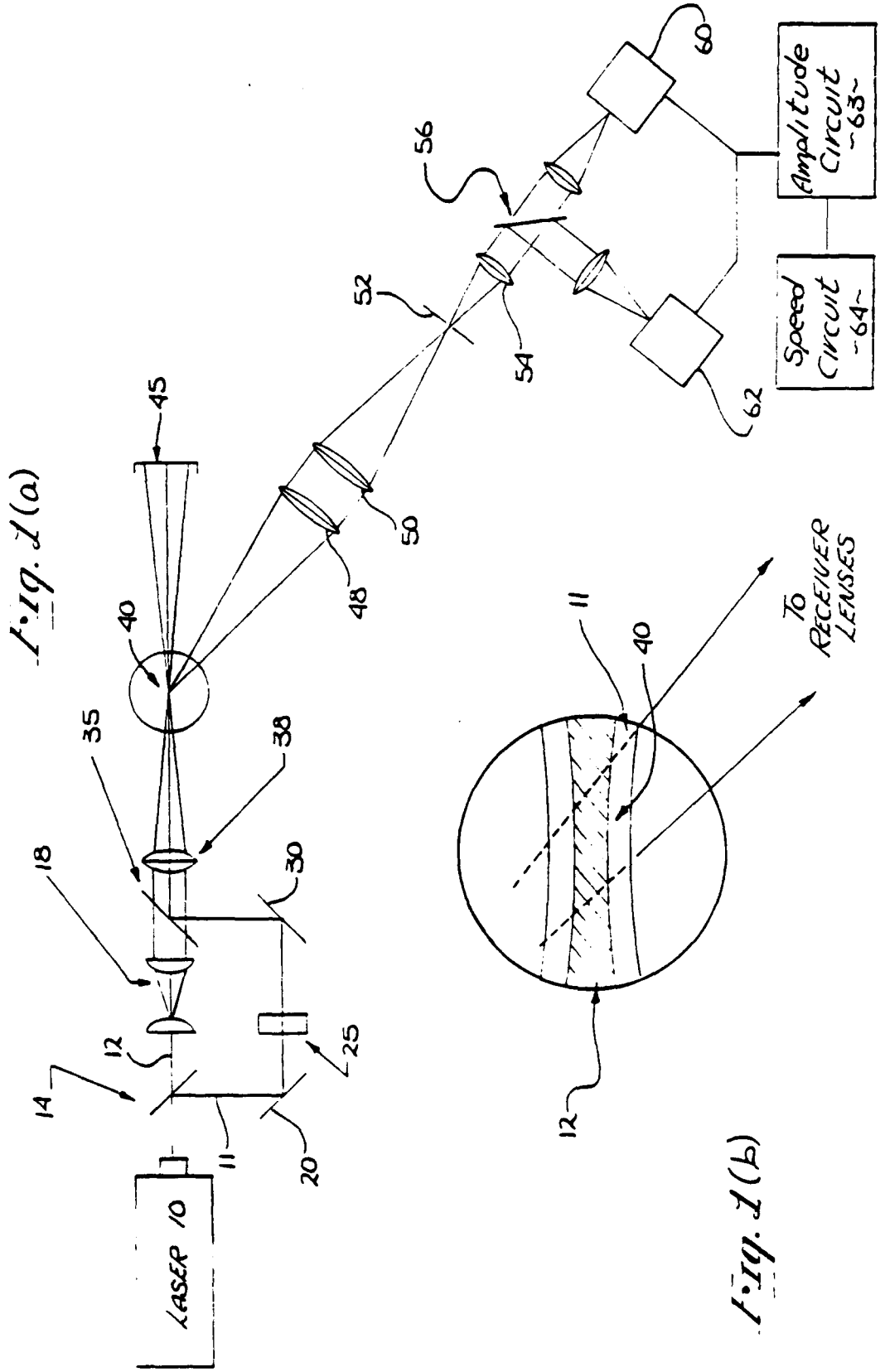
LASER 10
14
12
18
35
40
45
38
30
25
11
20
48
50
52
54
56
60
62
Amplitude Circuit -63-
Speed Circuit -64-
TO RECEIVER LENSES

Fig. 1(a)

Fig. 1(b)

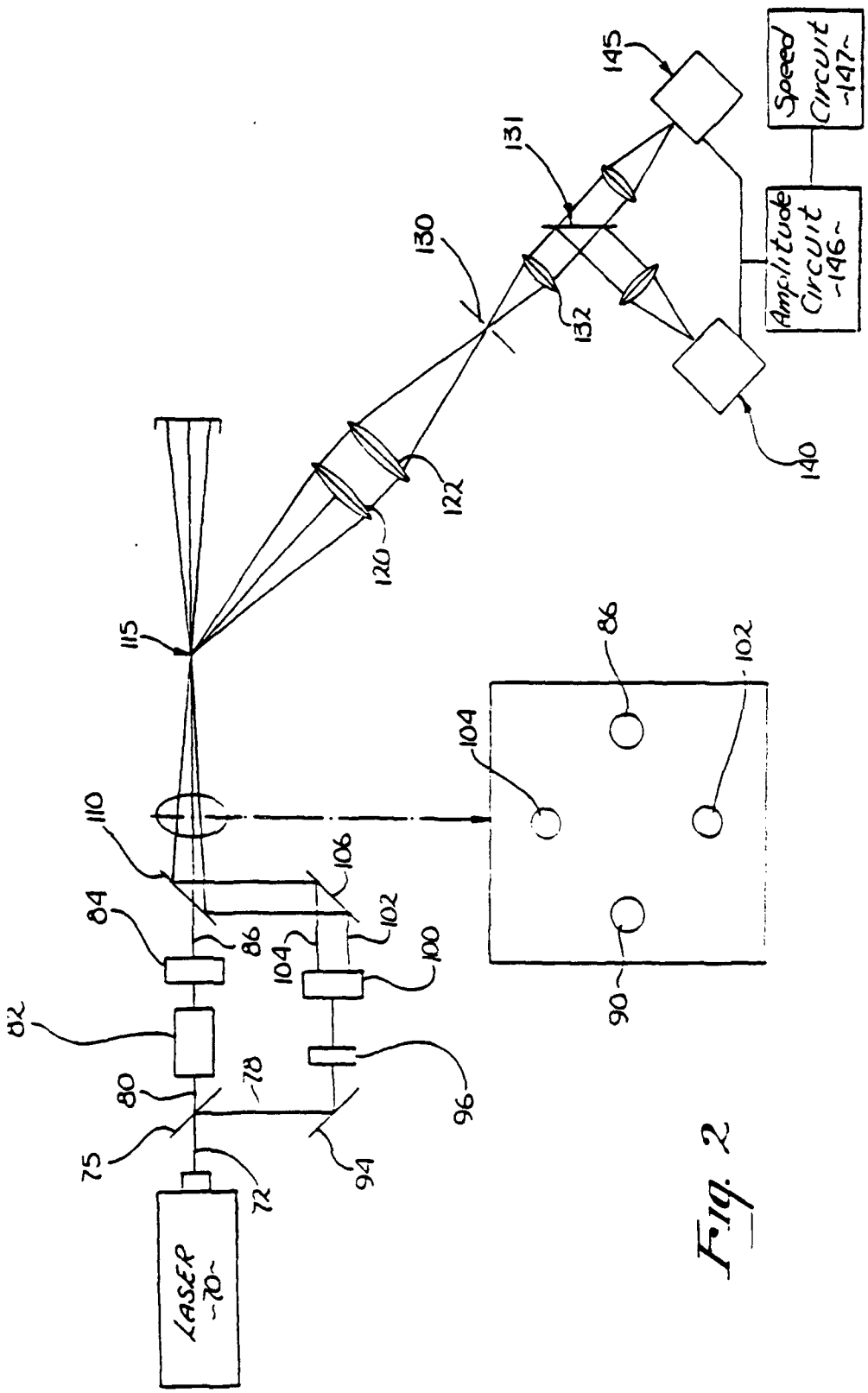
LASER -70-
72
75
80
78
82
84
86
90
94
96
100
102
104
106
110
115
120
122
130
131
132
140
145
Amplitude Circuit -146-
Speed Circuit -147-

Fig. 2

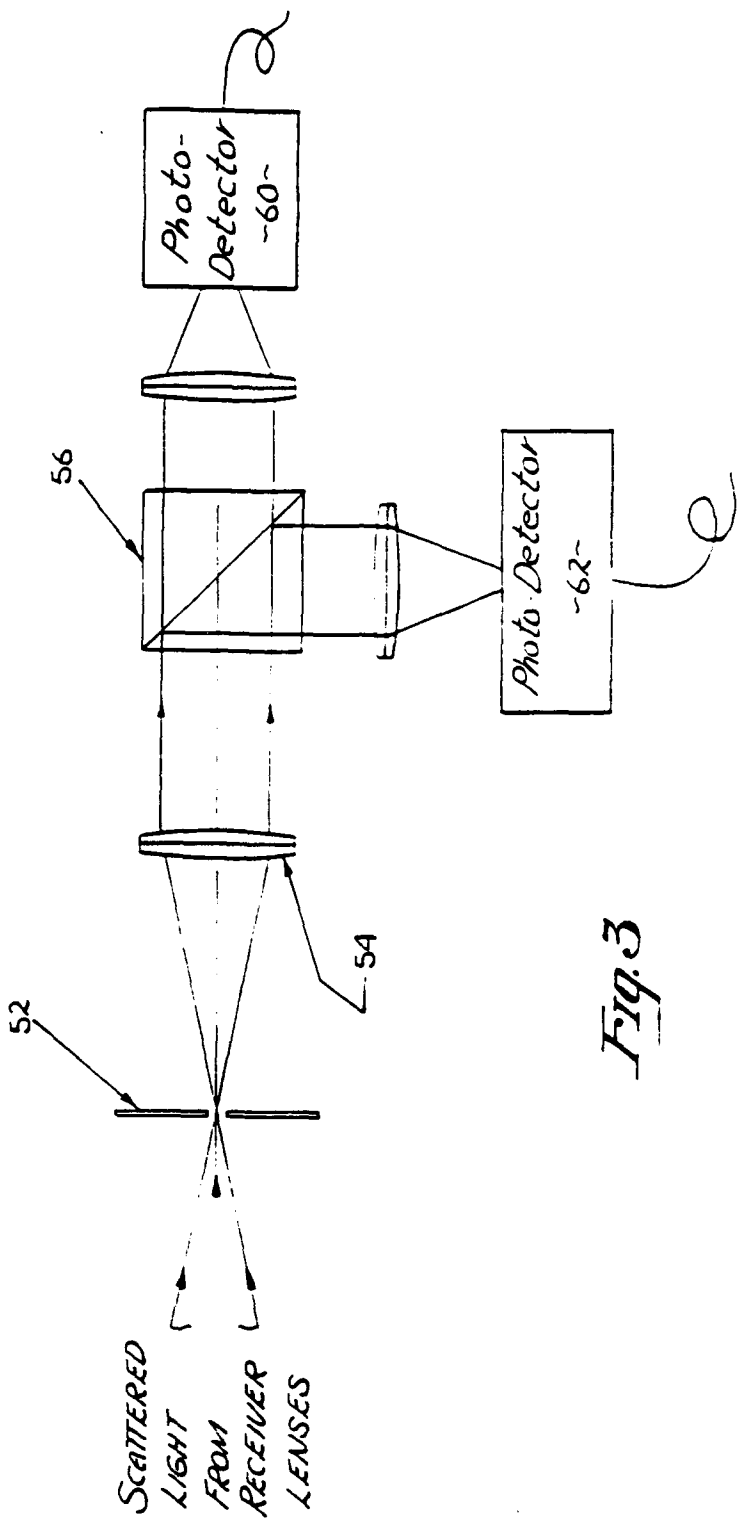
Photo-Detector -60-
56
Photo Detector -62-
54
52
SCATTERED LIGHT FROM RECEIVER LENSES

Fig. 3

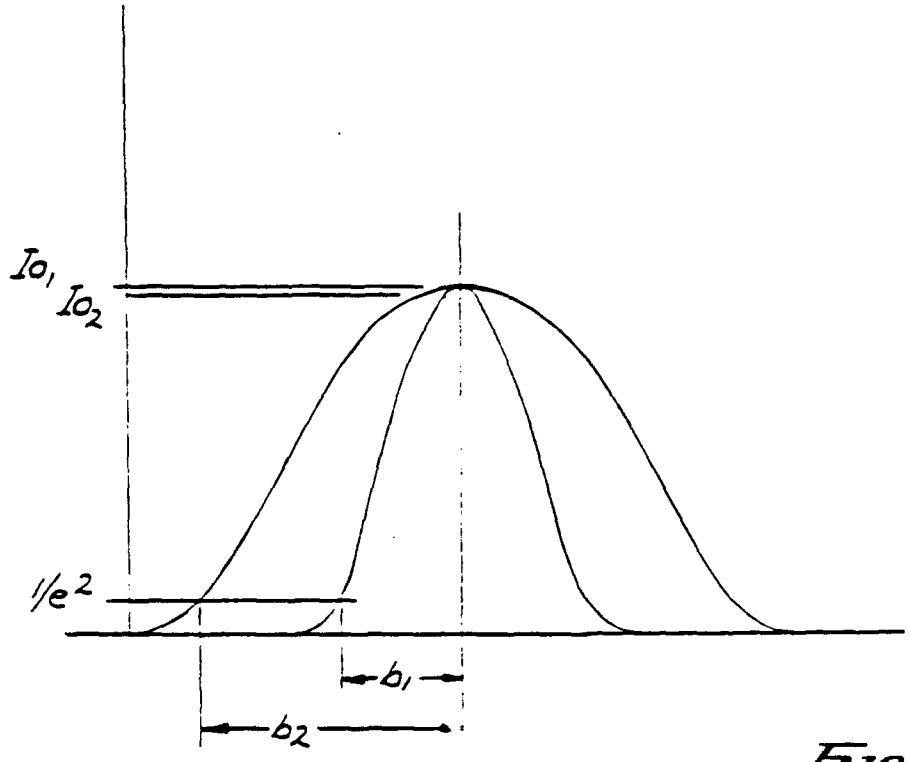

Fig. 4

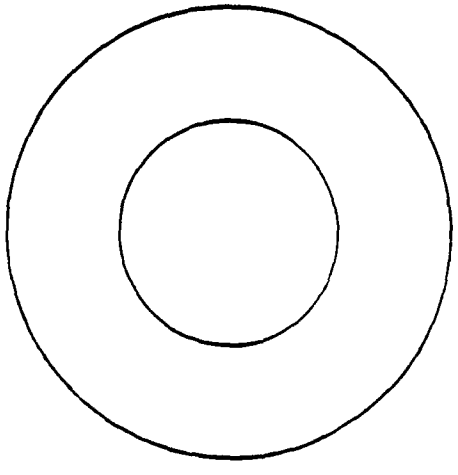

Fig. 5

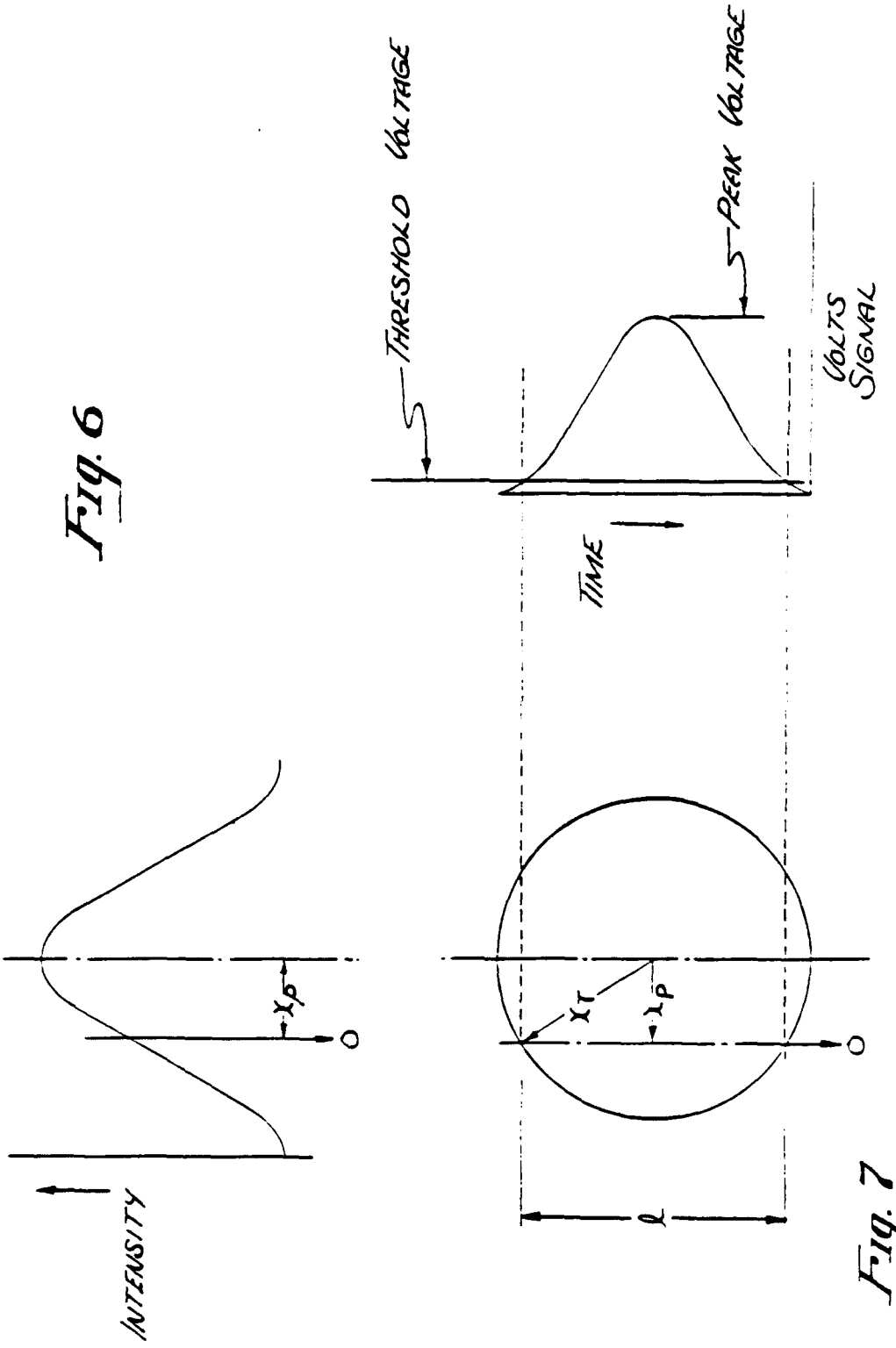
THRESHOLD VOLTAGE
PEAK VOLTAGE
VOLTS SIGNAL
TIME
INTENSITY
x_ρ
0
x_τ
λ_ρ
0
ℓ

Fig. 6

Fig. 7

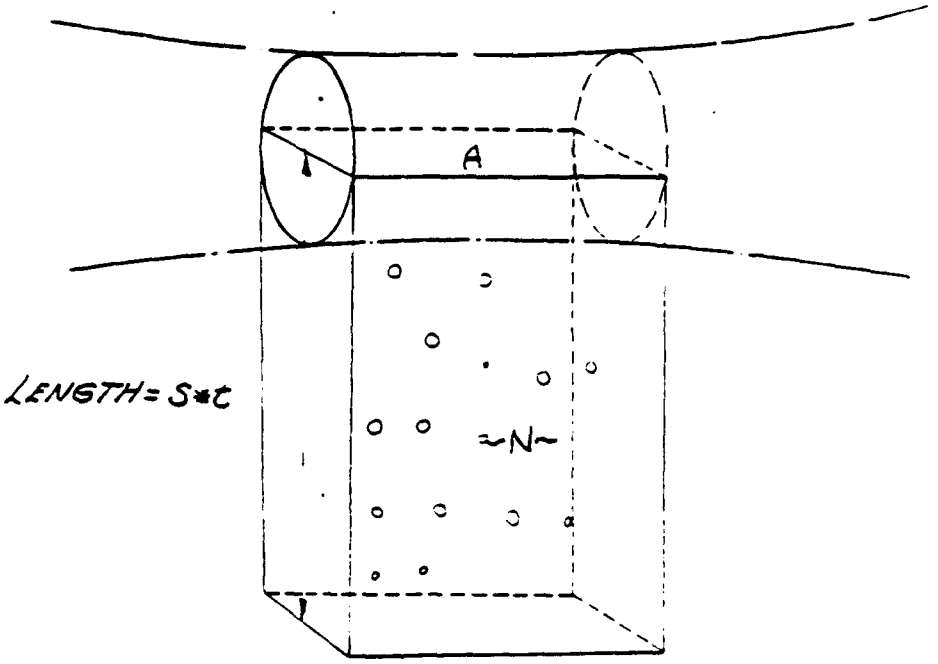

SAMPLE VOLUME = A*S*t

Fig. 8

METHOD AND APPARATUS TO DETERMINE THE SIZE AND VELOCITY OF PARTICLES USING LIGHT SCATTER DETECTION FROM CONFOCAL BEAMS

This invention was made with United States Government support under AFOSR contract F49620-86-C-0078 awarded by the Air Force. The Government has certain rights in this invention.

BACKGROUND OF THE INVENTION

1. Field of the Invention

The present invention relates to the field of determining the size, speed, and other parameters of particles, droplets, bubbles, or the like using laser light scattering.

2. Art Background

The measurement of particles, aerosols, liquid drops, bubbles and the like associated with industrial processes, atmospheric monitoring, combustion processes, agricultural applications of chemicals, cavitation studies, and the like has long been of importance. There have been a number of techniques developed that employ laser light scattering to determine the size of particles, drops, bubbles, or the like (hereinafter collectively referred to as "particles"). These techniques utilize one or more of a number of physical phenomena associated with the light scattering to obtain a measurable quantity that may be related to the particle size. The phenomena include the amplitude or intensity, the angular distribution, and the phase shift of the scattered light. Laser light extinction may also be used with other parameters to obtain additional information on the particles. Systems using the phase shift of the scattered light have been described by the inventor, W. D. Bachalo, in articles entitled, "Method for Measuring the Size and Velocity of Spheres by Dual-Beam Light-Scatter Interferometry", Applied Optics, Vol. 19, Feb. 1, 1980; "Phase/Doppler Spray Analyzer for Simultaneous Measurements of Drop Size and Velocity Distributions", and U.S. Pat. No. 4,540,283. Methods using the angular distribution of the scattered light have been described by J. Swithenbank, J. M. Beer, D. S. Taylor, D. Abbott, and G. C. McCreath, "Laser Diagnostic Technique for the Measurement of Droplet and Particle Size Distribution", *Progress in Astronautics and Aeronautics*, Vol. 53, ed., B. T. inn, 1977; and, E. D. Hirleman and S. Wittig, "In Situ Optical Measurement of Automobile Exhaust Gas Particulate Size Distributions: Regular Fuel and Methanol Mixtures", 16th Symposium (International) on Combustion, MIT, August 1976.

In the present disclosure, the system described utilizes the detection of the amplitude (intensity) of the light scattered by particles to obtain a measurement of their size and speed. The light scattered may be related to the particle size using the well-known Mie theory if the particles are homogeneous and spherical. Calibration with particles of known size may also be used to obtain the functional relationship between the particle size and the scattered light intensity received over a fixed solid angle. A significant difficulty arises when using laser beams with Gaussian (or other nonuniform) intensity profiles. The problem with detecting the peak value of the signal obtained from the scattered light is that this peak value is not only dependent upon the particle size, but also its trajectory through the measurement volume. Since the particle trajectories are random, an uncertainty in the measurement that must be resolved. When designing an in-situ nonintrusive device, this problem places constraints on the implementation of the technique in the field.

At least two viable methods have been proposed to deal with the problem of the Gaussian beam intensity distribution. Holve, D. J., and Self, S., "Optical Particle Sizing for In Situ Measurements", *Journal of Applied Optics*, Vol 18, No. 10, May 1979, pp. 1646–1652, utilized an inversion technique somewhat analogous to methods used in Computer Aided Tomography (CAT) systems. The numerical inversion scheme is used to unfold the dependence of the signals produced by light scattered by particles traversing the sample volume, formed by the laser beam and receiver optics, on random trajectories. A calibration procedure utilizing monodispersed particles of known size is used to define the sample volume and signal amplitude with respect to the particle size.

The second method for removing the ambiguity associated with the Gaussian beam intensity has been described by the inventor, W. D. Bachalo, in U.S. Pat. No. 4,329,054 which was issued on May 11, 1982. Subsequent disclosures of similar approaches have been described by R. J. Adrian in U.S. Pat. No. 4,387,993, issued June 14, 1983; by Apostolos Goulas, et al., in U.S. Pat. No. 4,348,111, issued Sept. 7, 1982; and R. A. Knollenberg in U.S. Pat. No. 4,636,075, issued Jan. 13, 1987. In each case, two concentric or coaxial beams are used having different wavelengths or polarizations. A beam having one wavelength or polarization is focused to a smaller diameter and directed to the center of a larger beam. In this way, the central uniform intensity of the larger beam may be identified. Only particles passing through the central portion of the larger beam will also produce signals on the small beam. When a signal is received from the small beam, the peak amplitude of the signal from the large beam is read and used to obtain the particle size. The method as described by Bachalo has the disadvantage of requiring a relatively large beam diameter ratio (5:1 to 7:1) between the small (pointer) and large (data) beams. A large beam diameter ratio is necessary to ensure that the incident intensity upon the particle from the large beam is known with sufficient accuracy. This requirement acts as a constraint on the upper limit of particle number densities (particle/cc) in which the system will operate satisfactorily.

Nonetheless, instruments based upon this concept have been developed by Hess and Spinoza (see U.S. Pat. No. 4,537,507, issued Aug. 27, 1985), and by Yeoman, M. L., Azzopardi, B. J., White, H. J., Bates, C. J., and Roberts, P. J., "Eng. Appl. of Laser Velocimetry", Winter Annual Meeting ASME, 1982. Upon careful calibration, the instruments were found to perform satisfactorily. As discussed by Bachalo, the method may be combined with the laser Doppler velocimeter to obtain simultaneous particle size and velocity measurements.

In the cases cited, the requirement for the rather large beam diameter ratios limits the application of the system to rather dilute particle fields. The method of Knollenberg which uses an elongated beam shape, overcomes this problem. However, the optical depth of field of the receiver and the need to measure particles on random trajectories also limits the application of the method.

The present invention discloses a means for significantly improving the above-mentioned technique to remove the serious limitation in high number density particle fields, presented by the need for large beam diameter ratios, allow the simultaneous measurement of

particle size, speed, and the sample volume cross-section. A mathematical formulation is given to determine where each particle passed through the Gaussian beam intensity profile and hence, to determine the incident intensity upon the particle. In addition, determination of the individual particle trajectories will allow the measurement of the sample volume diameter for each particle size class. Finally, the particle trajectory through the sample volume along with the transit time will be demonstrated as a means for measuring the speed of the particle. The method has the significant advantage of requiring a beam diameter ratio of only two to three.

SUMMARY OF THE INVENTION

An apparatus for sizing particles, droplets, bubbles, or the like employing laser light scattering is disclosed. A laser is used for generating two beams of light having different wavelengths or polarizations. The beams with different wavelengths may be generated by an argon ion laser or by two different lasers (e.g. Helium Neon and Helium Cadmium). Two beams with orthogonal polarizaions may be produced by partitioning a single linearly polarized beam and rotating the polarization of one by 90°. One of the beams is then expanded using a conventional beam expander and then redirected to be coaxial with the first beam. The beams are then focused to a common focal region. One beam is from two to our times larger in diameter than the other. An optical collection apparatus for sensing the light scattered caused by the particles, droplets, bubbles or the like passing through the focused beams has an axis extending into the focused beams. The axis of the collection apparatus may be aligned with the transmitted beams in the forward or back direction (on-axis detection) or at some suitable angle to the beams (off-axis detection). The collection apparatus includes receiver lenses which focus the scattered light through the beam splitter onto a first photo-detector, and light reflected from the beam splitter is directed onto a second photo-detector. The photo-detectors sense the scattered light from the beams with separate wavelengths or polarizations and produce proportionate voltage amplitudes. The peak voltages are determined from the information sensed by the light collection apparatus. A mathematical formulation is used with the known beam diameters and intensities along with two measured signal voltage amplitudes to determine the particle trajectory through the beams and hence, particle size. The technique also allows for the determination of the sample volume cross-section and particle speed, thus allowing the determination of particle number density and volume flux.

BRIEF DESCRIPTION OF THE DRAWINGS

FIG. 1 is a schematic of the preferred optical system of the present invention.

FIG. 2 is a schematic of an alternate optical system which incorporates the teachings of the present invention.

FIG. 3 is a more detailed schematic of the collection apparatus illustrated in FIGS. 1 and 2.

FIG. 4 is a graph of Gaussian beam intensity profiles of the first and second laser beams comprising the sample volume.

FIG. 5 is an end view of the sample volume of FIG. 4.

FIG. 6 is a graph illustrating a particle passing through the sample volume at a distance Xp from the center.

FIG. 7 is illustrates an end view of the sample volume and particle passing therethrough at a distance Xp from the center.

FIG. 8 illustrates the volume swept by particles passing through the sample volume in time t.

DETAILED DESCRIPTION OF THE INVENTION

An apparatus for sizing particles, droplets, bubbles, or the like (collectively "particles"), particularly suited for making in-situ nonintrusive measurements of the size, number density, and volume flux in a wide range of environments is disclosed. The apparatus utilizes known or predictable particle light scattering characteristics to obtain a size measurement from the measurement of the light scattering intensity. Ambiguity, associated with the Gaussian beam intensity and random particle trajectories through it, is eliminated with the use of a second coaxial beam having a smaller diameter. A mathematical analysis is provided to illustrate how this technique may be optimized such that the method can be used in high number density environments, and make efficient use of the available signals. In the following description, numerous specific details ae set forth such as wavelengths, beam diameter ratios, etc., however, it will be apparent to one skilled in the art that the invention may be practised without these specific details. In other instances, well known devices and components, structures and electrical processing circuits have not been described in detail in order to obscure the present invention unnecessarily.

Referring now to FIG. 1, the apparatus for determining the size of particles includes a laser 10. The laser beams employed by the present invention are generated, in the presently preferred embodiment, by a single laser 10 producing linearly polarized light. However, it will be appreciated that a laser capable of generating two wavelengths, or two separate lasers to provide two separate light wavelengths, could also be used. The light generated by laser 10 is partitioned into two beams 11 and 12 using a beam splitter 14. The beam 12 is increased in diameter using a beam expander denoted generally by the numeral 18. Beam 11 is directed by a reflector 20 through a polarization rotator 25 to rotate the polarization of beam 11 by 90°. The beam 11 is then directed by a reflector 30 to a second beam splitter 35 and made coaxial with the first beam 11. The coaxial beams 11 and 12 are then passed through a focusing lens 38 which causes the beams to focus at a common point. In the present embodiment, the beams 11 and 12 have orthogonal polarizations and the intensities are approximately equal. Where the light scattering by particles produces significant depolarization of the scattered light, different light wavelengths are utilized. As shown in FIG. 1 beams 11 and 12 are focused to form a sample volume 40. Beam stop 45 terminates beams 11 and 12 downstream from the sample volume 40. A light collection apparatus is provided for collecting the light scattered by particles passing through the sample volume 40. The collection apparatus includes receiver lenses 48 and 50 which define a solid angle of collection extending into the focused beams, and focus the scattered light through an aperture 52 and lens 54 onto a polarization beam splitter 56. Light passing through polarization beam splitter 56 is received by a first photo-detector 60, and light reflected off of beamsplitter 56 is received by photo-detector 62. Photo-detectors 60 and 62 are coupled to an amplitude circuit 63 which determines the

proportionate voltage amplitudes. As will be described below, the proportionate voltages are used to determine particle trajectory through beams 11 and 12. The amplitude circuit 63 is coupled to a speed circuit 64, which as will be discussed, determines the speed of a particle passing through the sample volume 40.

The focused beams 11 and 12, as shown schematically, establish two confocal beam diameters. Note than in FIG. 1, the focused beams 11 and 12 have been shown in an enlarged form to illustrate the confocal beam pattern. As shown, beams 12 and 11 have opposite polarizations. Particles passing through the focused beams will scatter light with an intensity that is a function of their diameter and index of refraction, as well as the incident light intensity which is a function of their trajectory through the beams. As will be discussed, the amplitude of the light scattered simultaneously from both beams contains sufficient information to determine the particle size. This information may be predicted by the well-known Mie light scattering theory.

An alternative embodiment of the transmitting optics is shown in FIG. 2, which includes the use of beam splitters to form two pairs of beams that are oriented orthogonal to each other. A laser 70 generates a beam 72 which is directed onto a beamsplitter 75 forming two laser beams 78 and 80. Beam 80 is expanded by beam expander 82 with the now expanded beam split by a beam splitter 84 into two parallel beams 86 and 90. Beam 78 is directed by reflector 94 through a polarization rotator 96 and beam splitter 100 thereby forming two beams 102 and 104. Beams 102 and 104 are directed by reflector 106 onto beam combiner 110 such that a beam matrix results as shown in enlarged form in FIG. 2. These four beams 86, 90, 102 and 104, are then focused to a common crossover region thereby forming a sample volume 115. Particles passing through the focused beams will scatter light that form orthogonal interference fringes in the plane of the receiver lenses 120 and 122. The temporal frequency of this scattered light will be at the Doppler difference frequency. This is the well-known laser Doppler velocimeter technique. This technique can be incorporated with the present invention to provide the particle size and two components of the velocity vector in the plane orthogonal to the beam projection axis.

As shown in FIG. 2, the light scattering is sensed by a collection apparatus (as also disclosed in FIG. 1) which includes lenses 120 and 122 which define a solid angle of collection extending into two focused beams. This collection apparatus may be located at any preferred angle to the transmitted beams including the backscatter direction. The light scattered within the solid angle by particles passing through the sample volume 115 is collected and focused by the receiver lenses 120 and 122 onto an aperture 130. This aperture serves to admit only light scattered by particles crossing the laser beams in the appropriate region wherein they are completely focused. The intersection of the image of the aperture 130 and the focused laser beams serve to define the sample volume. The sample volume 115 is defined by the overlap of the focused laser beams and the image of the aperture in the collection apparatus. It is well known that the relative sample volume size will vary with the particle diameter, as will be discussed below.

In both the embodiments of FIGS. 1 and 2, the collected scattered light is, as will be discussed, focused onto photodetectors (in FIG. 1, detectors 62 and 60; in FIG. 2, detectors 140 and 145) which are coupled to a signal amplitude circuit 146 (FIG. 2) and 63 (FIG. 1). Sizing means (not shown) is coupled to the signal amplitude detection means in each embodiment for determining the size of the particles passing through the sample volume, as will be discussed, based upon the amplitudes of the collected signals. In addition, a speed circuit 64 (FIG. 1) and 147 (FIG. 2) is coupled to the signal amplitude detection means for determining the speed of the particle passing through the sample volume.

Referring now to FIG. 3, the collection apparatus of the present invention includes receiver lenses (lenses 48 & 50 in FIG. 1; lenses 120 and 122 in FIG. 2) which collect the scattered light onto the aperture 52 (130 in FIG. 2). As shown in FIG. 3, in both embodiments of FIGS. 1 and 2, a collimating lens 54 (132 in FIG. 2) disposed beyond the aperture is used to collimate the light before entering the polarizing beam splitter 56 (131 in FIG. 2) (a dichroic beam splitter is used if different wavelengths are used for the laser beams). Additional lenses may be used to focus the light onto the photodetectors. Thus, the receiver optics selectively separate light scattered from the small and large beams by their polarizations and direct the scattered light to their respectively photo-detectors. It will be appreciated that although the illustrated embodiments utilize a polarization beam splitter to separate the light scattering components, a variety of other means can be used. In addition, a combination of light wavelength and polarization could be utilized to ensure complete separation of the signals. For the purposes of the description below, references to optical elements will refer to the elements identified in FIG. 1, however, it will be appreciated that the methods described herein are equally applicable to the embodiment disclosed in FIG. 2.

The receiver system serves to produce two signals with amplitudes proportional to the particle diameter and the trajectory through the large beam 11 and small beam 12. These signals have nominal Gaussian shapes. The signals are coupled to linear preamplifiers that preserve the amplitude information, and amplitude circuit 63 determines the amplitude of the signals. These devices consist of well known electronic circuitry and are not described further in this Specification. Two simultaneous signals will only be accepted when the particle passes within the diameter of the small focused beam 12.

Referring briefly to FIG. 4, the beam intensities at the sample volume 40 is illustrated. As shown, distance b_1 is the distance from the maximum intensity of the central beam 12; and b_2 is the distance from the maximum intensity of beam 11, where the intensity falls to $1/e^2$ of the maximum. An end view of the sample volume 40 is shown in FIG. 5.

Referring now to FIGS. 6 and 7, a particle passing on an arbitrary path through small beam 12 will produce a signal from detectors 60 and 62 (in the embodiment of FIG. 2, detectors 140 and 145). In order to determine the incident intensity on the particle, the trajectory defined by the distance x_p from the center of the Gaussian beam must be known. The well known equation describing the Gaussian beam intensity is given as

$$I = I_o \exp[-2x^2/b^2]$$

where I_o is the peak intensity of the beam which may be measured, x is the radius coordinate of the beam, and b is defined by convention as the radius wherein the inten-

sity I is equal to 1/e (e=2.7183) of the peak intensity, I_o. The radius b may also be measured for each beam. Thus, for beams 11 and 12, the equations are:

$$I_{11} = I_{o11} \exp\{-2x_{11}^2/b_1^2\}$$

$$I_{12} = I_{o12} \exp\{-2x_{12}^2/b_2^2\}$$

where the subscripts 11 and 12 refer to beams 11 and 12 (or in the case of the embodiment of FIG. 2, beams 102/104 and 86/90, respectively). Considering now the light scattered by a particle, the scattering parameters Q_{11} and Q_{12} may be specified. These coefficients may be computed if the characteristics (shape and material) of the particles are known or they can be determined by calibration with samples which have predetermined sizes. The scattering coefficients depend on such well known parameters as diameter, index of refraction, incident light wavelength and polarization, angle of light collection, and shape of the particles. These scattering coefficients are generally computed or obtained by calibration as a function of the size of the particle such that if Q can be obtained, a look up table can then be used to obtain the diameter d. Thus, Q is specified as a function of d as Q(d).

Given an arbitrary particle path x_p measured from the center of the beams and shown schematicaly in FIGs. 4, 5, 6 and 7, the scattered intensity may be expressed as:

$$I_{scat1} = I_{o11} Q_{11}(d) \exp\{-2x_p^2/b_1^2\}$$

$$I_{scat2} = I_{o12} Q_{12}(d) \exp\{-2x_p^2/b_2^2\}$$

Taking the ratio of the two equations yields:

$$I_{scat1}/I_{scat2} = \frac{I_{o11}\, Q_{11}(d)}{I_{o12}\, Q_{12}(d)} \exp\left[-2x_p^2\left(\frac{1}{b_1^2} - \frac{1}{b_2^2}\right)\right]$$

Solving for x_p results in the following:

$$x_p = \left\{\frac{1}{2}\left(\frac{b_1^2 b_2^2}{b_1^2 - b_2^2}\right)\ln\left[\left(\frac{I_{scat1}}{I_{scat2}}\right)\left(\frac{I_{o12}}{I_{o11}}\right)\left(\frac{Q_{12}(d)}{Q_{11}(d)}\right)\right]\right\}^{1/2}$$

where ln is the natural logarithm. In this expression, the ratio $Q_{12}(d)/Q_{11}(d)$ may be determined easily by calculating the light scattering for the respective polarizations which is the only parameter that is different between the two quantities. The incident beam intensities, I_{o11} and I_{o12} are measured apriori. Measurements of I_{scat1} and I_{scat2} are made for each particle based on the signal measurements. Thus, x_p can be obtained explicitly from the measured quantities for each particle size and trajectory. With xp determined, the equations may be rearranged as

$$Q_{11}(d) = \frac{I_{scat1}}{I_{o11}} \exp\{-2x_p^2/b_1^2\}$$

$$Q_{12}(d) = \frac{I_{scat1}}{I_{o12}} \exp\{-2x_p^2/b_2^2\}$$

to obtain $Q_{11}(d)$ and $Q_{12}(d)$. These values are then used in the respective lookup tables to obtain redundant measurements of the diameter of the particles. As mentioned, the lookup tables can be generated using the Mie theory or by direct calibration. Even if the Mie theory is used, calibration is still required to determine the constants that describe the collection efficiencies and gains of the system. This requirement and procedure is well-known.

Particles scatter as a function of their diameter. For example, for particles, the scattered light intensity increases approximately with the diameter squared. Since a scattered light level above a given threshold level must be scattered before the particle is detected, this will set an extreme radius within which the particle must pass before it is detected. The other dimension of the sample volume is set by the image of the receiver aperture. Because of the Gaussian incident intensity distribution (see FIGS. 4 and 6), the maximum radius for detection will be a function of the particle size. This change in the sampling cross section must be taken into account to prevent biasing the measured size distribution towards the large particles which have an effectively larger target for detection.

Using the aforementioned technique for determining the radius of the particle trajectory, x_p, a statistical distribution of the radii may be formed for each particle diameter. From this, the maximum radii for each partical diameter $x_{max}(d)$ can be determined which then defines the sampling cross section for each particle size measured. This method also includes any variances that may arise as a result of the measurement environment. The above mentioned sampling cross-section bias is then removed by multiplying the number of samples, n(d), for each particle size class in the measured statistical distribution by the ratio of the largest sampling cross section to that of the respective particle size as:

$$n(d)_c = \frac{x_{max}(d_{max}) \cdot n(d)}{x_{max}(d)}$$

where d_{max} is the largest size in the distribution. The average radii for each size class may also be used for this purpose and, in fact, is more reliable considering the statistics.

Knowledge of the radii of particle transit also provides necessary information for obtaining the particle's speed. Since the focused beam is circular, the path length through the beam as shown in FIG. 6 is known. The path length between the points where the signal exceeds a threshold level and where it falls below the threshold is determined as:

$$T = Q_1(d) I_{01} \exp\{-2x_t^2/b_1^2\}$$

where T is the set threshold level and x_t is the beam radius at the intensity level that produces a signal to the threshold level. Based on the analyses to this point, Q(d), b_1, and I_o are known. Therefore, the equation can be used to solve for x_t given as:

$$x_t = b_1\left[\frac{1}{2}\ln\left(\frac{T}{Q_1(d) \cdot I_{01}}\right)\right]$$

The particle path length between where the signal exceeds the threshold to where it falls below is given simply as:

$$l = 2[x_t^2 - x_p^2]^{\frac{1}{2}}$$

where x_p and x_t are deduced from the above relationships. A counter and a fixed frequency clock is used to measure the time, t, between when the signal exceeds the threshold to where it falls below the threshold again. The particle speed is then obtained as

$$S = X_p/t$$

The second approach illustrated in FIG. 2 utilizes the interference fringes formed by the pairs of crossed beams to obtain two components of particle velocity. This method consists of the well-known laser Doppler velocimeter (LDV) method. Combining this method with the present method allows the simultaneous measurement of particle size and velocity.

Given the measurements of the particle speed, sampling cross section, and number of particles counted per second, the particle number density can be obtained. This is accomplished by determining a swept volume as shown in FIG. 8 with a cross-sectional area defined by the sampling cross section and a length given by S multiplied by t, where t is the sampling time. For accuracy, the sample volume and speed must be determined for each particle size. The number density is then given as:

$$N = \sum_{i=1}^{m} \frac{n_i(d)}{A_i(d) \cdot S_i(d)\, t}$$

where $n_i(d)$ is the number of particles in each size class i of which there are m size classes, $A_i(d)$ is the corresponding sampling cross-sectional area for particle size d, $S_i(d)$ is the speed of particle size class d.

Other useful parameters may be extracted given the above parameters. Thus, the system revealed provides a versatile measurement technique for particle field diagnostics. Although the present invention has been described with reference to FIGS. 1-8, it will be appreciated that the Figures are for illustration only, and are not limitations on the invention. Numerous other optical structures and arrangements may be used which incorporate the teachings of the present invention as disclosed herein.

I claim:

1. An apparatus employing laser light scattering for determining the size of a particle, comprising:

laser beam generation means for generating first and second laser beams having Gaussian beam intensities;

beam expansion means in optical alignment with said first laser beam for expanding the diameter of said first beam;

light directing means for directing said first and second beams and combining said beams such that said second beam is disposed within and coaxial with said first beam;

focussing means in optical alignment with said light directing means for focussing said first and second beams such that they converge and said first beam is disposed within and coaxial with said second beam, thereby forming a sample volume;

collection means for sensing light scattered by a particle passing through said sample volume, said collection means converting said scattered light into electrical signals;

amplitude means coupled to said collection means for determining the amplitude of said electrical signals representing said scattered light;

trajectory determining means coupled to said amplitude means for calculating the trajector (x_p) of a particle passing through said sample volume, said trajectory being defined by:

$$x_p = \left\{ \frac{1}{2} \frac{(b_1^2 b_2^2)}{(b_1^2 - b_2^2)} \ln \left[\frac{(I_{scat1})}{I_{scat2}} \frac{(I_{02})}{I_{01}} \frac{(Q_2(d))}{Q_1(d)} \right] \right\}^{\frac{1}{2}}$$

where:

x_p = distance from the center of said second beam in said sample volume;

b_1 = distance from the maximum intensity of said second beam in said sample volume;

b_2 = distance from the maximum intensity of said first beam in said sample volume;

I_{01} = peak intensity of said first beam;

I_{02} = peak intensity of said second beam;

I_{scat1} = scattered light intensity of said first beam;

I_{scat2} = scattered light intensity of said second beam;

Q_1 = scattering parameter of said first beam;

Q_2 = scattering parameter of said second beam;

sizing means coupled to said trajectory determining means for determining the diameter of said particle from said particle's trajectory;

whereby the size of said particle is determined.

2. The apparatus as defined by claim 1, wherein said I_{scat1} and I_{scat2} values are determined by said trajectory determining means from the expressions:

$$I_{scat1} = I_{o1} Q_1(d) \exp\left[-2x_p^2/b_1^2\right]$$

$$I_{scat2} = I_{o2} Q_2(d) \exp\left[-2x_p^2/b_2^2\right].$$

3. The apparatus as defined by claim 2, wherein said sizing means includes look-up table means for relating said $Q_1(d)$ and $Q_2(d)$ values to said particle diameter (d), such that inputting said $Q_1(d)$ and $Q_2(d)$ values into said look-up table means results in an output corresponding to a diameter (d).

4. The apparatus as defined by claim 3, further including speed means coupled to said amplitude means for determining the speed of said particle passing through said sample volume.

5. The apparatus as defined by claim 4, wherein said collection means includes first and second photo-detectors for sensing light scattered by said particle through each of said first and second beams, respectively, said photo-detectors being coupled to said amplitude means.

6. The apparatus as defined by claim 5, wherein said photo-detectors sense said scattered light once said light exceeds a threshold value defined as:

$$T = Q_1(d) I_{o1} \exp\left[-2x_t^2/b_1^2\right]$$

where:

T = threshold value;

x_t = beam radius at the intensity level which produces a signal at said threshold level.

7. The apparatus as defined by claim 6, wherein the path length of said particle between where said electrical signals exceeds said threshold levels to where said signals fall below said level is defined as:

$$l = 2\left[x_t^2 - x_p^2\right]^{\frac{1}{2}}$$

8. The apparatus as defined by claim 7, wherein said speed means determines the time t when said signal exceeds said threshold value, the speed(s) of said particle being defined as:

$$X = x_p/t$$

9. The apparatus as defined by claim 8, wherein said speed means further determines the number of density of particles passing through said sample volume from the expression:

$$N = \sum_{i=1}^{M} \frac{n_i(d)}{A_i(d) \cdot S_i(d)t}$$

where:

N = number density of said particles;

$n_i(d)$ = number of particles in each size class i of M size classes;

$A_i(d)$ = sample cross-section area for particle class size d;

$S_i(d)$ = speed of said particle in size class d.

10. An apparatus employing laser light scattering for determining the size of a particle, comprising:

laser beam generation means for generating first and second laser beams hving Gaussian beam intensities;

beam expansion and splitting means in optical alignment with said first laser beam for expanding the diameter of said first beam and splitting said first beam into at least two parallel coplaner beams disposed in a first plane;

polarizanon and beam splitting means in optical alignment with said second beam and splitting said second beam into at least two parallel coplanar beams disposed in a second plane;

light detecting means for directing said first and second beam such that said first plane is disposed approximately at a known angle with respect to said second plane;

focussing means in optical alignment with said light directing means for focussing said first and second beams such that they converge thereby forming a sample volume;

collection means for sensing light scattered by a particle passing through said sample volume, said collection means converting said scattered light into electrical signals;

amplitude means coupled to said collection means for determining the amplitude of said electrical signals representing said scattered light;

trajectory determining means coupled to said amplitude means for calculating the trajectory (x_p) of a particle passing through said sample volume, said trajectory being defined by:

$$x_p = \left\{ \frac{1}{2} \frac{(b_1^2 - b_2^2)}{(b_1^2 - b_2^2)} \ln \left[\frac{(I_{sca1})}{I_{sca2}} \frac{(I_{02})}{I_{01}} \frac{(Q_2(d))}{Q_1(d)} \right] \right\}^{\frac{1}{2}}$$

where:

x_p = distance from the center of said second beam in said sample volume;

b_1 = distance from the maximum intensity of said second beam in said sample volume;

b_2 = distance from the maximum intensity of said first beam in said sample volume;

I_{01} = peak intensity of said first beam;

I_{02} = peak intensity of said second beam;

I_{sca1} = scattered light intensity of said first beam;

I_{sca2} = scattered light intensity of said second beam;

Q_1 = scattering parameter of said first beam;

Q_2 = scattering parameter of said second beam;

sizing means coupled to said trajectory determining means for determining the diameter of said particle from said particle's trajectory;

whereby the size of said particle is determined.

11. The apparatus as defined by claim 10, wherein said I_{sca1} and I_{sca2} values are determined by said trajectory determining means from the expressions:

$$I_{sca1} = I_{01} Q_1(d) \exp\left[-2x_p^2/b_1^2\right]$$

$$I_{sca2} = I_{02} Q_2(d) \exp\left[-2x_p^2/b_2^2\right].$$

12. The apparatus as defined by claim 11, wherein said sizing means includes look-up table means for relating said $Q_1(d)$ and $Q_2(d)$ values to said particle diameter (d), such that inputting said $Q_1(d)$ and $Q_2(d)$ values into said look-up table means results in an output corresponding to a diameter (d).

13. The apparatus as defined by claim 12, further including speed means coupled to said amplitude means for determining the speed of said particle passing through said sample volume.

14. The apparatus as defined by claim 13, wherein said collection means includes first and second photodetectors for sensing light scattered by said particle through each of said first and second beams, respectively, said photo-detectors being coupled to said amplitude means.

15. The apparatus as defined by claim 14, wherein said photo-detectors sense said scattered light once said light exceeds a threshold value defined as:

$$T = Q_1(d) I_{01} \exp\left[-2x_t^2/b_1^2\right]$$

where:

T = threshold value;

x_t = beam radius at the intensity level which produces a signal at said threshold level.

16. The apparatus as defined by claim 15, wherein the path length of said particle between where said electrical signals exceeds said threshold levels to where said signals fall below said level is defined as:

$$l = 2[x_t^2 - x_p^2]^{\frac{1}{2}}$$

17. The apparatus as defined by claim 16, wherein said speed means determines the two orthogonal velocity components using a laser Doppler velocimeter.

18. The apparatus as defined by claim 17, wherein said known angle is 90°.

19. The apparatus as defined by claim 17, wherein said speed means further determines the number density of particles passing through said sample volume from the expression:

$$N = \sum_{i=1}^{M} \frac{n_i(d)}{A_i(d) \cdot S_i(d)t}$$

where:

N = number density of said particles;

$n_i(d)$ = number of particles in each size class i of M size classes;

$A_i(d)$ = sample cross-section area for particle class size d;

$S_i(d)$ = speed of said particle in size class d.

20. A method employing laser light scattering for determining the size and trajectory of a particle comprising the steps of generating first and second laser beams having Gaussian beam intensities;

expanding the diameter of said first beam;

directing said first and second combining said beams such that said second beam is disposed within and coaxial with said first beam;

focussing said first and second beam such that they converge, thereby forming a sample volume;

sensing light scattered by a particle passing through said sample volume, and converting said scattered light into electrical signals;

determining the amplitude of said electrical signals representing said scattered light;

determining the trajectory (x_p) of a particle passing through said sample volume, said trajectory being defined by

$$x_p = \left\{ \frac{(b_1^2 b_2^2)}{(b_1^2 - b_2^2)} \ln \left[\frac{(I_{sca1})}{I_{sca2}} \frac{(b_{02})}{o1} \frac{(Q_2(d))}{Q_1(d)} \right] \right\}^{\frac{1}{2}}$$

where:

x_p = distance from the center of said second beam in said sample volume;

b_1 = distance from the maximum intensity of said first beam in said sample volume;

b_2 = distance from the maximum intensity of said second beam in said sample volume;

I_{o1} = peak intensity of said first beam;

I_{02} = peak intensity of said second beam;

I_{sca1} = scattered light intensity of said first beam;

I_{sca2} = scattered light intensity of said second beam;

Q_1 = scattering parameter of said first beam;

Q_2 = scattering parameter of said second beam;

determining the diameter of said particle from said particle's trajectory;

whereby the size and trajectory of said particle is determined.

21. The method as defined by claim **20**, wherein said I_{sca1} and I_{sca2} values are determined by said trajectory determining means from the expressions:

$$I_{sca1} = I_{o1} Q_1(d) \exp\{-2x_p^2/b_1^2\}$$

$$I_{sca2} = I_{o2} Q_2(d) \exp\{-2x_p^2/b_2^2\}.$$

22. The method as defined by claim **20**, wherein said size of said particle is determined using look-up table means for relating said $Q_1(d)$ and $Q_2(d)$ values to said particle diameter d such that inputting said $Q_1(d)$ and $Q_2(d)$ values into said look-up table means results in an output corresponding to a diameter d.

23. The method as defined by claim **21**, further including the step of determining the speed of said particle passing through said sample volume.

24. The method as defined by claim **22**, wherein said sensing step includes the use of first and second photodetectors.

25. The method as defined by claim **23**, wherein said collection means includes first and second photo-detectors for sensing light scattered by said particle through each of said first and second beams, respectively, said photo-detectors being coupled to said amplitude means.

26. The method as defined by claim **24**, wherein said photo-detectors sense said scattered light once said light exceeds a threshold value defined as:

$$T = Q_1(d) I_{o1} \exp\{-2x_t^2/b_1^2\}$$

where:

T = threshold value;

x_t = beam radius at the intensity level which produces a signal at said threshold level.

27. The method as defined by claim **25**, wherein the path length of said particle between where said electrical signals exceeds said threshold levels to where said signals fall below said level is defined as:

$$l = 2[x_t^2 - x_p^2]^{\frac{1}{2}}.$$

28. The method as defined by claim **26**, wherein said speed means determines the time t when said signal exceeds said threshold value, the speed(s) of said particle being defined as:

$$S = x_t/t.$$

* * * * *